WATES, MEIRING & BARNARD

Report to the

WATER RESEARCH COMMISSION

on

GENERIC SIMULATION MODEL FOR OPENCAST MINE WATER SYSTEMS

by

A M van Niekerk

WRC Report No. 528/1/97
ISBN 1 86845 361 8

PRETORIA
1997

NOTE

The computer program and manual,
as well as answers to any queries
regarding its application, are obtainable
from the author stationed at Wates, Meiring & Barnard

P O Box 6001
HALFWAY HOUSE
1685

Telephone (011) 315-0316

WATER RESEARCH COMMISSION

GENERIC SIMULATION MODEL FOR OPENCAST MINE WATER SYSTEMS

Table of Contents

List of Tables

List of Figures

List of Symbols

Symbol	Definition	Dimensions
		-
A_s	Surface area of pyrite	m^2
A	Reaction rate constant	-
a	Radius of coal/rock fragment or particle	m
A_{surf}	Surface area of pyrite per unit volume of coal/rock	m^2/m^3
a	Spherical particle radius	m
A	Cross sectional area	m^2
b	Stoichiometric ratio between pyrite and oxidant consumption	-
B(T)	Function to account for the temperature sensitivity of bacterial catalysis	-
B	Biotic scaling factor	-
b_{py}	Stoichiometric ratio	kg FeS_2/kg O_2
b_{Fe}	Stoichiometric ratio	kg Fe/kg O_2
C_o	Oxidant concentration	mol/m^3
C	Oxygen concentration	mg/m^3
C_{O2}	Oxygen concentration in spoils	kg/m^3
C	Oxygen concentration	kg/m^3
C	Actual oxidant concentration at the beginning of the time step	kg/m^3
C_{in}	Influent flow chemical concentration	kg/m^3
C_{out}	Outflow chemical concentration	kg/m^3
C	Chemical constituent concentration	kg/m^3
$D_{O2\,N2}$	Binary diffusion coefficient	m^2/sec
D_c	Diffusion coefficient	m^2/sec
d	Particle diameter	m
D	Dilution ratio of water	-
D_o	Diffusion coefficient	m^2/sec
D_{to2}	Effective diffusion coefficient of oxygen	m^2/sec
D_{tco2}	Effective diffusion coefficient of carbon dioxide	m^2/sec
D_1	Effective oxygen diffusion coefficient in pore space	m^2/sec
D_2	Effective oxygen diffusion coefficient into particle	m^2/sec
$D_{t\,O2}$	Effective oxygen diffusion coefficient	m^2/sec
D_o	Oxygen diffusion coefficient in air	m^2/sec
E_a	Activation energy	kJ/mole
E	Mass of oxygen consumed per unit mass of pyrite oxidised	kg FeS_2/m^3
E	Mass of oxygen consumed per unit mass of sulphur oxidised	kg O_2/kg S
F	Infiltration depth	mm
F(T)	Probability distribution function	-
F	Faraday constant	-
F_{py}	Pyrite content of spoils	kg/kg
F	Accumulated infiltration losses from start of runoff	mm
f	The instantaneous infiltration rate	mm/hr
f_c	The limiting, steady minimum infiltration rate	mm/hr
f_o	Initial maximum infiltration rate at the start of the storm	mm/hr
G_{py}	Pyrite content	kg FeS_2/kg coal
G_a	Empirical constant	-
G_b	Empirical constant	-
g	Acceleration due to gravity	m/s^2

Symbol	Definition	Dimensions
$H(O_2)$	Step function to account for the sensitivity of pyrite oxidation to the presence of available oxygen	-
H	Catalytic factor (= 10)	-
I	Ionic strength	-
I_a	Initial obstruction	mm
k	Decay constant or slope factor for a given soil	-
K	Oxygen concentration in particle	mg/m^3
K_d	Bacterial decay rate	-
K_{Fe}	Half saturated constant with respect to ferrous ion concentration	mg/ℓ
K_s	First order reaction rate constant	m/sec
K_c	Surficial reaction rate	$mol/m^2/sec$
K	Oxidant required to leach pyrite from a unit volume of coal/rock	mol/m^3
K_{ox}	Pyrite oxidation rate constant	m/sec
K_H	Half saturated constant with respect to hydrogen ion [H^+] concentration	mg/ℓ
ℓ	fragment half thickness	m
M_{py}	Pyrite mass oxidised in a time step	kg FeS_2/m^3 spoils/month
N_i	Molar flux	$mole/m^2/sec$
N_{o2}	Molar flux of oxygen	$mole/m^2/sec$
N_{co2}	Molar flux of carbon dioxide	$mole/m^2/sec$
n	Manning roughness coefficient	-
n	Number of electrons involved in the reaction (= 1)	-
P_{co2}	Carbon dioxide partial pressure	atm
P	Permeability	m/month
P	Accumulated rainfall at time t	mm
P	Wetted perimeter	m/m
$P_{(x)}$	Probability of detecting x pyrite grains in a sample	-
P	Total gas pressure	atm
P	Accumulated rainfall	mm
Q	Accumulated runoff	mm
Q_{py}	Stoichiometric oxygen requirement	kg O_2/kg pyrite oxidised
Q_{car}	Surficial carbonate dissolution rate	$mole/cm^2/sec$
Q_{py}	Oxygen consumption	$mole/m^3/sec$ or $kg/m^3/sec$
Q_{Fe}	Oxygen consumption	$mol/m^3/sec$ or $kg/m^3/sec$
Q	Oxygen consumption rate	kg $O_2/m^3/sec$
q	Flow rate	m^3/s
q_L	Lateral inflow per unit length along the x-axis	$m^2/s/m$
Q_{in}	Inflow from the next upper element	$m^3/month$
Q_{out}	Outflow to the next lower element	$m^3/month$
Q_{evap}	Nett evaporation loss from the impoundment	$m^3/month$
Q_d	Demand abstraction from impoundment	$m^3/month$
Q_{spill}	Spillage/decant from the impoundment	$m^3/month$
Q	Oxygen consumption rate	$kg/m^3/month$
Q_{py}	Oxygen consumption due to pyrite oxidation	$kg/m^3/month$
Q_{Fe}	Oxygen consumption due to ferrous iron oxidation	$kg/m^3/month$

Symbol	Definition	Dimensions
R_c	Chemical reaction rate	-
R_{py}	Pyrite oxidation rate, expressed on fractional basis	mole/mole/sec or kg/kg/sec
R	Pyrite oxidation rate	mol/sec
R	Universal gas constant	kJ/mol/K
r_s	Particle radius	m
R	Hydraulic radius (A/P)	m^2/m
$R_{CO2,O2}$	Ratio of molar flux of carbon dioxide to molar flux of oxygen	-
R_{py}	Pyrite oxidation rate, usually expressed on a fractional basis	mole/mole/sec or kg/kg/sec
R_{fe}	Ferrous iron oxidation rate	mole/m^3/sec or kg/m^3/sec
S	Water saturation of total porosity (fraction)	-
S(t)	Sulphate production	kg SO_4/m^2/sec
S	Potential maximum retention of soil	mm
S_f	Friction slope	m/m
S_o	Bed slope	m/m
t	Time from beginning of storm	hr
t	Time	sec
T	Temperature	K
T	Hydraulic residence time	days
T_1	Geometric means of the fast residence times	days
T_2	Geometric means of the slow residence time	days
T_d	Time for complete pyrite oxidation, if the process is diffusion limited	sec
T_c	Time for complete pyrite oxidation, if the process is kinetically controlled	sec
T_{do}	Model parameter at a reference oxidant concentration of C_o	month
T_{co}	Model parameter at a reference oxidant concentration of C_o	month
V_e	Water volume at the end of time step	m^3
V_o	Water volume at the beginning of time step	m^3
V	Volume of impoundment	m^3
V	Water volume in the flushed part of the spoils	m^3
V	Fraction of flow which migrates along the fast (preferential) flow path	-
v_o	Number of spherical particles per unit volume	$1/m^3$
v	Average velocity	m/s
X_t	Fraction of pyrite remaining at the end of time step	kg/kg
X_o	Fraction of pyrite remaining at start of time step	kg/kg
x	Distance down plane	m
x*	distance into dump	m
X	Position of reaction front in dump	m
X	Pyrite fraction remaining (in coal)	kg/kg
x	Number of discrete pyrite grains in the sample	-
x	Distance into dump	m
X_c	Fraction of remaining carbonate	-
X	Viable bacterial mass	mg/l
X_T	Proportion of maximum metabolic rate	-
X_{pH}	Proportion of maximum metabolic rate	-
X_o	Proportion of maximum metabolic rate	-
Y_o	Oxygen partial pressure	atm

Symbol	Definition	Dimensions
Y_i	Mole fraction of component I	mole/mole
Y_{O2}	Molar concentration of oxygen	mole/mole
Y_{CO2}	Molar concentration of carbon dioxide	mole/mole
y	Water depth	m
Z_i	Ionic charge	
Z	Dimension	m
Z	Vertical distance	m

Greek Symbols

Symbol	Definition	Dimensions
θ_t	Total (air-filled plus water-filled) porosity	m^3/m^3
θ_a	Air-filled porosity	m^3/m^3
θ_w	Water-filled porosity	m^3/m^3
ρ_s	Spoils fragment density	kg/m^3
ρ_b	Bulk spoils density	kg/m^3
ρ_w	Water density (~ 1 000)	kg/m^3
σ_1^2	Variance of ℓnT for the fast flow path	-
σ_2^2	Variance of ℓnT for the slow flow path	-
α	Pyrite surface area per unit volume of fragment	m^2/m^3
δ	Effective fragment thickness, within which pyrite is oxidised	m
ρ	Particle density	kg/m^3
ρ_{coal}	Coal density (~1,6)	ton/m^3
α	First order rate constant	-
λ	Mean number of grains per sample	-
ΔH_a	Actual free hydrogen ion concentration [H^+] increase	$mole/m^3$
ΔH_t	Generated free hydrogen ion concentration [H^+] increase	$mole/m^3$
ρ_c	Particle carbonate density	$mole/m^3$
γ_i	Activity coefficient	-
ℓ	Stoichiometric ratio of pyrite oxidised per unit oxygen utilised	mole FeS^2/mole O_2
ρ_s	Pyrite content of dump	kg FeS_2/m^3
ρ_s	Sulphur density in particle	kg S/m^3
θ_p	Particle porosity	m^3/m^3
γ	Henry's law constant	-
∂_s	Sulphate production per mass of sulphur oxidised	kg SO_4/kg S
ρ_s	Sulphur density in dump	-
ζ	Tortuosity	-
θ_{sat}	Saturated moisture content	-
θ_i	Initial moisture content	-
Ω	Sorptivity	m
ΔX	Fractional change in pyrite content during previous time step	-
ΔF_f	Change in ferrous iron mass in flushed fraction of spoils in previous time step	kg Fe
ΔF_{nf}	Change in ferrous iron mass in non-flushed fraction of spoils in previous time step	kg Fe

WATER RESEARCH COMMISSION

GENERIC SIMULATION MODEL FOR OPENCAST MINE WATER SYSTEMS

Acknowledgements

We would like to thank the Water Research Commission for the support of the project to develop a generic simulation model for opencast mine water systems. The project will hopefully contribute to a better understanding of such mine water systems.

We also appreciate the opportunity to use components of the model on a number of coal mining operations.

The members of the Project Steering Committee are thanked for their valuable contributions and advice on the project, including:

Dr TC Erasmus:	Water Research Commission
Mr HM du Plessis:	Water Research Commission
Mr DA Salmon:	AMCOAL
Mr JD Wells (deceased):	Digby Wells and Associates
Mr JNJ Viljoen:	Ingwe Collieries
Mr CF Rademan:	Sasol Coal
Mr SAP Brown:	Department of Water Affairs and Forestry
Mr JH Louw:	Department of Minerals and Energy

WATER RESEARCH COMMISSION

GENERIC SIMULATION MODEL FOR OPENCAST MINE WATER SYSTEMS

Executive Summary

1. INTRODUCTION

Opencast mining has become increasingly attractive as an economical coal recovery technique over the past decades. Several large opencast collieries are in operation on the Eastern Transvaal Highveld. These mining operations result in substantial disturbance of the natural hydrological cycle in the mining area. Opencast mining operations are also known to contribute a substantial salt, specifically sulphate load, to impoundments on the Eastern Transvaal Highveld. A recent water quality management study indicated that opencast mining contributes approximately 67% of the total sulphate load discharged to Witbank Dam.

Although numerous research projects have been launched to investigate various aspects of acid mine draining and saline water generation by collieries, no integrated model currently exists which can reliably predict the total mine water volume and quality from an opencast mine. Colliery management needs a predictive tool to analyse different mine water management options. A water and water quality model for an opencast mine would be an indispensable tool in arriving at the optimum mine water management strategy for a specific mine. The model must however be versatile enough to allow re-assessment of the mine water system after any change in the mining plan, which occurs periodically.

The principle aim of the research project is to formulate and develop an integrated water quality model which can be used to predict water flow and a number of water quality variables on any opencast mining operation. The following specific objectives were identified for the project:

- Development of a model which can be used to predict the water balance on an opencast mining operation including runoff, seepage and groundwater recharge.
- Development of a model which can be applied to any opencast mining environment with any combination of catchment areas, opencast pits, spoil areas, waste rock dumps, etc.
- The model must be able to simulate water flow and water quality from an opencast mine over the entire life of the mine. It must be sufficiently versatile to allow the simulation to be conducted with any time series input of daily or monthly rainfall and runoff.
- The model must be able to predict a number of water quality variables at any selected point within the mine water circuits. The selected water quality variables include TDS (or any other conservative element), sulphate and pH.

2. GENERAL CHARACTERISTICS OF MINING SPOILS

Spoils material presents a complex granular medium for the migration of water. The water flow is typically described as pseudo-karst, with preferential flow paths playing a significant role. A certain minimum moisture content has to be satisfied before flow can be initiated. It is also common to observe incomplete wetting of spoils subjected to rainfall recharge from the surface. The mathematical description of water migration through spoils has up to now been mainly by empirical methods.

Pyrite (FeS_2) is a common mineral in coal mining spoils and weathers to produce iron, sulphate and acidity products. The two main mechanisms of pyrite oxidation are summarised below:

$$FeS_2 + 3½O_2 + H_2O \rightarrow Fe^{2+} + 2\,SO_4^{2-} + 2H^+$$

$$FeS_2 + 14Fe^{3+} + 8H_2O \rightarrow 15Fe^{2+} + 2\,SO_4^{2-} + 16H^+$$

The further oxidation of the ferrous iron is recognised as the rate limiting reaction in the overall pyrite oxidation process:

$$14Fe^{2+} + 14H^+ + 3½O_2 \rightarrow 14Fe^{3+} + 7H_2O$$

Several more complex models of the oxidation of pyrite and associated minerals such as pyrrhotite have been developed.

Numerous mathematical models have been developed to predict the kinetics of pyrite oxidation in a spoils environment. Most models recognise the mass transfer (diffusion) and kinetic (chemical reaction) limitations and the sensitivity to the presence of an oxidant (oxygen and/or ferric iron). A shrinking-core type representation of the spoils particle within which pyrite oxidation takes place is commonly employed. Field observations of pyrite oxidation rates compared to the laboratory measurements under ideal conditions are very different. Field observations of pyrite oxidation rates indicate that severe limitations exist with respect to the transfer of oxidant (O_2/Fe^{3+}) into the spoils, transfer of the oxidation products from the spoils and the availability of a transport medium (water) to flush the oxidation products from the spoils.

A number of different minerals can participate in the neutralisation of pyrite oxidation products. The most common neutralising minerals include calcite, magnesite and dolomite. Feldspars also contribute to the neutralisation of acidity, but are generally slow reacting. The typical neutralisation reactions involving dolomite are summarised hereunder:

$$CaMg(CO_3)_2 + 4H^+ \rightarrow Ca^{2+} + Mg^{2+} + 2H_2CO_3 \text{ at } pH \leq 6.2$$

$$2CaMg(CO_3)_2 + 4H^+ \rightarrow 2Ca^{2+} + 2Mg^{2+} + 4HCO^-_3 \text{ at } pH \geq 6.2$$

The neutralisation kinetics are complicated and depends on numerous factors. Calcite dissolution rate is very sensitive to pH and the rate increases rapidly at $pH \leq 5$. The total neutralisation potential may also not be effectively available for reacting with pyrite oxidation products. Estimates of the available neutralisation capacity indicated that only 20 - 30% of the total carbonate minerals may actually participate in these reactions.

The chemistry of spoils water is influence by a large number of ionic species including:

- Acidity, $[H+]$ and alkalinity, $[OH^-]$, $[HCO_3^-]$, $[CO_3^{2-}]$

- Gaseous species, $[O_2]$, $[H_2CO_3^*]$, $[CO_2]$
- Iron, $[Fe^{2+}]$, $[Fe^{3+}]$
- Major cationic species, $[Ca^{2+}]$, $[Mg^{2+}]$
- Major anionic species, $[SO_4^{2-}]$

The presence of ionic species is influenced by the formation of soluble complexes, precipitation as insoluble salts, oxidation and reduction reactions. The redox potential in the spoils environment determines the relative concentration of ferrous and ferric iron. Iron forms many different sulphate and hydroxide complexes. Iron precipitates may include melanterite, jarosite and ferric hydroxide and influence the presence of dissolved iron species. The presence of carbonate and bicarbonate at different carbon dioxide partial pressures dominates the resultant pH and buffer capacity of the spoils water.

Microbial action can accelerate the pyrite oxidation process. This typically involves two bacterial species, *Thiobacillus ferro-oxidans* and *Thiobacillus thio-oxidans*. Microbial catalysis can increase the ferrous iron and pyrite oxidation rates by several orders of magnitude. Microbial action is sensitive to environmental conditions with optimum temperatures of 25-35°C, optimum pH of 2,5 - 4,5 and a minimum requirement for dissolved oxygen of more than 0,01 atm partial pressure.

Migration of oxygen in an unsaturated porous medium takes place in a number of different ways. These mechanisms of oxygen transport can be broadly classified into:

- oxygen transport via the water infiltration into the porous media.
- barometric pumping occurring due to fluctuations in atmospheric pressure. Atmospheric pressure changes are seldom more than 5 - 10%. In accordance with the ideal gas laws, movement of atmospheric constituents due to barometric pumping would typically be less than 50 - 100 mm, per metre depth of porous media.
- convective transport of oxygen under conditions created by, for example burning spoils.
- successive cycles of wetting and drying can also act as a mechanism for the transport of oxygen into a body of porous spoils. Wetting results in the displacement of air contained in the porous media. Drying results in ingress of air from the surrounding atmosphere into the porous spoils. These successive cycles occur over a long time scale, compared to the other oxygen transport mechanisms.
- advective transport of oxygen may also take place depending on several factors including wind patterns, geometry of the spoil/discard dump, local topography, grading within the dump and the effect of coal burning on or within the spoils body.

Diffusion is considered to be the main transport mechanisms supplying oxygen for pyrite oxidation processes to the interior of the opencast mine spoils body. A number of mathematical models have been developed to simulate the diffusion of oxygen into a homogeneous spoils body containing reactive pyrite minerals. These models are based on the assumption that oxygen is the rate limiting reactant, pyrite oxidation rate is much

faster than the oxygen supply to the pyrite oxidation sites and that a uniform distribution of pyrite exist throughout the spoils body.

3. HYDROLOGICAL ASPECTS OF MINE WATER SYSTEMS

Opencast mining operations extensively disturb the natural environment. The drainage characteristics of the natural surfaces are modified accordingly. Runoff simulation on a mine complex has to cater for a number of different surface types, including:

- natural pre-mined surface
- pit slopes and floor
- access ramps
- overburden spoil heaps
- levelled and profiled spoils
- levelled, topsoiled and vegetated spoils
- haul roads
- cultivated lands

The generic opencast mine water model can simulate the surface runoff from these different surface types using one of three different approaches:

- importation of a rainfall/runoff file generated by an independent hydrological model
- Soil Conservation Services (SCS) model
- Kinematic Flow (KF) model

4. DESCRIPTION OF GENERIC MINE WATER MODEL

The generic mine water model is designed to simulate the water flow and associated water quality over the operational life of an opencast pit. The simulation is done for a selected hydrological sequence and operates at a monthly time-step.

The opencast pit is subdivided into a number of individual mining blocks to allow the mine scheduling to be incorporated into the model. The status of each mining block then progressively changes from unmined, to prestripped, to mined and eventually to rehabilitated. The surface runoff and rainfall recharge characteristics of a mining block changes as its status changes. Each mining block is further subdivided into up to 10 horizontal layers. This allows the simulation of the vertical spatial variation of oxygen and water migration.

The generic opencast mine water model incorporates the three main sources of water to a pit water system, including:

- surface runoff from the different natural and disturbed surfaces draining towards the pit

- groundwater ingress from the surrounding aquifers which are intersected by the mining operations
- recharge to the spoils due to the infiltration of rainfall through the rehabilitation cover

Water storage and accumulation are also catered for in terms of the following features:

- spoils water which may accumulate in pit floor depressions
- surface runoff which may accumulate in depressions formed on the rehabilitated surface of the spoils body

Water quality algorithms allow the simulation of calcium, magnesium, sulphate, pH, alkalinity and iron species. The following chemical and geochemical characteristics are catered for in the model:

- quality of rainfall
- quality of recharge (infiltration) water entering the spoils body
- pyrite oxidation of the spoils body resulting in the release of oxidation products such as iron, sulphate and acidity
- neutralisation of pyrite oxidation products by dolomite and calcite minerals
- pollution washoff from dirty areas which will be transported by surface runoff

The conceptual flow diagram for the configuration of an opencast mining operation in terms of the model is shown on Figure A.1.

4.1 Water flow aspects

The surface runoff is computed using the hydrological models incorporated into the generic model. These models include the Soil Conservation Services (SCS) model and the Kinetic Flow (KF) model.

Rainfall recharge to the spoils is calculated on the basis of a seasonal distribution of infiltration, depending on the type of spoils rehabilitation cover. Allowance is made for levelled spoils, levelled and topsoiled spoils, levelled topsoiled and vegetated spoils.

Groundwater inflow to the opencast pit must be specified in terms of a flow per unit length of high wall or mined pit perimeter.

Water migration through the spoils is of particular importance in the model. A certain minimum spoils moisture content must be satisfied before the initiation of seepage to the next spoils layer. The spoils material is characterised in terms of a fraction in contact with migrating spoils water (due to the presence of preferential flow paths). A coarse and five spoils fraction are also defined, each with different water retention and permeability characteristics. Water then migrates through successive spoils layers until it finally reaches the pit floor.

All excess water generated in the opencast pit drains to the pit floor sump before discharge to an external pit water storage facility.

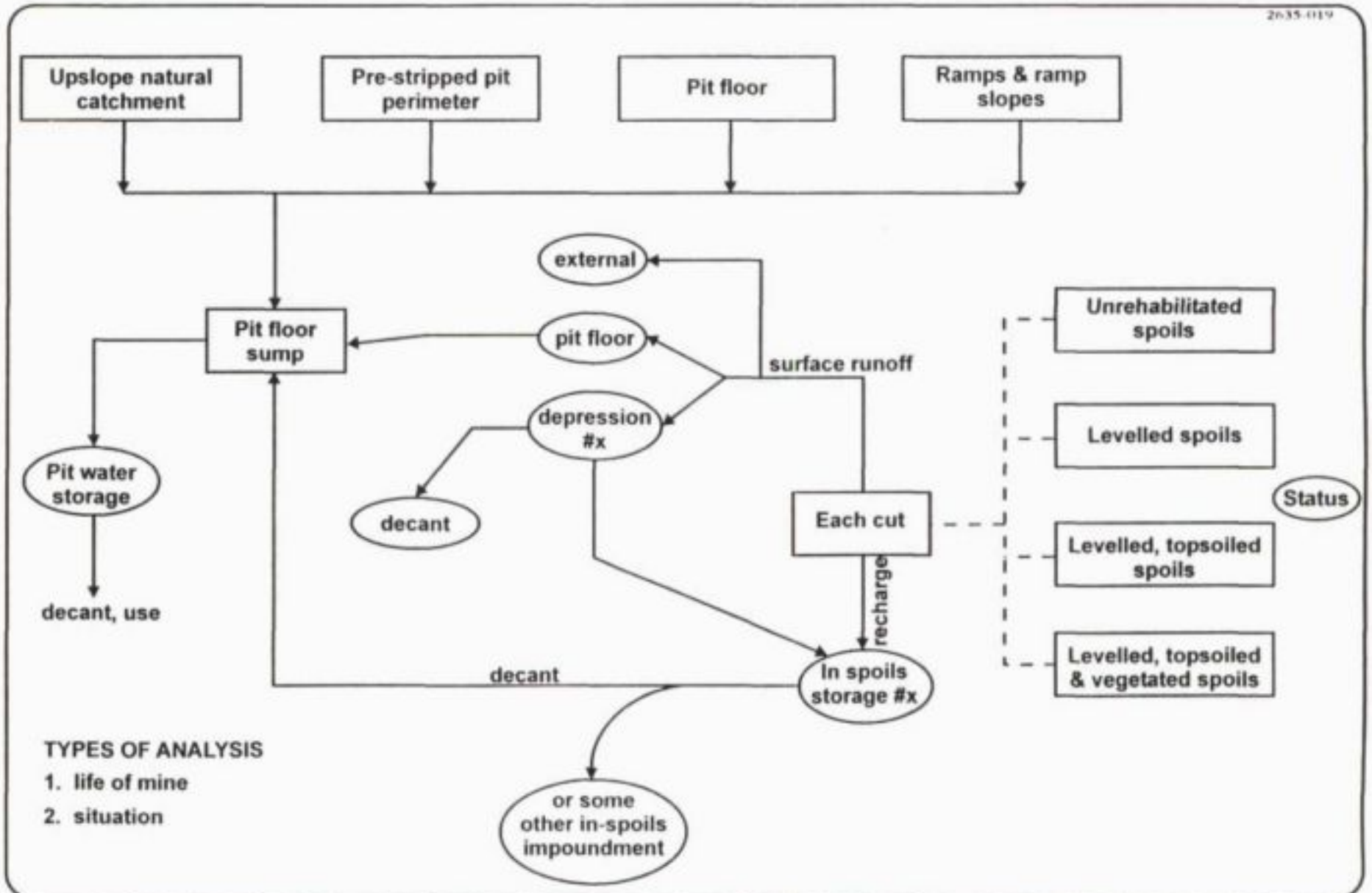

FIGURE A.1 : CONCEPTUAL FLOW DIAGRAM OF GENERIC MINE WATER MODEL

4.2 Water quality aspects

The water quality of the surface runoff is defined using an algorithm for the surface generation of pollutants and washoff from polluted surfaces. The quality of groundwater entering the pit is defined by the model user.

The model simulates the modification of the spoils water quality by a number of different processes:

- pyrite oxidation which releases oxidation products including iron (Fe^{2+}), sulphate (SO_4^{2-}) and acidity (H^+). The pyrite oxidation rate is calculated on the basis of the local concentration of oxidants (O_2 and Fe^{3+}) and remaining pyrite content.

- Ferrous iron undergo further oxidation depending on the redox potential in the local spoils environment. The ferrous iron will be oxidised to ferric iron which is an oxidant and will further stimulate pyrite oxidation. The redox potential is computed as a function of the local oxygen concentration in the spoils.

- Acidity generated in the process of pyrite oxidation is neutralised by carbonate minerals. The spoils typically contains a mix of calcite and dolomite which is reacted during neutralisation. The neutralisation process will only proceed if available carbonate minerals can be mobilised.

The slow pyrite weathering and migration of water through the spoils allow sufficient time for the application of the principles of chemical equilibrium. It is assumed that chemical equilibrium exist between the different ionic species in solution. Complexes and precipitates form depending on the ionic strength and relative free concentration of ionic species. The model also keeps an inventory of the accumulated precipitated salts to allow subsequent resolution if dictated by the local water chemistry.

5. CONCLUSIONS AND RECOMMENDATIONS FOR FURTHER RESEARCH

Development of a generic opencast mine water model has confirmed that the water system is indeed very complex. A large number of mining, hydrological, geochemical and other variables have to be taken into consideration. The project also confirmed that quasi-empirical models and prediction models based on some average rainfall and typical mine configuration can be very misleading in the prediction of mine water flow and quality.

As the environmental pressures on mining and related operations increase to cut back on the pollution load emanating from such operations, it will become increasingly important to develop accurate prediction tools to assess the generation of excess polluted water from opencast mining operations. Opencast mine water systems are further complicated by the fact that they are open to hydrological influences. This is unlike a closed circuit industrial process, where the water circuit and balance are typically dictated largely by production rates. Opencast mining operations will have to take due cognisance of the environmental risks associated with different hydrological events. The generic model allows such risk assessment by analysing the response of a mining operation to different hydrological sequences. This allows one to develop a quantitative understanding of the risk associated with extreme rainfall/runoff events.

The generic model can also be used to conduct a sensitivity analysis to develop an understanding of the response of the opencast mine water system to different variables.

This allows the mine operator to develop, for example, an understanding of the sensitivity of excess mine water production to different mining sequences. The benefit associated with accelerated spoils levelling, topsoiling and vegetation can now be quantified in terms of a reduction in excess water make. Sensitivity analyses in general confirmed that it is essential to have reliable information and data on mine scheduling and mine layout, accurate prediction of runoff associated with a different type of disturbed surfaces, reliable information on the recharge through the rehabilitation cover into the spoils and the geochemical characteristics of the spoils, specifically in terms of reactive pyrite and available carbonate minerals.

The data inputs to the generic opencast mine water model is onerous, but these inputs are required as minimum to develop a reliable understanding of the mine water system. The initial use of the model for a specific opencast pit, therefore requires the commitment of adequate resources and time to prepare the input data. Once the model has been configured with the available input data, it then becomes very easy to use and it is possible to look at a number of different mining schedules, rehabilitation strategies, hydrological sequences, etc. without further substantial input requirements.

The practical application of the model to the mining industry will, however, require further training and exposure of mining engineers, environmental officers and water system managers to the model. It is therefore recommended that the Commission gives consideration to the sponsoring of workshops to expose people to the model, develop confidence in the application of the model and to form a nuclear user group which can, in future, assist in the enhancement and refinement of the model.

Consideration should also be given to further research in a number of aspects which we now understand to be critical in the simulation of an opencast mine water system. These aspects include the following:

- Runoff generation from surfaces disturbed or modified by opencast mining operations. A large body of knowledge exists on rainfall/runoff characteristics for small and large catchments in South Africa. The Commission has, in the past, sponsored the development and verification of these models on different types of catchments. We have applied the best available knowledge to the generic mine water model. It is, however, appropriate to launch a research project to confirm the rainfall/runoff characteristics from surfaces, disturbed or modified by mining. These surfaces include access ramps and ramp slopes, pit floors, mining spoils in different states and different levels of rehabilitation.

- The recharge (infiltration) of rainfall through the rehabilitation cover into the spoils material is a dominant influence over the long term in any opencast mine water system. The Commission has already undertaken research on this topic and we believe that the research work should be continued.

- There is still a general lack of knowledge on the hydrodynamic characteristics of different South African spoils materials. The water retention and water flow characteristics need to be established for a broad spectrum of South African spoils, using techniques which have been applied with success internationally. The model had to rely on international experience and this needs to be extrapolated to South African conditions.

- There is also a general lack of information on the geochemical characteristics and the geochemical behaviour of South African spoils. It is only in recent times that static acid based accounting tests and kinetic leach column tests have been conducted. We need to expand our knowledge to include some full scale research work on the long term behaviour of spoils material under

controlled conditions. In general it would appear that the pyrite mineral contained in coal spoils is slowly oxidised and that the pyrite oxidation products are slowly mobilised from the spoils. It will be of value to our understanding of the geochemical behaviour of spoils to undertake full scale investigations into the migration of oxygen within actual spoils bodies and the accumulation of oxidation products.

WATER RESEARCH COMMISSION

GENERIC SIMULATION MODEL FOR OPENCAST MINE WATER SYSTEMS

1. INTRODUCTION

Opencast mining has become increasingly attractive as an economical coal recovery technique over the past decades. Several very large opencast collieries are in operation on the Eastern Transvaal Highveld. These mining operations result in substantial disturbance of the natural hydrological cycle in the mining area. Opencast mining operations are also known to contribute a substantial salt, specifically sulphate load, to impoundments on the Eastern Transvaal Highveld. A recent water quality management study indicated that opencast mining contributes approximately 67% of the total sulphate load discharged to Witbank dam.

The Department of Water Affairs and Forestry recently shifted the emphasis in the management of the national water resources. Water quality in any specific catchment is now managed on the basis of the Receiving Water Quality Objectives (RWQO) approach. The Receiving Water Quality Objectives approach is not the only instrument available to the Department in implementing a water quality management strategy for a catchment. It is however one of the most powerful instruments available to a regulatory agency. The RWQO approach caters for the allocation of waste loads of pollutants in a specific catchment to each of the major mining and industrial operations. The allowable waste load will be monitored at the final discharge point from a mining or industrial complex. It will be up to the colliery or industry to develop and implement a water system which will reliably achieve the allocated waste load.

Although numerous research projects have been launched to investigate various aspects of acid mine draining and saline water generation by collieries, no integrated model currently exists which can reliably predict the total mine water volume and quality from an opencast mine. Colliery management needs a predictive tool to analyse different mine water management options. A water and water quality model for an opencast mine would be an indispensable tool in arriving at the optimum mine water management strategy for a specific mine. The model must however be versatile enough to allow reassessment of the mine water system after any change in the mining plan, which occurs periodically.

Some first generation opencast mine water quality models were developed for selected collieries on the Eastern Transvaal Highveld. These models were hard wired for a specific colliery and have no general application to other collieries. The approach to certain of the water quality aspects in these models were also fairly empirical. There is a need in the mining industry to develop a generic opencast mine water quality model which can be applied after appropriate input of relevant physical and geochemical characteristics to any colliery.

There is also a need in the mining industry for the development of a tool which integrates the large amount of knowledge which has been accumulated on various aspects of coal mining and the impact of coal mining on water and water quality. Several models exist to predict the water quality emanating from sub-elements of a mining operation, such as a tailings dam or a discard dump. These submodels need to be integrated into a unified and overall colliery water quality model.

A generic model can be used to simulate and predict the effluent flow and pollution waste load emanating from a colliery complex under different hydrological conditions. Mine management will require such a modelling tool to determine whether a specific water management strategy will meet the pollution waste load allocation set by the Department of Water Affairs and Forestry.

The key issues to be addressed by the opencast mine water model include:

- The relative importance of pit perimeter and pit floor runoff, runoff from spoils areas, seepage from unrehabilitated spoils and rehabilitated spoils to the total opencast pit water balance.
- The relative importance of different water sources to the pit salt or sulphate balance.
- How will different mining schedules impact water flow and water quality.
- Can the seasonality of South African rainfall be exploited to better manage opencast mine water systems.
- What is the relative importance of flow from the regional groundwater body to the opencast pit.
- What is the impact of the opencast mining operation on the water yield from the natural catchment within which mining takes place.
- Seasonal and long term trends in water production and water quality from the opencast mine need to be understood.
- How can the opencast mine water balance and quality be modified by implementation of evaporation ponds, irrigation fields and periodic discharge to the public stream.

The main benefits arising from the development of a generic opencast water quality model include:

- Analysis and optimisation of mine water systems.
- Prediction of impact on water systems and circuits by changing mining plans or schedules.
- Quantification of the impact on the total mine water system by different spoils and waste rehabilitation strategies or rehabilitation rates.
- Definition of the risk of exceeding a certain allocated waste load by analysing long hydrological rainfall and runoff records.

The principle aim of the research project is to formulate and develop an integrated water quality model which can be used to predict water flow and a number of water quality variables on any opencast mining operation. The following specific objectives were identified for the project:

- Development of a model which can be used to predict the water balance on an opencast mining operation including runoff, seepage and groundwater recharge.
- Development of a model which can be applied to any opencast mining environment with any combination of catchment areas, opencast pits, spoil areas, waste rock dumps etc.
- The model must be able to simulate water flow and water quality from an opencast mine over the entire life of the mine. It must be sufficiently versatile to allow the simulation to be conducted with any time series input of daily or monthly rainfall and runoff.

- The model must be able to predict a number of water quality variables at any selected point within the mine water circuits. The selected water quality variables include TDS (or any other conservative element), sulphate and pH.

2. LITERATURE REVIEW

2.1 Physical spoils properties

Opencast mine spoils are composed of rock and soil fragments remaining after blasting, removal and relocation of coal overburden and interburden strata. The spoils fragment size distribution ranges from micrometres (μm) to meters (m). Spoils can, therefore, not be considered as a uniform media with homogenous physical and chemical properties.

The interparticle voids filled by air and/or water are significant to the migration of water and gases (oxygen, carbon dioxide) through the spoils body. The porosity of a spoils body can be computed as a function of the mass densities - refer to **Figure 2.1**:

- total (air-filled plus water-filled) porosity :

$$\Theta t = e / (1 + e) \qquad \textbf{(2.1.1)}$$

- air-filled porosity :

$$\Theta a = (1 - S).e / (1+e) \qquad \textbf{(2.1.2)}$$

- water-filled porosity:

$$\Theta_w = S.e/(1+e) = \Theta t - \Theta a \qquad \textbf{(2.1.3)}$$

where:

$e = (\rho_s - \rho_b) / (\rho_b - S.\rho_w)$

ρ_s = spoils fragment density (kg/m^3)

ρ_b = bulk spoils density (kg/m^3)

ρ_w = water density (~ 1 000 kg/m^3)

S = water saturation of total porosity (fraction)

Water percolating through the spoils material will act as a carrier medium to remove pyrite oxidation and leaching products from the spoils profile. The hydrodynamic properties of spoil material are, however, not readily amenable to mathematical description.

The top 5 m of spoils are typically subject to diurnal and seasonal temperature variations. The effect of fluctuating temperature reduces with increasing depth and remains reasonably constant (15 - 20°C) below 10 m from the surface.

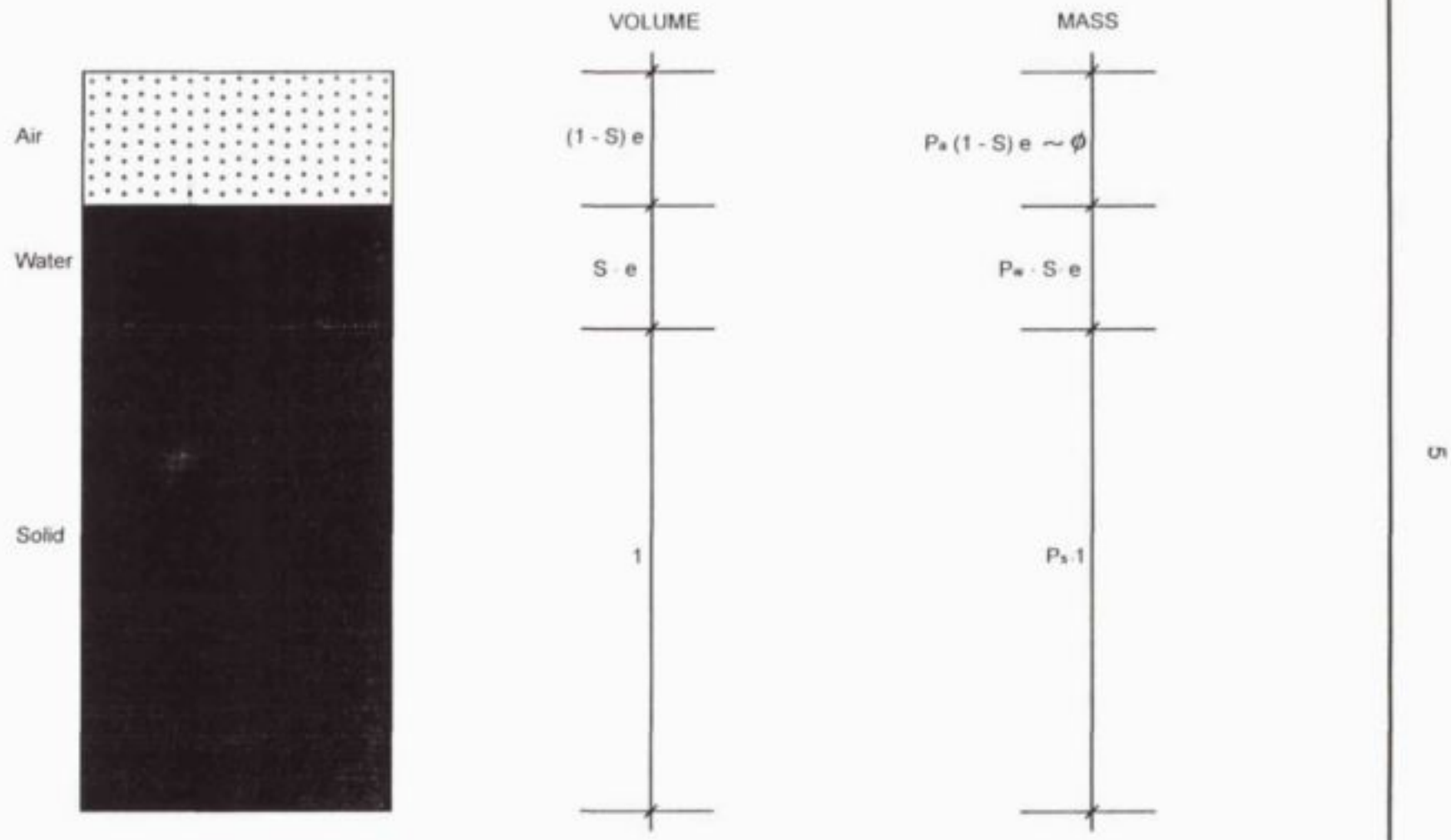

FIGURE 2.1 : VOLUME AND MASS FRACTIONS OF SPOILS MATERIAL

Typical spoils body physical properties are listed hereunder:

Spoil property	Range
• Pyritic sulphur content (% S)	0,02 - 4,0
• Spoils fragment density (kg/m^3)	2 200 - 2 700
• Bulk density (kg/m^3)	1 200 - 1 800
• Percentage coarse fragments, > 2 mm (%)	50 - 90
• Total porosity (v/v)	0,25 - 0,5
• Tortuosity (m/m)	2 - 10

Table 2.1 : Typical physical properties of spoils

2.2 Water migration through spoils

Water migration through spoils is primarily driven by:

- Infiltration/recharge via the rehabilitation cover to the spoils.
- Condensation/evaporation cycles within the spoils.
- Groundwater ingress from surrounding aquifers.

The water flow through spoils material is frequently approximated by pseudo-karst flow. This flow pattern is characterised by multiple flow paths and extreme ranges in geohydrological properties, such as hydraulic conductivity. The location and magnitude of flow paths are to a large extent controlled by rock stratigraphy, mining method, blasting method, contouring methods etc.

Spoils ridges and valleys, for example, vary in particle sizes. Larger spoils blocks tend to roll into spoils valleys, segregating from the smaller spoils particles which remain on the ridges. Flow paths are mainly associated with poorly consolidated spoils and local concentrations of bulky spoils. Geohydrological tests performed on spoils indicated that these preferential paths may not be interconnected and that flow is sometimes forced to migrate through areas of relatively low permeability.

The spatial variation in physical properties of spoils results in complex flow and water migration pathways. For example, a lense of relatively compacted/impermeable material may act as an aquiclude and may result in the formation of a localised perched water table within the spoils. The result is a highly variable and generally unpredictable flow pattern.

Elboushi (1975) has indicated that only 10 - 20% of the rock/spoils surfaces are effectively flushed during recharge/infiltration events. The remaining spoils body (80 - 90%) will accumulate pyrite oxidation products without flushing, except during extreme recharge events. The accumulated oxidation products will only become available during inundation/flooding of the pit spoils and may then be mobilised. Stromberg *et al.* (1994) also confirmed at the Aitik mine site in northern Sweden, that only 20% of the waste rock mass contributed substantially to the mobilisation of sulphate and copper from the waste rock dumps. It would also seem that the fraction of wetted spoils particle surfaces depends on the depth and intensity of the rainfall

recharge event. Severe storms (40 - 50 mm/hour) could result in a high degree (80 - 90%) of wetting of the spoils material, while low rainfall events may not result in any significant recharge.

Eriksson and Destouni (1994) found that the flow through a heterogeneous spoils medium is often characterised by the formation of relatively slow and relatively fast preferential flow paths. The true flow pattern is obviously not this simple. Rather, a range of slow and rapid flow paths typically exists in a spoils media. The flow chracteristics in spoils can be represented by a bi-modal probability distribution (refer to **Figure 2.2(a)**) which is expressed as:

$$f(T) = \frac{\upsilon}{T(2\pi\sigma_1^2)^{1/2}} \exp\left[-\tfrac{1}{2}(\ell nT-\ell nT_1)^2/\sigma_1^2\right] + \frac{(1-\upsilon)}{T(2\pi\sigma_2^2)^{1/2}} \exp\left[-\tfrac{1}{2}(\ell nT-\ell nT_2)^2/\sigma_2^2\right] \quad \textbf{(2.2.1)}$$

where:

T	=	hydraulic residence time (days)
υ	=	fraction of flow which migrates along the fast (preferential) flow path.
T_1, T_2	=	geometric means of the fast and slow residence times, respectively.
σ_1^2, σ_2^2	=	variance of lnT for the fast and slow flow paths, respectively.
$f(T)$	=	probability distribution function.

Typical probability distribution parameter values used at the Aitik mine site were:

	Geometric mean residence time (T)	Variance of lnT (σ^2)
Rapid flow path	1 yr	1,0
Slow flow path	60 yrs	0,3

Table 2.2 : Probability distribution parameters of water migration models (Aitik mine, Sweden)

The presence of preferential flow paths in a spoils body has an influence on the maximum level and temporal variation in pollutant flux emanating from the spoils body. The preferential flow paths typically result in the production of a reduced pollutant concentration in the spoils leachate, but also in the long-term slow release of pollutants. Water migrating along the slow and restricted flow paths will typically contain relatively high pollutant concentrations. This is due to the prolonged contact time between the water and oxidation products of the pyrite weathering process. Oxidation products may however remain in the poorly flushed spoils for a long time due to the restricted availability of a transport medium and the limited solubility of some oxidation products.

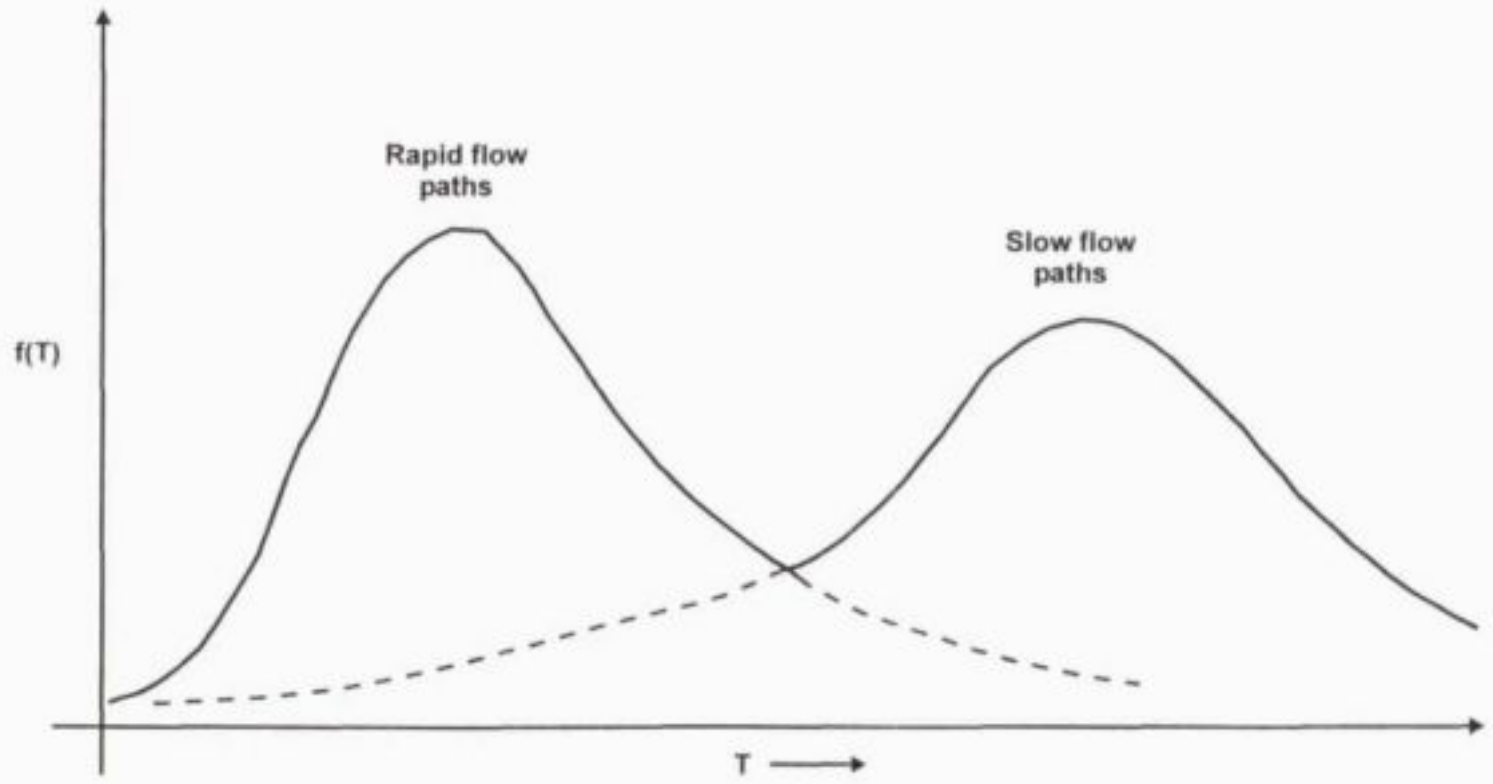

FIGURE 2.2(a) : PROBABILITY DISTRIBUTION OF WATER RESIDENCE TIME IN A SPOILS COLUMN

Jaynes (1983) employed an empirical technique to describe the pseudo-karst flow pattern through fractured spoils. The spoils body is divided into several horizontal layers. The water leaving any layer is allocated to the underlying layers in proportion to the **inverse** of the separating distance between layers - refer to Figure 2.2(b). Water migrating between two discrete horizontal layers, does not interact with the intervening layers. The fraction of water infiltrating/recharging to the top layer i, is then:

$$(d_i)^{-1} / \sum_{j=1}^{n} (d_i)^{-1} \qquad \textbf{(2.2.2)}$$

Water leaving any layer will be partitioned to the underlying layers in proportion to the inverse of the separating distance. The fraction of water leaving layer i and entering layer j is equal to:

$$(d_j - d_i)^{-1} / \sum_{k=i+1}^{n} (d_k - d_i)^{-1} \qquad \textbf{(2.2.3)}$$

The total flow from all overlying layers to layer j is then:

$$Q_j = \sum_{i=1}^{n} [(d_j - d_i)^{-1} / \sum_{k=i+1}^{n} (d_k - d_i)^{-1}] Q_i \qquad \textbf{(2.2.4)}$$

Water migration through waste rock piles and spoils heaps is, therefore, frequently characterised by rapid flow along preferential flow paths. Seasonal variation in seepage flow is common and periodic flushing of oxidation products takes place.

Elboushi (1975) also demonstrated that less than one half of the moisture retention (field capacity) of a granular/rocky material is required to initiate flow. This can be ascribed to incomplete wetting of the granular material. It was also postulated that the complete field capacity has to be satisfied for fine-grained waste/spoils ($\leq$ 0,15 mm size) before seepage flow would be established.

Gottschlich *et al.* (1987) experimented on coal discard material, containing particles in the size range 2 - 16 mm. The liquid hold-up (retention) in the experimental discard columns was established to be 0,1 - 0,15 m^3/m^3 discard volume. The dynamic fraction of the total hold-up was estimated to be 78%.

Harries and Ritchie (1981) measured moisture contents ranging from 0,05 to 0,12 m^3/m^3 in the Rum Jungle mine spoils/waste rock dumps.

Rogowski and Weinrich (1981) developed a relatively simple, but useful model of water migration through spoils material. Water moves primarily along preferential flow paths and relatively independent of the fines fraction in the spoils (refer to **Figure 2.2(c)**). For the purposes of defining water migration, a distinction is made between:

- Coarse spoils fragments (particle size > 2 mm) with a relatively low water retention and high saturated permeability.

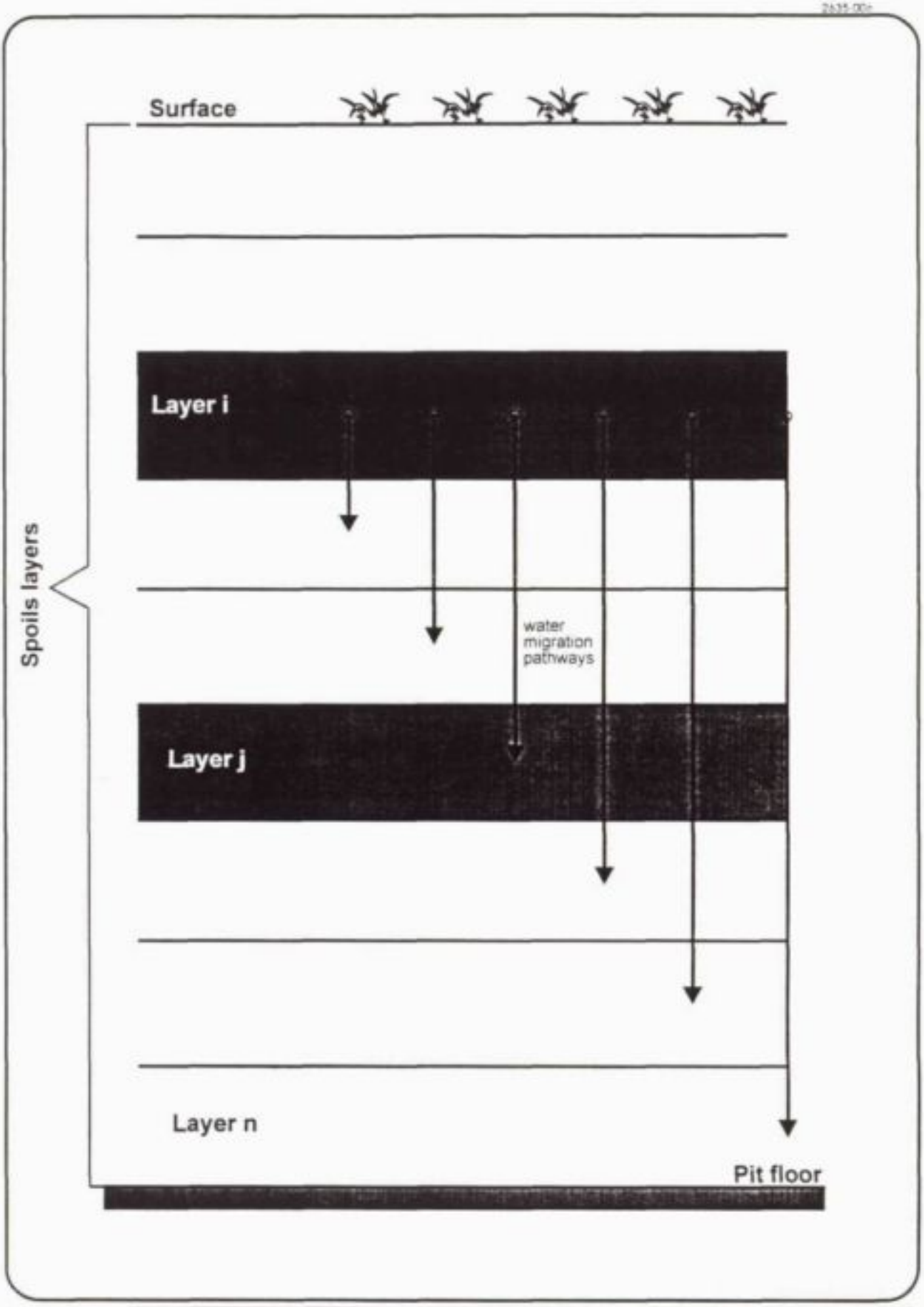

FIGURE 2.2(b) : JAYNES MODEL FOR WATER MIGRATION IN SPOILS

- Fine spoils fraction (particle size ≤2 mm) with a higher water retention and low saturated permeability.

A fraction of the spoils may never be wetted to any significant degree by water migration, except by a moisture condensation mechanism. Water entering the spoils has to satisfy the water retention of the coarse and fine fractions respectively, before migrating towards the next spoils layer. Rogowski (1980) employed the following moisture related spoils properties:

- Coarse fraction water retention = 0,07 m^3/m^3 spoils
- Fine fraction water retention = 0,13 - 0,14 m^3/m^3 spoils
- Total spoils porosity = 0,37 m^3/m^3 spoils

Pionke *et al.* (1980) observed a water-filled porosity of 11 - 12% for coal spoils particles in the size range 2 - 8 mm.

The flow velocity of water migrating through a saturated spoils material was observed to be similar to the measured saturated permeability. The water flow velocity for spoils was in the range of 0,5 - 1 mm/sec (43 - 86 m/day).

2.3 Pyrite oxidation

2.3.1 Geochemistry

Pyrite (FeS_2) is a common mineral in coal bearing strata. Two mechanisms of pyrite oxidation have been identified:

$$FeS_2 + 3½O_2 + H_2O \rightarrow Fe^{2+} + 2\,SO_4^{2-} + 2H^+$$

$$FeS_2 + 14Fe^{3+} + 8H_2O \rightarrow 15Fe^{2+} + 2\,SO_4^{2-} + 16H^+$$

The further oxidation of the ferrous iron is recognised as the rate limiting reaction in the overall pyrite oxidation process:

$$14Fe^{2+} + 14H^+ + 3½O_2 \rightarrow 14Fe^{3+} + 7H_2O$$

This latter reaction may be catalysed by bacterial action. The ferric iron may precipitate as a hydroxide under favourable pH conditions to release further acidity:

$$Fe^{3+} + 3H_2O \rightarrow Fe(OH)_3(s) + 3H^+$$

The autocatalytic nature of the pyrite oxidation process is shown in **Figure 2.3.1**.

Irrespective of the pyrite oxidation route, the molar ratio dictates that the oxidation of 1 mole of FeS_2 requires 3,5 moles of O_2 and produces 2 moles of acidity (H^+). In an alkaline environment, the ferrous iron will oxidize and precipitate as goethite ((FeOOH) which requires a further 0,25 moles O_2 and produces a further 2 moles acidity (H^+).

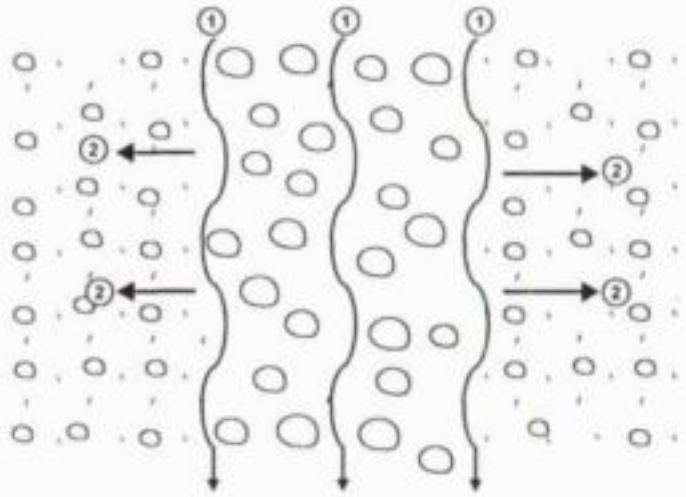

① Water migration routes via coarse fraction

② Water migration into fines fraction, under capillary action

FIGURE 2.2 (c) : CONCEPTUAL MODEL OF MOISTURE MIGRATION IN SPOILS

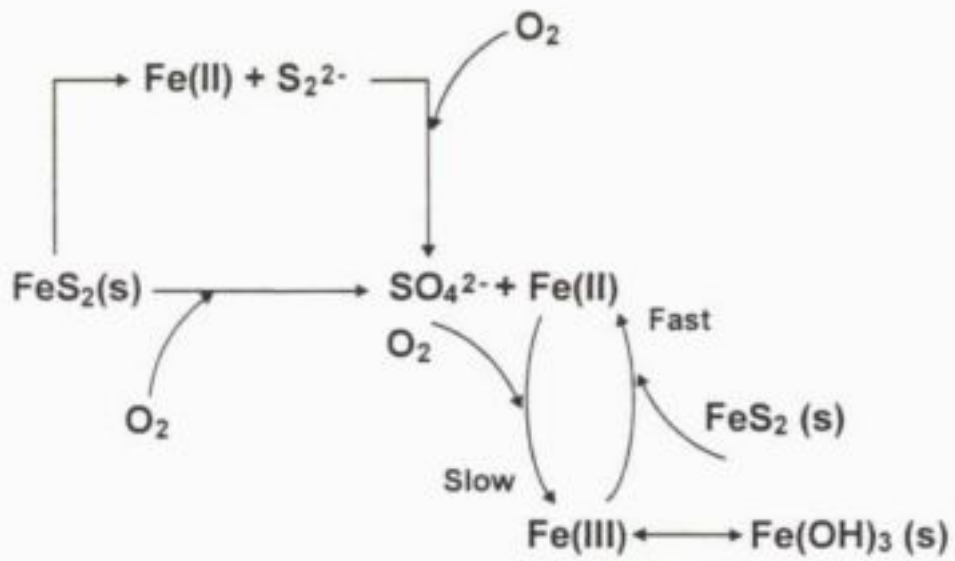

FIGURE 2.3.1 : PYRITE AUTOCATALYTIC OXIDATION MODEL

The oxidation of pyrite by ferric iron as the oxidant in a **low pH environment** can be written in a general form as:

$$FeS_2 + (2 + 12x)Fe^{3+} + (8x)\ H_2O$$

$$\rightarrow (3 + 12x)Fe^{2+} + (14x)H^+ + (2x)\ HSO_4^- + 2(1-x)S^\circ$$

Previous research by Cathles (1983) has indicated that the most appropriate value for x is 0,6 in a low pH environment, which results in the expression:

$$FeS_2 + 9{,}2Fe^{3+} + 4{,}8H_2O \rightarrow 10{,}2Fe^{2+} + 8{,}4H^+ + 1{,}2HSO_4^- + 0{,}8S^\circ$$

It must be stressed that this stoichiometry of pyrite oxidation applies only to specific conditions, including high ferric iron concentration, low pH ($\leq$ 2,0), and no available dissolved oxygen.

Barnes and Romberger (1968) stated that no thermodynamically reasonable mechanism has been identified by which **significant** pyrite oxidation can take place in the absence of oxygen or some other oxidizing agent, such as ferric iron.

Pyrrhotite [$Fe_{(1-x)}S$] is commonly found in some zinc, nickel and copper deposits. Pyrrhotite will also oxidize to form acidic products by the following reactions:

$$Fe_{(1-x)}S + (2 - x/2)\ O_2 + xH_2O \rightarrow (1-x)Fe^{2+} + SO_4^{2-} + 2xH^+$$

$$Fe_{(1-x)}S + (2 - 2x)\ Fe^{3+} \rightarrow (3 - 3x)\ Fe^{2+} + S^\circ$$

Elemental sulphur may be further oxidised to sulphate. Partial oxidation of pyrrhotite, resulting in the accumulation of elemental sulphur, has been observed at nickel mining operations.

Kleinman *et al.* (1981) formulated three steps/stages in the pyrite oxidation process:

- **Stage I** occurs at relatively high pH ≥ 4,5 with the following two reactions taking place:

$$FeS_2 + 3½O_2 + H_2O \rightarrow Fe^{2+} + 2SO_4^{2-} + 2H^+$$

$$Fe^{2+} + ¼O_2 + 2½H_2O \rightarrow Fe(OH)_3 + 2H^+$$

  These reactions proceed abiotically and the oxidation of ferrous iron is rapid at pH ≥ 5,0. The nett result is a leachate containing high sulphate concentrations and low acidity and iron concentrations.

- **Stage II** occurs as the pH continues to drop below 4,5, typically in the range 2,5 ≤ pH ≤ 4,5. The same reactions as in Stage I still dominate, but bacterial activity now catalyses them, specifically the oxidation of ferrous iron. The leachate contains elevated sulphate concentrations and acidity. The dissolved iron concentrations are also increasing due to the increased solubility of ferric iron at pH < 3,5.

- **Stage III** is initiated as the pH continues to drop to pH ≤ 2,5. The ferric iron activity is increased by the further increased solubility and the decreased precipitation of $Fe(OH)_3$. The following two reactions become dominant:

$$FeS_2 + 14Fe^{3+} + 8H_2O \rightarrow 15Fe^{2+} + 2SO_4^{2-} + 16H^+$$

$$Fe^{2+} + ¼O_2 + H^+ \rightarrow Fe^{3+} + ½H_2O$$

  Ferric iron then becomes the primary oxidant of pyrite and the availability of the ferric iron is dictated by the oxidation of ferrous iron. The leachate contains high concentrations of sulphate, iron and acidity. The ferric iron : ferrous iron ratio is largely determined by the redox potential in the spoils environment.

2.3.2 Kinetics of pyrite oxidation

The kinetics of pyrite oxidation within a spoils fragment can be described using a shrinking core model (Levenspiel, 1968). Jaynes (1983) refined the generic shrinking core model for use in a spoils environment with pyrite oxidation. He developed an expression for the oxidation rate, assuming a first order reaction with respect to oxidant (O_2 and/or Fe^{3+}) concentration and pyrite surface area - refer to **Figure 2.3.2(a)**.

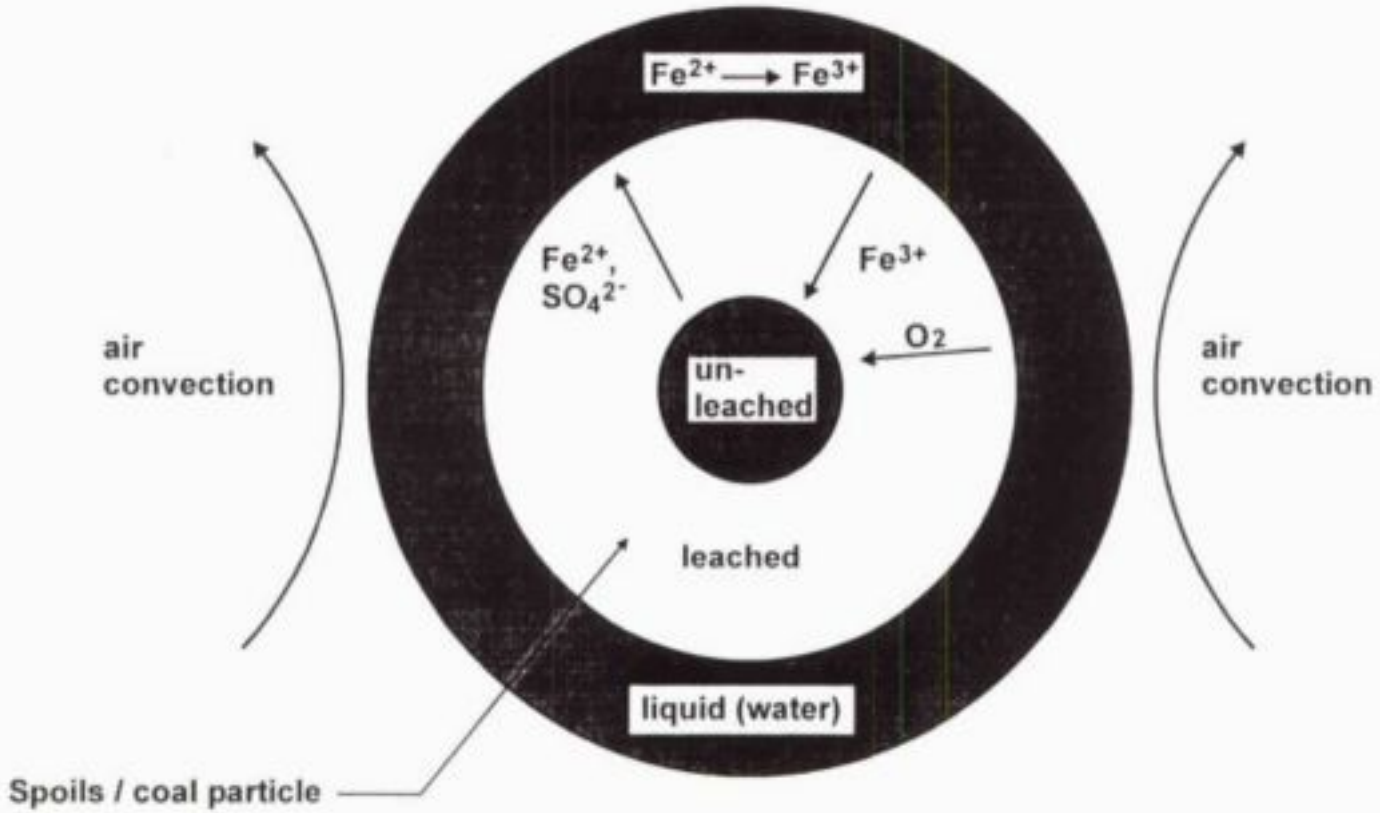

FIGURE 2 : SHRINKING CORE MODEL FOR THE LEACHING OF PYRITE FROM COAL

$$\frac{dX}{dt} = \frac{-1}{2T_d(1-X) + T_c} \qquad \textbf{(2.3.2.1)}$$

where:

X = pyrite fraction remaining (kg/kg)

T_d = time for complete pyrite oxidation, if the process is diffusion limited (sec).

T_c = time for complete pyrite oxidation, if the process is kinetically controlled (sec).

Assuming a simple spoils fragment shape in the form of a thin plate, then:

$$T_d = \frac{\rho_{py} \cdot \ell^2}{2b.D_c.C_o} \qquad \textbf{(2.3.2.2)}$$

where:

ρ_{py} = pyrite density in fragment (mole/m^3)

ℓ = fragment half thickness (m)

b = stoichiometric ratio between pyrite and oxidant consumption (1/3,5)

D_c = diffusion coefficient (m^2/sec)

C_o = oxidant concentration (mole/m^3)

and

$$T_c = \frac{\rho_{py} \cdot \ell}{b.K_s.C_o.\alpha.\delta} \qquad \textbf{(2.3.2.3)}$$

where:

K_s = first order reaction rate constant (m/sec)

α = pyrite surface area per unit volume of fragment (m^2/m^3)

δ = effective fragment thickness, within which pyrite is oxidised (m)

In general, diffusion is the rate-limiting step for pyrite oxidation as reflected hereunder by typical T_c and T_d values used by Jaynes (1983) in his model formulation:

	Oxidant = O_2 (0,21 mole fraction)	**Oxidant = Fe^{3+} (50 mg/l)**
T_d	86 yrs	111 years
T_c	13 yrs	2 years

In general for pure pyrite crystals, the pyrite oxidation rate is of the form

$$R = K_s.A_s.C_o \qquad \textbf{(2.3.2.4)}$$

where:

R = pyrite oxidation rate (mole/sec)

K_s = pyrite oxidation rate constant (m/sec)

A_s = surface area of pyrite (m^2)

The experimentally observed values for the rate constant, K_s, are summarised hereunder:

Reference	Oxidant	
	Ferric iron (Fe^{3+})	**Oxygen (O_2)**
Clark (1965)	$8,1 - 8,6 \times 10^{-10}$	18×10^{-10}
Singer & Stumm (1968)	$1,0 - 4,4 \times 10^{-9}$	—
Osurf (1970)	$4,4 \times 10^{-9} - 7,5 \times 10^{-10}$	$4,4 - 12 \times 10^{-10}$
Pionke *et al* (1980(a))	—	$8,2 \times 10^{-10}$

Table 2.3.2 : Pyrite oxidation rates observed for pure pyrite crystals, (K_s in m/h)

The pyrite (pure granules) oxidation rate was also observed to be inversely related to particle size. This can be explained by the approximate expression for the specific particle surface area:

$$A_s = 6/\rho.d$$

where:

A_s = surface area per unit mass (m^2/kg)

ρ = particle density (kg/m^3)

d = particle diameter (m)

Morin and Hutt (1994) employed an empirical expression for the pyrite oxidation rate which is frequently based on kinetic (leach column) test results. The experimentally observed pyrite reaction rates are frequently of an exponentially declining type and the observed reaction rate then approaches a steady state, which can be employed in modelling.

Sharer *et al.* (1994) used the following empirical equation for the **abiotic** surficial pyrite oxidation rate:

$$K_c = A(0,33\ pH)^{0.7} \exp(-E_a/RT)C_o \qquad \textbf{(2.3.2.5)}$$

Where:

K_c = surficial reaction rate (mole/m²/sec)

A = reaction rate constant

E_a = activation energy (kJ/mole)

R = universal gas constant (kJ/mole/K)

T = temperature (K)

C_o = oxygen concentration (mole/m³)

The abiotic pyrite oxidation rate is therefore also a weak function of the ambient pH-level.

The oxidation rate of pyrite by ferric iron is about ten times (one order of magnitude) faster than the oxidation rate by oxygen, at equivalent concentrations of ferric iron and oxygen.

Cathles (1983) developed a model to simulate the removal of pyritic sulphur from coal stockpiles. The research was motivated by the requirement to reduce the sulphur content of coal burned in American power stations. It was demonstrated that pyritic sulphur can be removed from coal by controlled leaching using a ferric sulphate solution. The model included aspects of pyrite sulphur oxidation, movement of air by convection through coal stockpiles and heat generation in the coal stockpiles. The pyrite leaching process in coal stockpiles was described as a number of sequential steps involving:

- Oxygen saturation of the water film coating of the coal/rock fragment. The oxygen is assumed to be supplied by convective air movement.
- Bacterial catalysis of ferrous to ferric iron oxidation in the liquid film, utilizing oxygen.
- Diffusion of ferric iron into the coal/rock fragment to react with pyrite to form sulphur, sulphate and ferrous iron.
- Counter-diffusion of the pyrite oxidation products via the leached rim of the coal/rock particle.

Pyrite oxidation rate is typically much faster than the ferric iron diffusion rate. The result is a coal/rock fragment with a shrinking core, consisting of a leached rim, surrounding a diminishing core of unreacted material.

The pyrite oxidation kinetics observed by Cathles (1983) may find application in a large spoils body containing carbonaceous shale with dispersed pyritic sulphur granules. The pyrite oxidation rate equation is:

$$\frac{dX}{dt} = \frac{-3X^{2/3} \cdot B(T) \cdot H(O_2)}{6 \cdot T_e \cdot X^{1/3} \cdot (1-X^{1/3}) + T_c} \qquad \textbf{(2.3.2.6)}$$

where:

X = remaining pyrite fraction in coal (kg/kg)

$B(T)$ = function to account for the temperature sensitivity of bacterial catalysis

$H(O_2)$ = step function to account for the sensitivity of pyrite oxidation to the presence of available oxygen

T_d = time factor to account for the diffusional transport of the oxidant through the coal fragment (sec)

T_c = time factor to account for the pyrite oxidation rate (sec)

The following expressions were developed for the two time factors:

$$T_c = \frac{K.a}{K_{ox}.A_{surf}.\delta.C_o} \qquad \textbf{(2.3.2.7)}$$

$$T_d = \frac{K.a^2}{6.D_c.C_o} \qquad \textbf{(2.3.2.8)}$$

where :

K = oxidant required to leach pyrite from a unit volume of coal/rock (mole/m^3)

a = radius of coal/rock fragment (m)

K_{ox} = pyrite oxidation rate constant (m/sec)

A_{surf} = surface area of pyrite per unit volume of coal/rock (m^2/m^3)

D_c = diffusion coefficient of ferric iron in coal/rock (m^2/sec)

δ = leached rim depth (m)

C_o = concentration of ferric iron oxidant (mole/m^3)

The Cathles model is derived from similar principles as the Jaynes model, both using a mixed kinetic shrinking core approach, but on different coal/rock particle shapes. The typical model values for T_c and T_d at 20°C and particle radius of 1 cm:

	Oxidant (Fe^{3+} = 50 mg/l)	
	Theory	**Observation**
T_d	193 years	83 years
T_c*	55 - 181 years	17 years

** The experimentally observed values for the T_c time factor were much lower than theoretically predicted.*

Cathles (1983) also expressed the rate of oxygen consumption within the coal stockpile as:

$$\frac{dO_2}{dt} = \rho_{coal} (1 - \Theta_i) Q_{py} . G_{py} . [dX/dt] \quad \textbf{(2.3.2.9)}$$

where:

ρ_{coal} = coal density (approximately 1,6 ton/m^3)

Θ_i = stockpile porosity (m^3/m^3)

Q_{py} = stoichiometric oxygen requirements (kgO_2/kg pyrite oxidised)

G_{py} = pyrite density ($kgFeS_2$/kg coal)

The mass transfer of oxygen due to advective air movement into the coal stockpile is not strictly applicable to a dense spoils environment. Diffusional transport of oxygen is assumed to be more appropriate under the latter conditions.

The Cathles model also assumes a uniform and relatively high moisture migration rate through the coal stockpile. The situation in a South African spoils body is very different, considering the relatively low annual precipitation under local conditions.

It must be appreciated that the Cathles model was primarily developed for pyrite leaching from porous coal stockpiles, using ferric iron as oxidant. Some aspects of the model formulation may be extrapolated to the situation in a relatively dense spoils body/discard dump. Hydrometallurgical models, which simulate commercial heap leaching operations, generally focus on the reaction and transport of reaction products in and around the **individual** ore/rock particle. The mass transfer problem of providing the oxidant from outside the dump to the particles within is not considered. A constant oxidant (oxygen or ferric iron) concentration surrounding the individual spoils/rock particles is usually assumed. In natural systems, where forced ventilation and pumped oxidant recirculation is absent, these approximations are not appropriate.

Harries and Ritchie (1981) derived pyrite oxidation rates from temperature profiles at a dump on the Rum Jungle Mine in Australia. The pyrite oxidation rate, expressed in mass of oxygen consumed per unit surface area of the dump was 2,52 kg O_2/m^2/year (43 ton SO_4/ha/year). This is substantially higher than the sulphate production observed on coal mining spoils bodies in South Africa. A simple first order reaction was used to simulate pyrite oxidation under conditions of a constant external source of oxidant (O_2/Fe^{3+}):

$$\frac{dX}{dt} = -\alpha X \quad \textbf{(2.3.2.10)}$$

where :

α = first order rate constant

This model was demonstrated to have application over relatively short periods of time (20 - 200 days) and up to approximately 63% oxidation of the available pyrite.

Helz *et al.* (1987) suggested that pyrite oxidation rates exceed the transport rates of oxidation products from coal stockpiles. This may result in the accummulation of oxidation products such as gypsum, melanterite, goethite, jarosite etc. in coal stockpiles. The leachate quality would therefore be saturated with the solid phase of these oxidation products.

The oxidation of ferrous iron to ferric iron may also influence the pyrite oxidation rate. If the ferrous iron is not removed by oxidation or precipitation, then the pyrite oxidation process may be retarded. The **abiotic** oxidation rate of ferrous iron is influenced by the iron concentrations, pH and oxygen partial pressure:

$$\frac{d[Fe^{2+}]}{dt} = [Fe^{2+}][O_2](K_1/[H^+]^2 + K_2) \qquad \textbf{(2.3.2.11)}$$

where :

$[Fe^{2+}]$	=	ferrous iron concentration (mole/l)
$[O_2]$	=	oxygen concentration (mole/mole) or partial pressure (atm)
K_1	=	$1,3 \times 10^{-15}$ (mole^2/l^2/sec)
$[H^+]$	=	hydrogen ion concentration (mole/l)
K_2	=	$1,7 \times 10^{-9}$ (l/sec)

The ferrous iron oxidation rate is shown as a function of pH on **Figure 2.3.2(b)**.

Pionke *et al.* (1980(b)) found in experimentation using spoils particles in the size range 2 - 8 mm, that the pyrite oxidation rate was the limiting process for freshly exposed material. The diffusion of pyrite oxidation products, however, is the rate limiting step for weathered spoils material. This supports the application of "shrinking core" type kinetic models to describe the pyrite oxidation process.

Literature values for the pyrite oxidation rate under ideal conditions with no restriction on the availability of oxidants vary from 0,06 - 0,16 g SO_4/kg pyrite/hour. For a 30 m high spoils heap, containing 0,5% sulphur and with a bulk density of 1600 kg/m^3, this is equivalent to 4 710 - 12 560 ton SO_4/ha/year.

Field observations on the Eastern Transvaal Highveld opencast mines indicated a sulphate production rate emanating with seepage from spoils bodies of 2 - 8 ton SO_4/ha/year. This is obviously much lower than the observations under controlled and ideal conditions. It demonstrates the severe restrictions in the field with respect to pyrite oxidation, including the mass transfer of oxidants into the spoils pore volume, mass transfer of oxidation products from the spoils particle surface and flushing/removal of oxidation products from the spoils particle surfaces.

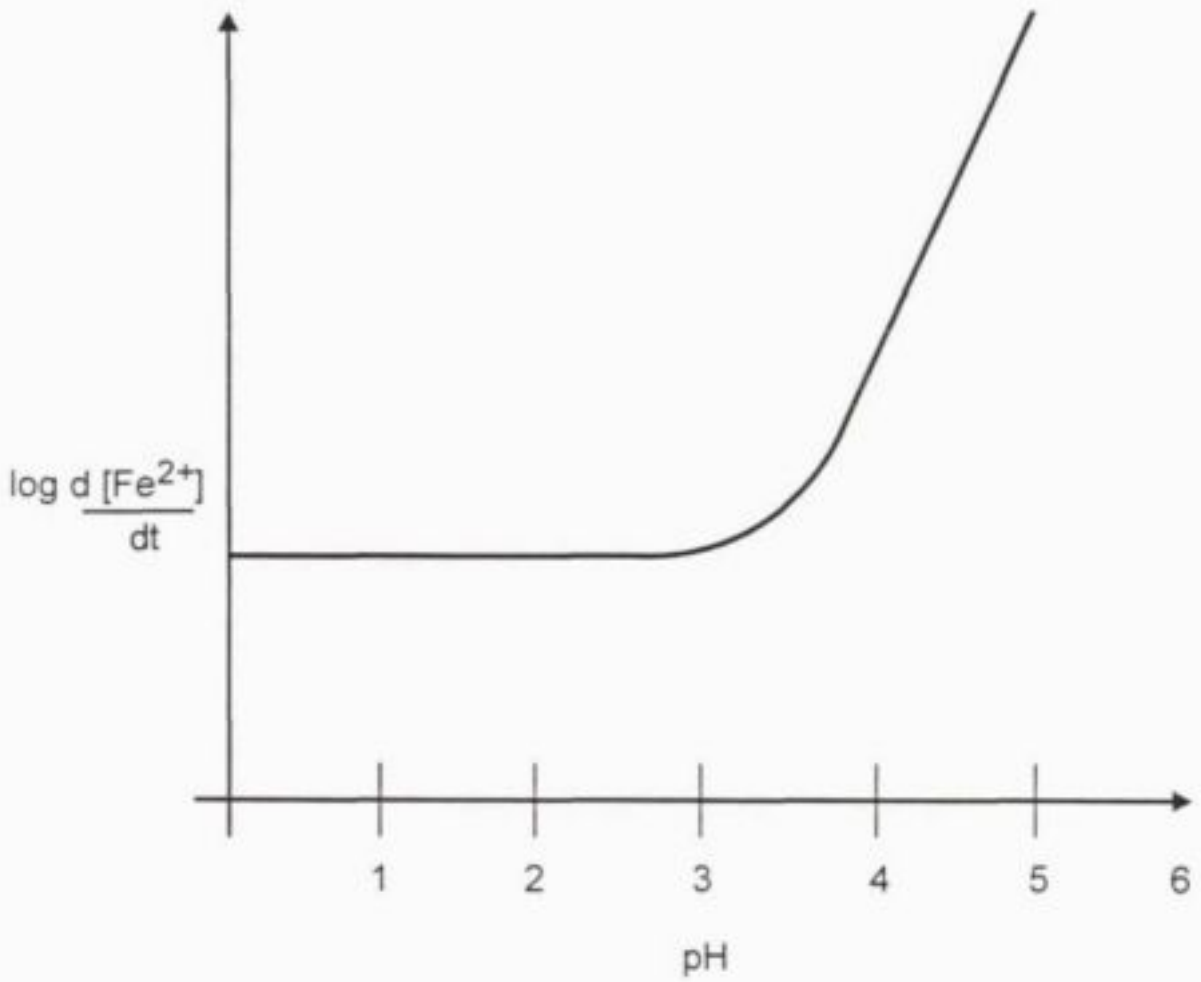

FIGURE 2.3.2(b) : FERROUS IRON OXIDATION RATE AS A FUNCTION OF pH (abiotic conditions)

Scharer *et al.* (1994) conducted an evaluation of pyrite oxidation in **tailings** containing 35% FeS_2 (very high) on a mass basis. They observed the following pyrite oxidation rates as 21°C.

- abiotic oxidation = 0,038 mole/kg/month
  = 3,65 kgSO_4/ton tailings/month
- biotic oxidation = 1,17 mole/kg/month (@ pH = 3)
  = 112 kg SO_4/ton tailings/month

Catalysis of the pyrite oxidation process by *Thiobacillus ferro-oxidans* was, therefore, able to increase the reaction rate by a factor of 31.

2.3.3 Pyrite geology

A large number of different sulphide minerals can produce acidic oxidation products. The most common sulfide minerals contained in coal deposits and associated strata include pyrite, marcasite, sphalerite, galena and chalcopyrite - refer to **Table 2.3.3.**

Coal typically contains sulphur in different forms including:

- pyritic sulphur
- sulphate sulphur
- organic sulphur

The oxidation of organic sulphur compounds may increase the sulphate concentration, but does not contribute to the formation/release of acidity, as reflected by the following reaction:

$$X\text{-}S + 2\,O_2 \rightarrow SO_4^{2-} + X^{2+}$$

Marcasite (FeS_2 in the rhombic crystal form) is much more reactive than pyrite (FeS_2 in the cubic crystal form).

Pyrite is typically not uniformly distributed throughout a rock mass, most of the pyrite exists in localised regions of high density, called clusters. Rymer *et al.* (1991) proposed the use of a Poisson distribution to describe the stochastic properties of pyrite distribution in a rock mass:

$$P(x) = \exp(-\lambda)^x/x! \qquad \textbf{(2.3.3)}$$

where :

x = number of discrete pyrite grains in the sample

λ = mean number of grains per sample

$P(x)$ = probability of detecting x pyrite grains in a sample

The Poisson distribution approaches a continuous probability distribution if x is defined as the number of discrete pyrite grains per 10 000 (or some arbitrary large number) non-pyrite mineral grains.

Mineral	Composition
Pyrite	FeS_2
Marcasite	FeS_2
Pyrrhotite	$Fe_{1-x}S$
Smythite, Greigite	Fe_3S_4
Mackinawite	FeS
Amorphous	FeS
Chalcopyrite	$CuFeS_2$
Chalcocite	Cu_2S
Bornite	Cu_5FeS_4
Arsenopyrite	FeAsS
Realgar	AsS
Orpiment	As_2S_3
Tetrahedrite and Tennenite	$Cu_{12}(Sb,As)_4S_{13}$
Molybdenite	MoS_2
Sphalerite	ZnS
Galena	PbS
Cinnabar	HgS
Cobalitite	CoAsS
Niccolite	NiAs
Pentlandite	$(Fe,Ni)_9S_8$

Table 2.3.3 : Common sulphide containing minerals

2.4 Geochemistry of neutralisation

Neutralisation of the pyrite oxidation products (specifically acidity) is mainly achieved by calcite and dolomite. Aluminosilicate minerals, such as clays and feldspars, may also contribute to the process. The conventional neutralisation reactions include:

Calcite

$CaCO_3 + 2H^+ \rightarrow Ca^{2+} + H_2CO_3$ at pH ≤ 6.2

$2CaCO_3 + 2H^+ \rightarrow 2Ca^{2+} + 2HCO_3^-$ at pH ≥ 6.2

Dolomite

$CaMg(CO_3)_2 + 4H^+ \rightarrow Ca^{2+} + Mg^{2+} + 2H_2CO_3$ at pH ≤ 6.2

$2CaMg(CO_3)_2 + 4H^+ \rightarrow 2Ca^{2+} + 2Mg^{2+} + 4HCO_3^-$ at pH ≥ 6.2

The nett oxidation/neutralisation reactions in an **acidic** environment can be summarised:

$$FeS_2 + 3½O_2 + H_2O \rightarrow Fe^{2+} + 2SO_4^{2-} + 2H^+$$

$$CaCO_3 + 2H^+ \rightarrow Ca^{2+} + H_2CO_3$$

$$H_2CO_3 \rightleftarrows H_2O + CO_2(g)$$

The molar ratio of calcium to sulphate is then $[Ca]/[SO_4] = 0,5$ in an **acidic** environment ($pH \leq 3$ typically).

The nett oxidation/neutralisation reactions in a mildly acidic to **alkaline** ($pH \geq 6,2$) environment can be summarised:

$$FeS_2 + 3¾O_2 + 3½H_2O \rightarrow Fe(OH)_3(s) + 2SO_4^{2-} + 4H^+$$

$$4CaCO_3 + 4H^+ \rightarrow 4Ca^{2+} + 4HCO_3^-$$

The molar ratio of calcium to sulphate is then $[Ca]/[SO_4] = 2,0$.

Analysis of the molar ratio of calcium (or calcium plus magnesium) and sulphate in the spoils water/leachate gives an indication of the local environmental conditions under which pyrite oxidation takes place. A lower molar ratio would indicate an acidic environment (low pH) and a higher molar ratio would indicate an alkaline environment (high pH).

Common minerals which typically contribute to the neutralisation of acidity include calcite ($CaCO_3$), magnesite ($MgCO_3$), dolomite ($CaMg(CO_3)_2$) and ankerite ($CaFe(CO_3)_2$).

Morin and Hutt (1994) found that feldspars are slow reacting, but can also contribute to the neutralisation of acidity. The stoichiometry of these neutralisation reactions can be complex and tend to be site specific. The rate and nature of feldspar neutralisation are dependant on several factors including type of feldspar mineral, environmental conditions (specifically pH) and acid generation.

The neutralisation reactions involving the three most common feldspars are summarised below:

- **Calcium feldspar (anorthite)at $3,5 \leq pH \leq 4,5$**

$$FeS_2 + 13/2H_2O + 15/4O_2 + ½CaAl_2Si_2O_8$$

$$\rightarrow Fe(OH)_3 + 2SO_4^{2-} + ½Ca^{2+} + Al^{3+} + H_4SiO_4$$

at $pH \geq 7,0$

$$FeS_2 + 13/2H_2O + 15/4O_2 + 2CaAl_2Si_2O_8$$

$$\rightarrow Fe(OH)_3 + 2SO_4^{2-} + 2Ca^{2+} + 4Al(OH)_3 + 4H_4SiO_4$$

- **Potassium feldspar** **at 3,5 ≤ pH ≤ 4,5**

$$FeS_2 + 15/2H_2O + 15/4O_2 + KAlSi_3O_8$$

$$\rightarrow \quad Fe(OH)_3 + 2SO_4^{2-} + K^+ + Al^{3+} + 3H_4SiO_4$$

at pH ≥ 7,0

$$FeS_2 + 15/2H_2O + 15/4O_2 + 4KAlSi_3O_8$$

$$\rightarrow \quad Fe(OH)_3 + 2SO_4^{2-} + 4K^+ + 4Al(OH)_3 + 12H_4SiO_4$$

- **Sodium feldspar (albite)** **at 3,5 ≤ pH ≤ 4,5**

$$FeS_2 + 15/2H_2O + 15/4O_2 + NaAlSi_3O_8$$

$$\rightarrow \quad Fe(OH)_3 + 2SO_4^{2-} + Na^+ + Al^{3+} + 3H_4SiO_4$$

at pH ≥ 7,0

$$FeS_2 + 15/2H_2O + 15/4O_2 + 4NaAlSi_3O_8$$

$$\rightarrow \quad Fe(OH)_3 + 2SO_4^{2-} + 4Na^+ + 4Al(OH)_3 + 12H_4SiO_4$$

The molar ratio of cations to sulphate will vary substantially, depending on the specific neutralisation reaction and the ambient pH as reflected below:

Mineral	pH approximately 4	pH approximately 7
Calcite	1,0	2,0
Calcium feldspar	0,25	1,0
Potassium feldspar	0,5	2,0
Sodium feldspar	0,5	2,0

Table 2.4(a): Molar ratio of cations to sulphate in neutralisation product water

Jaynes (1983) quoted work done by Wentzler (1977) to describe the neutralisation of acidity by carbonate minerals. The carbonate dissolution rate can be expressed as:

$$Q_{car} = -K_c[H^+] \qquad \textbf{(2.4.1)}$$

where :

Q_{car} = surficial carbonate dissolution rate (mole/cm^2/sec)

K_c = rate constant

= $2,9 \times 10^{-6}$ ℓ/cm^2/sec

If one assumes the carbonate mineral particles to be spherical and dispersed in the spoils environment, the carbonate dissolution (per particle) can be expressed as:

$$\frac{dX_c}{dt} = \frac{3\,X_c^{\frac{1}{3}}\,K_c[H^+]}{\rho_c . r_s} \qquad \textbf{(2.4.2)}$$

where :

X_c = fraction of remaining carbonate

ρ_c = particle carbonate density (mole/m^3)

r_s = particle radius (m)

The neutralisation rate per unit spoils volume can then be based on the particle dissolution rate and the particle density per unit spoils volume.

Jaynes (1983) used an empirical model to estimate the neutralisation capacity of gangue material in stabilising the spoils pH, refer to **Figure 2.4(a)**. The gangue material is assumed to include aluminosilicates and other clays. The empirical model stated that:

$$\Delta H_a = \Delta H_r\,[1 - \exp\,(G_b\,(G_a - pH))] \qquad \textbf{(2.4.3)}$$

where:

ΔH_a = actual free hydrogen ion concentration [H$^+$] increase in solution (mole/m^3)

ΔH_r = generated free hydrogen ion concentration [H$^+$] increase (mole/m^3)

G_b, G_a = empirical constants

The neutralisation of acid mine drainage by carbonate minerals can however be severely restricted due to the coating of the minerals by ferric hydroxide.

Siderite ($FeCO_3$) is also a common carbonate mineral, but does not contribute to the effective neutralisation of acid mine water. In a low pH environment, it will act as a buffering agent in accordance with the reaction:

$$FeCO_3 + 2H^+ \rightarrow Fe^{2+} + H_2CO_3 \quad (Ksp = +6.0)$$

Additional acidity may in fact be generated when the ferrous iron is oxidised to ferric iron, and the ferric iron precipitates as a hydroxide.

Dilution of acid mine drainage (AMD) with water containing dissolved carbonate species, such as bicarbonate, is also an approach to achieve neutralisation. The resulting pH after blending of AMD and water can be estimated on the basis of the following two expressions:

$$[H^+]_f = [H^+]\,D - [HCO_3^-]\,(1-D) \qquad \textbf{(2.4.4)}$$

for $[H^+]_f > [HCO_3^-]_f$

$$[H^+]_f = 10^{-11.37}/([HCO_3^-]\,(1-D) - [H^+]D) \qquad \textbf{(2.4.5)}$$

for $[H^+]_f \leq [HCO_3^-]_f$

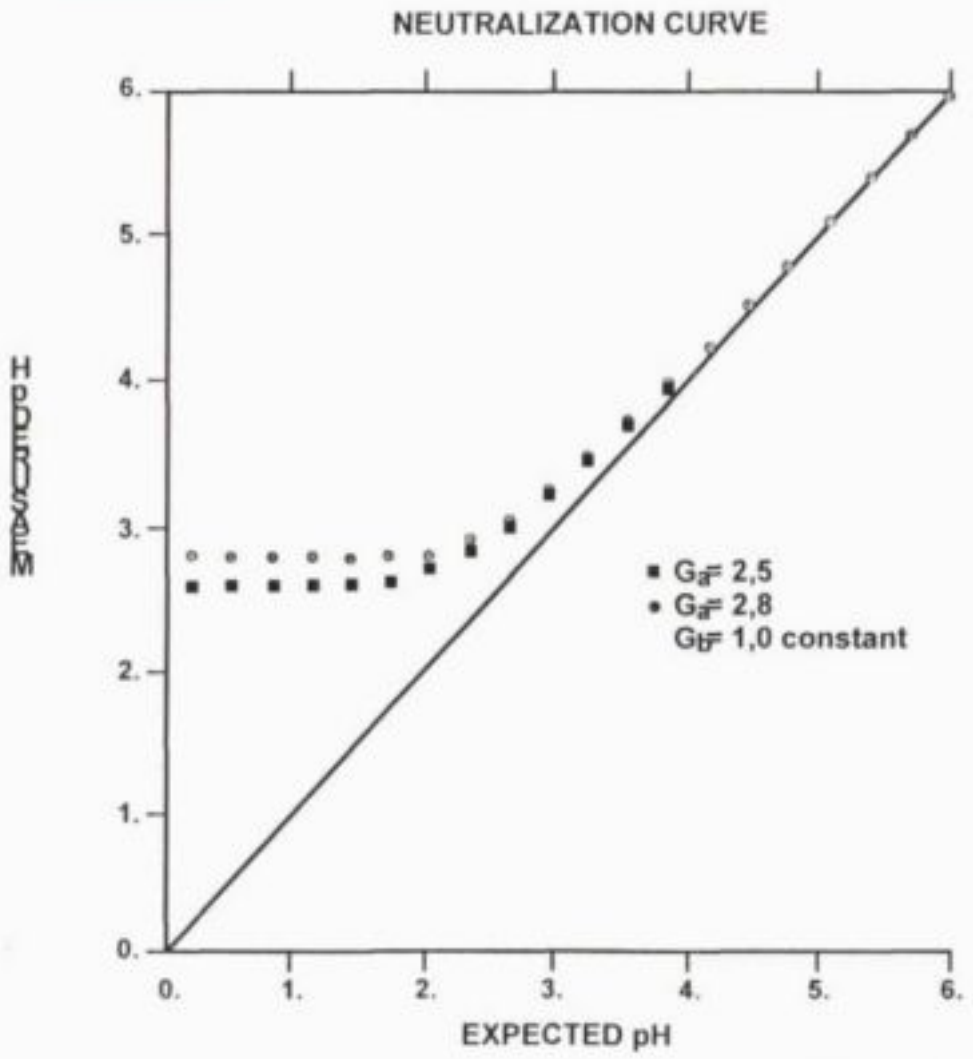

FIGURE 2.4 (a) : JAYNES EMPIRICAL MODEL FOR SPOILS NEUTRALISATION

where :

$[H^+]_f$ = final hydrogen ion concentration (mole/ℓ)

$[H^+]_i$ = initial hydrogen ion concentration (mole/ℓ)

$[HCO_3^-]_i$ = initial bicarbonate concentration (mole/ℓ)

$[HCO_3^-]_f$ = final bicarbonate concentration (mole/ℓ)

D = dilution ratio of water : AMD

There is a critical dilution, depending on the initial pH and alkalinity, beyond which the final pH of the neutralised acid mine drainage increases rapidly.

The definition of $[H^+]_i$ includes the hydrogen ion concentration as well as the equivalent acidity of dissolved metal species such as Fe^{3+}, Fe^{2+} and Al^{3+}.

$$[H^+]_i = [H^+] + 3[Fe_{tot}] + 3[Al^{3+}]$$

A number of different minerals are effective in buffering (not necessarily neutralising) the mine water system:

Mineral	Buffering in pH-range
Calcite, $CaCO_3$	5,5 - 6,9
Dolomite, $CaMg(CO_3)_2$	5,3 - 6,8
Siderite, $FeCO_3$	5,1 - 6,0
Kaolinite, $Al_2Si_2O_5(OH)_4$	3,7 - 4,3
Gibbsite, $Al(OH)_3$	3,7 - 4,3
Ferric hydroxide, $Fe(OH)_3$	3,3 - 3,7
Goethite, FeOOH	2,1 - 2,2
Jarosite, $KFe_3(SO_4)(OH)_6$	?

Table 2.4(b): Buffering minerals in spoils environment (Blowes 1983)

Kinetic humidity cell tests conducted by Ferguson and Morin (1991) on waste rock indicated that only 27% of the total available neutralisation potential (NP) was effectively utilised in neutralising the acid production taking place during pyrite oxidation.

The molar ratio of Alkalinity : (Ca + Mg) gives an indication of the nett neutralisation reaction involving calcite/dolomite. In an acidic environment:

$$CaCO_3 + 2H^+ \rightarrow Ca^{2+} + H_2CO_3$$

$$H_2CO_3 \rightleftharpoons H_2O + CO_2(g)$$

The ratio [Alk]/[Ca] = 0

In an alkaline environment:

$$2CaCO_3 + 2H^+ \rightarrow \quad 2Ca^{2+} + 2HCO_3^-$$

The ratio [Alk]/[Ca] = 1

The actual situation in a spoils environment is somewhere between these two theoretical extremes, but can be used as an indication of the environmental conditions existing at the micro-sites where pyrite oxidation occurs. The precipitation and dissolution of gypsum ($CaSO_4.2H_2O$) can however distort the theoretical ratio's of [Alk]/[Ca] and [Ca]/[SO_4]. Even if the spoils water is alkaline a significant fraction of CO_2 may be lost, which reduces the consumption of neutralising minerals such as calcite/dolomite. The true situation in a spoils environment lies between the acidic and alkaline extremes. Acidic micro-environments results in the loss of CO_2 as neutralisation takes place. In general:

- If a large excess of neutralisation capacity is present, then the [Alk]/[Ca + Mg] tends to be 1/1 (little loss of CO_2) in the alkaline environment.

- If the neutralisation capacity becomes depleted, then the [Alk]/[Ca + Mg] tends to zero due to the substantial loss of CO_2 in the predominantly acidic environment.

Morin and Hutt (1994) proposed the use of kinetic tests to assess the relative rates of pyrite oxidation and neutralisation reactions. The ABA static test results (acid production potential and neutralisation potential) are compared to the rate at which these potentials are manifested in the kinetic test (humidity cell or leach column). The flushing of a waste rock/spoils material may result in the preferential depletion of neutralising minerals, over and above the requirement for neutralisation of pyrite oxidation products.

Flushing is sensitive to the dissolution of calcite and dolomite:

$$CaCO_3(s) \rightleftharpoons Ca^{2+} + CO_3^{2-} \qquad Ksp = 8,39$$

$$CaMg(CO_3)_2(s) \rightleftharpoons Ca^{2+} + Mg^{2+} + 2CO_3^{2-} \qquad Ksp = 16,97$$

Percolating water may contain as much as 50 - 100 mg Ca/l and 60 - 120 mg $CaCO_3$/l alkalinity (in a closed system at pH 7,0 - 7,5), due to the dissolution of calcite. The alkalinity may be consumed when coming into contact with acid generating pyrite oxidation cells.

The dissolution rates of these minerals are, therefore, sensitive to the degree of saturation of the percolating spoilswater with respect to calcium, magnesium and carbonate. Dolomite dissolves at much slower rates compared to calcite. In general, the dissolution rate of calcite is dependant on:

- Magnesium content, with the highest dissolution rates obtained from rocks containing 1 - 2,5% MgO.

- Impurities such as disseminated clays delay the calcite dissolution rate.

The dissolution of calcite is pH-dependant, with very rapid dissolution at low pH values - refer to **Figure 2.4(b)** (Busenberg and Plummer, 1986).

2635-032

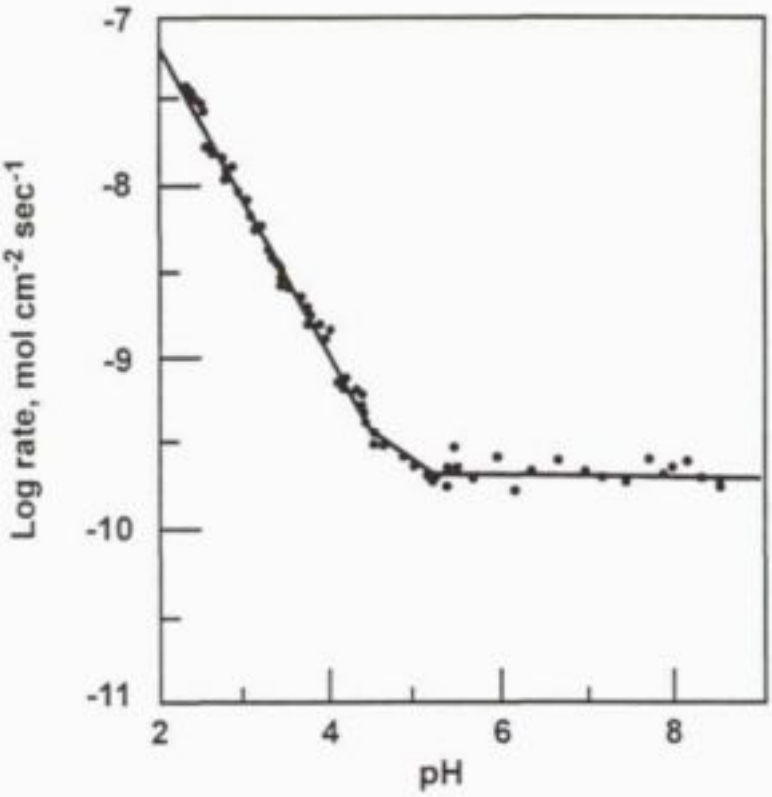

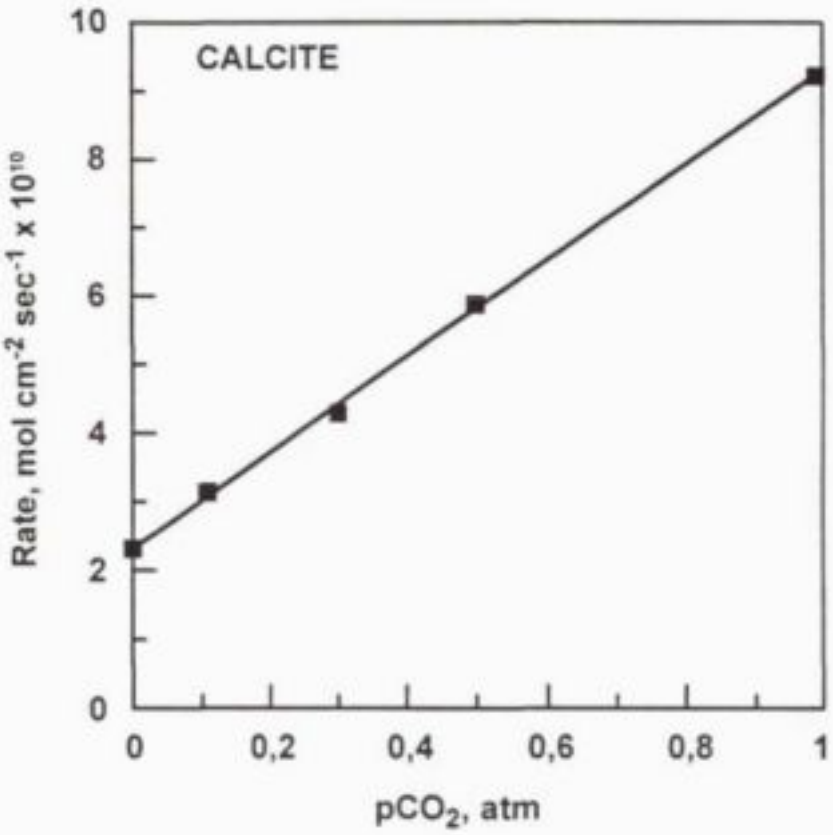

FIGURE 2.4 (b) : CALCIUM CARBONATE DISSOLUTION AS A FUNCTION OF pH AND CARBON DIOXIDE PARTIAL PRESSURE (after Busenberg and Plummer, 1986)

2.5 Aqueous phase chemistry

Spoils water prediction models typically account for the presence of the following ionic species in solution:

- Acidity, [H+] and alkalinity, [OH^-], [HCO_3^-], [CO_3^{2-}]
- Gaseous species, [O_2], [$H_2CO_3^*$], [CO_2]
- Iron, [Fe^{2+}], [Fe^{3+}]
- Major cationic species, [Ca^{2+}], [Mg^{2+}]
- Major anionic species, [SO_4^{2-}]

Some acid mine drainage prediction models also account for the initial inventory of minerals such as pyrite, calcite, dolomite, feldspars etc.

The activity of ionic species is dependant on the total ionic strength of the aqueous solution. The Davies equation is typically employed to calculate the activity coefficients:

$$\log\gamma_i = -0{,}5\, Z_i^2 \left[I^{0.5}/(1 + I^{0.5}) - 0{,}3I\right] \qquad \textbf{(2.5.1)}$$

where :

γ_i = activity coefficient

I = ionic strength

= approx $2{,}5 \times 10^{-5}$ (TDS)

TDS = total dissolved solids (mg/l)

Z_i = ionic charge

The presence of ferric iron is largely dictated by the solid phase equilibrium with amorphous ferric hydroxide and by the formation of aqueous complexes. The precipitation of ferric iron is described as follows:

$$Fe^{3+} + 3H_2O \rightarrow Fe(OH)_3\,(s) + 3H^+$$

$$\log (Ksp) = 4{,}9 = \log [Fe^{3+}]/[H^+]^3$$

The presence of **ferric iron species** is also influenced by the formation of soluble hydroxide and sulphate complexes:

$$Fe^{3+} + H_2O \rightleftarrows Fe(OH)^{2+} + H^+ \qquad \log K = -2{,}94$$

$$Fe^{3+} + 2H_2O \rightleftarrows Fe(OH)_2^+ + 2H^+ \qquad \log K = -5{,}70$$

$$2Fe^{3+} + 2H_2O \rightleftarrows Fe_2(OH)_2^{4+} + 2H^+ \qquad \log K = -5{,}22$$

$$Fe^{3+} + 3H_2O \rightleftarrows Fe(OH)_3^\circ\,(aq) + 3H^+ \qquad \log K = -12{,}0$$

$Fe^{3+} + 4H_2O$	$\rightleftarrows$	$Fe(OH)_4^- + 4H^+$	log K = -21,60
$Fe^{3+} + HSO_4^-$	$\rightleftarrows$	$Fe\,HSO_4^{2+}$	log K = 0,60
$Fe^{3+} + SO_4^{2-}$	$\rightleftarrows$	$Fe\,SO_4^+$	log K = + 3,96
$Fe^{3+} + 2SO_4^{2-}$	$\rightleftarrows$	$Fe\,(SO_4)_2^-$	log K = + 5,38
HSO_4^-	$\rightleftarrows$	$H^+ + SO_4^{2-}$	log K = -1,14
$(\alpha)FeOOH + 3H^+$	$\rightleftarrows$	$Fe^{3+} + 2H_2O$	log K = +1,55

The presence of ferrous iron species can be explained by the formation of soluble sulphate and hydroxide complexes (Cathles, 1979):

$Fe^{2+} + SO_4^{2-}$	$\rightleftarrows$	$FeSO_4^\circ$	log K = +2,20
$Fe^{2+} + HSO_4^-$	$\rightleftarrows$	$Fe\,HSO_4^+$	log K = +1,10
$Fe^{2+} + H_2O$	$\rightleftarrows$	$Fe\,O^+ + H^+$	log K = -9,48
$Fe^{2+} + 2H_2O$	$\rightleftarrows$	$Fe\,(OH)_2^\circ + 2H^+$	log K = -20,60
$Fe(OH)_2 + 2H^+$	$\rightleftarrows$	$Fe^{2+} + 2H_2O$	log K = +12,85

Ferric iron tends to form much stronger complexes with hydroxide and sulphate compared to ferrous iron. This implies that although the redox potential may indicate that Fe^{2+} should be oxidised to Fe^{3+}, the opposite may be true due to complex formation reactions.

The presence of calcium and magnesium is also influenced by complex ion formations and the solubility of gypsum:

$Mg^{2+} + SO_4^{2-}$	$\rightleftarrows$	$MgSO_4^\circ$	Ksp = +2,23
$Ca^{2+} + SO_4^{2-}$	$\rightleftarrows$	$CaSO_4^\circ$	Ksp = +2,32
$CaSO_4.2H_2O(s)$	$\rightleftarrows$	$Ca^{2+} + SO_4^{2-} + 2H_2O$	Ksp = -4,62

Furthermore, the presence of ionic species is determined by the solubility of certain solid phase forms:

$FeSO_4.7H_2O(s)$	$\rightleftarrows$	$Fe^{2+} + SO_4^{2-} + 7H_2O$	Ksp = -4,58
$\frac{1}{3}KFe_3(SO_4)_2(OH)_6(s) + 2H^+$	$\rightleftarrows$	$\frac{1}{3}K^+ + Fe^{3+} + \frac{2}{3}SO_4^{2-} + 2H_2O$	Ksp = -3,07
$\frac{1}{3}NaFe_3(SO_4)_2(OH)_6(s) + 2H^+$	$\rightleftarrows$	$\frac{1}{3}Na^+ + Fe^{3+} + \frac{2}{3}SO_4^{2-} + 2H_2O$	Ksp = -1,76

The precipitation of jarosite is important to the equilibrium aqueous chemistry, especially at low pH conditions, when ferric iron is in solution:

$$K^+ + 3Fe^{3+} + 2SO_4^{2-} + 6H_2O \rightleftarrows KFe_3(SO_4)_2(OH)_6 + 6H^+$$

There is, however, some uncertainty with respect to the solubility constants of K-jarosite and Na-jarosite.

Siderite is also likely to form in the presence of ferrous iron and carbonate alkalinity (pH ≥ 6.4). The specific siderite formation reactions include:

$$Fe^{2+} + H_2CO_3 \rightarrow FeCO_3(s) + 2H^+$$

$$Fe^{2+} + HCO_3^- \rightarrow FeCO_3(s) + H^+$$

$$Fe^{2+} + CO_3^{2-} \rightarrow FeCO_3(s) \qquad \log K = 10.4$$

The formation of siderite therefore in general releases acidity, which can further consume calcite/dolomite. The alternative postulate for the formation of siderite in the presence of calcite is a simple ion exchange reaction:

$$Fe^{2+} + CaCO_3(s) \rightarrow Ca^{2+} + FeCO_3(s)$$

This simple formation model does not release/consume acidity in the process, but obviously uses calcite which could have been used for neutralisation of acidity.

The redox potential (E_h) of acid mine water is typically determined by the ferrous/ferric iron redox couple. The Nernst equation can be used to describe the ferrous/ferric equilibrium:

$$E_h = E_o - RT/nF.\ell n([Fe^{2+}]/[Fe^{3+}]) \qquad \textbf{(2.5.2)}$$

Where:

$[Fe^{2+}],[Fe^{3+}]$	=	activities of the free ferrous/ferric ion species (mole/l)
R	=	ideal gas constant
T	=	temperature (K)
F	=	Faraday constant
n	=	number of electrons involved in the reaction (= 1)

It is not appropriate to use the total ferrous ion and total ferric ion concentrations in these calculations. Correction must be made for the complexed forms of these dissolved iron species. Ferric iron (Fe^{3+}) forms strong complexes with sulphate and hydroxide. The most common dissolved complexes include $FeSO_4^+$, $Fe(SO_4)^{2-}$, $Fe(OH)^{2+}$, $Fe_2(OH)_2^{4+}$ and $Fe(OH)_2^+$. The **free** ferric ion typically constitutes a small percentage (< 10%) of the total ferric iron in solution (Nordstrom *et al.* 1979).

Ferrous iron forms weak complexes and the only complex of significance is $FeSO_4^\circ$.

Iron precipitates which can also play a role in the equilibrium of dissolved concentrations of ionic species include:

- Melanterite $FeSO_4.7H_2O$
- Copiapite $Fe(II).Fe(III).(SO_4)_6.(OH)_2.2H_2O$

- Coquimbite $Fe_2(SO_4)_3.9H_2O$
- Jarosite $KFe_3(SO_4)_2.(OH)_6$
- Ferric hydroxide (amorphous) $Fe(OH)_3$
- Goethite FeOOH

Melanterite and copiapite (yellow) typically form where acid rock drainage is drawn to an exposed surface by capillary forces and water evaporates leaving the relatively soluble precipitates behind. Copiapite is also known to undergo ion exchange reactions with divalent and trivalent ions such as Mg^{2+}, Cu^{2+}, Zn^{2+}, Cd^{2+} and Al^{3+}. Melanterite, copiapite and coquimbite precipitates are typically only associated with extremely acidic mine water, $pH \leq 1,5$.

Jarosite (yellow) precipitation is more common in the range $1,5 \leq pH \leq 2,5$. Some uncertainty still remains with respect to the thermodynamic constants assumed for jarosite. A kinetic restriction may exist in the precipitation of jarosite. This restriction may be overcome by the presence of adequate surface area, such as bacterial/algal slimes etc.

Ferric hydroxide (amorphous) appears to control the presence of dissolved ferric iron in acid mine waters, in the pH range $2,5 \leq pH \leq 3,5$.

Iron is the fourth most common element in the earth's crust and participates in a multitude of abiotic and biotic processes. The stable equilibrium state of iron as a function of redox potential and pH is depicted in **Figure 2.5**.

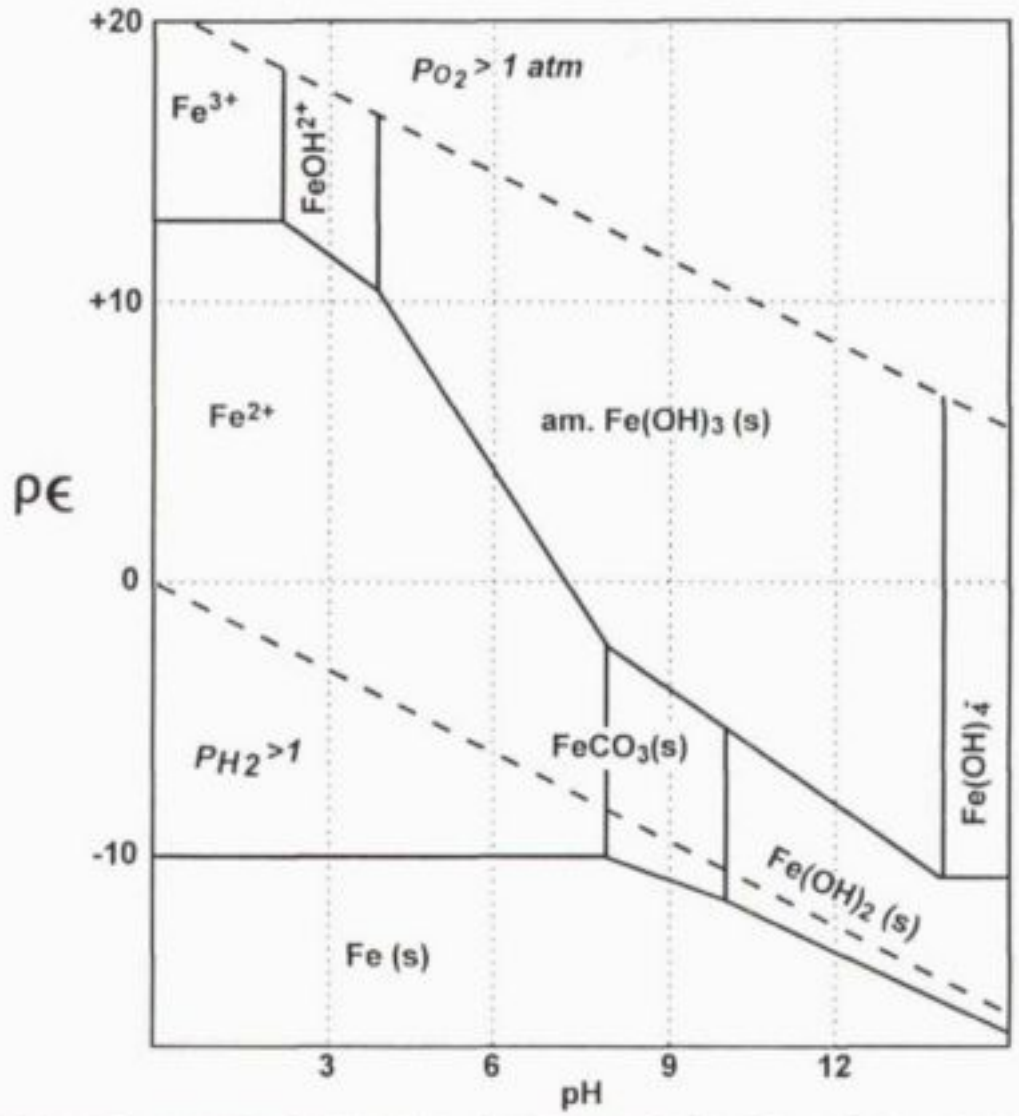

FIGURE 2.5 : EQUILIBRIUM CHEMISTRY OF IRON

Species	Formation equation Expressed in terms of components in the chemical equilibrium model	log K (I=0) (Temperature = 25°C)
Dissolved[12]		
Fe^{3+} - FREE		
$FeSO_4^+$	$Fe^{3+} + SO_4^{2-} \rightleftarrows FeSO_4^+$	4,04
$Fe(SO_4)_2^-$	$Fe^{3+} + 2SO_4^{2-} \rightleftarrows Fe(SO_4)_2^-$	5,38
$FeOH^{2+}$	$Fe^{3+} + H_2O \rightleftarrows FeOH^{2+} + H^+$	- 2,19
$Fe(OH)_2^+$	$Fe^{3+} + 2H_2O \rightleftarrows Fe(OH)_2^+ + 2H^+$	- 5,7
$Fe_2(OH)_2^{4+}$	$2Fe^{3+} + 2H_2O \rightleftarrows Fe_2(OH)_2^{4+} + 2H^+$	- 2,9
Solid		
$FePO_4.2H_2O(s)$	$Fe^{3+} + PO_4^{3-} + 2H_2O \rightleftarrows FePO_4.2H_2O(s)$	26,4
$Fe(OH)_3(s)$	$Fe^{3+} + 3H_2O \rightleftarrows Fe(OH)_3(s) + 3H^+$	- 3,2 ± 0,2
α-FeOOH(s)	$Fe^{3+} + 2H_2O \rightleftarrows$ α-FeOOH(s) $+ 3H^+$	- 3,02 ± 0,35
γ-FeOOH(s)	$Fe^{3+} + 2H_2O \rightleftarrows$ γ-FeOOH(s) $+ 3H^+$	- 0,5
α-$Fe_2O_3(s)$	$2Fe^{3+} + 3H_2O \rightleftarrows$ α-$Fe_2O_3(s) + 6H^+$	0,48 ± 0,23
$Fe(SO_4)(OH)(s)$	$Fe^{3+} + SO_4^{2-} + H_2O \rightleftarrows Fe(SO_4)OH(s) + H^+$	0,7
$KFe_3(SO_4)_2(OH)_6(s)$	$K^+ + 3Fe^{3+} + 2SO_4^{2-} + 6H_2O \rightleftarrows KFe_3(SO_4)_2(OH)_6(s) + 6H^+$	—
$Fe_3(SO_4)_2(OH)_5$	$3Fe^{3+} + 2SO_4^{2-} + 7H_2O \rightleftarrows Fe_3(SO_4)_2(OH)_5.2H_2O(s) + 5H^+$	2,7
$H_3OFe_3(SO_4)_2(OH)_6(s)$	$H_3O^+ + 3Fe^{3+} + 2SO_4^{2-} + 6H_2O \rightleftarrows H_3OFe_3(SO_4)_2(OH)_6(s) + 6H^+$	10,98
$NaFe_3(SO_4)_2(OH)_6(s)$	$Na^+ + 3Fe^{3+} + 2SO_4^{2-} + 6H_2O \rightleftarrows NaFe_3(SO_4)_2(OH)_6(s) + 6H^+$	8,92
$AgFe_3(SO_4)_2(OH)_6(s)$	$Ag^+ + 3Fe^{3+} + 2SO_4^{2-} + 6H_2O \rightleftarrows AgFe_3(SO_4)_2(OH)_6(s) + 6H^+$	13,78
$PbFe_6(SO_4)_4(OH)_{12}(s)$	$Pb^{2+} + 5Fe^{3+} + 4SO_4^{2-} + 12H_2O \rightleftarrows PbFe_6(SO_4)_4(OH)_{12}(s) + 12H^+$	27,36

Table 2.5 : Equilibrium equations for principal iron species (Smith et al (1988))

Smith *et al.* (1988) conducted research into the bacterial oxidation of ferrous iron by *Thiobacillus ferro-oxidans*. Experiments were conducted in the pH range 1,8 - 2,1. In this pH range the dominant dissolved ferrous and ferric iron species were Fe^{2+}, $FeSO_4^{\circ}$, Fe^{3+}, $FeSO_4^{+}$ and $Fe(SO_4)_2^{-}$. Ferric iron precipitated as the hydroxide when the pH increased above pH 2,0 → 2,5. The principle iron species were computed on the basis of a chemical equilibrium model which incorporated the equations listed in **Table 2.5**.

2.6 Microbial action

Two bacterial species are known to accelerate the pyrite oxidation process; *Thiobacillus ferro-oxidans* and *Thiobacillus thio-oxidans*. These autotrophic bacteria are sensitive to temperature, with an optimum temperature of about 30°C. Virtually no bacterial action takes place below 4°C and above 55°C.

Bacterial catalysis can substantially accelerate the pyrite oxidation process. Singer and Stumm (1970) indicated that the ferrous iron oxidation rate (considered to be the rate limiting reaction in the overall pyrite oxidation process) can be accelerated by six orders of magnitude in the presence of bacteria.

The microbial catalysis of the pyrite oxidation process is also sensitive to pH, with an optimum range of $2,5 \leq pH \leq 4,0$. Scharer *et al.* (1991) used the following biotic pyrite oxidation rate to account for the pH sensitivity:

$$K = B.\exp(-E_a/RT)/(1 + 10^{2.5-pH} + 10^{pH-4}) \qquad \textbf{(2.6.1)}$$

B = biotic scaling factor, typically 16-35

The United States Bureau of Mines is currently developing a predictive model of acid mine drainage from waste rock and spoils dumps. The bacterial catalysis of the pyrite oxidation process is modelled by an evaluation of the viable bacterial density. A modified Monod-type expression is used with allowance for bacterial growth and death as a function of the limiting substrate $[Fe^{2+}]$ concentration and pH.

$$\frac{dX}{dt} = \mu_m X[[H^+]/(K_h+[H^+])].[[Fe^{2+}]/(K_f+[Fe^{2+}])]-K_d X^2 \qquad \textbf{(2.6.2)}$$

where:

X = viable bacterial mass (mg/l)

μ_m = maximum growth rate (approximately 0,1/hour)

K_h = half saturated constant with respect to hydrogen ion $[H^+]$ concentration
= 0,1 mmol/l = 0,1 mg/l

K_f = half saturated constant with respect to ferrous iron $[Fe^{2+}]$ concentration
= 2,0 mmol/l = 110 mg Fe/l

K_d = bacterial decay rate
= 0,005 mmol/l/hour

The autotrophic bacterial growth using oxidation of ferrous iron as energy source, typically yields 0,4 mg bacterial mass/mmole iron oxidised, which is equivalent to 7 mg/g Fe^{2+}.

Bacterial catalysis however requires favourable environmental conditions for metabolism. *Thiobacillus ferro-oxidous* is sensitive to at least the following three environmental conditions:

- **Temperature**

  The bacterial species is mesophyllic, with an optimum temperature in the range of 25 - 35°C. The inhibition of bacterial action under sub-optimal temperatures can be described by the equation:

  $$X_T = -1{,}25 \times 10^{-5} T^3 - 4{,}4 \times 10^{-4} T^2 + 0{,}066\ T - 0{,}25 \quad \textbf{(2.6.3)}$$

  for $4°C \leq T \leq 55°C$

  where:

  X_T = proportion of maximum metabolic rate

  T = temperature (°C)

- **pH**

  Thiobacillus ferro-oxidans is also sensitive to pH. At low pH, cell activity decreases, probably due to acid attack of the cell membrane. High pH, on the other hand, also results in decreased efficiency of metabolic processes. The pH dependance can be described by the following equation:

  $$X_{pH} = -0{,}35\ pH^2 + 2{,}3\ pH - 2{,}7 \quad \textbf{(2.6.4)}$$

  for $1{,}54 \leq pH \leq 4{,}95$

  X_{pH} = proportion of maximum metabolic rate

- **Dissolved oxygen**

  Thiobacillus ferro-oxidans can survive at low oxygen concentrations, but requires oxygen as an electron acceptor for ferrous iron oxidation. The influence of oxygen on the metabolic rate is expressed by the following equations:

  $$X_o = 1{,}0 \quad \text{for } Y_o > 0{,}01 \text{ atm} \quad \textbf{(2.6.5)}$$

  $$X_o = Y_o/0{,}01 \quad \text{for } Y_o < 0{,}01 \text{ atm} \quad \textbf{(2.6.6)}$$

  where:

  X_o = proportion of maximum metabolic rate

  Y_o = oxygen partial pressure (or dissolved oxygen concentration) in atm.

Tests conducted by Scharer *et al.* (1991) indicated that *Thiobacillus ferro-oxidans* did not actively grow at a temperature less than 6°C, with healty growth at 21°C. The Arrhenius activated energy for bacterial pyrite oxidation was found to be E_a = 25,6 kcal/mole (doubling for every 10°C temperature rise).

2.7 Oxygen migration in the spoils environment

The presence of oxygen is important to sustain the pyrite oxidation process. Oxygen is an essential reagent in all the pyrite oxidation process reactions, including the further oxidation of products such as ferrous iron. No thermodynamically favourable mechanism, which does not involve oxygen, has been identified for the natural oxidation of pyrite.

An inverse relationship is frequently observed between oxygen (O_2) concentration and carbon dioxide (CO_2) concentration in the spoils environment. The consumption of oxygen in the spoils environment may be be attributed to:

- pyrite oxidation processes
- soil bacterial respiration

The production of CO_2 can be attributed to the same two processes. The neutralisation of acidity by carbonate minerals may also produce carbon dioxide. The generalised neutralisation reaction involving calcite demonstrates this generation mechanism:

$$FeS_2 + 2CaCO_3 + 3¾O_2 + 1,5H_2O$$

$$\rightarrow \quad Fe(OH)_3 + 2SO_4^{2-} + 2Ca^{2+} + 2CO_2(g)$$

The relationship between the oxygen consumption and the corresponding carbon dioxide production depends on the environmental conditions in the spoils environment:

- In an acidic environment (pH < 4,0), with some carbonate mineral (M - CO_3) present, then:

$$FeS_2 + 3½O_2 + H_2O \rightarrow Fe^{2+} + 2SO_4^{2-} + 2H^+$$

$$M\text{-}CO_3 + 2H^+ \rightarrow M^{2+} + H_2CO_3(aq)$$

  In an acidic environment, the carbonic acid would be virtually completely undissociated (in the H_2CO_3 form) and the equilibrium between H_2CO_3(aq) and CO_2(g) would be governed by Henry's Law. In the extreme case where all H_2CO_3(aq) is exsolved, the molar ratio between CO_2 generation and O_2 consumption is then 1/3,5 = 0,29.

- In a mildly acidic environment (pH ≥ 4,0) the oxidation of ferrous iron and the subsequent precipitation of ferric iron would consume further oxygen and generate further acidity:

$$Fe^{2+} + ¼O_2 + 2,5H_2O \rightarrow Fe(OH)_3 + 2H^+$$

$$M\text{-}CO_3 + 2H^+ \rightarrow M^{2+} + H_2CO_3(aq)$$

In the extreme case, where all $H_2CO_3(aq)$ is exsolved, the molar ratio between CO_2 generated and O_2 consumptiion is then 2/3,75 = 0,53.

- In an alkaline environment, the acidity generated by the pyrite oxidation process would also be neutralised by carbonate minerals. The carbonic acid would however dissociate to form soluble bicarbonate and carbonate species. Very little CO_2 would be exsolved and no specific molar ratio between CO_2 generation and O_2 consumption would exist.

Jaynes (1983) reported an experimentally observed molar ratio of CO_2 generated : O_2 consumption of 0,30. This would indicate that acidic conditions existed in the micro-environment in which these reactions are taking place.

2.7.1 Diffusion Processes

The expression for diffusional mass transfer of a gas in one dimension can be expressed as:

$$N_i = \frac{-D_f P}{RT} \cdot \frac{dY_i}{dZ} \qquad \textbf{(2.7.1.1)}$$

where:

N_i = molar flux (mole/m^2/sec)

D_{fi} = diffusion coefficient (m^2/sec)

P = total gas pressure (atm)

R = Universal gas constant (8,31 kPa.cm^3/mole/K)

T = absolute temperature (K)

Y_i = mole fraction of component i (mole/mole)

Z = dimension (m)

In the spoils environment, the one dimensional gas diffusion expression has to be adjusted for the porosity, Θa (air-filled porosity) and for the tortuosity, ζ, of the spoils:

$$N_i = \frac{\Theta a\, D_f\, P}{\zeta \cdot R.T} \cdot \frac{dY_i}{dZ} \qquad \textbf{(2.7.1.2)}$$

The following numerical values are commonly used for air-filled porosity and tortuosity:

	Air-filled porosity (Θa)	**Tortuosity (ζ)**
Coarse spoils	0,12	5
Fine spoils	0,06	10

The air-filled porosity is sensitive to the moisture content of the spoils.

Three gaseous species of significance are typically present in the spoils environment : nitrogen (N_2), oxygen (O_2) and carbon dioxide (CO_2). This is particularly relevant in an acidic spoils environment where some CO_2 is exsolved during the calcite/dolomite dissolution processes. The gas diffusion coefficient is however sensitive to gas composition, relative gas flux rates, temperature and pressure. In a quasi-steady state situation, it can be assumed that nitrogen is a stagnant gas with mainly oxygen and carbon dioxide as mobile gases. The generalised equation for diffusional mass transfer is then:

$$N_{O2} = \frac{-D_{f\,O2}P}{RT} \cdot \frac{dY_{O2}}{dZ} \qquad \textbf{(2.7.1.3)}$$

$$N_{CO2} = \frac{-D_{f\,CO2}P}{RT} \cdot \frac{dY_{O2}}{dZ} \qquad \textbf{(2.7.1.4)}$$

where:

$$D_{f\,O2} = \frac{D_{O2,CO2} \cdot D_{O2,N2}}{D_{O2,N2} \cdot Y_{CO2} + D_{O2,CO2} \cdot Y_{N2} + R_{CO2,O2} \cdot D_{O2,N2} \cdot Y_{O2}}$$

$$D_{f\,CO2} = \frac{D_{O2,CO2} \cdot D_{CO2,N2}}{D_{CO2,N2} \cdot Y_{O2} + D_{O2,CO2} \cdot Y_{N2} + D_{CO2,N2} \cdot Y_{CO2} / R_{CO2,O2}}$$

and;

N_{O2} = molar flux of oxygen (mole/m^2/sec)

N_{CO2} = molar flux of carbon dioxide (mole/m^2/sec)

$D_{f\,O2}$ = effective diffusion coefficient of oxygen (m^2/sec)

$D_{f\,CO2}$ = effective diffusion coefficient of carbon dioxide (m^2/sec)

Y_{O2} = molar concentration of oxygen (mole/mole)

Y_{CO2} = molar concentration of carbon dioxide (mole/mole)

$D_{O2,CO2}$ = diffusion coefficient for oxygen-nitrogen gas pair (m^2/sec)

$D_{CO2,N2}$ = diffusion coefficient for carbon dioxide nitrogen gas pair (m^2/sec)

and

$R_{CO2,O2}$ = N_{CO2}/N_{O2}

The effective diffusion coefficient for oxygen in a nitrogen-oxygen-carbon dioxide system is shown in **Figure 2.7.1** as a function of gas composition and relative gas flux rates.

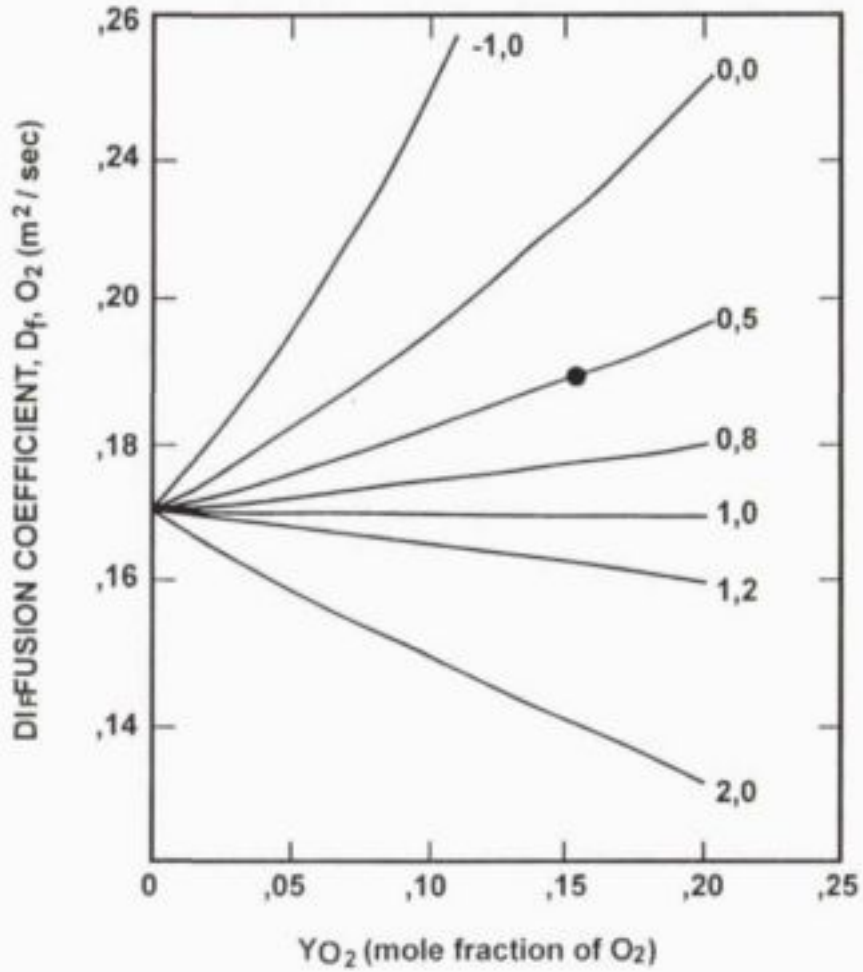

- Nitrogen - oxygen - carbon dioxide system
- N_2 mole fraction = 0,79
- Environment, 20°C, 101 kPa
- Curves show different values of the flux ratio R202.02 = N_C0_2 / $N0_2$

FIGURE 2.7.1 :VARIATION OF THE FICKIAN DIFFUSION COEFFICIENT OF OXYGEN

The diffusion coefficients for the gas pairs of interest are summarised hereunder at 20°C (293K) and standard pressure (101 kPa):

Gas pair	D (m^2/sec)
• oxygen-nitrogen	$2,02 \times 10^{-5}$
• carbon dioxide-nitrogen	$1,59 \times 10^{-5}$
• oxygen-carbon dioxide	$1,59 \times 10^{-5}$

Significant deviations from the simple binary gas diffusion behaviour are, therefore, possible in a complex multiple-gas environment.

If the **spoils environment** is **not acidic**, then the situation can be simulated as a binary gas system consisting of two components, nitrogen (N_2) and oxygen (O_2).

The general diffusion equation for a two component gas system is:

$$N_i = \frac{-D_{ij}}{1-(1-R_j)Y_i} \cdot \frac{P}{RT} \cdot \frac{dY_i}{dz} \quad \textbf{(2.7.1.5)}$$

where:

$i = O_2$ and $j = N_2$

If we further assume the atmospheric pressure to be constant, then $N_i = -N_j$ and $R_j = N_j/N_i = 1$, and

$$N_{O2} = -D_{O2,N2} \cdot \frac{P}{RT} \cdot \frac{dY_{O2}}{dz} \quad \textbf{(2.7.1.6)}$$

where:

N_{O2} = molar oxygen flux (mole O_2/m^2/sec)

$D_{O2,N2}$ = binary diffusion coefficient (m^2/sec)

The rehabilitation covers of spoils bodies typically contain active plant growth with associated soil microbial activity. The microbial respiration rates in the soil surface layers vary substantially. Jaynes (1983) employed the following range of soil cover respiration rates in his model:

$1,2 \times 10^{-12} - 12 \times 10^{-12}$ mole/cm^3/sec

Bennett and Ritchie (1991) derived the internal oxygen consumption rate from oxygen concentration profiles in waste rock dumps at the Aitik Mine in northern Sweden. The average oxygen consumption rate was 0,32 kg/m^3/year (0,34 kg FeS_2/m^3/year), assuming that oxidation of one mole pyrite, consumes the equivalent of 3,5 moles O_2 in an acidic environment. It would, therefore, take approximately 50 years, with no restriction to the oxygen supply into the interior of the waste rock dumps to exhaust the pyrite.

The migration of oxygen in unsaturated porous media may take place in a number of ways. These mechanisms of migration may be broadly classified into:

- Oxygen transport via the water infiltration into the porous media.
- Barometric pumping occuring due to fluctuations in atmospheric pressure. Atmospheric pressure changes are seldom more than 5 - 10%. In accordance with the ideal gas laws, movement of atmospheric constituents due to barometric pumping would typically be less than 50 - 100 mm per metre depth of porous media.
- Convective transport of oxygen under conditions created by, for example, burning spoils.
- Successive cycles of wetting and drying can also act as a mechanism for the transport of oxygen into a body of porous spoils. Wetting results in the displacement of air contained in the porous media. Drying results in ingress of air from the surrounding atmosphere into the porous spoils. These successive cycles occur over a long time scale, compared to the other oxygen transport mechanisms.
- Advective transport of oxygen may also take place depending on several factors including wind patterns, geometry of the spoil/discard dump, local topography, grading within the dump and the effect of coal burning on or within the spoils body.

Diffusion is considered to be the main transport mechanism supplying the oxygen required for the pyrite oxidation processes to the interior of opencast mine spoils bodies. Spoils material characteristics do not typically allow the advective movement of air through the spoils, except in situations where an uncovered spoils body is exposed to strong wind action. Placement of the spoils back into the preceding mining cuts is therefore not conducive to advective air movement through the spoils. Barometric "pumping" can only effectively aerate the outer surface of a spoils body, within the constraints of the typical variation in barometric pressure in the South African interior.

2.7.2 Oxygen consumption

Oxygen consumption within spoils can mainly be attributed to three processes:

- pyrite oxidation
- ferrous iron oxidation
- respiration by bacterial and other microscopic life forms

The oxygen consumption due to pyrite oxidation can be expressed as:

$$Q_{py} = -R_{py} \cdot F_{py} \cdot \rho_b / b \qquad \textbf{(2.7.2.1)}$$

where:

Q_{py} = oxygen consumption (mole/m^3/sec or kg/m^3/sec)

R_{py} = pyrite oxidation rate, usually expressed on a fractional basis (mole/mole/sec or kg/kg/sec)

$F_{\rho y}$ = pyrite content of spoils (kg/kg)

ρ_b = bulk density of spoils (kg/m^3)

ρ = stoichiometric ratio of mole pyrite oxidised per mole oxygen utilised (mole FeS_2/mole O_2) = 1/3,5 = 0,2857 mole FeS_2/mole O_2.

The oxygen consumption due to oxidation of ferrous iron can be expressed as:

$$Q_{Fe} = -R_{Fe}/b$$

where:

Q_{Fe} = oxygen consumption (mole/m^3/sec or kg/m^3/sec)

R_{Fe} = ferrous iron oxidation rate (mole/m^3/sec or kg/m^3/sec)

b = stoichiometric ratio of mole Fe^{2+} oxidised per mole O_2 utilised (mole Fe^{2+}/mole O_2) = 1/0,25 = 4 mole Fe^{2+}/mole O_2
= 6,975 kg Fe^{2+}/kg O_2

2.7.3 Oxygen diffusion modelling

Ritchie (1977) developed a mathematical model to simulate the oxygen diffusion into a homogenous waste rock/spoils body. The model assumes that oxygen (O_2) is the rate-limiting reactant in the oxidation of pyrite. The pyrite oxidation rate is, therefore, governed by the rate at which oxygen can be transported from the atmosphere to the internal reaction sites within the dump. Ritchie assumed that oxygen was transported by a diffusional process. The model was developed for a relatively flat, semi-infinite body of spoils, with the top face exposed to the atmosphere. A planar moving boundary formulation was adopted with a moving reaction front located between the top surface of the dump and the base of the dump. The region above the moving reaction front was assumed to be fully oxidised, while the region below the moving reaction front was unoxidised, refer to **Figure 2.7.3(a)**.

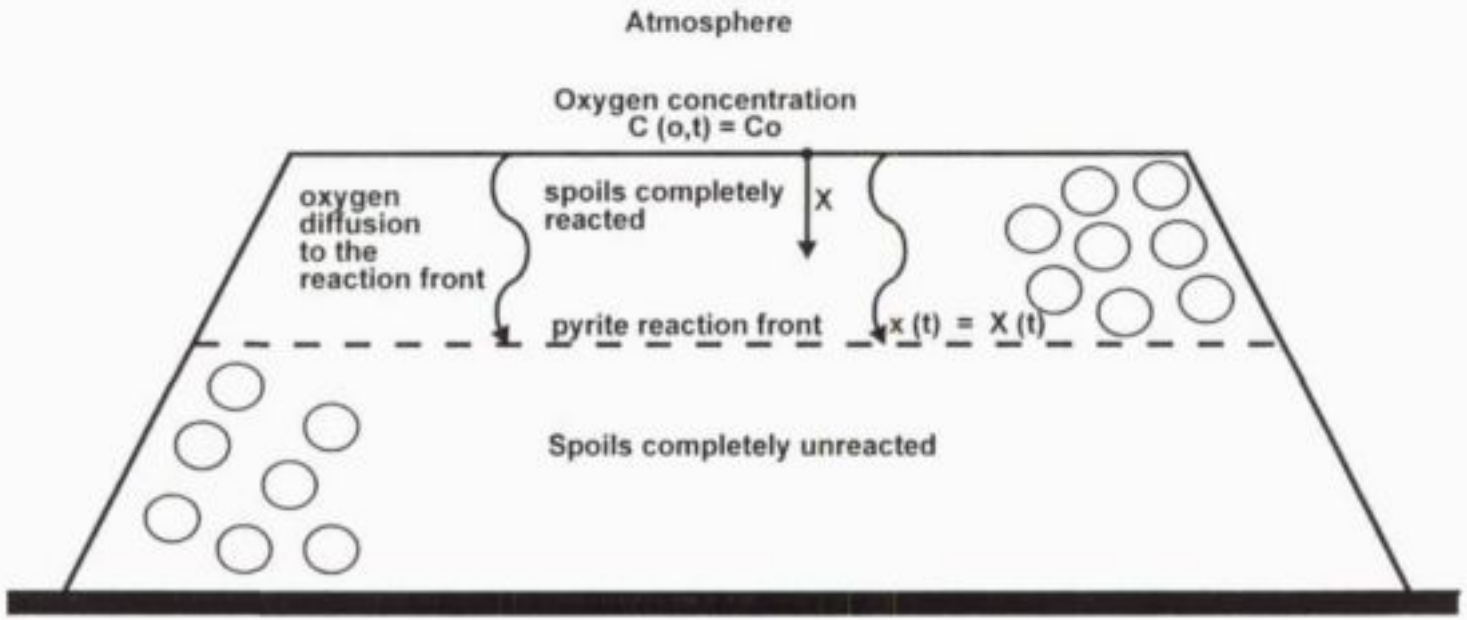

FIGURE 2.7.3(a) : SCHEMATIC PRESENTATION OF THE RITCHIE PYRITE OXIDATION MODEL

The diffusion equation governing the migration of oxygen is:

$$\Theta_a \frac{dC}{dt} = D_{to2} \frac{\partial^2 C}{\delta x^2} \qquad \textbf{(2.7.3.1)}$$

where:

Θ_a = dump air porosity (m^3/m^3)

C = oxygen concentration (mg/m^3)

D_{to2} = effective oxygen diffusion coefficient (m^2/sec)

x = distance into dump (m)

X = position of reaction front in dump (m)

The boundary conditions can be stated as follows:

C(x=0) = Co

C(x=X) = 0

The position of the reaction front can be described by the following expression:

$$D_{to2} \frac{\partial C}{dx}(x = X) = -E.\rho_s .dX/dt \qquad \textbf{(2.7.3.2)}$$

where:

E = mass of oxygen consumed per unit mass of pyrite oxidised (kg O_2/kgFeS_2)

ρ_s = pyrite content of dump (kg FeS_2/m^3)

The oxygen concentration at any position and time in the spoils dump is:

$$C(x,t) = C_o[1 - erf[x/2(D.t)^{½}]/erf(\alpha) \qquad \textbf{(2.7.3.3)}$$

where $D = D_{to2}/\Theta_a$

The model paramenter α is found from the transcendental equation:

$$(\pi\alpha)^{½}.\exp(\alpha^2).erf(\alpha) = \Theta_a C/(E.\rho_s) \qquad \textbf{(2.7.3.4)}$$

The position of the reaction front at any point in time is then:

$$X(t) = 2.\alpha (D.t)^{½} \qquad \textbf{(2.7.3.5)}$$

Davis and Ritchie (1986) developed a two-stage oxygen diffusion model to simulate pyrite oxidation in waste rock/spoils dumps (refer to **Figure 2.7.3(b)**). The first stage consisted of oxygen diffusion from the atmosphere through the pore space to the individual reacting particles located in the dump. The second stage consisted of oxygen diffusion within the reacting particles. The model was based on a number of assumptions:

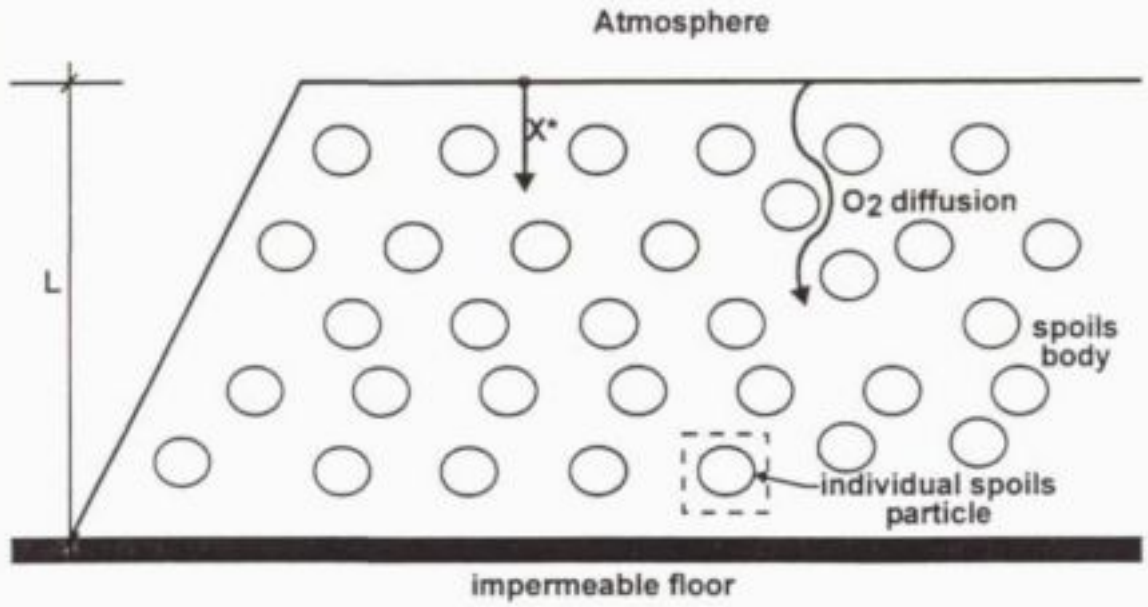

MACROSCOPIC SPOILS DUMP MODEL

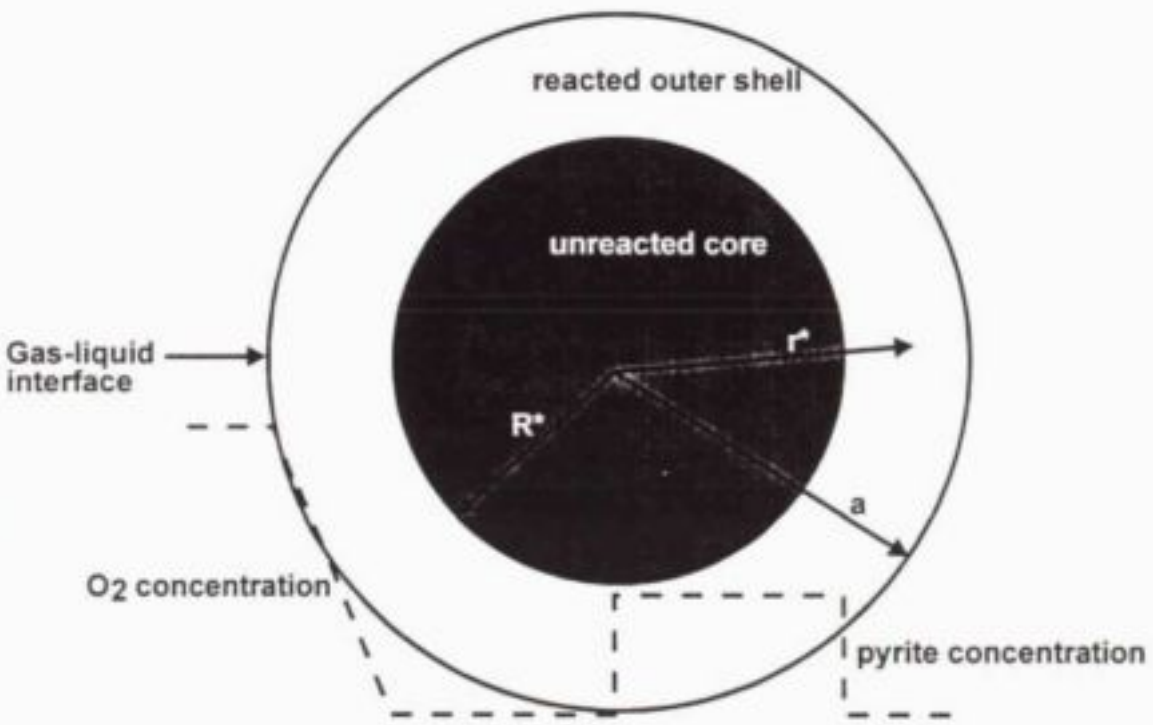

MACROSCOPIC SPOILS PARTICLE MODEL

FIGURE 2.7.3(b) : SCHEMATIC PRESENTATION OF DAVIS AND RITCHIE SPOILS OXIDATION MODEL

- All reactants in the pyrite oxidation process are available, with only oxygen as the rate-limiting reactant.
- The pyrite oxidation rate is much faster than the rate at which oxygen can be supplied to the reaction sites.
- Oxygen mass transfer is driven by concentration gradients in the dump pore space and within the individual particles.
- Pyrite is evenly disseminated throughout the waste rock/spoils particles, which results in a shrinking core formulation of the pyrite oxidation process within each particle.

The expressions governing the mass transfer of oxygen in the dump pore space are summarised hereunder:

$$\Theta_a \frac{dC}{dt^*} = D_1 \frac{\partial^2 C}{dx^{*2}} - Q \qquad \text{for} \quad 0 \le x \le L \qquad \textbf{(2.7.3.6)}$$

with boundary conditions

$$C(x^* = O) = C_o$$

$$\frac{dC}{dx^*}(x^* = L) = O$$

$$C(t^* = 0) = O$$

where

Θ_a = air-filled porosity (m^3/m^3)

C = oxygen concentration in pore space (mg/m^3)

D_1 = effective oxygen diffusion coefficient in pore space (m^2/sec)

x^* = distance into dump (m)

t^* = time (sec)

L = depth of dump (m)

Q = oxygen consumption rate ($kgO_2/m^3/sec$)

The oxygen consumption rate can be computed on the basis of the number of reacting particles per unit volume.

$$Q = \upsilon . D_2 . 4\pi a^2 \frac{\partial K}{\partial r^*}(r^* = a) \qquad \textbf{(2.7.3.7)}$$

where:

υ = number of spherical particles per unit volume
= $3(1-\Theta_a) / 4\pi a^3$

D_2 = effective oxygen diffusion coefficient into particle (m^2/sec)

a = spherical particle radius (m)

K = oxygen concentration in particle (mg/m^3)

Thus $Q = 3(1-\Theta_a) D_2 a \cdot \frac{\partial K}{\partial r^*} (r^* = a)$ **(2.7.3.8)**

The expressions governing the mass transfer of oxygen within the reacting particles can be summarised as follows:

$$\frac{\partial K}{\partial t^*} = D_2 \cdot \frac{\partial^2 K}{\partial r^{*2}} + \frac{2D_2 \partial K}{r^* \partial r^*} \quad \textbf{(2.7.3.9)}$$

for $R < r^* < a$

with R = radial position of reacting surface (m)

The boundary conditions relevant to a specific reacting particle can be stated as:

$K(r^* = R) = 0$ and $K(r^* = R) = \gamma C$ **(2.7.3.10)**

$$\frac{E\rho_s \cdot \partial R}{(1-\Theta_p)\partial t^*} = \frac{D_2 \partial K}{\partial r^*}$$

where:

E = mass of oxygen consumed per unit mass of sulphur oxidised (kgO_2/kgS)

ρ_s = sulphur density in particle (kgS/m^3)

Θ_p = particle porosity (m^3/m^3)

γ = Henry's Law constant

The oxygen concentration in the pore space (C) and the oxygen concentration at the particle surface can be related using Henry's Law:

$C = \gamma . K(r = a)$ **(2.7.3.11)**

where:

γ = Henry's Law constant

Davis (1983) developed **approximate solutions** to obtain the oxygen concentrations in the pore space of the dump as a function of time and position. The **upper bound approximate solutions** to the dimensionless oxygen concentration profile in the dump depends on the location of the planar moving front, behind which the particles are totally reacted. The position of the planar front, X, can be solved from the trancendental equation:

$$t = tc + X^2/2 + tc\sqrt{\beta} \, . \, X \, . \, \tanh [\sqrt{\beta}.(1-X)] \qquad \textbf{(2.7.3.12)}$$

where:

$$tc = 1/(6k)$$

$$\beta = 6k$$

$$k = \gamma(1-\Theta_s) \, D_2/D_1(L/a)^2$$

The upper bound solutions for the oxygen concentrations, $t \geq tc$, can be summarised:

- $0 \leq x \leq X(t)$

$$u(x, t) = 1 - x/X[t - tc - X^2/2]/[t - X^2/2] \qquad \textbf{(2.7.3.13)}$$

- $X(t) \leq x \leq 1$

$$u(x, t) = [tc.\text{Cosh}\sqrt{\beta}.(1-x)] \, / \, [(t - X^2/2) \, \text{Cosh}\sqrt{\beta}.(1-X)] \qquad \textbf{(2.7.3.14)}$$

The dimensionless expressions are based on the following transformations:

$$u = C/C_o \qquad \_ = K/\gamma C_o$$

$$x = x^*/L \qquad r = r^*/a$$

$$R = R^*/a$$

In most cases, the model parameter, β is large and the approximate analytic solutions can be further simplified:

$$\beta = 6k = t\gamma.D_2(1-\Theta_a)L^2/D_1a^2 \qquad \textbf{(2.7.3.15)}$$

The oxygen concentration profiles then become:

$$u(x,t) = 1 - (\sqrt{\beta} \, . \, X) \, / \, (1 + \sqrt{\beta} \, . \, X) \quad \text{for } 0 \leq x \leq X(t)$$

$$u(x,t) = \exp[-\sqrt{\beta}(x - X)]/[1 + \sqrt{\beta}.X] \quad \text{for } X(t) \leq x \leq 1$$

In the region above the moving planar front, the oxygen concentration decreases linearly with distance from the top of the waste/spoils dump surface. The dimensionless oxygen concentration is equal to:

$$u(x,t) = 1 - (\sqrt{\beta} \, . \, X) \, / \, (1 - \sqrt{\beta} \, . \, X) \text{ at the planar front} \qquad \textbf{(2.7.3.16)}$$

$$= 1 - 1/[1 + (\sqrt{\beta}X)^{-1}]$$

The oxygen concentration decreases exponentially below the planar moving front.

The sulphate production rate in the waste/spoils body can be expressed as:

$$S(t) = L.\partial_s.\rho_s/\zeta_{sl} \cdot 1/(2t\text{-}tc)^{1/2} \quad \textbf{(2.7.3.17)}$$

where:

$S(t)$ = sulphate production ($kgSO_4/m^2/sec$)

∂_s = sulphate production per mass of sulphur oxidised ($kgSO_4/kgS$)

ρ_s = sulphur density in dump

ζ_{sl} = $L^2E.\rho_s/(D_1u_o)$

E = mass of oxygen consumed per unit mass of sulphur oxidised (kgO_2/kgS)

The Davis model has been calibrated on highly reactive waste rock/spoils dumps, containing readily oxidizable pyrite. The dumps were all highly acidic and produced an estimated sulphate load of 60 $tonSO_4/ha/a$. This is approximately one order of magnitude higher than the typical sulphate production rates observed in opencast spoils bodies on the Eastern Transvaal Highveld coalfields.

The model assumes that pyrite oxidation products do not accumulate within the waste rock/spoils body. The pyrite oxidation is also assumed to be restricted to the primary oxidation reaction, yielding ferrous iron and sulphate. It is clear that the model does not recognise factors which could restrict the rate at which pyrite oxidation products are mobilised from a waste rock/spoils dump such as precipitation, neutralisation, and flushing. The variability of the geochemical properties of waste rock and spoils is also not reflected in the model.

Yanful (1991) investigated the diffusion of oxygen into fine-grained tailings material. The effective diffusion coefficient was again expressed as:

$$D_3 = \frac{\Theta_a D_2}{\zeta}$$

where:

Θ_a = air-filled porosity

ζ = tortuosity (= 5 for spoils)

The oxygen diffusion coefficients:

- water = $2 \times 10^{-5}\ cm^2/sec$
- air = $0{,}178\ cm^2/sec$

The effective diffusion coefficient therefore decreases rapidly beyond a spoils moisture content of 70 - 80%.

3. HYDROLOGICAL ASPECTS OF MODELLING OPENCAST MINE WATER SYSTEMS

The nature of open-pit mining operations implies that the original drainage areas are undisturbed by nature, with only a small percentage of impervious areas. The catchment characteristics will, however, change extensively as mining progresses, resulting in progressive disturbance of the natural surfaces. Drainage on a mining complex can take place from the following types of surfaces:

- original pre-mined surface,
- pit slopes,
- pit floor,
- access ramps,
- overburden spoil heaps,
- levelled and profiled spoils,
- levelled, topsoiled and vegetated spoils,
- access roads,
- cultivated lands.

Each of these surfaces will exhibit a different response to rainfall, both in terms of runoff and infiltration. In order to correctly simulate the various types of surfaces and develop a generic model for application on any mine site, three hydrological simulation approaches were adopted. The approaches incorporated into the model are all based on well-tested and commonly-used techniques, which have been adapted to open-pit mine water systems.

The three hydrological approaches applied are:

- **Importation of separately generated runoff files**

  If available, the user may input a runoff file generated by any method or a file which has been generated through a monitoring program. The data layout must be detailed in an ASCII format, and once imported will be transparent to the operation of the model.

- **Soil Conservation Service (SCS) model**

  The SCS model is an empirical method relating the accumulated runoff from a catchment to the rainfall which has fallen on the catchment. It is particularly applicable for catchments of 8 km^2 or less and has been adapted for South African conditions. This method is well-tested, well-documented and accepted in Southern Africa.

- **Kinematic flow theory**

  The use of kinematic flow theory has been extensively researched in the past decade and many models exist that employ this technique. The value of the technique is the simulation of the true behaviour of the catchment with realistic parameters, rather than an empirical approach. The empirical methods assume a unique travel time for each point in the catchment. This neglects the change in depth of flow with time and movement down the catchment, which can lead to increase in velocity. The kinematic equations are simplified hydrodynamic equations and can be modified to account for losses and abstraction in a realistic manner.

All three hydrological approaches are described in more detail in the following sections including the data requirements.

3.1 Generation of runoff files

3.1.1 Background

It is often found that the data input required for the execution of hydrological models is not readily available. In general the empirical models require less data than the kinematic methods, but even these data are often difficult to obtain.

The collection of data and assessment of appropriate hydrological parameters describing a catchment response require the attention of an experienced hydrologist. This may, therefore, be carried out separately from opencast mine water modelling itself. If surface runoffs are already generated, it is necessary to import these values into the generic opencast mine water model.

Recorded rainfall/runoff data, although sparse at present, could in the future become an additional source of data. A one-year data base of recorded runoffs could, therefore, be incorporated into the model for a short term simulation. Although the recording period is limited, the data are recorded on site and, therefore, have value in terms of local applicability. The ability to import this type of hydrological data is imperative.

3.1.2 Methodology

The different surface drainage characteristics of the different types of areas outlined above requires a separate flow file for each element. The modelling methods (SCS and kinematic models) allow for the incorporation of factors to simulate the hydrological response of various surfaces. As the hydrological modelling is carried out independently in this case, it is assumed that the flow for each type of surface will be separately generated before importation into the generic mine water model.

Due to the model configuration it is possible for either the runoff simulation approaches or the importation option to be used independently of the simulation or reporting components of the generic mine water model.

As the model of the generic opencast mine water system is dynamically constructed and can have any number of elements, the user will be prompted for the input file for each different type of surface at data entry. When the hydrological model is run, it will determine whether import data is required or not. If the files are available these data will be accessed and stored in the data-base for later use.

3.2 Soil Conservation Service (SCS) model

3.2.1 Background

The Soil Conservation Service or SCS model was originally developed by Mocklus and has been extensively modified over the past three decades. It is most applicable for catchment sizes of 8 km^2 or less and slopes not exceeding 30%. This method has been tested and modified for South African conditions by Cousons (1976), Arnold (1980), Schulze (1982), Hope (1984) and Schmidt and Schulze (1984). The SCS method can be used for the estimation of runoff depth, runoff volume, peak discharge and can be used to generate a flow hydrograph.

3.2.2 Runoff Equations

The runoff in the SCS method is calculated using an empirical method describing the relationship between accumulated rainfall and accumulated runoff. An index is included in the relationship, which describes the surface response characteristics.

Runoff is deemed to begin after the interception and depression storage components have been satisfied, plus any infiltration which occurs before runoff takes place. This is satisfied by a rainfall amount termed the initial abstraction (Ia). Additional infiltration losses, occurring after the runoff has started, are termed the total retention (F), which increases to a maximum value of S.

This leads to the relationship which assumes the ratio of actual retention to maximum retention, is equal to the ratio of the runoff to the rainfall minus the initial abstraction.

Therefore:

$$\frac{Q}{(P - Ia)} = \frac{F}{S} \qquad \textbf{(3.2.2.1)}$$

where:

Q = accumulated runoff (mm)

P = accumulated rainfall (mm)

F = accumulated infiltration losses (mm) from start of runoff

S = potential maximum retention of soil (mm)

Ia = initial abstraction (mm)

When runoff has started taking place, all rainfall will either become surface runoff or infiltration.

Therefore:

$$P - Ia = F + Q \qquad \textbf{(3.2.2.2)}$$

To avoid having to estimate both Ia and S, the following empirical relationship is set up:

$$Ia = cS \qquad \textbf{(3.2.2.3)}$$

Therefore solving equations (3.2.2.1) and (3.2.2.2) and substituting (3.2.2.3) gives;

$$Q = \frac{(p - cS)^2}{P + (1 - c)S} \qquad \textbf{(3.2.2.4)}$$

This equation can, therefore, predict runoff depth Q from rainfall depth P for a catchment described by c and S. Equation (3.2.2.4) applies only where rainfall exceeds initial abstraction.

The value of S is related to the soil type, cover conditions and moisture status of the catchment. A dimensionless curve number (see Appendix A) was created to produce a more linear relationship and reflects the catchment response index to rainfall:

$$CN = \frac{25\,400}{S + 254} \qquad \textbf{(3.2.2.5)}$$

It is also possible to solve for S for application on a well-gauged catchment to determine appropriate CN values.

3.2.3 Rainfall

The SCS methodology was designed to work with daily rainfall as the basic input. Generally in South Africa, these data are easily accessible from the Weather Bureau. Time and rainfall intensity are not included in the analysis method.

It has generally been accepted that one-day rainfall be used as the basic rainfall data input. The 24-hour rainfall has been recommended (Schulze and Arnold, 1979), but conversion factors vary regionally and by recurrence interval and are, therefore, not easily determined. Daily rainfall values can be obtained from Adamson (1981) for 2 400 stations in Southern Africa, and for various recurrence intervals.

Maps of maximum expected one-day rainfall are available, but must be treated with caution. It is rather recommended to obtain values from tabulated weather station records (Adamsom, 1980). If more than one record is available, preference should be given to the longer records and/or the more closely related MAP values.

3.2.4 Soil Groups

Soil type is of prime importance in assessing and evaluating the hydrological response of a catchment. Various types of soil regulate the absorption, retention and release of water in different ways and to varying degrees. Important factors defining soil characteristics are its infiltration rate, permeability and water storage capacity.

The four basic soil groups, defined by the US Department of Agriculture, were adopted in South Africa and three additional intermediate soil groups were defined due to the wide spectrum of soils found in South Africa. The soil descriptions are given in **Table 3.2.4**.

Soil Groups	Class	Description
A	Low storm flow potential	Infiltration rate is high and permeability unrestricted. Soil depth is high and well-drained. Infiltration = 25 mm/hr Permeability > 7,6 mm/hr

Soil Groups	Class	Description
A/B		
B	Moderately low storm flow potential	Moderate infiltration rate, effective depth and drainage. Permeability is slightly restricted Infiltration = 13 mm/hr Permeability = 3,8 to 7,6 mm/hr
B/C		
C	Moderately high storm flow potential	Infiltration rate slow or deteriorates rapidly. Permeability restricted. Soil depth shallow. Infiltration = 6 mm/hr Permeability = 1,3 to 3,8 mm/hr
C/D		
D	High storm flow potential	Very slow infiltration rates and severally restricted permeability. Very shallow soils; High shrink potential. Infiltration = 3 mm/hr Permeability < 1,3 mm/hr

Table 3.2.4 : Soil classification for SCS methodology (Schmidt and Schulze, 1987)

3.2.5 Land Use and Treatment Classes

In order to assess the runoff from a catchment the surface conditions must be considered. In the SCS methodology, this is incorporated into the CN value through a classification of the land use and surface status (terracing, etc). The classes incorporate land use and treatment combinations as found in practice. If non-typical conditions are found, interpolation between classes can be carried out.

The basic classification is by land use, with a secondary classification by type of operation within the land use. The following is a list of the basic land use classifications:

- Cultivated land - Fallow
  - Row crops
  - Small grain crops
  - Close-seeded legumes or rotation meadows
  - Sugar cane
- Grassland
- Meadow
- Woods
- Orchards
- Forest
- Urban/Suburban

3.2.6 Hydrological Conditions

The runoff potential of a catchment is affected by the prevailing hydrological conditions of the catchment at the time of assessment. This makes some allowance for the antecedent moisture conditions of the soil. The hydrological conditions is defined as:

- Poor - high runoff potential
- Good - poor runoff potential

3.2.7 Calculation Procedure

Step 1. - Classify the surface in terms of hydrological condition, either good or poor.

Step 2. - From the tables of South African soil groups establish the soil type as A, A/B, B, B/C, C, C/D, or D.

Step 3. - Using the information from Steps 1 and 2 and the type of land use applicable to the catchment, obtain a Curve Number (CN) from the appropriate tables.

Step 4. - Calculate the maximum retention in the soil:

$$S = \frac{25400}{CN} - 254 \qquad \textbf{(3.2.7.1)}$$

Step 5. - Calculate the flow off the catchment;

$$Q = \frac{(P - cS)^2}{P + (1 - c)S} \qquad \textbf{(3.2.7.2)}$$

where:

c - the co-efficient of initial abstraction
≈ 0,1 recommended by Schmidt and Schulze (1987)

P - the accumulated rainfall (mm) at time t
≈ to be read from raw data provided.

3.2.8 Parameter Tables

The tables contained in Appendix A are taken from Schmidt and Schulze (1987), and represent the curve numbers by land use and the soil classification for use in the SCS methodology and defined for South African conditions.

3.3 Kinematic flow model

3.3.1 Background

The kinematic approach to the routing of flood waves was first introduced by Lighthill and Whitham (1955). Henderson and Wooding (1964) used this approach to model the runoff hydrograph resulting from excess rain on a plane. This approach has since been incorporated in models such as SWMM, WITWAT and WITSKM to model overland flow. Although these models were essentially developed for the analysis of urban drainage systems, the kinematic method has also been used to model runoff off from essentially rural catchments by Constantinides (1982) in the Kine 2 model and by Holden (1993).

The kinematic method has advantages over time-area methods in that its basis is founded in hydraulic theory and the non-linearity of the surface flow process is taken into account. The theory is simpler than the general hydrodynamic equations. The simpler numerical solutions result in faster

computer programs. This approach can be used to route flood waves down channels, pipes and through aquifers.

3.3.2 Kinematic flow theory

The equations of flow on which the kinematic theory is based are the St Venant equations. These equations describe one-dimensional flow of an incompressible, homogeneous fluid. The flow must be gradually varied and have a hydrostatic pressure distribution at any given section, and the steady-state resistance laws are assumed to describe friction and turbulence. The equations consist of the continuity or mass balance equation and the dynamic equation. The continuity equation can be derived by taking a mass balance around an element of fluid - refer to Figure 3.3.2.

The resulting equation is:

$$\frac{\partial q}{\partial x} + \frac{\partial A}{\partial t} = q_L \qquad \textbf{(3.3.2.1)}$$

where:

q = the flow rate (m^3/s)

A = the cross sectional area (m^2)

t = time (s)

q_L = the lateral inflow per unit length along the x-axis ($m^3/s/m$)

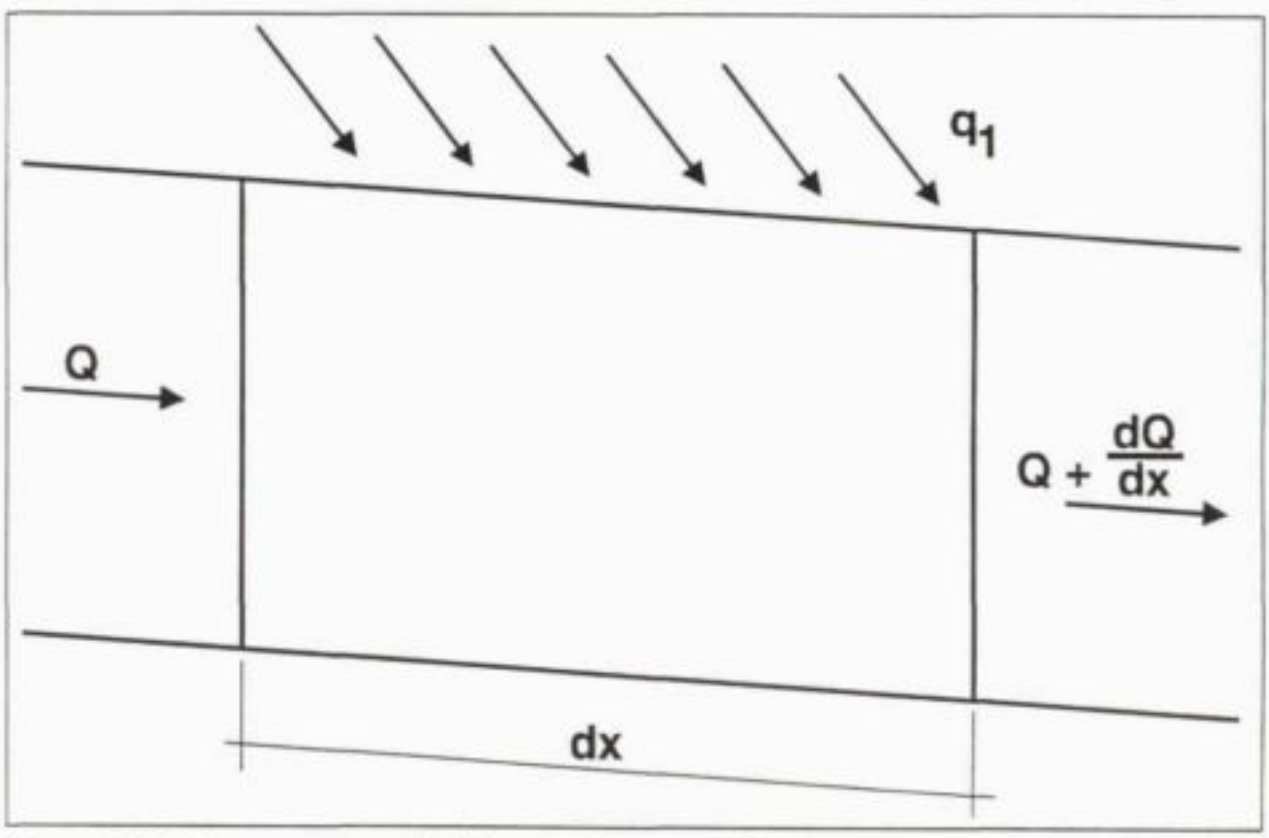

Figure 3.3.2 : Components required for mass balance of fluid element

The dynamic equation is derived using Newton's second law of motion. This equation is derived in classical hydraulics textbooks such as Chow (1959) and will not be repeated here. The equation can be expressed as:

$$S_f = So - \frac{\partial y}{\partial x} - \frac{v}{g} \cdot \frac{\partial v}{\partial x} - \frac{1}{g}\frac{\partial v}{\partial t} \qquad \textbf{(3.3.2.2)}$$

where:

S_f = friction slope (m/m)

So = bed slope (m/m)

y = water depth (m)

x = distance down plane (m)

v = average velocity (m/s)

g = acceleration due to gravity (m/s^2)

The terms in the dynamic equation are all slopes with $\delta y/\delta x$ the water surface slope, $v/g\ \delta v/\delta x$ and $1/g\ \delta v/\delta t$ being acceleration slopes.

Some of the terms of the dynamic equation can be ignored under certain circumstances. Henderson (1966) showed that the last two terms are generally an order of magnitude smaller than $\delta y/\delta x$, while Stephenson and Meadows (1986) showed that the acceleration terms are often insignificant or cancel one another out.

The kinematic approximation is that the friction slope $S_f \approx S_o$ and the other terms of the dynamic equation can be ignored. Stephenson (1981) showed that, in overland flow, the term $\delta y/\delta y$ is generally an order of magnitude smaller than the ground slope S_o. Holden (1993) showed that a typical plane of length 100 m has kinematic flow numbers in excess of 10 using the dimensionless kinematic flow number:

$$K = (S_o L)/(Y_o Fro)$$

where S_o and L are the slope and length of a rectangular plane subject to steady rainfall, Y_o is the equilibrium flow depth at the downstream end, and Fro is the Froude number at Y_o. This was considered by Woolhiser and Ligget (1967) to indicate that the kinematic approximation is adequate.

The kinematic approximation implies that the flow is uniform and that there is a single-valued relationship between the flow (Q) and the flow depth (y) such that Q = Q(y) and y = y(Q). The relationship generally takes the form

$$Q = cY^m \qquad \textbf{(3.3.2.3)}$$

The Manning equation is one of the more popular relationship used to relate Q to y and for a rectangular plane can be expressed as:

$$Q = AR^{2/3}\sqrt{S_o}/n \qquad \textbf{(3.2.2.4)}$$

where:

A = cross section area (m^2)

R = hydraulic radius (A/P)

P = wetted perimeter (m/m)

n = Manning roughness coefficient

S_f is replaced by S_o for the kinematic approximation. For a rectangular plane of width W, the hydraulic radius can be approximated by y which leads to

$$Q = Wy^{5/3} \cdot \sqrt{S_o}/n \qquad \textbf{(3.3.2.5)}$$

The continuity equation can be written as:

$$\frac{\partial Q}{\partial x} + \frac{dA}{dQ} \cdot \frac{\partial Q}{\partial t} q_L \qquad \textbf{(3.3.2.6)}$$

with A replaced by $\frac{dA}{dQ} \cdot \frac{\partial Q}{\partial t}$

dQ/dA is the wave velocity c and the equation becomes:

$$\frac{\partial Q}{\partial x} + \frac{1}{c} \cdot \frac{\partial Q}{\partial t} = q_L \qquad \textbf{(3.3.2.7)}$$

3.3.3 Numerical Solution to Equation

The kinematic equations are non-linear, partial differential equations. These equations do have analytical solutions for simple cases. Normally numerical techniques have to be employed to solve the equations. The finite difference scheme approach has been used to solve the equations. Constantinides (1982) and Holden (1993) described and tested some of the possible finite difference schemes. The schemes most often used are derivatives of that derived by Cunge (1969). The so-called Muskinghum-Cunge method was tested by Holden (1993) and shown to be stable and relatively accurate. The approach is outlined below.

Consider the computational cell shown in Figure 3.3.3.

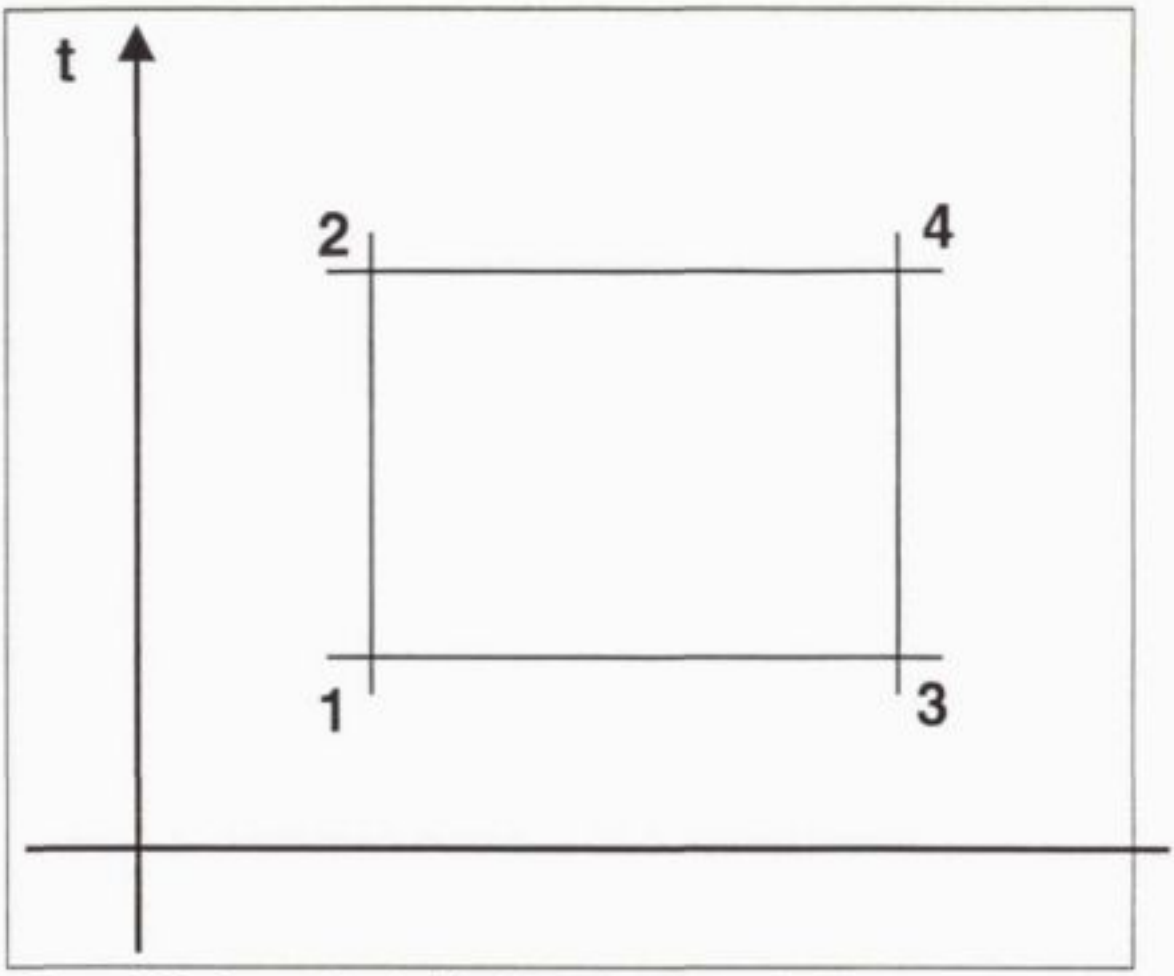

Figure 3.3.3 : Computational cell for kinematic routing methodology

Preismann (1961) presented a general expression for the finite difference formulation of the kinematic equation as follows.

$$[\varphi (Q_3 - Q_1) + (1 - \varphi) (Q4 - Q2)]/\Delta x + [\Theta(Q2 - Q1) + (1 - \Theta) (Q_4 - Q_9)]/(\Delta t.c) = q_L \quad \textbf{(3.3.3.1)}$$

The approximation of the partial differential equation by a finite-difference scheme introduces numerical diffusion. This error can be estimated by using a Taylor expansion of the terms of the continuity equation, which results in:

$$R = [\Theta - 1/2] + CR[\varphi - 1/2] \frac{\partial^2 Q}{\partial x^2} \delta x + (\text{higher order terms}) \quad \textbf{(3.3.3.2)}$$

For the error term to be zero we require:

$$O = [\Theta\ 1/2] + CR\ [\varphi - 1/2] \quad \textbf{(3.3.3.3)}$$

where CR is the Courant number = $c\Delta t/\Delta x$

If the friction slope $S_f = S_o - \delta g/\delta x$, Kousis (1983) showed that the continuity equation could be written as:

$$\frac{\partial Q}{\partial x} + \frac{1}{c}\frac{\partial Q}{\partial t} = \frac{-Q}{2WcS_f}\cdot\frac{\partial^2 Q}{\partial x^2} \qquad \textbf{(3.3.3.4)}$$

By putting S_f = So and matching the numerical diffusivity to the hydraulic diffusivity the following results:

$$\Delta x\,[(\Theta - 1/2) + CR\,(\varphi - 1/2)]\,\frac{d^2Q}{\partial x^2} = \frac{-Q}{2WcS_o}\cdot\frac{\partial^2 Q}{\partial x^2}$$

which, solving for Θ gives:

$$\Theta = [1 - 2\,CR\,(\varphi - 0{,}5) - \frac{Q}{BoxCSo}]/2 \qquad \textbf{(3.3.3.5)}$$

Putting φ = 0, results in an unconditionally stable scheme which gives;

$$\Theta = [1 + CR) - Q/(BoxCSo)] / 2 \qquad \textbf{(3.3.3.6)}$$

Thus by varying Θ, the numerical and hydraulic diffusivity can be matched. This deals with the surface runoff component of the kinematic approach. This approach can be used for aquifer routing, and pipes and channels where backwater effects are unimportant. The remaining important component of the kinematic model would be the infiltration aspect.

3.3.4 Infiltration

The Hortonian approach to infiltration is used in this model. This approach considers the soils surface as a sieve which has the ability to separate rainfall into two basic components. The one component, for rainfall intensities exceeding the infiltration capacity of the soil, goes via overland flow to the stream channels, while the other goes through the groundwater flow to the stream channels or is returned to the air by evaporation. This is not strictly correct as underlying soil layers could cause perched water tables which result in interflow.

There are two methods that are often used to model Hortonian infiltration. These are the Horton equation which is an empirical exponential decay function:

$$f = f_c + (f_o - f_c)\exp(-kt) \qquad \textbf{(3.3.4.1)}$$

where:

- f = the instantaneous infiltration rate (mm/hr)
- f_c = the limiting, steady minimum infiltration rate (mm/hr)
- f_o = is the initial maximum infiltration rate at the start of the storm (mm/hr)
- k = the decay constant or slope factor for a given soil
- t = time from beginning of storm (hr)

The other approach is the Green-Ampt equation. This equation is simple and physically based. The model can be expressed as follows.

$$f = K_{sat} [1+ ((\Theta_{sat} - \Theta_i) - \Omega)/F] \quad \textbf{(3.3.4.2)}$$

where:

f	=	instantaneous infiltration rate (mm/hr)
Θ_{sat}	=	saturated moisture content
Θ_i	=	initial moisture content
Ω	=	sorptivity (m)
F	=	infiltration depth (mm)

Both of these approaches can be included in the kinematic model as alternative options.

4. DEVELOPMENT OF THE GENERIC MINE WATER MODEL

4.1 Modelling approach

The generic opencast mine water model is designed to simulate, predict and understand the water flow and water quality aspects of a single, selected opencast pit. The model, therefore, concentrates on the pit and does not attempt to integrate the pit water system with the total mine water complex, including coal beneficiation plants, discard dumps, slurry ponds, etc. Some allowance is made in the model for associated water-related infrastructure, such as pit water evaporation ponds.

The model is also a life-of-mine type model, which simulates the water-related aspects over the operational phase of an opencast pit. The model can be extended to simulate the post-mining behaviour of the pit.

The approach is to select a specific hydrological sequence (rainfall/runoff record) and to investigate the response of the mine water system over the operating life of the pit. Different hydrological sequences can be selected to test the sensitivity of the mine water system to different rainfall/runoff events.

This type of model must be distinguished from an operational type of model. An operational-type model specifies a certain opencast pit operational scenario in terms of geometry, status of spoils (unrehabilitated, levelled, topsoiled, vegetated, etc.), geochemical properties, etc. The specific pit opencast scenario is then tested for a hydrological sequence involving a large number of rainfall/runoff events. The operational-type models are designed to investigate the response of a specific pit status to different rainfall/runoff events and to conduct a risk assessment on, for example, flooding of the pit, etc. Operational model simulations are used to select or design the pit water-related infrastructure such as dewatering pumps, sump sizes, etc.

4.2 Conceptual presentation of mine workings

The opencast mine water model incorporates the important elements of a pit water system. The following sources of water are recognised in the model:

- Surface runoff from the different natural and disturbed surfaces draining towards the pit.
- Groundwater ingress from the aquifers which are intersected by the mine workings.
- Recharge to the spoils due to infiltration of rainfall and runoff.

Water storage and accumulation are also catered for in the model in terms of:

- Spoils water accumulating in pit floor depressions.
- Depressions on the surface of the spoils body to which surface runoff may flow and accumulate.
- Excess pit water storage ponds located outside the pit.

The model incorporates algorithms to describe the water quality in terms of sulphate concentration and acidity/alkalinity. The following chemical and geochemical aspects are catered for:

- Quality of the rainfall.
- Quality of the recharge (infiltration) water entering the spoils body.
- Pyrite oxidation in the spoils body resulting in the release of oxidation products such as acidity, iron and sulphate.
- Neutralisation of pyrite oxidation products.
- Pollutant washoff from surfaces such as the pit floor, access ramps, etc.

The conceptual flow diagram of the generic mine water model is shown in **Figure 4.2(a)**. The total pit area is subdivided into individual mining blocks, which each corresponds to approximately one month of surface disturbance by mining. This implies that an opencast pit with an anticipated mining life of 5 years would be divided into 60 individual blocks. The status of a specific mining block then changes from natural (undisturbed), pit floor, unrehabilitated spoils, levelled spoils, levelled and topsoiled spoils, and rehabilitated spoils. The surface runoff and recharge characteristics of a mining block would also change as the status of the block changes.

The surface runoff from a specific mining block could be diverted to one of three destinations:

- Discharge to a water body or adjacent catchment, outside the pit water system.
- Pit floor from where it reports to the pit floor sump.
- Depressions formed on the rehabilitated pit spoils surface. It is possible that more than one on-spoils depression is formed and the model allows the definition of more than one depression.

The surface recharge associated with a mining block depends on the status of the specific block. It is not intended to model the recharge mechanism itself. This model relies on an input generated by a specialised submodel, dealing specifically with spoils cover recharge. The recharge will migrate through the spoils and could eventually report to one of two destinations:

- The pit floor from where it flows to the pit floor sump.
- In-spoils impoundment. More than one in-spoils impoundment may exist and the model allows the selection of a specific in-spoils impoundment. Decant from any in-spoils impoundment may flow to the pit floor sump or may flow to an adjacent in-spoils impoundment.

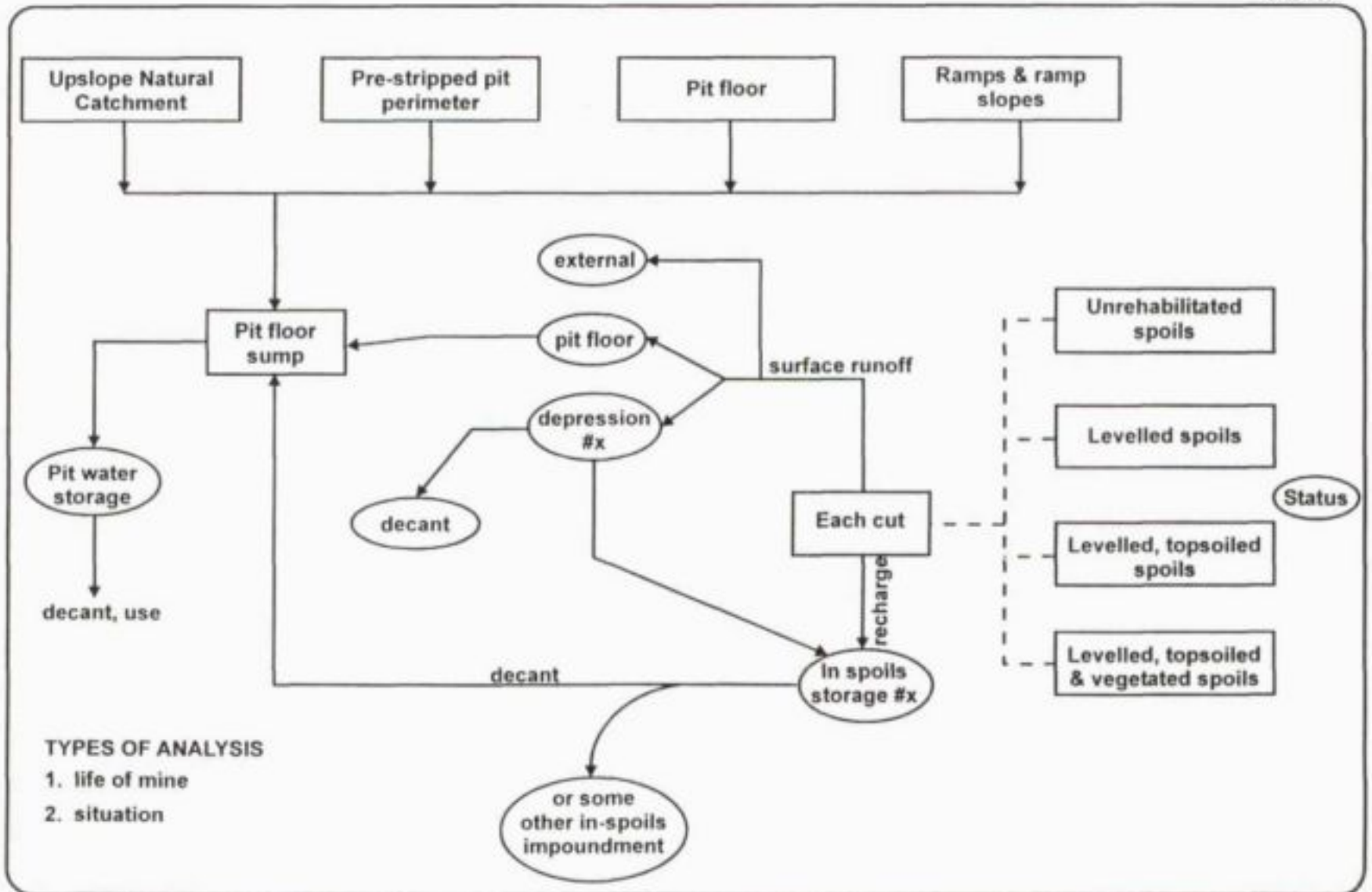

FIGURE 4.2 (a) : CONCEPTUAL FLOW DIAGRAM OF GENERIC MINE WATER MODEL

Groundwater flows typically do not constitute a significant component of the overall pit water system. Allowance is, however, made for a groundwater flow contribution from three separate aquifers. The groundwater flow may be directed to an in-spoils impoundment or to the pit floor sump directly. Groundwater flow contributions are sensitive to the pit geometry and pit size and will change over the life of the pit.

The pit water system can, furthermore, receive significant flow contributions from the upslope natural catchment, the pre-stripped pit perimeter and from ramps and ramp slopes. The runoff characteristics of these surfaces do not typically change much over the life of the pit. The size of these catchment surfaces may however be variable and may change over the life of the pit.

The excess pit water accumulates in a pit floor sump and during the operational life of the pit, this water is transferred to an external pit water storage facility. In the post-mining situation, the excess pit water accumulates in the pit and eventually inundates the spoils body.

Discretisation of the spoils body

A specific mining block may undergo frequent changes in status from an initial natural state to an eventual rehabilitated spoils status. The spoils within a specific mining block will be subjected to substantial moisture changes and water migration over time. It is, therefore, essential to recognise the vertical spatial variation in a mining block spoils with respect to water movement, oxygen diffusion, pyrite oxidation, accumulation and flushing of oxidation products.

A specific mining block is discretised into several horizontal layers to allow simulation of the spatial variation in spoils properties and related phenomena. **Figure 4.2(b)** shows the discretisation. The discretisation approach allows for the simulation of spatial variation with respect to:

- Geochemical properties such as pyrite content, neutralisation capacity etc.
- Spoils physical properties.
- Progressive moisture saturation of spoils material by recharge from the top.
- Pyrite oxidation rate as a function of oxygen concentration within the spoils body.
- Accumulation and flushing of pyrite oxidation products.

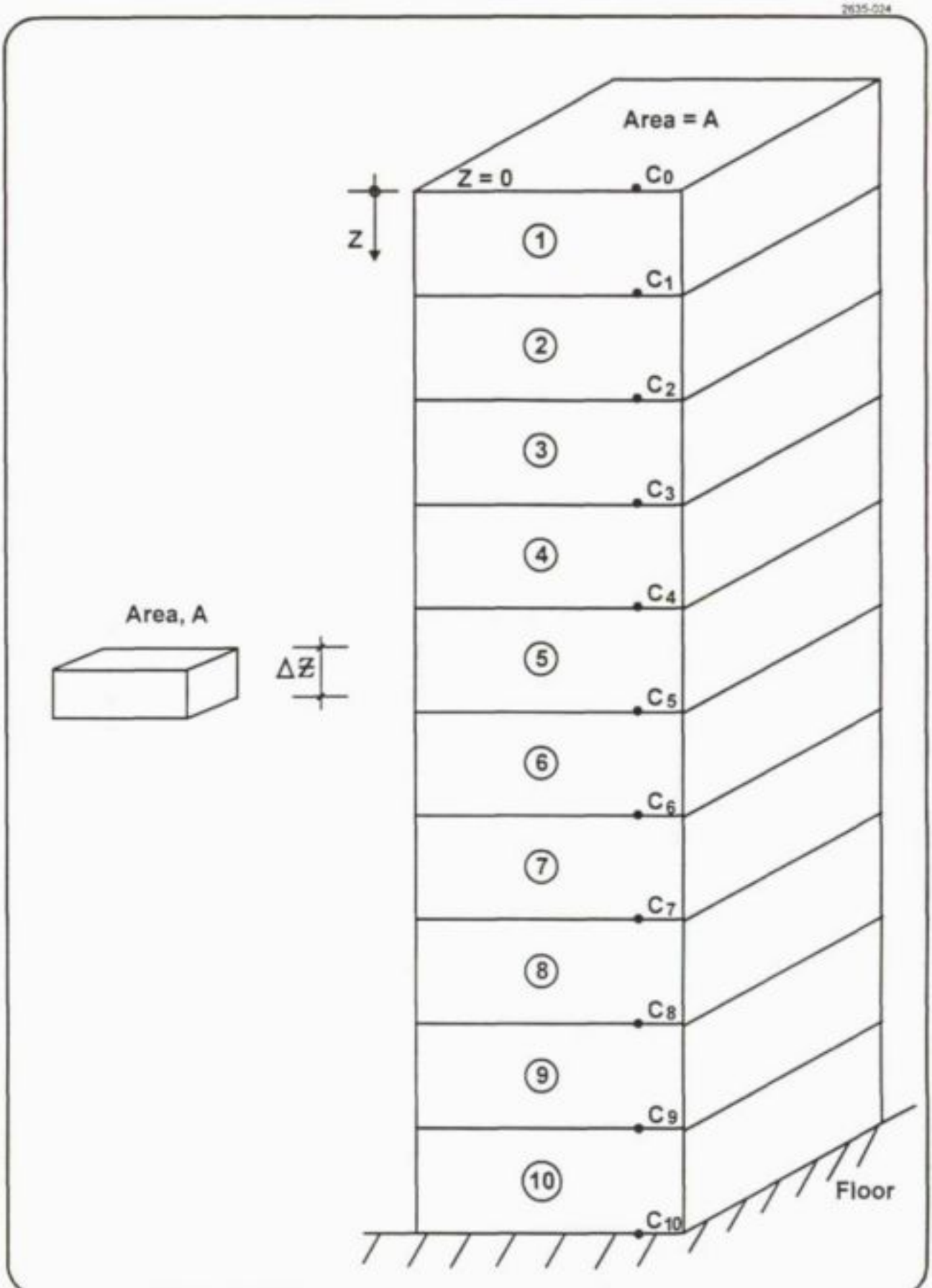

FIGURE 4.2 (b) : SCHEMATIC PRESENTATION OF DISCRETISATION OF A MINING BLOCK

The typical model inputs required for each of the mining blocks are:

- Area size (ha).
- Time-related changes in the status of a mining block.
- Destination of surface runoff and changes of this with time.
- Destination of recharge and changes with time.
- Pre-mining strata thickness (overburden, interburden and coal).
- Post-mining strata thickness, which can also be based on the thickness of overburden and interburden and the bulking factor.
- The location of the mining block relative to the perimeter of the mining operation. Information on outside blocks is employed to calculate the length of the pit perimeter along which groundwater may enter the pit water system.

The required geochemical input will be described in **Section 4.4** of this report.

4.3 Water balance aspects

The generic mine water system is shown on **Figure 4.2(a)** and includes several surface runoff, recharge and groundwater flow components. The approach to the mathematical description of these flow components is given below.

Surface runoff typically constitutes the biggest flow contribution to the overall water balance over the operational life of the mine. Surface runoff from disturbed surfaces also contributes a pollution load, due to the washoff from surface sources of pollution. The mathematical description of the runoff sub-models incorporated into the integrated generic mine water model is presented in **Chapter 3** of this report. The model allows for the importation of rainfall/runoff files generated by an independent hydrological simulation program or the generation of monthly runoff values using the Soil Conservation Services (SCS) model or the Kinematic Flow (KF) model.

Recharge (infiltration) via the spoils rehabilitation cover becomes progressively more important as mining progresses. In the post-mining situation, recharge typically dominates the water balance. Surface recharge is the topic of ongoing research and a parallel project entitled "Calibration of Models for the Design of Covers for Opencast Mine and Waste Rock Rehabilitation" is being carried out by the WRC. It is not the intention of this project to repeat the knowledge and models which are available to calculate recharge. Recharge is inherently a complex phenomenon and dependant on numerous factors including cover thickness, cover material, cover placement technique, surface slope, presence of local depressions, presence of macroscopic features such as cracks/crevices, vegetation, etc. The generic opencast mine water model deals with the recharge component of flow in two ways:

- It can be received from an independent model which calculates recharge on the basis of a specific hydrological rainfall record. The recharge should preferably be specified as a unit flow ($mm/m^2/month$) or a percentage of monthly precipitation.
- Default recharge values, which are based primarily on experience gained on the Mpumalanga Highveld Coalfields can be used. The recharge values are

defined as a percentage of monthly precipitation and incorporate a lag factor. The default values for recharge are summarised below for different spoils cover types:

Table 4.3(a) : Rainfall recharge to spoils with different covers (% of monthly rainfall)

Month	Levelled (no topsoil) (%)	200 mm topsoil (no vegetation) (%)	200 mm topsoil (vegetated) (%)	600 mm topsoil (vegetated) (%)
January	3,5	3,1	1,6	0,6
February	3,3	2,9	1,4	0,7
March	2,7	2,3	1,1	0,7
April	0,7	0,6	0,7	0,6
May	0,4	0,3	0,3	0,6
June	0,4	0,3	0,3	0,5
July	0,4	0,3	0,3	0,5
August	0,4	0,3	0,3	0,5
September	2,8	2,4	0,9	0,5
October	3,0	2,5	1,2	0,6
November	3,3	2,9	1,3	0,6
December	3,4	3,0	1,5	0,6
Total	**24**	**21**	**11**	**7**

Groundwater flows are accepted as inputs to the generic opencast mine water model. The groundwater flows should, therefore, be based on geohydrological models which run independently from the generic opencast mine water model. The model allows for input from three different aquifers and the following information is required as input:

- The time-related flow (m^3/month) for each aquifer.
- The split of the groundwater flow from each aquifer to the in-spoils impoundments and the pit floor sump.
- The flow per unit length of pit perimeter.

Default values for the groundwater flows are specified in terms of a flow per unit pit perimeter length per month. A default value can be entered for each aquifer and the model assumes that the groundwater reports to the pit floor sumps in the default situation.

Spoils water migration is a major consideration in the accurate description of the mine water system. The importance also increases with time and could dominate the opencast mine water balance in the post-mining situation. The description of water migration in the spoils environment is complicated by the heterogeneous nature of the

material. It has been attempted to develop a simple, but appropriate, approach to the description of water migration in spoils incorporating the following aspects:

- A small percentage of the spoils (typically 20 - 25%) effectively comes in contact with the migrating water.
- The part of the spoils that is in contact with migrating water, can be divided into a coarse fraction and fine fraction. The moisture retention and water movement pattern in the coarse and fine fractions are different.
- The spoils material has a large moisture deficit, which needs to be partially satisfied before flow will be initiated.
- The spoils material that is not in direct contact with migration water will be wetted by successive evaporation/condensation cycles.

The generic water migration pattern on the spoils body is shown in **Figure 4.3(a)**.

Considering a **unit volume** of spoils, the following material characteristics are required to predict water migration:

- Bulk density, ρ_b (default value = 1600 kg/m^3)
- Total porosity, Θ_t (default value = 0,30 m^3/m^3)
- Fraction of spoils in contact with the migrating water, f_t (default value = 0,25)

The fraction of spoils in contact with the migrating water is further subdivided into a coarse fraction (f_c) and a fine fraction (f_f). The mass of the two fractions can then be calculated as:

- Mass coarse fraction (per unit volume)

  $= \quad f_c.f_t.\rho_b$ **(4.3.1)**

- Mass fine fraction (per unit volume)

  $= \quad f_f.f_t.\rho_b$ **(4.3.2)**

The default values are for the coarse fraction, $f_c = 0,5$ and for the fine fraction, $f_f = 0,5$.

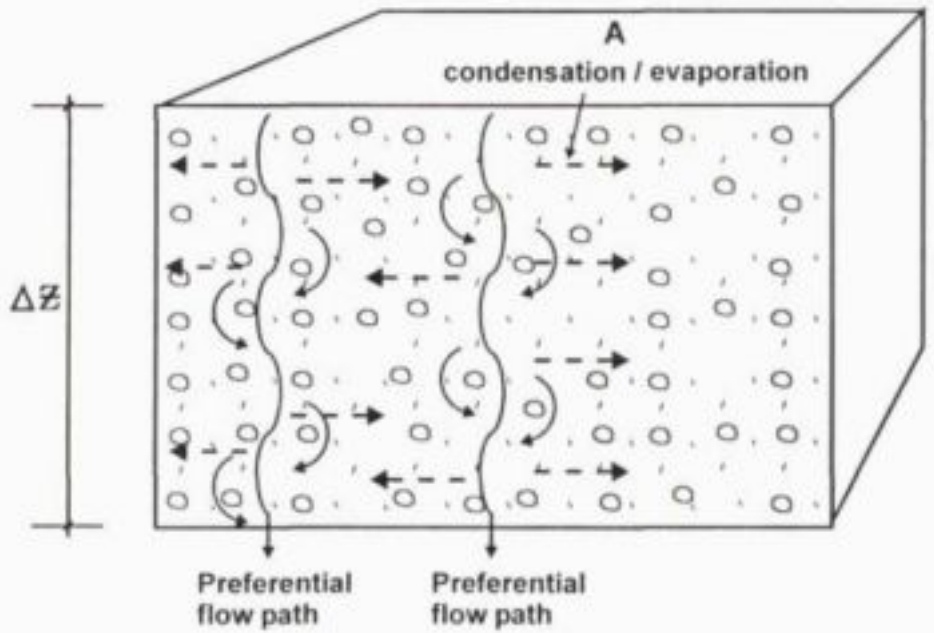

FIGURE 4.3 (a) : CONCEPTUAL MODEL OF SPOILS WATER MIGRATION PATTERNS

The water retention by the different spoils fractions must be satisfied, before initiation of free flow down the spoils. The respective water retentions by the coarse and fine fractions are as follows:

- Coarse fraction water retention (per unit mass of spoils)

  $= \quad S_c \cdot (f_c.f_t.\rho_b)$ **(4.3.3)**

- Fine fraction water retention (unit mass of spoils)

  $= \quad S_f \cdot (f_f.f_t.\rho_b)$ **(4.3.4)**

  where:

  S_c = coarse spoils fraction water retention (kg water/kg dry spoils)

  S_f = fine spoils fraction water retention (kg water/kg dry spoils)

The default values for S_c = 0,04 kg water/kg dry spoils and S_f = 0,09 kg water/kg dry spoils.

The prediction of the water migration rate in the different fractions is particularly difficult due to the heterogeneous nature of the material. A probabilistic approach is followed using a bi-modal probability distribution of permeability to predict the water migration rates for the spoils element. The water migration rate is generated (using a random number generator and the bi-modal probability distribution) for each spoils element at the initiation of the model run.

The water volume **in the spoils element** (surface area A and depth ΔZ) will vary between the following extremes:

- Minimum value corresponding to the required wetting of the coarse and fine fractions:

  $V_{min,s}$ (m^3 water) = $(S_c.f_c + S_f.f_f)\, f_t.\rho_b\, (\Delta Z.A)/1000$ **(4.3.5)**

- Maximum value corresponding to the saturation of the coarse and fine fractions:

  $V_{max,s}$ (m^3 water) = $\Theta_t.f_t.\rho_b.(\Delta Z.A)/1000$ **(4.3.6)**

The **maximum** outflow from the spoils element can be computed as:

$$Q_{out,\,max} = P.A.\Theta_t.f_t \quad \textbf{(4.3.7)}$$

where:

P = permeability (m/month)

A = cross sectional area of spoils element

The degree of moisture saturation for a specific spoils block can then be calculated as:

$$So = [V_{o,s}/V_{max,s} - V_{min,s}/V_{max,s}] / [1 - V_{min,s} / V_{max,s}]$$

where:

$V_{o,s}$ = water volume in spoils block at the start of a time step (m^3)

S_o = degree of moisture saturation at the start of a time step (m^3/m^3)

The outflow from the spoils element during the time step is:

$$Q_{out} = Q_{out,max} S_o \delta$$

where:

Q_{out} = outflow from spoils element (m^3/month)

δ = flow parameter

The volume of water in the spoils element can be computed using the general expressions (refer to Figure 4.3(b)):

$$\frac{dV}{dt} = Q_{in} - Q_{out} \qquad \textbf{(4.3.8)}$$

and over a specific time step of one month then :

$$V_e = V_o + Q_{in} - Q_{out} \qquad \textbf{(4.3.9)}$$

where:

V_e = water volume at the end of the time step (m^3)

V_o = water volume at the beginning of the time step (m^3)

Q_{in} = inflow from the next upper element (m^3/month)

Q_{out} = outflow to the next lower element (m^3/month)

As a first estimate, no flow from the spoils element will take place until the necessary wetting of the spoils has occured thus:

if $V_o \leq V_{min}$ then $Q_{out} = 0$

$V_e = V_o + Q_{in}$

if $V_o > V_{min}$ then $Q_{out} = Q_{out}$

$V_e = V_o + Q_{in} - Q_{out}$

with a check that if $V_e \leq V_{min}$

then $V_e = V_{min}$ and $Q_{out} = V_o + Q_{in} - V_{min}$

with a check that if $V_e \geq V_{max}$

then $V_e = V_{max}$ and $Q_{out} = V_o + Q_{in} - V_{max}$

The general expression for the simulation of the water balance of an impoundment as shown on **Figure 4.3(c)** is:

$$V_e - V_o = \frac{dV}{dt} = Q_{in} - Q_{evap} - Q_d - Q_{spill}$$

where:

V	=	volume of the impoundment (m^3)
V_o	=	volume of impoundment at the start of the time step (m^3)
V_e	=	volume of impoundment at the end of the time step (m^3)
Q_{in}	=	influent flow to the impoundment, such as runoff, seepage etc. (m^3/month)
Q_{evap}	=	nett evaporation loss from the impoundment (m^3/month)
	=	Ao (E - P)
Q_d	=	demand abstraction from impoundment (m^3/month)
Q_{spill}	=	spillage/decant from the impoundment (m^3/month)

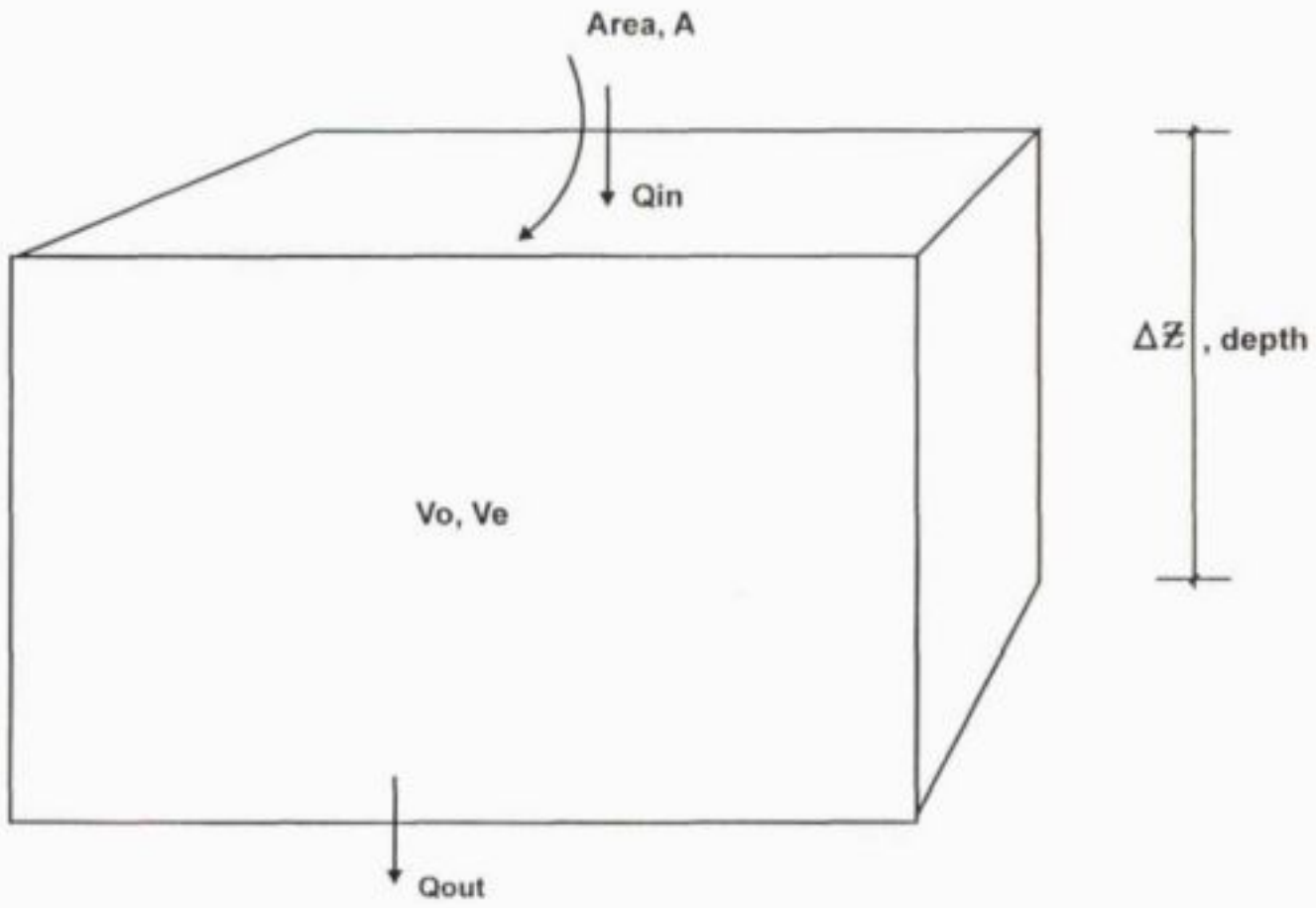

FIGURE 4.3 (b) : WATER BALANCE COMPONENTS OF A SPOILS ELEMENT

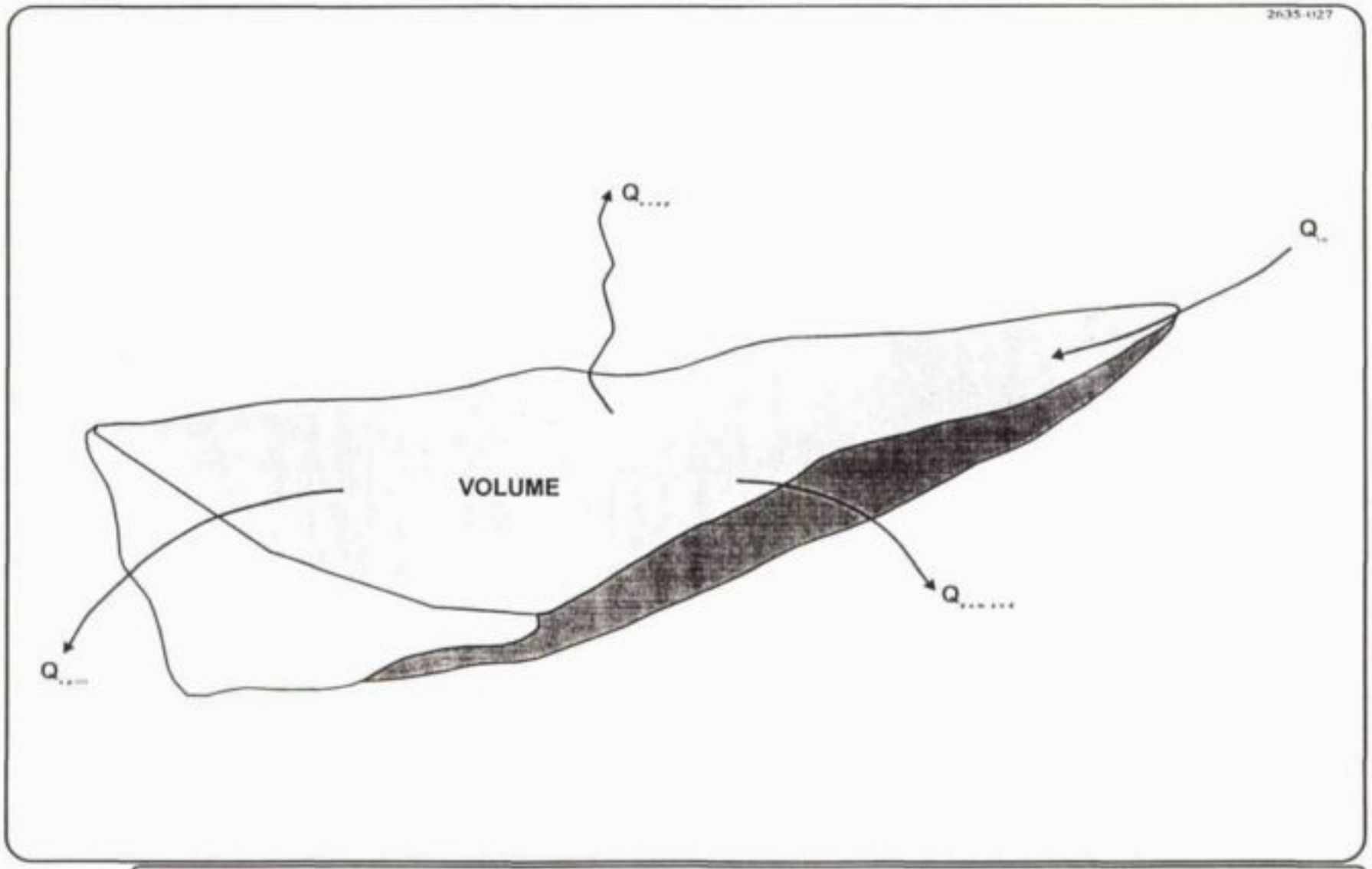

FIGURE 4.3 (c) : GENERAL WATER BALANCE COMPONENTS OF AN IMPOUNDMENT

In general

if $V_o \leq V_{min}$,	then	Q_d	=	0
		Q_{spill}	=	0
if $V_e \geq V_{max}$,	then	Q_{spill}	=	$V_e - V_{max}$
		V_e	=	V_{max}
if $V_e \leq 0$,	then	V_e	=	0

4.4 Spoils water quality aspects

The spoils water quality is modified by several different processes as water migrates through the spoils. These processes include:

- The pyrite oxidation process which releases a number of oxidation products, including iron (Fe^{2+}), sulphate (SO_4^{2-}) and acidity (H^+). The pyrite oxidation rate is sensitive to the presence of oxidants (O_2 and Fe^{3+}) and oxidisable pyrite mineral.

- The ferrous iron may undergo further oxidation depending on the redox potential of the local spoils environment. The ferrous iron will be oxidised to ferric iron, which is itself an oxidant and will stimulate further pyrite oxidation. The redox potential is primarily a function of the local presence of oxygen in the spoils.

- The acidity generated in the process of pyrite oxidation may be neutralised by carbonate minerals. Spoils typically contain a mixture of calcite and dolomite, which will react during the neutralisation process. The neutralisation process will release carbonate, calcium and magnesium to the spoils water.

- The generally slow pyrite weathering and slow migration of water through the spoils allow sufficient time for application of the principles of chemical equilibrium. It is, therefore, assumed that chemical equilibrium exists between the different ionic species in solution. Precipitates may form if over-saturation develops with respect to any specific salt. An inventory of the accumulated salt species is kept to allow subsequent resolution if dictated by the ambient water chemistry.

The pyrite oxidation process is driven by the available oxygen in the local spoils environment. It is assumed that the oxygen diffuses into the spoils environment and that consumption takes place due to microbial respiration (in the rehabilitation cover) and pyrite oxidation (in the body of spoils).

The geochemical characteristics of the spoils body are defined in terms of the acid generation potential and the neutralisation potential. These properties are highly variable and the assumption of some average geochemical characteristic for the entire spoils body is not realistic. The model therefore uses a probabilistic approach to the geochemical characterisation of each spoils element. The acid generation potential (sulphur content) and neutralisation potential can be described by log-normal probability distributions. The statistical parameters specifying the probability distribution can be based on field testing such as ABA tests. The geochemical

properties of a specific spoils element are then fixed using a random number generator and the probability distribution for acid generation potential and neutralisation potential respectively.

The ionic species incorporated in the model include hydrogen ion (H^+), hydroxide ion (OH^-), carbon dioxide (CO_2/H_2CO_3), bicarbonate (HCO_3^-), carbonate (CO_3^{2-}), ferrous iron (Fe^{2+}), ferric iron (Fe^{3+}), sulphate (SO_4^{2-}), calcium (Ca^{2+}) and magnesium (Mg^{2+}).

A correlation between sulphate and TDS can be used to calculate the total ionic strength. This can then be used in the correction of activity coefficients for the individual ionic species.

A stepwise approach is followed to compute the change in spoils water chemistry after each successive time-step - refer to **Figure 4.4(a)**.

The atmosphere contains oxygen at a partial pressure of 0,21 atm. This corresponds to an atmospheric oxygen concentration of 0,30 kg/m^3 (at P=1 atm and T = 293K). The partial pressure of CO_2 in the atmopshere is 0,00035 atm. The model uses the simplifying assumption that as the oxygen is consumed in the spoils, the remaining nitrogen and carbon dioxide partial pressures increase in proportion to the decrease in oxygen partial pressure:

$$P_{co2} = [0,00035/0,79]\,[0,21.]\,[0,3-C_{o2}]/0,3 \qquad \textbf{(4.4.1)}$$

where

P_{co2} = carbon dioxide partial pressure (atm)

C_{o2} = oxygen concentration in spoils (kg/m^3)

4.4.1 Diffusion of Oxygen

The diffusion of oxygen to the pyrite minerals in the spoils body is considered to be one of the rate-limiting steps in the weathering process. The model assumes that oxygen diffusion into the spoils is driven by a concentration gradient. A mining block is, therefore, discretised in a vertical dimension to allow the description of the oxygen migration process. The typical mining block discretisation is shown on **Figure 4.4.1**.

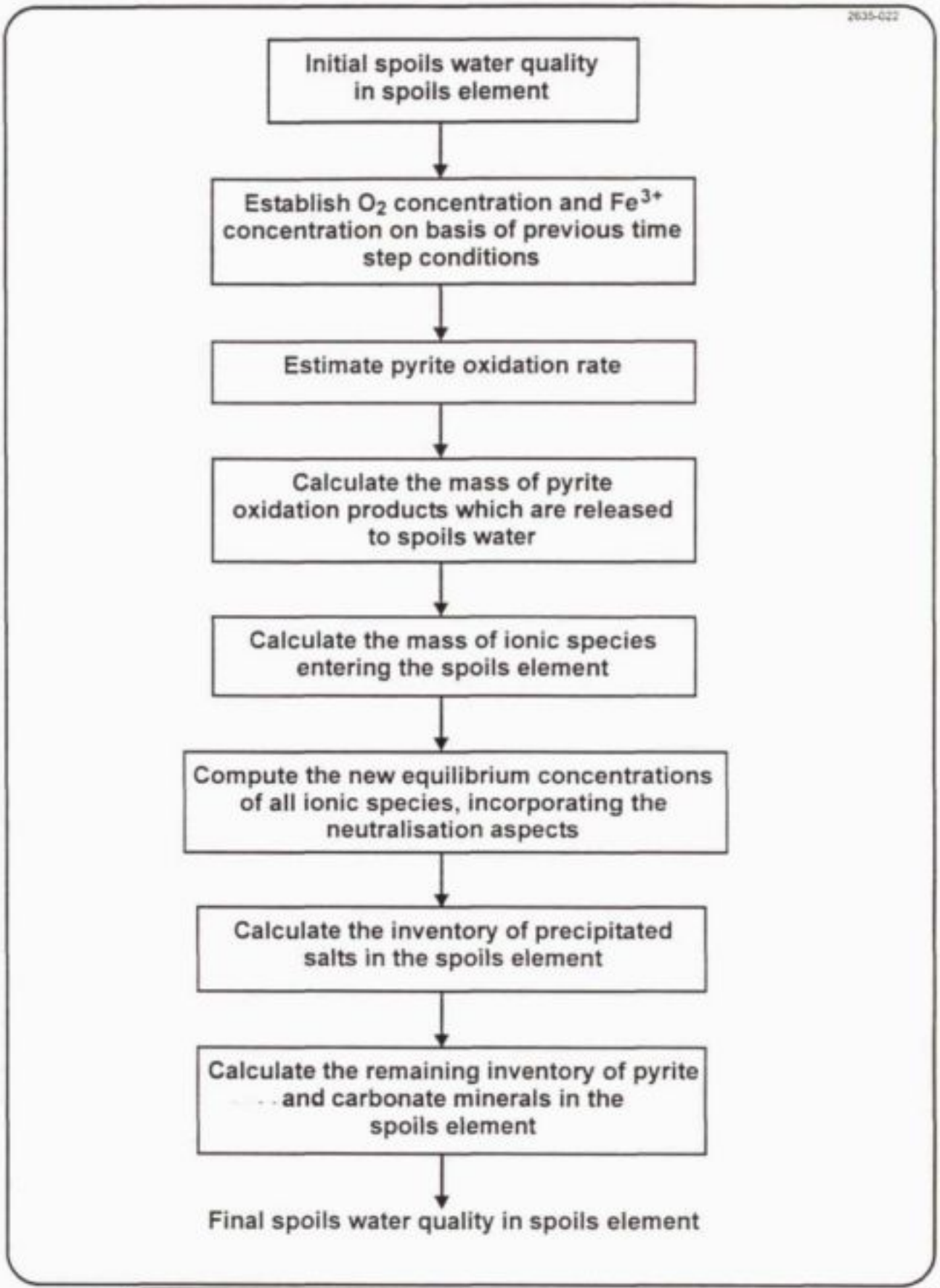

FIGURE 4.4 (a) : GENERIC SOLUTION OF AQUATIC CHEMISTRY FOR A SPOILS ELEMENT

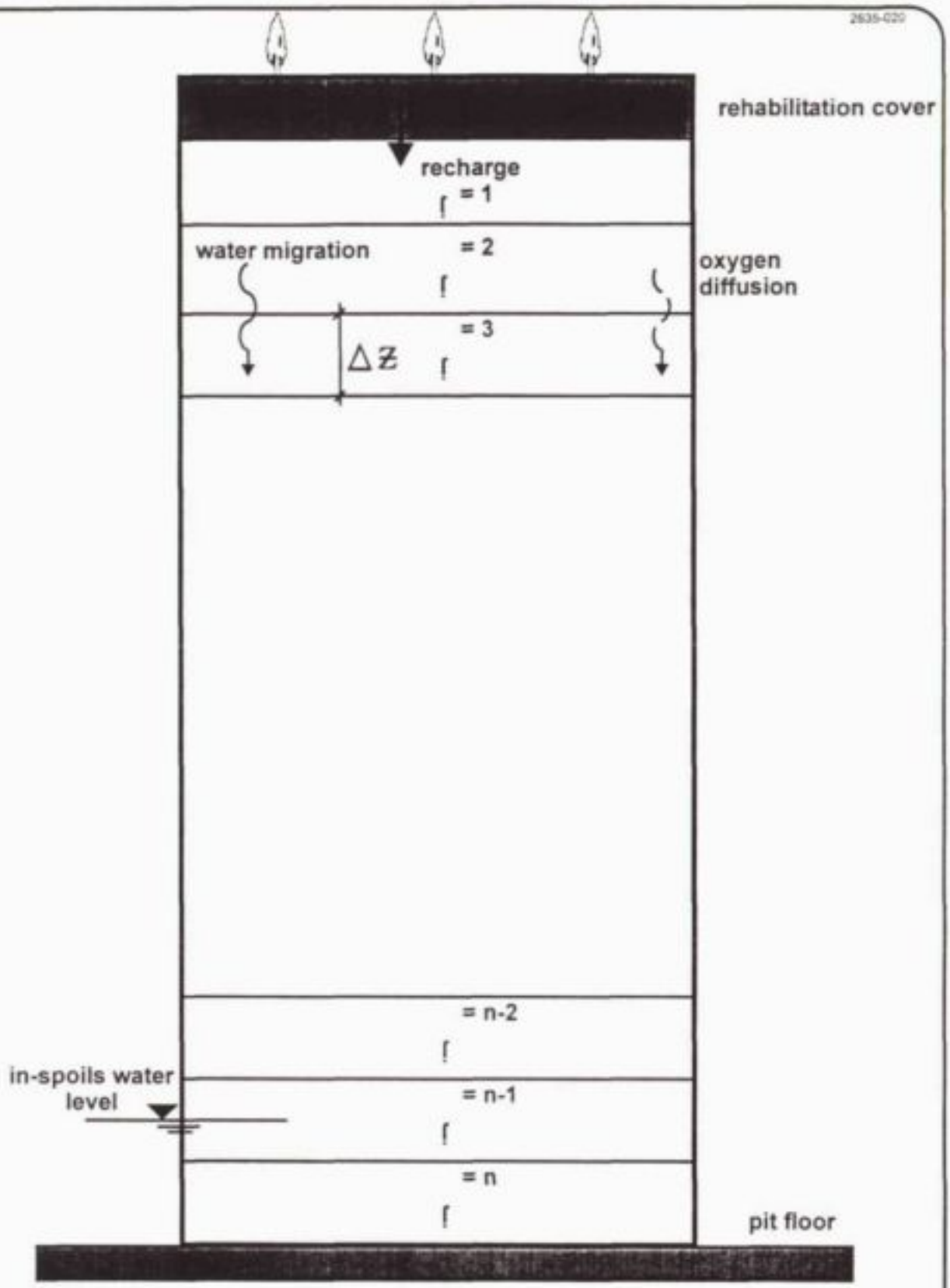

FIGURE 4.4.1 : DISCRETIZATION OF MINING BLOCK TO ALLOW VERTICAL SPATIAL MODELLING OF GAS MIGRATION

The general expression for the diffusion of oxygen is:

$$\Theta_a \cdot \frac{\partial C}{\partial t} = D_{f,o2} \cdot \frac{\partial^2 C}{\partial Z^2} - Q \qquad \textbf{(4.4.1.1)}$$

where :

C = oxygen concentration (kg/m^3)

Θ_a = air-filled porosity (m^3/m^3)

$D_{f,o2}$ = effective oxygen diffusion coefficient (m^2/sec)

Q = oxygen consumption rate ($kg/m^3/month$)

Z = vertical distance (m)

The geochemical processes of concern take place very slowly and can be approximated by a pseudo-steady state approach. This allows the simplification of the general diffusion equation to:

$$D_{f,o2} \cdot \frac{\partial^2 C}{\partial Z^2} = Q \qquad \textbf{(4.4.1.2)}$$

The effective oxygen diffusion coefficient in a spoils environment:

$$D_{f,o2} = \frac{\Theta_a . D_o}{\zeta} \qquad \textbf{(4.4.1.3)}$$

where:

D_o = oxygen diffusion coefficient in air

= 2.02×10^{-5} m^2/sec at 1 atm and 293K

ζ = tortuosity (default value = 5)

The air filled porosity, Θ_a, is a function of the spoils moisture content. We will assume that the spoils is saturated with moisture and the corresponding water volume (per unit volume of spoils) is:

$$V_{mois} = S_c . f_c . \rho_b + S_f . f_f . \rho_b \qquad \textbf{(4.4.1.4)}$$

The remaining air-filled porosity of the spoils is:

$$\Theta_a = \Theta_t - V_{mois} \qquad \textbf{(4.4.1.5)}$$

A numerical technique will be employed to compute the oxygen concentration at various levels in the spoils. A central difference equation will be used to approximate the second order differential:

$$\frac{\partial^2 C}{\partial Z^2} = \frac{C(Z_{n+1}) - 2C(Z_n) + C(Z_{n-1})}{(\Delta Z)^2} \qquad \textbf{(4.4.1.6)}$$

The general finite difference equation is then:

$$C(Z_{n+1}) - 2C(Z_n) + C(Z_{n-1}) = Q(Z_n).(\Delta Z)^2/D_t) \quad \textbf{(4.4.1.7)}$$

The finite difference equations for a mining block with ten spoils elements are summarised hereunder:

$$C_2 - 2C_1 + C_0 = Q_{12}.\Delta Z^2 / D_{t12}$$

$$C_3 - 2C_2 + C_1 = Q_{23}.\Delta Z^2 / D_{t23}$$

$$C_4 - 2C_3 + C_2 = Q_{34}.\Delta Z^2 / D_{t34}$$

$$C_5 - 2C_4 + C_3 = Q_{45}.\Delta Z^2 / D_{t45}$$

$$C_6 - 2C_5 + C_4 = Q_{56}.\Delta Z^2 / D_{t56}$$

$$C_7 - 2C_6 + C_5 = Q_{67}.\Delta Z^2 / D_{t67}$$

$$C_8 - 2C_7 + C_6 = Q_{78}.\Delta Z^2 / D_{t78}$$

$$C_9 - 2C_8 + C_7 = Q_{89}.\Delta Z^2 / D_{t89}$$

$$C_{10} - 2C_9 + C_8 = Q_{9,10}.\Delta Z^2 / D_{t9,10}$$

$$C_{11} - 2C_{10} + C_9 = Q_{10}.\Delta Z^2 / D_{t10}$$

$$C_{11} = C_9 \text{ (gradient across pit floor =0)}$$

The oxygen concentrations can be solved by the successive Liebman iteration procedure (Gerald, 1968), starting with assumed concentrations:

$$C_1 = \tfrac{1}{2}[C_2 + C_0 - Q_{12}(\Delta Z)^2/D_{t12}]$$

$$C_2 = \tfrac{1}{2}[C_3 + C_1 - Q_{23}(\Delta Z)^2/D_{t23}]$$

$$C_3 = \tfrac{1}{2}[C_4 + C_2 - Q_{34}(\Delta Z)^2/D_{t34}]$$

$$C_4 = \tfrac{1}{2}[C_5 + C_3 - Q_{45}(\Delta Z)^2/D_{t45}]$$

$$C_5 = \tfrac{1}{2}[C_6 + C_4 - Q_{56}(\Delta Z)^2/D_{t56}]$$

$$C_6 = \tfrac{1}{2}[C_7 + C_5 - Q_{67}(\Delta Z)^2/D_{t67}]$$

$$C_7 = \tfrac{1}{2}[C_8 + C_6 - Q_{78}(\Delta Z)^2/D_{t78}]$$

$$C_8 = \tfrac{1}{2}[C_9 + C_7 - Q_{89}(\Delta Z)^2/D_{t89}]$$

$$C_9 = \tfrac{1}{2}[C_{10} + C_8 - Q_{9,10}(\Delta Z)^2/D_{t9,10}]$$

$$C_{10} = \tfrac{1}{2}[C_9 + C_9 - Q_{10}(\Delta Z)^2/D_{t10}]$$

Note that the atmospheric concentration of oxygen is:

$$C_0 = 0{,}30 \text{ kg/m}^3 \text{ (P=1 atm and T = 293K)}$$

and that:

$$Q_{xy} = (Q_x + Q_y)/2 \quad \textbf{(4.4.1.8)}$$

$$D_{bxy} = (D_{bx} + D_{by})/2 \quad \textbf{(4.4.1.9)}$$

The oxygen consumption is based on the previous time step information on pyrite oxidation and ferrous iron oxidation:

$$Q_{py} = -\Delta X \cdot F_{py} \cdot \rho_b / b_{py} \quad \textbf{(4.4.1.10)}$$

where:

Q_{py} = oxygen consumption due to pyrite oxidation (kg/m^3/month)

ΔX = fractional change in pyrite content during previous time step

F_{py} = pyrite content of spoils ($kgFeS_2/kg$ spoils)

ρ_b = spoils bulk density (kg/m^3)

b_{py} = stoichiometric ratio

= 1,07 $kgFeS_2/kg\ O_2$

$$Q_{Fe} = -\Delta F / b_{Fe} \quad \textbf{(4.4.1.11)}$$

where:

Q_{Fe} = oxygen consumption due to ferrous iron oxidation (kg/m^3/month)

$\Delta F = \Delta F_f + \Delta F_{nf}$

and:

ΔF_f = change in ferrous iron mass in flushed fraction of spoils in previous time step (kgFe)

ΔF_{nf} = change in ferrous iron mass in non-flushed fraction of spoils in previous time step (kgFe)

b_{Fe} = stoichiometric ratio

= 6,97 $kgFe/kg\ O_2$

4.4.2 Pyrite oxidation rate

Several researchers have in the past made successful use of "shrinking core" type models to describe the oxidation of pyrite in the presence of an oxidant. The two common oxidants to be considered are oxygen and ferric iron. In both cases the pyrite oxidation rate can be expressed in the form:

$$\frac{dX}{dt} = \frac{-1}{2T_d(1-X_o) + T_c} = \Delta X \quad (dt = 1 \text{ month}) \quad \textbf{(4.4.2.1)}$$

where:

X = fraction of pyrite remaining (kg/kg)

X_o = fraction of pyrite remaining at start of time step (kg/kg)

T_d = time-related parameter, which is linked to oxidant diffusion processes

T_c = time-related parameter, which is linked to the reaction kinetics

This expression applies to the situation when the oxidant is present at a specified constant concentration. In the spoils environment, the oxidant concentration (availability) is variable and dependant on a number of environmental and kinetic constraints. The effect of oxidant concentration on pyrite oxidation rate can be accounted for by correcting the T_d and T_c parameters at every time step to reflect the actual conditions:

$$T_d = T_{do}/(C/C_o) \quad \textbf{(4.4.2.2)}$$

$$T_c = T_{co}/(C/C_o) \quad \textbf{(4.4.2.3)}$$

where:

T_{do} = model parameter at a reference oxidant concentration of C_o (month)

T_{co} = model parameter at a reference oxidant concentration of C_o (month)

C = actual oxidant concentration at the beginning of the time step (kg/m^3)

The default values for the model parameters are summarised below at the reference oxidant concentrations:

	Oxygen, O_2 (C_o = 0,30 kg.m^3)	**Ferric Iron, Fe^{3+} (C_o = 0,05 kg/m^3)**
T_{do}	1000 months	1000 months
T_{co}	150 months	200 months

The total pyrite oxidation rate is then:

$$\frac{dX}{dt} = -1/[2\,T_{d,O2}(1-Xo) + T_{c,O2}] - 1/[2\,T_{d,Fe}(1-Xo) + T_{c,Fe}] \quad \textbf{(4.4.2.4)}$$

where:

$T_{d,O2}$ = $T_{do,O2}/(C_{O2}/C_{o,O2})$

$T_{c,O2} = T_{oo,O2}/(C_{O2}/C_{o,O2})$

$T_{d,Fe} = T_{oo,Fe} / (C_{Fe}/C_{o,Fe})$

$T_{c,Fe} = T_{oo,Fe} / (C_{Fe}/C_{o,Fe})$

The model incorporates the catalytic effect of microbial action on pyrite oxidation. It is assumed that catalysis is particularly active in the pH range of $2 \leq pH \leq 4$. The catalytic effect on the pyrite oxidation rate can be expressed as:

$$\left(\frac{dX}{dt}\right)_{cat} \qquad \frac{dX}{dt}[1 + H(pH)] \qquad \textbf{(4.4.2.5)}$$

where:

$H(pH) = H[-0,35\,(pH)^2 + 2,3(pH) - 2,7]$

H = catalytic factor

= 10 (default)

This expression only applies in the pH range of $1,6 \leq pH \leq 5,0$.

The pyrite content in each cell of each mining block is quantified during the model initialisation of a simulation by:

- specifying a specific pyrite content, or
- generating a pyrite content from a probability distribution

The remaining pyrite is calculated after each time step:

$X_t = X_o + dX/dt$ **(4.4.2.6)**

where:

X_o = fraction of remaining pyrite at the start of the time step (kg/kg)

X_t = fraction of remaining pyrite at the end of the time step (kg/kg)

The mass of pyrite which has been oxidised in the time step:

$M_{py} = (X_o - X_t) \,.\, F_{py} \cdot \rho_b$ **(4.4.2.7)**

where:

M_{py} = pyrite mass oxidised in a time step ($kgFeS_2/m^3$ spoils/month)

F_{py} = natural pyrite content of spoils ($kgFeS_2$/kg spoils)

ρ_b = spoils bulk density (kg/m^3)

4.4.3 Pyrite Oxidation Products

The oxidation of pyrite will release oxidation products to the spoils water in accordance with the equation:

$$FeS_2 + 3½O_2 + H_2O \rightarrow Fe^{2+} + 2SO_4^{2-} + 2H^+$$

The oxidation of one mole pyrite will release:

- 1 mole Fe^{2+}
- 2 mole SO_4^{2-}
- 2 mole H^+

Therefore, the oxidation of one kg pyrite will release:

- 0,47 kg Fe^{2+}
- 1,60 kg SO_4^{2-}
- 0,0167 kg H^+

and:

$M_{Fe} = 0,47.M_{py}$ kg product/m^3 spoils/month

$M_{SO4} = 1,60.M_{py}$ kg product/m^3 spoils/month

$M_H = 0,0167M_{py}$ kg product/m^3 spoils/month

The hydrodynamic description of the spoils water migration distinguishes between two fractions in the spoils body:

- A fraction (f_i) of the spoils mass **in contact** with the migrating spoils water, and from which pyrite oxidation products are flushed.
- The remaining fraction (1 - f_i) of the spoils mass which is **not in contact** with migrating spoils water and from which the pyrite oxidation products are not flushed.

A water balance is compiled over the spoils fraction in contact with the migrating spoils water (refer to **Section 4.3** of the report), which incorporates for **each spoils element:**

- V_o = water volume at the beginning of the time step (m^3)
- V_i = water volume at the end of the time step (m^3)
- Q_{in} = influent flow from the next upper spoils element (m^3/month)
- Q_{out} = outflow to the next lower spoils element (m^3/month)

The mass balance for a chemical constituent in the flushed fraction of the spoils:

$$\frac{d(VC)}{dt} = Q_{in}.C_{in} - Q_{out}.C_{out} \pm R_c.V \qquad \textbf{(4.4.3.1)}$$

where:

V = water volume in the flushed part of the spoils (m^3)

C = chemical constituent concentration (kg/m^3)

C_{in} = influent flow chemical concentration (kg/m^3)

C_{out} = outflow chemical concentration (kg/m^3)

R_c = chemical reaction rate

The spoils element can be approximated as completely mixed from a chemical reaction and concentration perspective in which case the following approach can be adopted:

- The initial mass of a chemical in the spoils water, $V_o.C_o$.
- The further mass of a chemical introduced by the influent flow, $Q_{in}.C_{in}$.
- The total initial spoils water volume ($V_o + Q_{in}$) then contains a chemical mass ($V_o.C_o + Q_{in}.C_{in}$) at a concentration of ($V_o.C_o + Q_{in}.C_{in}$) / ($V_o + Q_{in}$).

The pyrite oxidation products (Fe^{2+}, SO_4^{2-}, H^+) are now introduced into this spoils water volume to increase the concentrations of these specific ionic species. It must be kept in mind that only a fraction (f_t) of the total pyrite oxidation products will be introduced into the active spoils water volume. Thus:

- **Ferrous iron** **(4.4.3.2)**

$$M_{Fe} = V_o.C_{Fe,o} + Q_{in}.C_{Fe,in} + 0{,}47.f_t.M_{py}\,(A\_Z)$$

$$C_{Fe} = M_{Fe} / (V_o + Q_{in})$$

- **Sulphate** **(4.4.3.3)**

$$M_{SO4} = V_o.C_{SO4,o} + Q_{in}.C_{SO4,in} + 1{,}60.f_t.M_{py}\,(A\_Z)$$

$$C_{SO4} = M_{SO4} / (V_o + Q_{in})$$

- **Hydrogen Ion** **(4.4.3.4)**

$$M_H = V_o.C_{H,o} + Q_{in}.C_{H,in} + 0{,}0167.f_t.M_{py}\,(A\_Z)$$

$$C_H = M_H / (V_o + Q_{in})$$

The increased concentration of these ionic species will result in a chemical imbalance. Neutralisation reactions, triggered by the release of acidity, are of specific importance. It has been observed in leach column tests of spoils material containing an excess of neutralisation capacity, that dolomite or

calcite will react in response to the presence of acidity. Spoils contain a variety of neutralising minerals including calcite, dolomite, feldspars etc. The model uses a complex dolomitic mineral of the general composition

$$Ca_x.Mg_y\ .\ CO_3$$

where:

$$x + y = 1$$

for the purposes of modelling. The calcium (and by implication magnesium) content of the neutralising mineral is specified. One can also specify a pseudo-stability constant for this neutralising mineral. Neutralisation will obviously only take place for as long as an excess of the neutralising mineral is available.

A new chemical equilibrium is calculated taking into account the redox potential in the spoils element (primarily a function of the local oxygen concentration), the chemical specification of the different ionic species and the chemical precipitation as insoluble salts. This new equilibrium then establishes the chemical concentrations at the end of the time step and in the outflow from the spoils element.

The water content of the spoils fraction not in contact with the migrating spoils water is assumed to be constant. This water volume is calculated on the basis of the moisture content:

$$V_{stag} = [S_c.f_c\ (1 - f_t)\ .\ \rho_b + S_t.f_t\ (1-f_t).\rho_b]\ A.\ \Delta Z \quad \textbf{(4.4.3.5)}$$

The pyrite oxidation products in the spoils fraction is assumed to accumulate in the available water volume. The following approach is adopted to calculate the chemical species concentrations in the non-flushed spoils fraction:

- The initial mass of a chemical in the spoils water = $V_{stag}.C_o$.
- The pyrite oxidation products (Fe^{2+}, SO_4^{2-}, H^+) are now introduced into this spoils water volume to increase the concentration of these specific ionic species. The specific ionic species will increase as follows:
- **Ferrous iron**

$$M_{Fe} = V_{stag}.C_{Fe,0} + 0{,}47\ (1 - f_t)\ M_{py}\ (A.\ \Delta Z)$$

$$C_{Fe} = M_{Fe}/V_{stag}$$

- **Sulphate**

$$M_{SO4} = V_{stag}.C_{SO4,0} + 1{,}60\ (1 - f_t)\ M_{py}\ (A.\ \Delta Z)$$

$$C_{SO4} = M_{SO4}/V_{stag}$$

- **Hydrogen ion**

$$M_H = V_{stag}.C_{H,0} + 0{,}0167\ (1 - f_t)\ M_{py}\ (A.\ \Delta Z)$$

$$C_H = M_H/V_{stag}$$

An inventory is kept of the following mass components:

- pyrite which can be oxidised
- neutralisation mineral
- chemical precipitates such as $CaSO_4.2H_2O$, $CaCO_3$, etc.

4.4.4 Spoils Water Chemistry

Complexing in the spoilswater solution occurs between all the major cationic species (Ca^{2+}, Mg^{2+}, Fe^{2+} and Fe^{3+}) and the anionic species SO_4^{2-}, CO_3^{2-} and OH^-. In speciating the solution, the principal cations are considered to be affected only via complexing with SO_4^{2-} and for Fe^{3+} also with OH^-. That is, complexing with CO_3^{2-}, and for Mg^{2+}, Ca^{2+} and Fe^{2+} with OH^-, is considered to have no affect on the principal cationic species. The geochemical model incorporates the following complexation reactions:

$$Ca^{2+} + SO_4^{2-} \rightleftarrows CaSO_4^{\circ},\ K_{CaS} = 10^{2.32}$$

$$Mg^{2+} + SO_4^{2-} \rightleftarrows MgSO_4^{\circ},\ K_{MgS} = 10^{2.23}$$

$$Fe^{2+} + SO_4^{2-} \rightleftarrows FeSO_4^{\circ},\ K_{Fe2S} = 10^{2.20}$$

$$Fe^{3+} + SO_4^{2-} \rightleftarrows FeSO_4^{+},\ K_{Fe3S} = 10^{3.96}$$

$$Fe^{3+} + OH^- \rightleftarrows FeOH^{2+},\ K_{Fe3OH1} = 10^{-16.94}$$

$$Fe^{3+} + 2OH^- \rightleftarrows Fe(OH)_2^{+},\ K_{Fe3OH2} = 10^{-33.70}$$

$$Fe^{3+} + 3OH^- \rightleftarrows Fe(OH)_3^{\circ},\ K_{Fe3OH3} = 10^{-54.0}$$

Mass balance relationships for the principal species are thus expressed in terms of the molar concentrations:

$$[Ca^{2+}]_t = [Ca^{2+}]_f + [CaSO_4^{\circ}]$$

$$[Mg^{2+}]_t = [Mg^{2+}]_f + [MgSO_4^{\circ}]$$

$$[Fe^{2+}]_t = [Fe^{2+}]_f + [FeSO_4^{\circ}]$$

$$[Fe^{3+}]_t = [Fe^{3+}]_f + [FeSO_4^{+}] + [FeOH^{2+}] + [Fe(OH)_2^{+}] + [Fe(OH)_3^{\circ}]$$

$$[Fe]_t = [Fe_{2+}]_t + [Fe^{3+}]_t$$

$$[SO_4^{2-}]_t = [SO_4^{2-}]_f + [CaSO_4^{\circ}] + [MgSO_4^{\circ}] + [FeSO_4^{\circ}] + [FeSO_4^{+}]$$

where

subscript '$_t$' = refers to total species (free and complexed)

subscript '$_f$' = refers to free species

For each of the sulphate complexes, an equilibrium relationship links free and complexed species, as follows:

$[Ca^{2+}]_f[SO_4^{2-}]_f / [CaSO_4^\circ] = K_{CaS} / f_\sigma^2 = K'_{CaS}$

$[Mg^{2+}]_f [SO_4^{2-}]_f / [MgSO_4^\circ] = K_{MgS} / f_\sigma^2 = K'_{MgS}$

where

K_{MgS} = complexation constant between Mg^{2+} and SO_4^{2-}

K_{CaS} = complexation constant between Ca^{2+} and SO_4^{2-}

and similarly

$[Fe^{2+}]_f [SO_4^{2-}]_f / [FeSO_4^\circ] = K_{Fe2S} / f_\sigma^2 = K'_{Fe2S}$

and

$[Fe^{3+}] [SO_4^{2-}] / [FeSO_4^+] = K_{Fe3S} f_m / (f_t . f_\sigma)$

$[Fe^{3+}] [OH^-] / [FeOH]^{2+} = K_{Fe3OH1} . f_\sigma / (f_t . f_m)$

$[Fe^{3+}] [OH^-]^2 / [Fe(OH)_2^+] = K_{Fe3OH2} / (f_t . f_m^2)$

$[Fe^{3+}] [OH^-]^3 / [Fe(OH)_3^\circ] = K_{Fe3OH3} / (f_t . f_m^3)$

where

f_t, f_σ, f_m = tri, di and monovalent activity coefficients

Recognizing that spoils water pH governs the $[OH^-]$ concentration and that the principal species Fe^{3+} is significantly affected by complexing with OH^-, speciation of the principal species will be pH dependant, i.e.

$pH = -\log_{10} (H^+)$

where

(H^+) = activity of H^+ ion = $f_m[H^+]$

and, $(H^+) [OH^-]$ = $K_w / f_m = K_w'$ ($K_w = 10^{-14}$)

i.e.

$$[Fe^{3+}]_t = [Fe^{3+}]_f \left\{ 1 + \frac{[OH^-]}{K^1_{Fe3OH1}} + \frac{[OH^-]^2}{K^1_{Fe3OH2}} + \frac{[OH^-]^3}{K^1_{Fe3OH3}} + \frac{[SO_4^{2-}]_f}{K^1_{Fe3S}} \right\}$$

$$[Fe^{3+}]_t = [Fe^{3+}]_f \left\{ 1 + \frac{K^1_w}{(H^+)K^1_{Fe3OH1}} + \frac{(K^1_w)^2}{(H^+)^2 K^1_{Fe3OH2}} + \frac{(K^1_w)^3}{(H^+)^3 K^1_{Fe3OH3}} + \frac{[SO_4^{2-}]_f}{K^1_{Fe3S}} \right\}$$

In addition, the relative concentrations of $[Fe^{2+}]_f$ and $[Fe^{3+}]$ depend on both pH and redox potential as determined by the partial pressure of oxygen:

$$Fe^{2+} + H^+ + \tfrac{1}{4} O_2 \rightarrow Fe^{3+} + \tfrac{1}{2} H_2O$$

$$\text{i.e. } [Fe^{3+}]_f / ([Fe^{2+}]_f \cdot (H^+) \cdot (pO_2)^{\frac{1}{4}}) = \frac{K_{ox} \cdot f_e}{f_t} = K^1_{ox}$$

$$\text{i.e. } [Fe^{3+}]_f / [Fe^{2+}]_f = K^1_{ox} \cdot (H^+)(pO_2)^{\frac{1}{4}}$$

If the spoils water pH, redox potential (O_2), total dissolved iron, $[Fe]_t$ and free $[SO_4^{2-}]_f$ species concentrations are known (via speciation of principal ionic matrix), then it is possible to determine $(Fe^{3+}]_f$ and $[Fe^{2+}]_f$, i.e. from the following expressions:

$$[Fe]_t = [Fe^{3+}]_t + [Fe^{2+}]_t$$

$$= [Fe^{3+}]_f \left\{ 1 + \frac{K^1_w}{(H^+)K^1_{Fe3OH1}} + \frac{(K^1_w)^2}{(H^+)^2 K^1_{Fe3OH2}} + \frac{(K^1_w)^3}{(H^+)^3 K^1_{Fe3OH3}} + \frac{[SO_4^{2-}]_f}{K^1_{Fe3S}} \right\}$$

$$+ \quad \frac{[Fe^{3+}]_f}{K^1_{ox}(H^+)(pO_2)^{\frac{1}{4}}} \cdot \left\{ 1 + \frac{[SO_4^{2-}]_f}{K^1_{Fe2S}} \right\}$$

Hence, if $[Fe]_t$ is known, solve for $[Fe^{3+}]_f$ and then for $[Fe^{2+}]_f$ i.e.

$$[Fe^{2+}]_f = [Fe^{3+}]_f / (K^1_{ox} \cdot (H^+)(pO_2)^{\frac{1}{4}})$$

Alkalinity in water containing carbonate, iron and sulphate species

Alkalinity is defined as the proton (H^+) accepting capacity relative to selected reference species (i.e. reference species for those subsystems capable of accepting/donating protons). The three subsystems capable of H^+ acceptance are

- the carbonate subsystem $H_2CO_3^* / HCO_3^- / CO_3^{2-}$,
- the ferric system ($Fe^{3+} / FeOH^{2+} / Fe(OH)_2^+ / Fe(OH)_3^\circ$)
- the sulphate system (SO_4^{2-} / HSO_4^-)
- water system (H^+ / OH^-).

The following chemical reactions (with corresponding equilibrium constants) are of significance in calculating spoilswater alkalinity:

$HCO_3^- + H^+ \rightleftarrows H_2CO_3^*, K_{C1}$

$H_2CO_3^* \rightleftarrows CO_2 + H_2O, K_{HC}$

$Fe^{3+} + OH^- \rightleftarrows Fe(OH)^{2+}, K_{Fe3OH1}$

$Fe^{3+} + 2OH^- \rightleftarrows Fe(OH)^{2+}, K_{Fe3OH2}$

$Fe^{3+} + 3OH^- \rightleftarrows Fe(OH)_3^\circ, K_{Fe3OH3}$

$H^+ + OH^- \rightleftarrows H_2O, K_w = 10^{-14}$

$SO_4^{2-} + H^+ \rightleftarrows HSO_4^-, K_{HS} = 10^{-1.14}$

For the sake of convenience, we select $H_2CO_3^*$, Fe^{3+}, SO_4^{2-} and pure water as reference species and define total alkalinity (TAlk) as follows:

$$TAlk = Alk\ H_2CO_3^* + Alk\ Fe^{3+} + Alk\ SO_4^{2-} + Alk\ H_2O$$

where

$$Alk\ H_2CO_3^* = 2[CO_3^{2-}]_t + [HCO_3^-]_t$$

$$Alk\ Fe^{3+} = [Fe(OH)^{2+}] + 2[Fe(OH)_2^+] + 3[Fe(OH)_3^\circ]$$

$$Alk\ SO_4^{2-} = -[HSO_4^-]$$

$$Alk\ H_2O = [OH^-] - [H^+]$$

In the region $pH \leq 8$, which is typical of spoils water:

$Alk\ H_2CO_3^* \simeq [HCO_3^-]_t = [HCO_3^-]$ since HCO_3^- does not complex significantly

$Alk\ H_2O \simeq -[H^+]$

and $Alk\ Fe^{3+}$ and $Alk\ SO_4^{2-}$ are as above, i.e.

$$TAlk \simeq [HCO_3^-] + \{[FeOH^{2+}] + 2[Fe(OH)_2^+] + 3[Fe(OH)_3^\circ]\} - [HSO_4^-] - [H^+]$$

If $[Fe^{3+}]_t$, pCO_2 and $[SO_4^{2-}]$ are known then:

- $[HCO_3^-] = K^1_{C1} \cdot K_{HC} \cdot pCO_2 / (H^+)$

  where

  K^1_{C1} = $K_{C1}/f_m = (H^+)\,[HCO_3^-] / [H_2CO_3^*]$

  K_{HC} = Henry's constant

  = $[H_2CO_3^*] / pCO_2$

  pCO_2 = partial pressure of CO_2 (atmosphere)

  thus

  Alk $H_2CO_3^*$ = $K^1_{C1} \cdot K_{HC} \cdot pCO_2 / (H^+)$

- Alk $Fe^{3+} = [FeOH^{2+}] + 2[Fe(OH)_2^+] + 3[Fe(OH)_3^\circ]$

$$= [Fe^{3+}]_f \left\{ \frac{K^1_w}{(H^+)K_{Fe3OH1}} + \frac{2(K^1_w)^2}{(H^+)^2 K_{Fe3OH2}} + \frac{3(K^1_w)^3}{(H^+)^3 K_{Fe3OH3}} \right\}$$

  and $[Fe^{3+}]_f$ is given by the relationship linking total dissolved iron, redox potential and pH

- Alk SO_4^{2-} = —$[HSO_4]$

  = —$(H^+)[SO_4^{2-}]_f / K^1_{HS}$

These equations indicate that if total dissolved iron, Fe_t, pH, free sulphate, $[SO_4^{2-}]_f$, pO_2 and pCO_2 are known, then one can calculate TAlk. This observation forms the basis for an aqueous-gas phase algorithm for determining pH if the TAlk value is known.

Algorithm I to calculate pH and species (free and complexed) concentrations for aqeuous-gas equilibrium

Input : <u>total</u> species concentrations for sulphate $[SO_4^{2-}]_t$, ferric iron $[Fe^{3+}]_t$, ferrous iron $[Fe^{2+}]_t$, calcium $[Ca^{2+}]_t$, magnesium $[Mg^{2+}]_t$ and total alkalinity [TAlk].

pO_2 and pCO_2, and ionic strength μ

$[Fe]_t = [Fe^{3+}]_t + [Fe^{2+}]_t$

1. Calculate activity coefficients f_m, f_{CI} and f_i using Davis equation

2. Calculate apparent equilibrium constant (K) values

3. Calculate pH {i.e. (H^+)}

   3.1 Assume (H^+) - initial guess should be too large, say $(H^+) = 0{,}01$ moles/l

3.2 Calculate $[Fe^{3+}]_f / [Fe^{2+}]_f$

i.e. $[Fe^{3+}]_f/[Fe^{2+}]_f = K'_{ox} . (pO_2)^{¼} . (H^+)$

3.3 Speciate principal ionic species (i.e. calculate free and complexed ferric iron, ferrous iron, calcium, magnesium and sulphate species):

Assume $[SO_4^{2-}]_f = [SO_4]_t$ i.e. $[SO_4^{2-}]_f$ too large in first approximation

$$[Ca^{2+}]_f = [Ca^{2+}]_t / (1 + [SO_4^{2-}]_f / K^1_{CaS})$$

$$[Mg^{2+}]_f = [Mg^{2+}]_t / (1 + [SO_4^{2-}]_f / K^1_{MgS})$$

$$[Fe^{3+}]_f = [Fe]_t / \left\{ 1 + \frac{K^1_w}{(H^+)K^1_{Fe3OH1}} + \frac{(K^1_w)^2}{(H^+)^2 K^1_{Fe3OH2}} + \frac{(K^1_w)^3}{(H^+)^3 K^1_{Fe3OH3}} \right\}$$

$$+ \quad \frac{[SO_4^{2-}]_f}{K^1_{Fe3S}} + \left(1 + \frac{[SO_4^{2-}]_f}{K_{Fe2S}} \right) / (K^1_{ox} \cdot pO_2^{½} (H^+))$$

$$[Fe^{2+}]_f = [Fe^{3+}]_f / \{K^1_{ox} \cdot pO_2^{½} (H^+)\}$$

$$CALFe^{2+}_t = [Fe^{2+}]_f (1 + [SO_4^{2-}]_f / K^1_{Fe2S})$$

Calculate $[SO_4^{2-}]_f$ for assumed value of $[SO_4^{2-}]_f$:

$$CALSO_4 = [SO_4^{2-}]_f \left\{ 1 + \frac{[Ca^{2+}]_f}{K^1_{CaS}} + \frac{[Mg^{2+}]_f}{K^1_{MgS}} + \frac{[Fe^{2+}]_f}{K^1_{Fe2S}} + \frac{[Fe^{3+}]_f}{K^1_{Fe3S}} \right\}$$

If $CALSO_4 > [SO_4]_t$ then reduce $[SO_4^{2-}]_f$

If $CALSO_4 < [SO_4]_t$ then increase $[SO_4^{2-}]_f$

Repeat the iteration from step 3.2

3.4 Adjust TAlk for the effect of oxidizing Fe^{2+} to Fe^{3+} ie.

$Fe^{2+} + H^+ + ¼O_2 \rightarrow Fe^{3+} + ½H_2O$

$\therefore \Delta Alk = [Fe^{2+}]_t - CALFe^{2+}$

$TAlk = TAlk + \Delta Alk$

3.5 For the assumed (H^+) value calculate alkalinity:

$AlkH_2CO_3 = [HCO_3^-] = K_{HC} . K_{C1}^{-1} . pCO_2/(H^+)$

$$AlkH_2O = -[H^+]$$

$$AlkFe = [Fe^{3+}]_T \left(\frac{K_w^1}{(H^+)K_{Fe3OH1}} + \frac{(K_w^1)^2}{(H^+)^2 K_{Fe3OH2}^1} + \frac{(K_w^1)^3}{(H^+)^3 K_{Fe3OH3}^1} \right)$$

$$AlkSO_4 = -(H^+)\,[SO_4^{2-}]_T / K'_{HS}$$

$$CALTAlk = AlkH_2CO_3 + AlkH_2O + AlkFe + AlkSO_4$$

3.6 Compare the calculated value for TAlk with input value (calculated TAlk varies monotorically with pH):

If CALTAlk < TAlk, reduce (H^+)

If CALTAlk > TAlk, increase (H^+)

Repeat the iteration from step 3.2.

3.7 $pH = -\log_{10}(H^+)$

Precipitation / dissolution of $Fe(OH)_3$ i.e. Fe_2O_3

Algorithm I determines free and complexed species concentrations in any spoils element under equilibrium conditions between species in the aqueous phase and gas phase (O_2 and CO_2). The solution may now be supersaturated with respect to any of a number of minerals, including $Fe(OH)_3$, $CaCO_3$, $FeCO_3$ and $CaSO_4$. These four minerals are considered as potential precipitants.

With regard to the above four minerals, only $Fe(OH)_3$ is likely to have a major impact on the principal ionic equilibrium and complexed species belonging to this matrix. This arises for two reasons. Firstly, pyrite oxidation is a major reaction under oxidative conditions. Secondly, $Fe(OH)_3$ is very insoluble under neutral and alkaline pH conditions. Consequently, and for the sake of shortening computation time, precipitation of $Fe(OH)_3$ was interlinked with dolomite, calcite, siderite dissolution and Algorithm I. Precipitation of the remaining minerals will be considered to affect only pH and the species concentrations of the dissolving mineral. For example, if $CaCO_3$ precipitation occurs, it will be assumed that sulphate and iron species are unaffected by this reaction.

Model for $Fe(0H)_3$ (i.e. Fe_2O_3) Precipitation

After completion of Algorithm I, the model assesses the saturation state with respect to $Fe(OH)_3$. $[Fe^{3+}]_T$ and $[OH^-]$, via pH, form part of the output from Algorithm I.

If $Fe(OH)_3$ supersaturated conditions prevail then this mineral will precipitate until saturation is attained. In this process, the only changes in $[Fe^{3+}]_T$ and Alkalinity arise from $Fe(OH)_3$ precipitation. Carbonate mineral dissolution and equilibrium with O_2 are not considered here. Consequently, the parameter $(TAlk - 3[Fe^{3+}]_T)$ remains constant and equal to the input value. Furthermore, in determining the saturation state established, (H^+) is varied and $(TAlk - 3[Fe^{3+}]_T)$

determined and compared with the input value. Because calculated (TAlk—$3[Fe^{3+}]_t$) varies monotonically with (H^+) (i.e. increasing (H^+) decreases calculated (TAlk—$3[Fe^{3+}]_t$) and vice versa), (H^+) can be systematically varied until input and calculated values are equal.

Once the saturated state has been determined, if the solution was found to be supersaturated with $Fe(OH)_3$ after Algorithm I then there will be a decrease in TAlk and this will cause dissolution of a carbonate mineral, i.e. $Fe^{3+} + 3MCO_3 + 3H^+ \rightarrow Fe(OH)_3 + 3M^{2+} + 3CO_2$. Thus, Alkalinity will increase by three times the molar mass of $Fe(OH)_3$ precipitated. Alkalinity and carbonate mineral in storage are then adjusted and Algorithm I repeated. Algorithm I is repeated once and thereafter Algorithm III is executed (i.e. $CaCO_3$ and $FeCO_3$ precipitation/dissolution). This repetition of Algorithm I is executed, whether carbonate mineral is in storage or not.

If $Fe(OH)_3$ undersaturated conditions prevail (i.e. at the start of this Algorithm II) and if no $Fe(OH)_3$ is in storage, the Algorithm II is not executed. If $Fe(OH)_3$ is in storage, the Algorithm II is carried out to obtain the output species concentrations.

$[Fe^{3+}]_t [OH^-]^3 = K_{spFeOH3} / (f_1 f_m^3) = K'_{spFeOH3}$ ($K_{spFeOH3} = 10^{-45.2}$)

Algorithm II for $Fe(OH)_3$ Precipitation / Dissolution

Input from Algorithm I includes $[SO_4^{2-}]_t$, $[Fe^{2+}]_t$, $[Fe^{2+}]_t$, $[Fe^{3+}]_t$, $[Fe^{3+}]_t$, TAlk, pH and also pCO_2.

The algorithm is based on the following precipitation reaction:

$Fe^{3+} + 3OH^- \_ Fe(OH)_3(s)$, $K_{spFeOH3} = 10^{-45.2}$

1. Determine saturation state:

   $(H^+) = 10^{-pH}$ and $[OH^-] = K'_w/(H^+)$

   Product = $[Fe^{3+}]_t [OH^-]^3$

   If Product > $K'_{SpFeOH3}$, then supersaturation exists and $ALKM_3Fe_3T$ = TAlk-$3[Fe^{3+}]_t$

   Continue to step (2) only if supersaturation exists or undersaturation exists with some $Fe(OH)_3$ in storage.

2. Determine equilibrium state of $Fe(OH)_3$ saturation :

   2.1 Assume $(H^+) = 10^{-pH}$

   2.2 $[Fe^{3+}]_t = K'_{SpFeOH3} (H^+)^3 / (K'_w)^3$

   2.3 $CAL[Fe^{3+}]_T$ equals calculated $[Fe^{3+}]_t$

$$CAL[Fe^{3+}]_t = [Fe^{3+}]_t \cdot \left\{ 1 + \frac{K'_w}{K'_{Fe3OH1}(H^+)} + \frac{(K'_w)^2}{K'_{Fe3OH2}(H^+)^2} + \frac{(K'_w)^3}{K'_{Fe3OH3}(H^+)^3} + \frac{[SO_4^{2-}]_t}{K'_{Fe3S}} \right\}$$

2.4 Calculate TAlk (i.e. CALTALK)

$AlkH_2CO_3 = K_{HC} \cdot K^1_{c1} \cdot pCO_2 / (H^+)$

$$AlkFe^{3+} = [Fe^{3+}]_t \left\{ \frac{K^1_w}{K^1_{Fe3OH1}(H^+)} + \frac{2(K^1_w)^2}{K^1_{Fe3OH2}(H^+)^2} + \frac{3(K^1_w)^3}{K^1_{Fe3OH3}(H^+)^3} \right\}$$

$AlkSO_4^{2-} = \quad -[SO_4^{2-}]_t (H^+) / K^1_{HS}$

$AlkH_2O = \quad -(H^+)$

$CALTALK = \quad AlkH_2CO_3 + AlkFe^{3+} + AlkSO_4^{2-} + AlkH_2O$

2.5 CAL(ALKM3Fe3T) = CALTALK - 3.CAL$[Fe^{3+}]_t$

2.6 If CAL(ALKM3Fe3T) > ALKM3Fe3T

increase (H^+)

If CAL(ALKM3Fe3T) < ALKM3Fe3T

decrease (H^+)

3. Calculate $pH = -\log_{10} (H^+)$

DELTA = $[Fe^{3+}]_t$ - CAL$[Fe^{3+}]_t$

Proceed with the following steps, if dolomite (x = 1, y = 1) is available in storage:

TALK = CALTALK + 3*DELTA

$[Ca^{2+}]_t = [Ca^{2+}]_t + 1{,}5$*DELTA

$[Mg^{2+}]_t = [Mg^{2+}]_t + 1.5$*DELTA

Adjust $CaMg(CO_3)_2$ in storage by -3 DELTA to account for $MgCa(CO_3)_2$ dissolution taking place

else, if $CaCO_3$ or $FeCO_3$ in storage:

TALK = TALK + 3*DELTA

$[Ca^{2+}]_t = [Ca^{2+}]_t + 3$*DELTA

else

$[Fe^{2+}]_t = [Fe^{2+}]_t + 3$*DELTA

Adjust $CaCO_3$ or $FeCO_3$ in storage by -3DELTA

4. $[Fe^{3+}]_t = CAL[Fe^{3+}]_t$ Only if DELTA is positive *OR*
DELTA negative and $Fe(OH)_3$ in storage

$[Fe]_t = [Fe^{3+}]_t + [Fe^{2+}]_t$

5. Repeat Algorithm I and then bypass Algorithm II to go to Algorithm III.

$CaCO_3$ and/or $FeCO_3$ Precipitation/dissolution

Solubility product relationships for these two minerals are

$[Ca^{2+}]_t [CO_3^{2-}]_t = K_{spCaCO3} / f_\sigma^2 = K'_{spCaCO3}$

$[Fe^{2+}]_t [CO_3^{2-}]_t = K_{spFeCO3} / f_\sigma^2 = K'_{FeCO3}$

After the sequence of computations involving Algorithm I and II has been completed precipitation and/or dissolution potentials for the above minerals are determined. If supersaturated, mineral is allowed to precipitate and pH, $[Ca^{2+}]_t$, $[Fe^{2+}]_t$ and TAlk are adjusted. If undersaturated, mineral is allowed to dissolve (only if in storage) and pH, $[Ca^{2+}]_t$, $[Fe^{2+}]_t$ and TAlk adjusted; if minerals are not in storage, no adjustment to pH, Ca_t or Fe^{2+}_t, are made.

As for $Fe(OH)_3$ precipitation, determination of saturated equilibrium state is complicated by the fact that pH changes with precipitation / dissolution. The rule of a solution algorithm (under prescribed CO_2 conditions) hinges around the fact that (TAlk-2$[Ca^{2+}]_t$) and (TAlk-2$[Fe^{2+}]_t$) remain constant with $CaCO_3$ and $FeCO_3$ precipitation/dissolution. Consequently, the solution is effected by adjusting pH and calculating (TAlk-2$[Me^{2+}]_t$) value for saturated equilibrium. Because the parameter (TAlk-2$[Me^{2+}]_t$) changes monotonically with change in pH, successive approximation on pH can be effected until the calculated value equals the input value.

Algorithm III for $CaCO_3$ Precipitation/dissolution

Input after completion of Algorithms I & II :

pH, $[Ca^{2+}]_t$, $[Ca^{2+}]_t$, $[Fe^{3+}]_t$, TAlk, $[SO_4^{2-}]_t$ and relevant equilibrium constants

For the carbonate system equilibrium:

$(H^+) [HCO_3^-] / [H_2CO_3] = K_{c1}/f_m = K'_{c2}$

$(H^+) [CO_3^{2-}] / [HCO_3^-] = f_m.K_{C2}/f_\sigma = K'_{C2}$

1. Determine input value for Alk-2$[Ca^{2+}]_t$ i.e.

ALKM2TCA = TAlk-2$[Ca^{2+}]_t$

2. Determine $CaCO_3$ saturation state:

2.1 Assume (H^+) = 0,01 mole

2.2 Calculate alkalinity for assumed (H^+) value

$$\mathrm{AlkH_2CO_3} = K_{HC} \cdot K^1_{c1} \cdot pCO_2 / (H^+)$$

$$\mathrm{AlkFe^{3+}} = [Fe^{3+}]_f \left\{ \frac{K^1_w}{K_{Fe3OH1}(H+)} + \frac{2(K^1_w)^2}{K^1_{Fe3OH2}(H^-)^2} + \frac{3(K^1_w)^3}{K_{Fe3OH3}(H^-)^3} \right\}$$

$$\mathrm{AlkSO_4} = -(H^+) \cdot [SO^{2-}_4]_f / K^1_{HS}$$

$$\mathrm{AlkH_2O} = -(H^+)$$

$$\mathrm{CAL(TALK)} = \mathrm{AlkH_2CO_3} + \mathrm{AlkFe^{3+}} + \mathrm{AlkSO_4} + \mathrm{AlkH_2O}$$

2.3 Calculate total calcium at $CaCO_3$ saturation

$$[HCO^-_3]_f = K_{HC} K^1_{C1} \cdot pCO_2 / (H^+)$$

$$[CO^{2-}_3]_f = K^1_{C2} \cdot [HCO^-_3] / (H^+)$$

$$\mathrm{CAL}[Ca^{2+}]_f = K^1_{SpCaCO3} / [CO^{2-}_3]_f$$

$$\mathrm{CAL}[Ca^{2+}]_t = \mathrm{CAL}[Ca^{2+}]_f \left\{ 1 + \frac{[SO^{2-}_4]_f}{K^1_{CaS}} \right\}$$

2.4 Calculate CAL(TALK) - 2CAL $[Ca^{2+}]_t$

If CAL(ALKM2CA) > ALKM2TCA

then reduce (H^+) and vice versa

3. Determine $CaCO_3$ precipitation / dissolution

DPOT = CAL$[Ca^{2+}]_t$ — $[Ca^{2+}]_t$

If DPOT is negative ($CaCO_3$ precipitates):

3.1 Put DPOT into $CaCO_3$ storage

3.2 Adjust the following parameters

$[Ca^{2+}]_t$ = CAL$[Ca^{2+}]_t$

TAlk = CAL(TALK)

pH = $-\log_{10}(H^+)$

If DPOT is positive ($CaCO_3$ dissolves)

3.3 If no $CaCO_3$ in storage then exit algorithm III

3.4 If $CaCO_3$ is in storage, then adjust $[Ca^{2+}]_t$, TAlk and pH as above and decrease $CaCO_3$ in storage by DPOT.

Algorithm IV for $FeCO_3$ Precipitation/dissolution

Input after completion of Algorithms I, II and III

$[Fe^{3+}]_t$, $[Fe^{2+}]_t$, TAlk, $[SO_4^{2-}]_t$

and relevant equilibrium and solubility product constants.

1. Determine input value for Alk—$2[Fe^{2+}]_T$, i.e.

   ALKM2TFE = TAlk -$2[Fe^{2+}]_t$

2. Determine $FeCO_3$ saturation state

   2.1 Assume (H^+) = 0,01 mole

   2.2 Calculate alkalinity for assumed (H^+) using the previous approach (Algorithm III, step 2.2)

   2.3 Calculate total Fe^{2+} at $FeCO_3$ saturation

$$[HCO_3^-]_f = K_{HC} K_{C1}^1 \cdot pCO_2 / (H^+)$$

$$[CO_3^{2-}]_f = K_{C2}^1 \cdot [HCO_3^-] / (H^+)$$

$$CAL[Fe^{2+}]_f = K_{SpFeCO3}^1 / [CO_3^{2-}]_f$$

$$CAL[Fe^{2+}]_t = CAL[Fe^{2+}]_f \left\{ 1 + \frac{[SO_4^{2-}]_f}{K_{Fe2S}^1} \right\}$$

   2.4 Calculate TAlk—$2[Fe^{2+}]_t$

   CAL(ALKM2TFE) = CAL(TAlk) —$2CAL[Fe^{2+}]_t$

   2.5 Compare calculated and input TAlk —$2[Fe^{2+}]_t$

   If CAL(ALKM2TFE) > ALKM2TFE

   then reduce (H^+) and vice versa

3. Determine $FeCO_3$ precipitation potential:

   DPOT = $CAL[Fe^{2+}]_t$ - $[Fe^{2+}]_t$

   If DPOT is negative ($FeCO_3$ precipitates):

   3.1 Put DPOT into $FeCO_3$ storage

   3.2 Adjust following parameters :

   $[Fe^{2+}]_t$ = $CAL[Fe^{2+}]_t$

TAlk = CAL(TALK)

$pH = -\log_{10}(H^+)$

If DPOT is positive ($FeCO_3$ dissolves)

3.3 If no $FeCO_3$ in storage → leave Algorithm IV

3.4 If $FeCO_3$ is in storage then adjust $[Fe^{2+}]_i$, TAlk and pH as above and decrease $FeCO_3$ in storage by DPOT.

Blend of different quality water

At each blending point, for each stream the following species concentrations will be known and available:

$[Fe^{3+}]_i$, $[Fe^{2+}]_i$, $[SO_4^{2-}]_i$, $[Mg^{2+}]_i$, $[Ca^{2+}]_i$, TAlk

These are all conservative parameters

If Q_i is flow from i^{th} stream and Q_T is ΣQ_i, then concentrations of each of the above species in the blended stream are calculated as):

$$[Fe^{3+}]_i = \sum_i \left([Fe^{3+}]_i \frac{Q_i}{Q_T} \right)$$

$$[SO_4^{2-}]_i = \sum_i \left([SO_4^{2-}]_i \bullet \frac{Q_i}{Q_T} \right)$$

$$[Mg^{2+}]_i = \sum_i \left([Mg^{2+}]_i \bullet \frac{Q_i}{Q_T} \right)$$

$$[Ca^{2+}]_i = \sum_i \left([Ca^{2+}]_i \bullet \frac{Q_i}{Q_T} \right)$$

$$[TAlk]_i = \sum_i \left(TAlk_i \bullet \frac{Q_i}{Q_T} \right)$$

These blended species concentrations then form the input to the above Algorithms I and II with the assumed oxygen and carbon dioxide partial pressures as $pO_2 = 0,21$ atm and $pCO_2 = 0,00035$ atm.

5. GEOCHEMICAL CHARACTERISATION OF OPENCAST MINE SPOILS

Geochemical characterisation of spoils is required to provide certain input parameters used in the generic opencast mine water model. Apart from this, geochemical characterisation is in itself useful to estimate the behaviour of spoils and predict the leachate quality that may emanate from the spoils.

5.1 Physical and hydraulic properties of spoils

Recharge and flow in spoils is primarily influenced by its physical and hydraulic properties. **Table 5.1** summarises the main physical and hydraulic parameters that can be readily determined for spoils. These parameters are also essential inputs to the generic opencast mine water model.

Table 5.1. Determination of physical and hydraulic properties of spoils

Property	Symbol	unit	Procedure
Bulk spoils density	ρ_b	kg/m^3	Measure spoil mass and volume. ρ_b = Mass/Volume
Spoils fragment density	ρ_s	kg/m^3	Measure volume and mass of fragment. ρ_s = Mass/Volume
Coarse fraction	f_c	-	Sieve analysis. (Fraction > 2 mm)
Fine fraction	f_f	-	Sieve analysis. (Fraction < 2 mm)
Coarse fraction water retention	S_c	kg/kg	Saturate coarse spoils column and wind dry at 20°C.
Fine fraction water retention	S_f	kg/kg	Saturate fine spoils column and wind dry at 20°C.
Total moisture content	S_t	kg/kg	$S_t = f_c.S_c + f_f.S_f$
Air filled porosity	θa	m^3/m^3	Pack column with saturated spoils. inundate from the bottom to exclude air. θa = Water volume/Spoils volume
Water filled porosity	θw	m^3/m^3	θw = (S_t . Spoils mass) / (ρ_w . Spoils volume)
Total porosity	θ_t	m^3/m^3	$\theta t = \theta a + \theta w$

5.2 Geochemical tests for the prediction of drainage quality

Various tests have been developed in an attempt to characterise the geochemistry of spoils. **Table 5.2.** summarises the main tests that have found application worldwide in the mine water field.

Of the kinetic **laboratory** tests the modified humidity cell and column leach test are frequently employed for the geochemical characterisation of coal mine spoils. The main difference between these tests lies in the use of crushed spoil(100% < 100 mm) in the modified humidity cell test, while the column leach test uses spoils without prior crushing.

Table 5.2. Static and kinetic tests used for the geochemical characterisation of waste rock and tailings

Static Tests	Objective	Advantages	Disadvantages
Acid base accounting	Determine potential for acid generation.	Rapid assessment. Initial screening test.	Does not simulate field conditions. Zone of uncertainty exists.
Kinetic Tests:			
British Columbia Research confirmation test	Confirm static test results. Used at gold and base metal mines.	Relatively simple. Rapid assessment	Ignores neutralisation. Does not predict reaction rates.
Shake flask weathering test	Determine rate of acid generation and accumulation of reaction products.	Simple to perform. Rapid assessment.	Reaction rates (short term) determined for submerged environment only.
Soxhlet extraction test	Confirm static test results.	Relatively simple. Rapid assessment.	Field conditions not simulated. Bacterial action not considered.
Humidity cell test	Determine reaction rates, used for tailings assessment.	Suitable for fine grained material.	Long test period. Preferential flow paths ignored. Influence of particle size ignored.
Large scale modified humidity cell test	Simulate reaction rates. Used for coarse material.	Spatial distribution of minerals accounted for. Oxidation products allowed to accumulate.	Long test period. Material crushed (100% <100mm)
Leach column test	Simulate geochemical reaction rates in field.	No prior crushing. Most accurate laboratory simulation of field conditions.	Long test period.
On site waste rock piles	Reaction rates under actual field conditions.	No prior crushing. Actual field conditions simulated.	Long testing period. Interpretation of results may be complex.

5.3 Practical application to case studies

A combination of the available geochemical tests, including acid base accounting, shake flask tests and leach column tests was used to assess the geochemical behaviour of four opencast coal mining pits on the Eastern Transvaal Highveld. The different spoils types are briefly described in **Table 5.3.**

Table 5.3. Description of spoils used for geochemical characterisation.

Identification no.	Description	Typical spoils water quality
Spoils A	Springs - Witbank coalfield. Approximately 10 years old. Coarse material.(50-100mm) Sandstone/siltstone/shale.	pH = 7,3-8,6 Sulphate(mg$CaCO_3$/l) = 2200-3900 Calcium(mg$CaCO_3$/l) = 1200-3000 Magnesium(mg$CaCO_3$/l)=1400-5600. Note: Typical quality of flooded spoils.
Spoils B	Springs-Witbank coalfield. Approximately 3 years old. Fine grained material.(<5mm). Sandstone /siltstone /shale.	pH = 3,1 Sulphate(mg$CaCO_3$/l) = 1200 Calcium(mg$CaCO_3$/l) = 350 Magnesium(mg$CaCO_3$/l) = 440 Note: Typical quality of flooded spoils.
Spoils C	Highveld coalfield. Approximately 6 years old. Coarse material.(50-100mm) Mainly shale with some sandstone. Highly weathered.	pH = 7,8-8,3 Sulphate(mg$CaCO_3$/l) = 250-560 Calcium(mg$CaCO_3$/l) = 100-330 Magnesium(mg$CaCO_3$/l) = 160-700 Note: Quality is a combination of surface runoff and spoils recharge.
Spoils D	Highveld coalfield. Approximately 6 months old. Mixture of coarse grained sandstone/shale and clayey organic matter. Little weathering.	pH = 7,3-8,6 Sulphate(mg$CaCO_3$/l) = 70-390 Calcium(mg$CaCO_3$/l) = 75-175 Magnesium(mg$CaCO_3$/l) = 80-205 Note: Quality is a combination of surface runoff and spoils recharge.

Note: all concentrations are expressed as equivalent $CaCO_3$

5.3.1 Physical and hydraulic properties

The physical properties of the spoils was determined according to the procedures previously described and are summarised in **Table 5.3.1.(a)**.

Table 5.3.1.(a). Physical properties of four different spoils.

	Spoils A	Spoils B	Spoils C	Spoils D
Spoils bulk density ρ_b (kg/m^3)	1471	1629	1283	1676
Total (saturated) moisture content S_t	10,7%	15,1%	12,8%	15,1%
Air filled porosity θ_a	25%	3%	28%	9%
Water filled (saturated) porosity θ_w	16%	25%	17%	25%
Total porosity θ_t	41%	28%	45%	34%

Columns (300mm diameter by 1000mm height) were constructed from perspex and packed with material from the above spoils (**Figure 5.3.1.(a)**). No crushing was conducted prior to packing of the columns. The hydraulic characteristics of the spoils were determined by flooding the columns and then allowing the columns to drain and monitoring the outflow. Useful flow parameters were determined, as summarised in **Table 5.3.1.(b).** The cumulative outflow volume and outflow rates from the columns are shown on **Figure 5.3.1.(b)** and **Figures 5.3.1.(c) & (d)**.

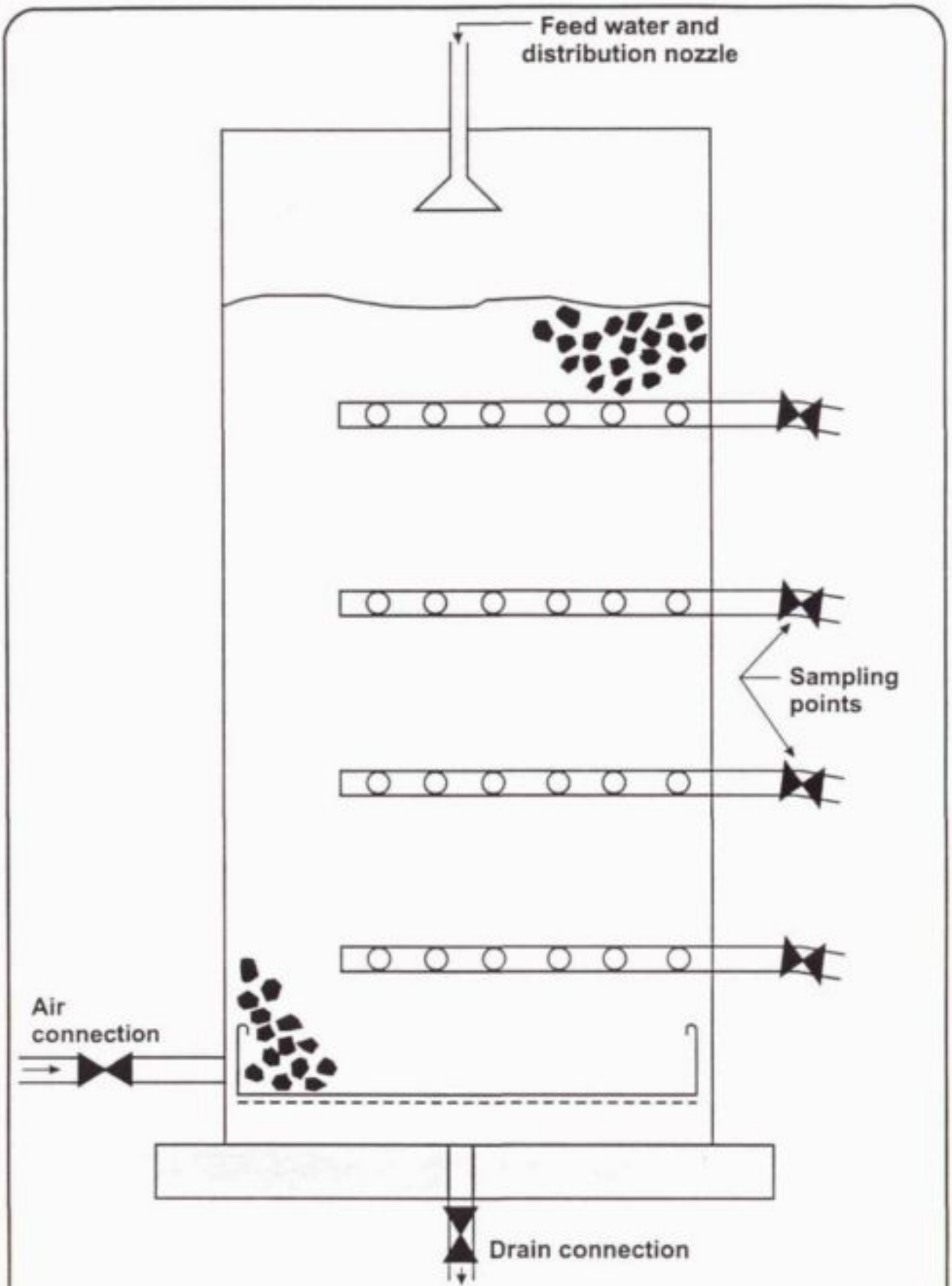

FIGURE 5.3.1 (a) : COLUMNS USED FOR LEACHING EXPERIMENTS ON SPOILS FROM FOUR OPENCAST PITS

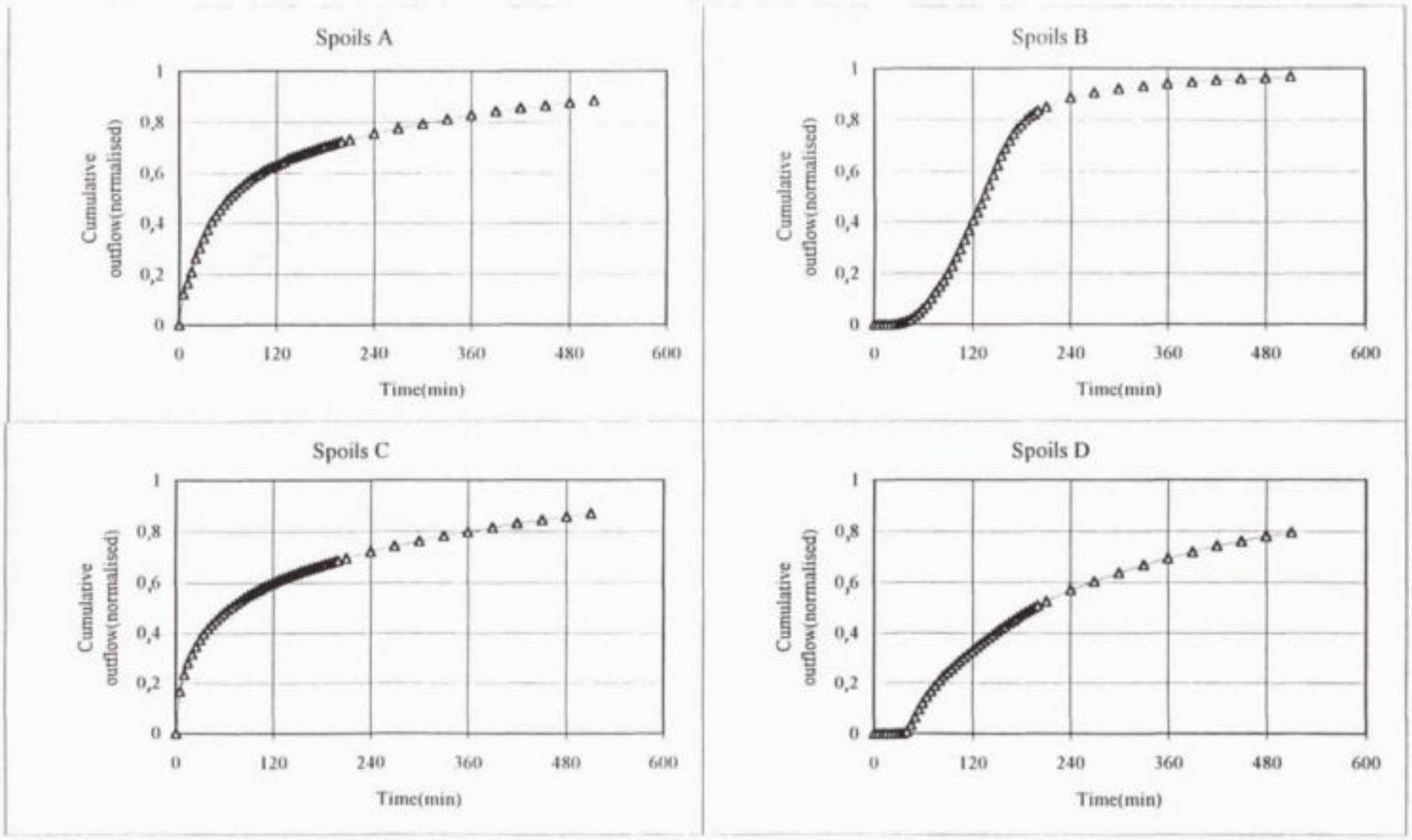

Figure 5.3.1(b) : Normalised cumulative outflow from different spoils

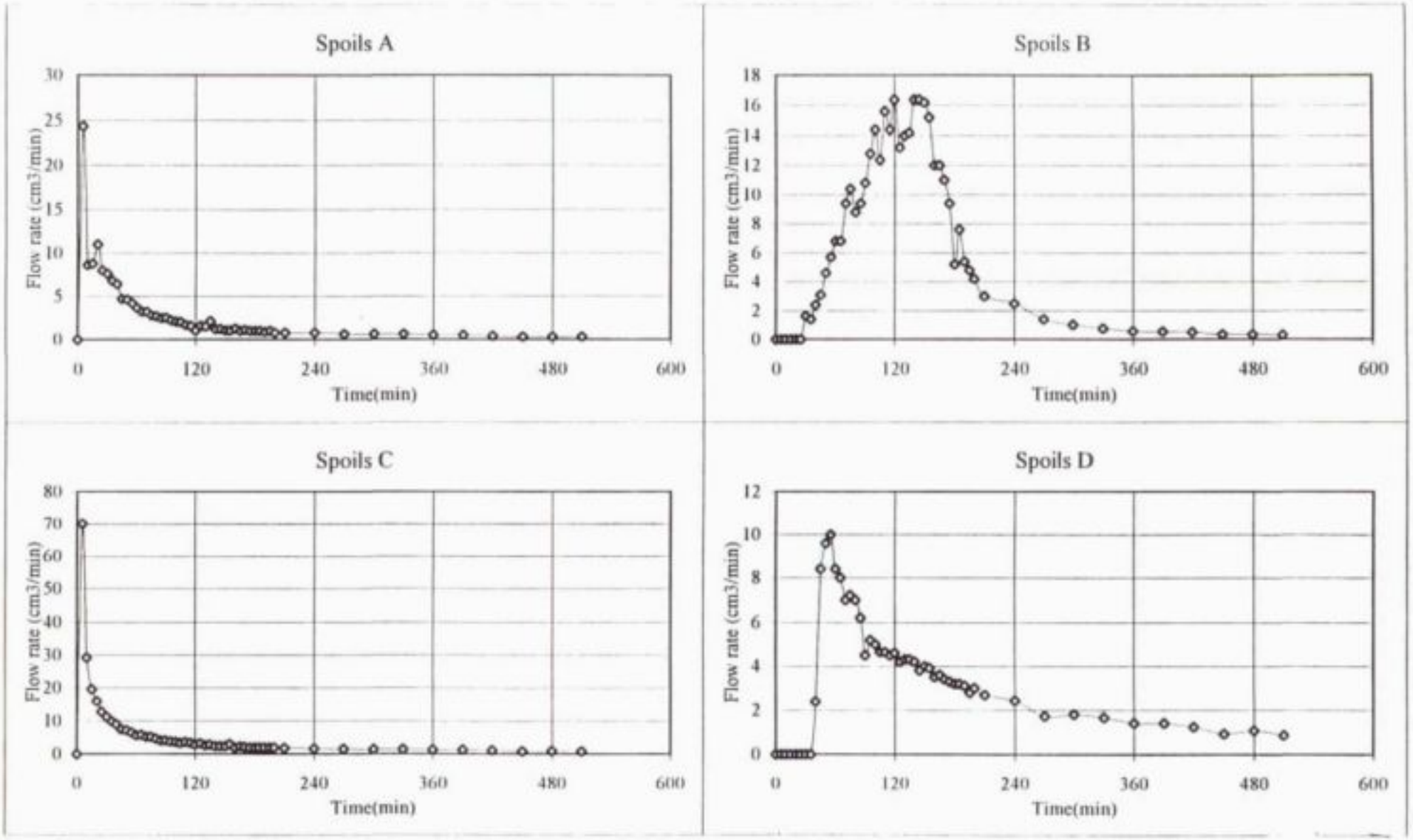

Figure 5.3.1(c) : Outflow rate from different spoils

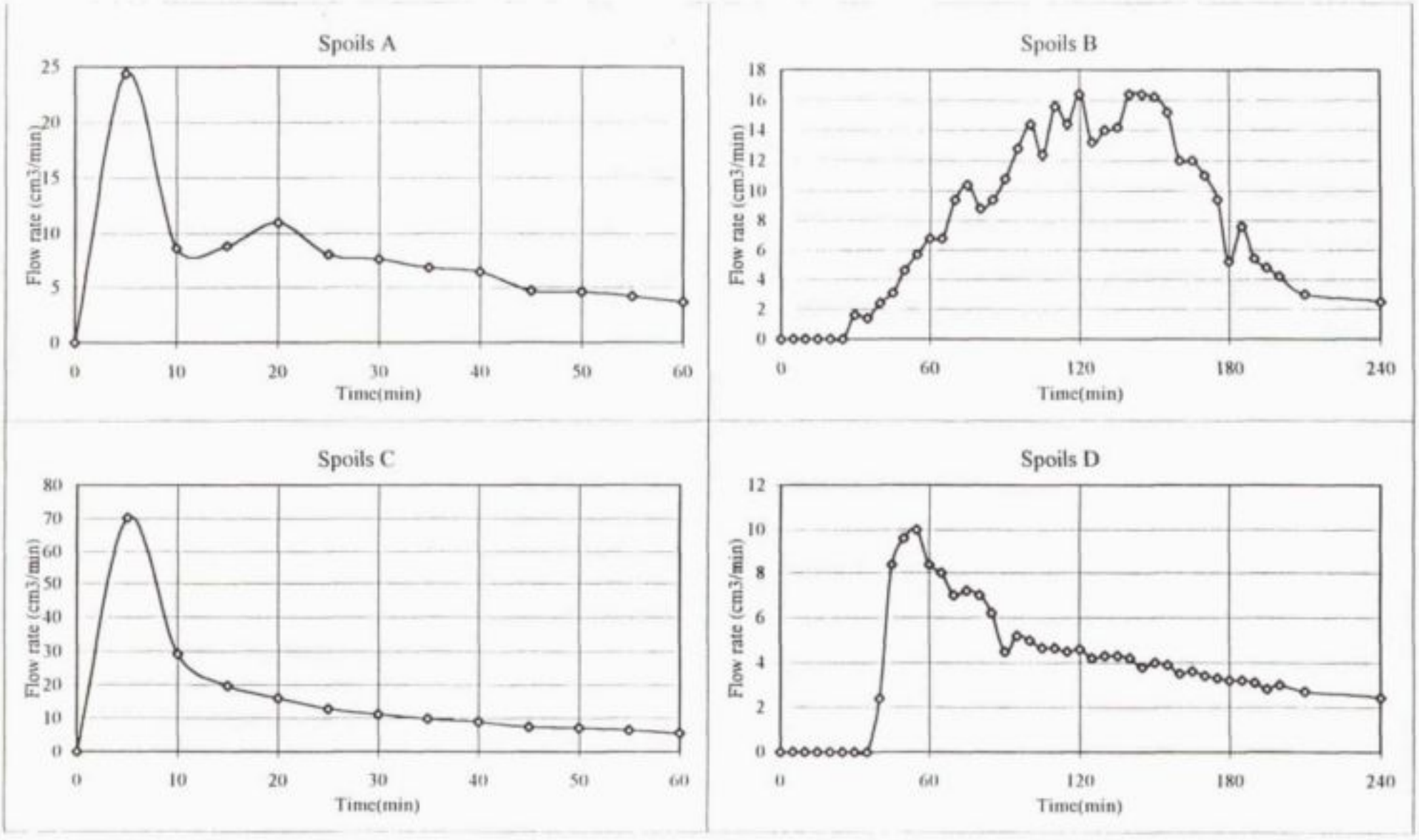

Figure 5.3.1(d) : Enlargement of Figure 5.3.1(c) to illustrate hydraulic properties of spoils

Table 5.3.1.(b). Hydraulic parameters determined for four different spoils.

Symbol	Description	Spoils A	Spoils B	Spoils C	Spoils D
t_{10}	Time for 10% of outflow (minutes)	3,8	70	2,8	56
t_{50}	Time for 50% of outflow (minutes)	62	134	68	195
t_{90}	Time for 90% of outflow (minutes)	645	270	720	990
T_{tnom}	Nominal retention time (minutes.)	65	128	64	129
T_{peak}	Time to reach peak value (minutes)	5	120	5	55
SCI	Short circuiting index. $= (T_{tnom}-T_{peak})/T_{peak}$	12,0	0,07	11,8	1,3

The results from the hydraulic tests are discussed below:

Spoils A:
Extensive short circuiting occurred through these spoils. This is substantiated by the high short circuiting index calculated for the spoils and is illustrated by the left skewness of the outflow curve. Enlargement of the flow curve indicates that flow through the spoils was initially dominated along preferential flow paths. This was followed by a second peak 20 minutes later, indicating flow along a set of more restrictive, but still significant, preferential flow paths. The remainder of the outflow (approximately 70%) migrated through the spoils in a typical porous media flow pattern.

Spoils B:
These fine grained spoils approximated plug flow behaviour, as indicated by the low short circuit index of SCI=0,07. The initial lag period before the first outflow appeared, reflects the inherent permeability of the spoils material. Variations in the outflow rate was observed and two approximately equally sized peaks appeared in the outflow. It is believed that migration through the spoils followed numerous parallel flow paths with similar characteristics, which presented a good approximation of classical porous media flow.

Spoils C:
This coarse spoils behaved similar to Spoils A in displaying extensive short circuiting. This is substantiated by the high short circuiting index (SCI) calculated for the spoils and is illustrated by the left skewness of the outflow curve. Enlargement of the flow curve indicates that flow through the spoils was initially dominated by a single set of preferential flow paths. The remainder of the outflow (approximately 75%) migrated through the spoils in a typical porous media type flow pattern.

Spoils D:
This spoils exhibited an outflow pattern due to the presence of preferential flow paths which seemed to vary in size and accounted for approximately 25% of the total outflow. The initial lay period reflects the limited permeability of the material, even along the preferential flow paths. The remainder of the outflow approximated porous media flow and the short circuiting index for the column was, although not ideal for plugflow, significantly lower than that of the coarse spoils A & C.

5.3.2 Acid base accounting

Acid base accounting was conducted on spoils samples as a preliminary test to assess the long term potential for acid mine drainage emanating from the spoils. The acid potential(AP) was based on the total sulphur content of the spoils (Sobek et al, 1978). This may overestimate the acid potential of weathered spoils due to the inclusion of sulphate salts, that are not necessarily acid forming. It was found that the accumulated sulphate salts (due to pyrite oxidation), led to an overestimate of less than 10% for the acid potential, which did not alter the interpretation of the results. The neutralisation potential(NP) was determined by first acidifying the spoils, and then titrating with a standard base to pH = 7. The interpretation of the results was based on the ratio of NP:AP (Smith,1990):

- NP:AP < 1:1 then there is a significant risk of acid mine drainage formation,
- 1 < NP:AP < 3:1 the leachate acidity is uncertain and further geochemical testing should be conducted
- NP:AP > 3:1 the leachate is likely to be neutral to alkaline.

Table 5.3.2 summarises the results from the acid base accounting tests. The saturated paste pH of the spoils was also measured, after mixing the pulverised material with distilled water. The objective of this was to determine the short term pH that could be expected in the leachates.

The acid base accounting test results are further evaluated against the observations from the leach column experiments in the section that follows.

Table 5.3.2. Acid base accounting results for four different spoils

	Spoils A	Spoils B	Spoils C	Spoils D
Saturated paste pH	6,8 - 8,0	4,7 - 5,2	5,4 - 6,4	6,4 - 8,0
Neutralization potential - NP($kgCaCO_3$/ton)	9,4	0,45	13,9	40,3
Acid potential - AP($kgCaCO_3$/ton)	6,2	6,7	20,9	11,6
Ratio NP:AP	1,5	0,07	0,7	3,5
Interpretation	Uncertain	Acid forming	Acid forming	Neutral /alkaline

5.3.3 Column leach tests

The columns used for the determination of the spoils hydraulic properties were also used to conduct long term leach tests over 240 days (8 months) for Spoils B, C and D, and 380 days (12 months) for Spoils A.

The columns were packed with uncrushed and unsieved spoils material. Using distilled water, a 30 mm water depth was applied to the spoils at weekly intervals. The generated leachate was collected over a three day period. The outlet was then closed and humidified air was passed through the spoils for four days, after which any additional leachate was collected before repeating the cycle. The primary objective of the leach column tests was to assess the maximum reaction rates occurring within the spoils, i.e. under conditions where oxygen was not the rate limiting reactant. The ponded water depth amounts to 1560mm/a which is twice the annual rainfall typically received on the Eastern Transvaal Highveld. The effective rainfall recharge to rehabilitated spoils with a vegetated soil cover may be as low as 10% of mean annual precipitation. The annual application of water to the experimental spoils therefore corresponded approximately to 20 years of recharge via the spoils.

Figure 5.3.3.(a), (b), (c) and **(d)** summarises the main water quality constituents measured in the leachate. The sulphate, calcium and magnesium concentrations are expressed as mg$CaCO_3$/l to allow direct stoichiometric comparisons. It should be noted that the column leachate quality was specific to the laboratory conditions under which the tests were conducted and may differ from the leachate produced under field conditions.

The cumulative sulphate, calcium and magnesium washed from the columns during the extended leaching experiments are illustrated on **Figure 5.3.3.(e)**. These time series plots provide insight into the mechanisms by which the different leachate qualities were produced and are discussed below:

Spoils A

The *acid base accounting tests* could not confirm whether these spoils would remain alkaline over the long term.

The leach column test indicated that the spoils did not become acidic over the period of testing. High concentrations of sulphate, calcium and magnesium initially reported in the leachate as a result of the flushing of accumulated pyrite oxidation products within the spoils. The leachate concentration stabilised after this, with the stoichiometric ratio between sulphate production and calcareous mineral dissolution approximating a ratio of 1:1. Sufficient calcareous minerals were available to neutralise the acidity formed. The dissolution of the calcareous minerals kept pace with the generation of acidity. A slight excess of calcareous minerals appears to be present, which effectively maintains a neutral/alkaline water.

Spoils B

The acid base accounting tests predicted an acidic leachate for Spoils B, which was confirmed by the column leach tests. The pH did, however, suddenly increase after 120 days, remained alkaline for 50 days and then declined to pH< 6 for the remainder of the test. This increase in pH was accompanied by a reduction in the sulphate concentration and a slight increase in the calcium concentration. It is believed that the oxygen supply to the column may have decreased during this period, which inhibited pyrite oxidation to the extent where the calcareous minerals could neutralise the acidity.

The mobilisation of calcareous minerals lagged behind the generation of acidity, resulting in a nett acidic leachate. The steady decline in Ca and Mg concentrations in the leachate also indicated the progressive loss of available neutralisation capacity.

Spoils C

The acid base accounting tests predicted an acidic leachate for Spoils C. This was substantiated by the column leach experiments, although fluctuations did occur. The leachate remained saturated with respect to gypsum($CaSO_4.2H_2O$) for the duration of the test and the true reaction rates may therefore have been underestimated due to the accumulation of gypsum in the spoils. The stoichiometric ratio of sulphate: (calcium + magnesium) was approximately 1:1, but with a slight deficiency in calcareous minerals compared to the generated acidity.

Spoils D

The acid base accounting tests predicted an alkaline leachate for these spoils, which was confirmed by the leaching experiments. The stoichiometric ratio of sulphate : (calcium + magnesium) varied from 1:1 to 2,4:1 and was 1,4:1 on average. Significant variations also occurred in the ratio of sulphate : magnesium. It was concluded that calcium carbonate and potentially magnesium carbonate precipitated within the spoils. This obscured the interpretation of the observed ratios between sulphate and (calcium and magnesium).

The rate of acid formation (as reflected by sulphate in the leachate) and the rate of neutralisation (as reflected by calcium and magnesium in the leachate) was determined for the different spoils and are summarised on **Figure 5.3.3.(f)**. These are pseudo-reaction rates, being a combination of accumulated pyrite oxidation products and those reaction products that formed in the interval between successive leachings. The true reaction rates were approached as the column leach tests progressed and the effect of leaching historically accumulated products became less significant. **Table 5.3.3.(a)** summarises the typical sulphate production and neutralisation rates calculated for the spoils under laboratory conditions. These sulphate production rates are significantly higher than the rates observed under field conditions, (typically of 0,01 kgCaCO3/ton/a), and indicate how the weathering of the spoils may be accelerated by column leach tests.

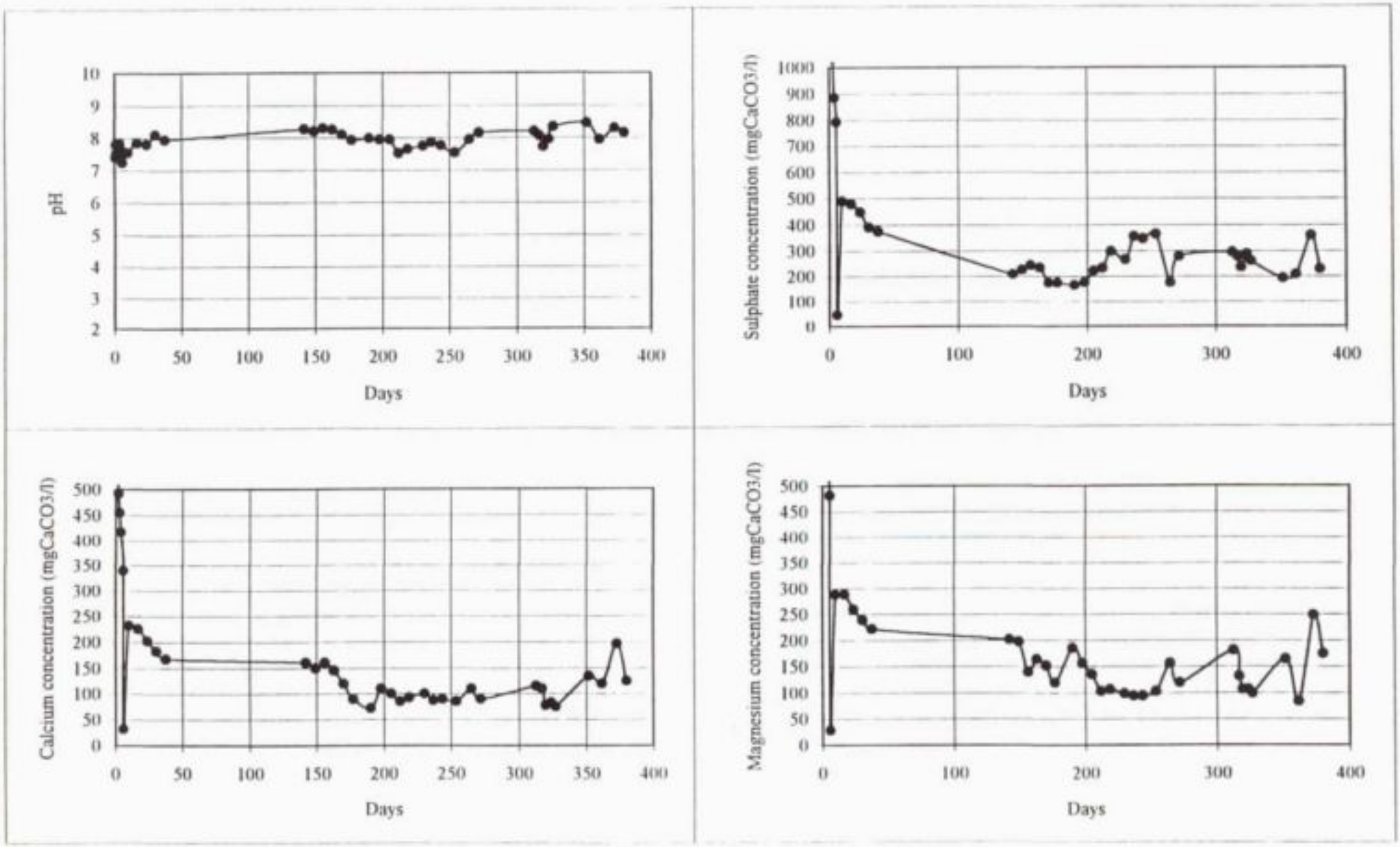

Figure 5.3.3.(a). Water quality of column leachate from Spoils A

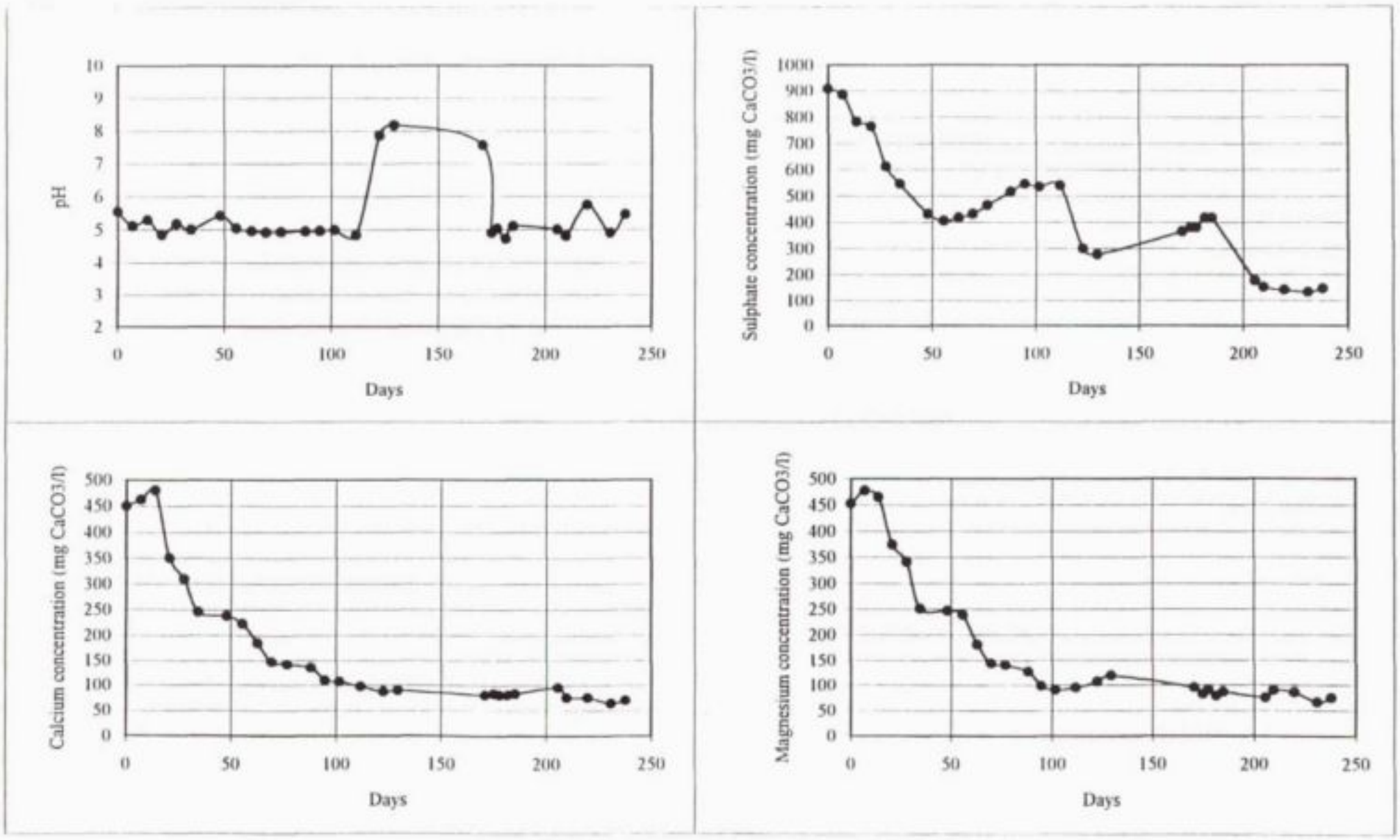

Figure 5.3.3.(b). Water quality of column leachate from Spoils B

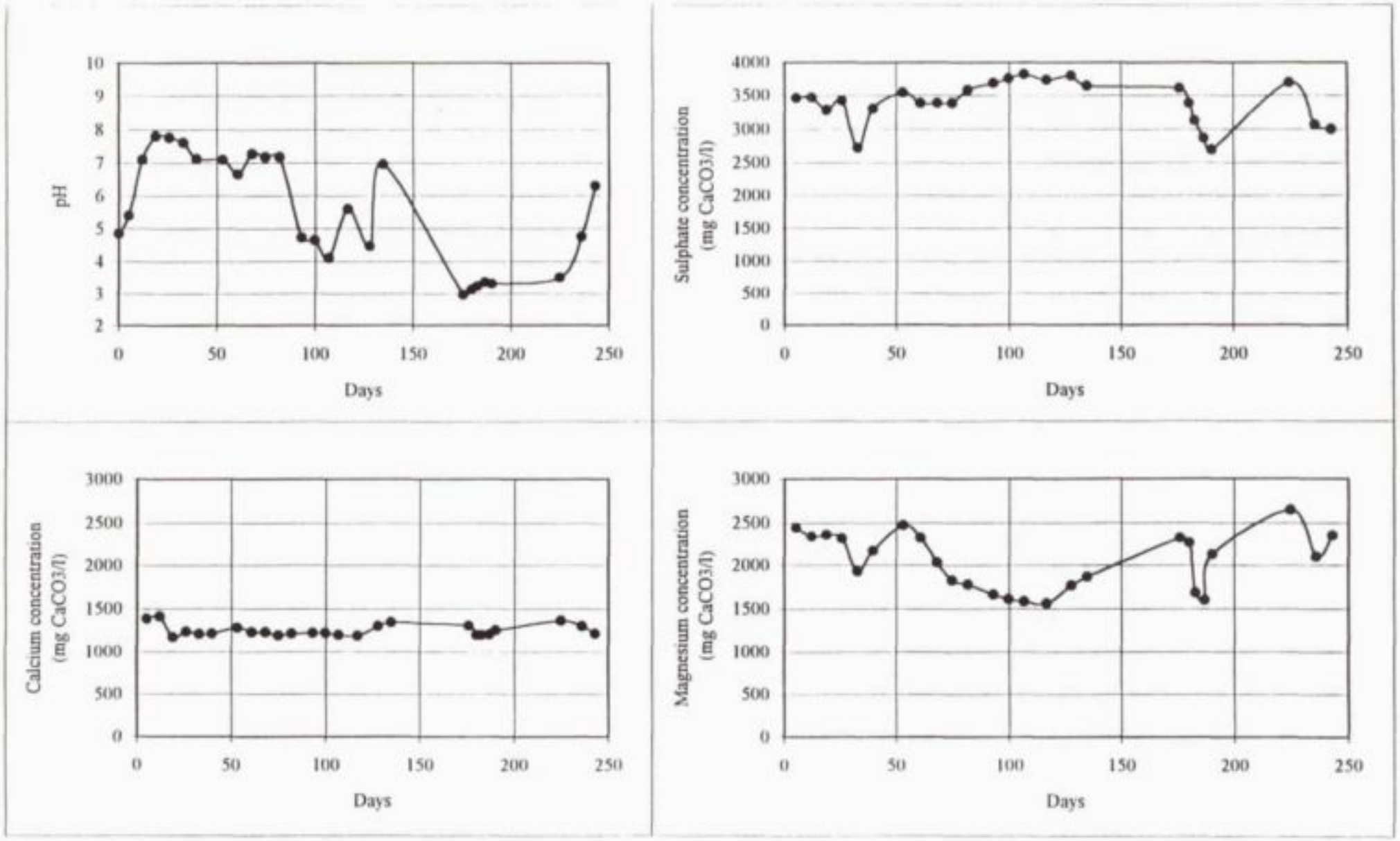

Figure 5.3.3.(c). Water quality of column leachate from Spoils C

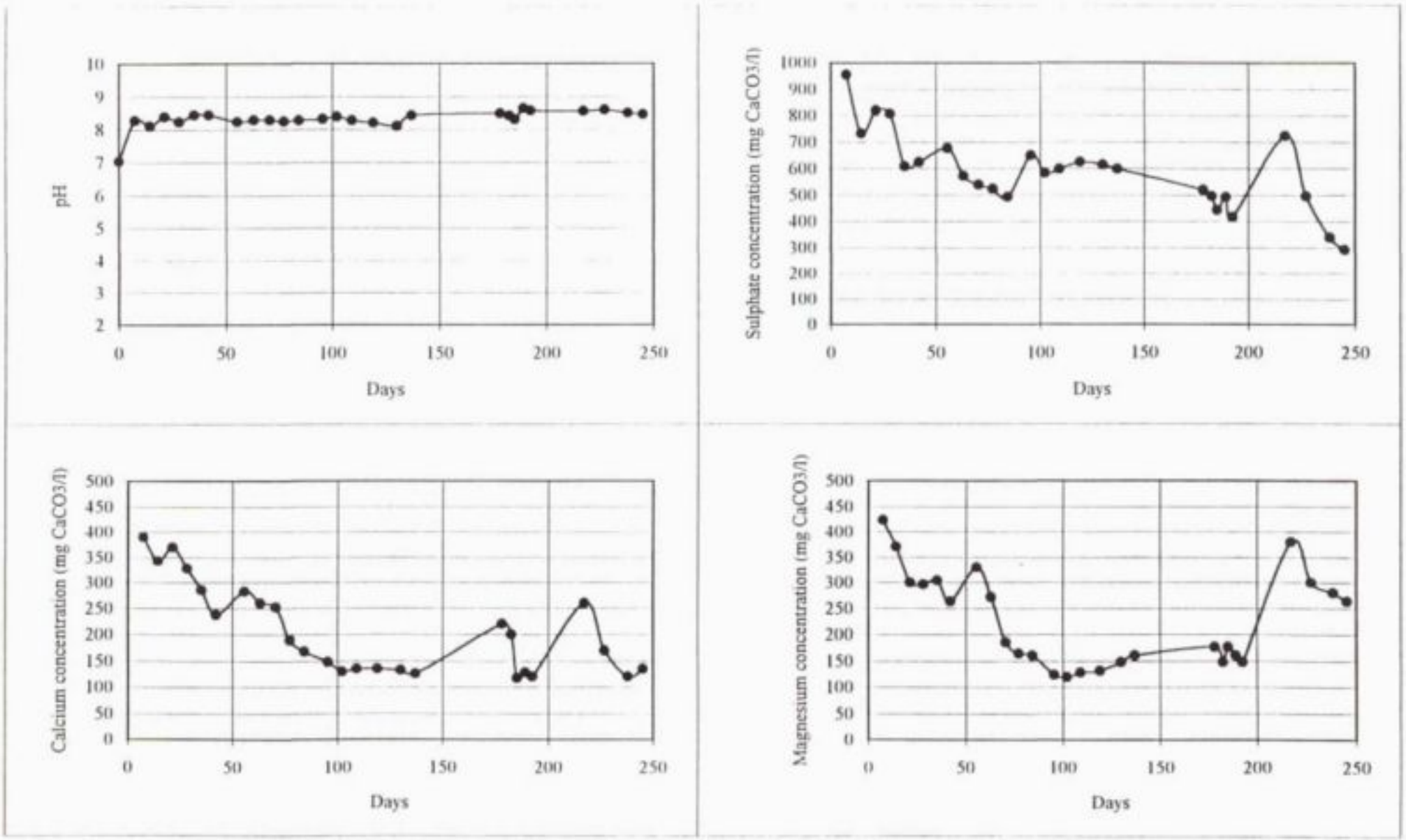

Figure 5.3.3.(d). Water quality of column leachate from Spoils D

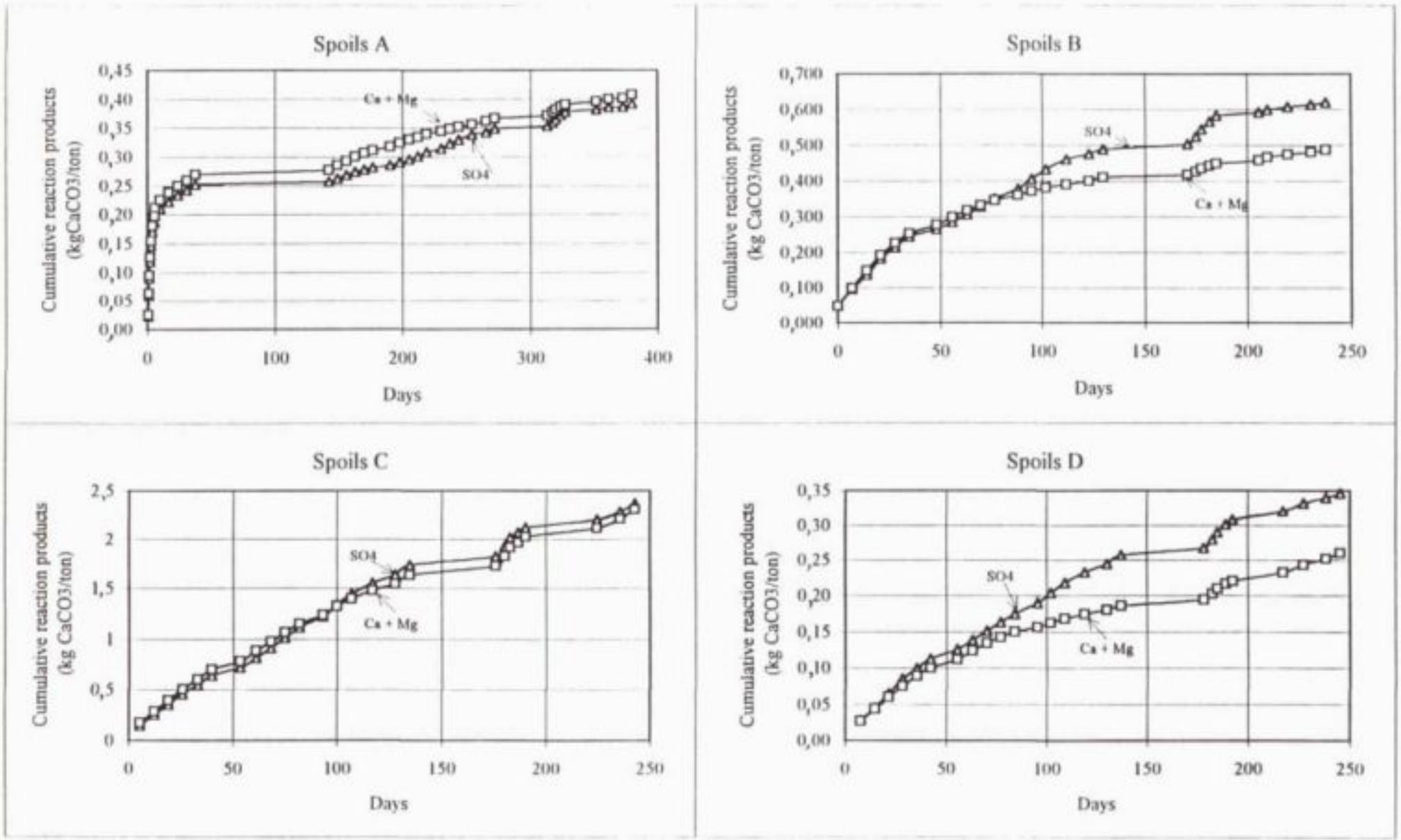

Figure 5.3.3.(e). Cumulative reaction products leached from different spoils.

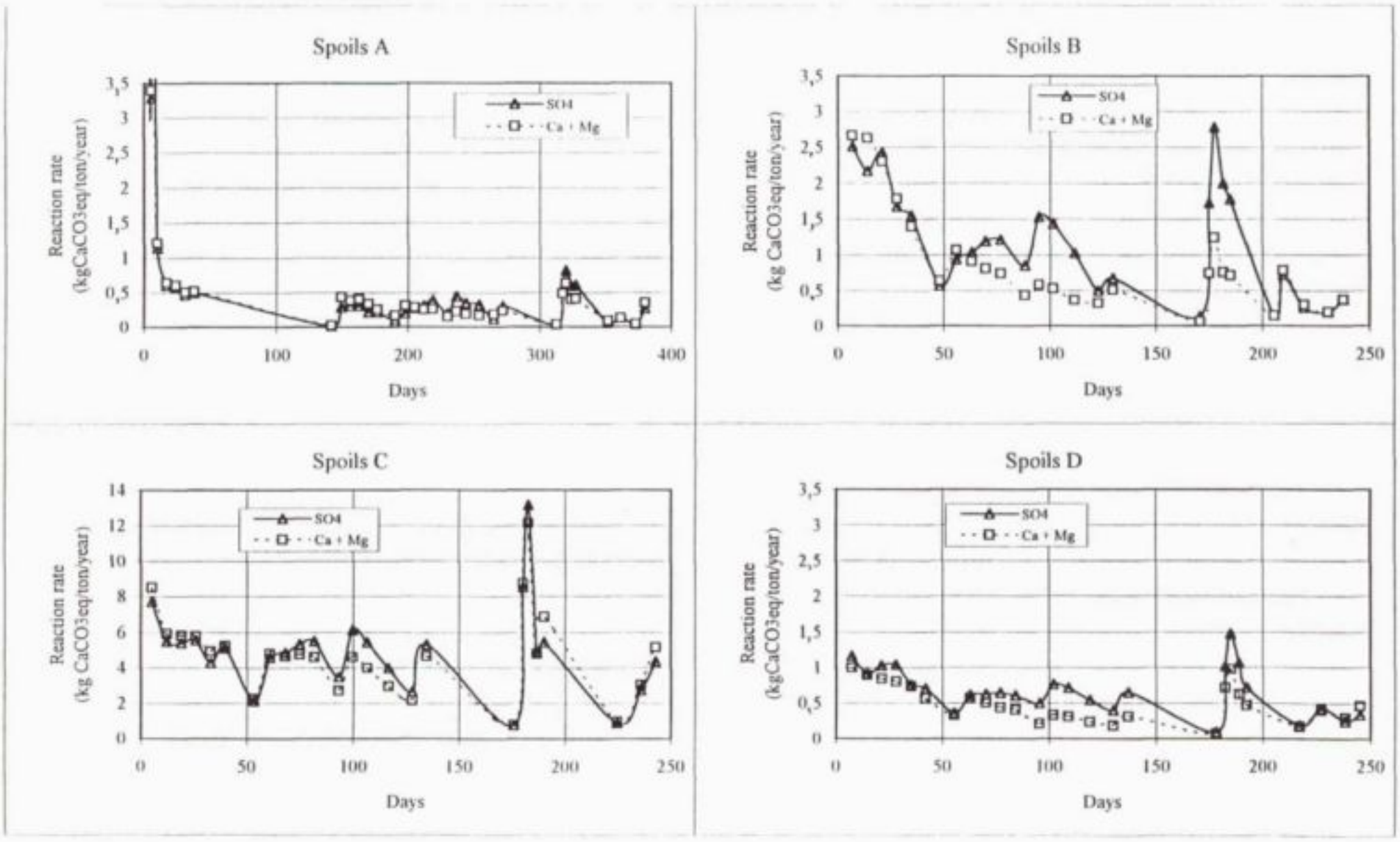

Figure 5.3.3.(f).Acid generation and neutralisation rates for different spoils.

The estimated times for the release of the full acid and neutralisation potentials (derived from the acid base accounting tests) under laboratory conditions are also indicated in the table. Care must be exercised in the interpretation of the results since the accumulation of calcium and magnesium in the spoils are not reflected in the results. The times for the release of the neutralisation potential of Spoils C and Spoils D are not indicated in the table, since it would not be a true reflection of the actual dissolution rate of calcareous minerals from these spoils, due to the precipitation of calcium and magnesium salts within the spoils.

The time for utilisation of the neutralisation potential for Spoils B was calculated to be approximately 1 year from the start of the leach test. This is evident from **Figure 5.3.3.(b)** which indicates how the calcium and magnesium concentrations decreased from 450mg$CaCO_3$/l at the start of the test to less than 70 mg$CaCO_3$/l after 240 days.

The time for depletion of the neutralisation potential from Spoils A was calculated to be in excess of that required for acid generation and confirmed that the spoils would not produce acidic leachate in the long term.

It should be noted that the acid generation and neutralisation calculations assume that all the minerals will react, which is unlikely to occur under natural field conditions. The oxidation rate of pyrite under field conditions is significantly lower than that occurring in the columns. This would then also apply to the neutralisation rates. The time required for pyrite oxidation to proceed to the extent where its effect becomes negligible may therefore be considerably longer under field conditions.

Table 5.3.3.(a). Acid generation and neutralisation production rates for different spoils in column leach experiments.

	Spoils A	**Spoils B**	**Spoils C**	**Spoils D**
Calcium + Magnesium leaching rate) (kg$CaCO_3$/ton/year)	0,27	0,61	Refer to text	Refer to text
Time for depletion of calcareous minerals under laboratory conditions.	35 years	1 year	Refer to text	Refer to text
Sulphate production rate (kg$CaCO_3$/ton/year)	0,31	0,98	5,12	0,65
Time for full oxidation of pyrite under laboratory conditions.	21 years	7 years	4 years	19 years

Note : Rates were based on 50 percentile values

The observed acid generation and neutralisation production rates serve as calibration inputs to the generic mine water simulation model. These rates reflect an upper limit with no restrictions on the availability of the oxidant (O_2).

The mass of sulphate, calcium and magnesium leached from the columns was determined and is summarised in **Table 5.3.4.(a)**.

Table 5.3.4.(a). Mass of oxidation products leached from different spoils during the long term column leach tests.

	Spoils A	Spoils B	Spoils C	Spoils D
Calcium ($kgCaCO_3$/ton)	0,18	0,2	0,9	0,12
Magnesium ($kgCaCO_3$/ton)	0,23	0,2	1,5	0,14
Calcium & Magnesium ($kgCaCO_3$/ton)	0,41	0,4	2,4	0,26
Neutralisation potential ($kgCaCO_3$/ton)	9,4	0,45	13,9	40,3
Sulphate ($kgCaCO_3$/ton)	0,39	0,62	2,4	0,35
Acid generation potential ($kgCaCO_3$/ton)	6,2	6,7	20,9	11,6

It is clear that the total oxidation of all pyrite will take a very long time. The leach column tests (simulating the field water migration over a 20 year period) only mobilised a small fraction (typically 5 - 10%) of the total acid generation potential. In practise it is generally observed that pyrite oxidation products tend to accumulate in the spoils, due to the low flushing rate with a rehabilitation cover.

6. DEMONSTRATION OF THE MINE WATER MODEL

The generic mine water model was employed to simulate the water make in a small opencast colliery.

6.1 Description of Mini-pit

The pit consists of an eastern and western portion respectively. The two portions will be mined concurrently and will therefore form a single, integrated mine water system. The total surface area of the pit is 85 ha.

The pit natural surface topography drops from south to north. Mining will take place against the natural slope as described below.

The pit will intercept the characteristic geology of the Mpumalanga Highveld Coalfields, with nearly horizontally-bedded, gentle undulating succession of shales, sandstone and coal. The average depth of the pit is 20 m.

The coal reserves are to be mined in cuts starting at the junction between the western and eastern portions of the pit. The cuts will start in an easterly direction across the eastern portion and a westerly direction across the western portion of the mini-pit – refer to **Figure 6.1(a)**. The mining will start from the box cut and progress in a general southerly direction. The pit was divided into 166 separate mining blocks with an average 3 to 4 blocks mined per month. A single cut across a portion of the pit will take about 4 months to mine. The pit will be continually mined through the low floor contour, running across the western portion of the mini-pit. The water that collects in the spoils body will decant into the open pit floor from where it will be pumped to the existing polluted water system.

The box cut will be filled and rehabilitated towards the end of the first year of mining. This will be achieved by using the overburden and hard rock spoils from the mining of the first series of blocks, further insloping of the low wall and the available stockpiles of topsoil.

The proposed mining plan allows for a single row of unrehabilitated spoils behind the open pit floor. Any particular row of unrehabilitated spoils will be in existence for about 4 to 6 months, before being levelled. The status of the mining blocks after the first and third years of mining are shown in **Figures 6.1(b)** and **6.1(c)** respectively. The levelling and topsoiling will be done to ensure that the post-mining topography will be free draining. During mining, the upslope surface runoff will be prevented from entering the pit by means of berms constructed along the southern edge of the opencast pit.

6.2 Modelling of pit water balance

The generic mine water model was used to assess the pit water make during active opencast mining operations. The pit was represented by the 166 individual mining blocks, with the status of each block in each of the 58 months of the mining and rehabilitation operation being input to the model. The coal reserves were assumed to be exploited after 48 months of mining. A further 10 months were allowed for the final rehabilitation of the pit to give a total of 58 months for the life of the mine. The block status types that are catered for in the model included:

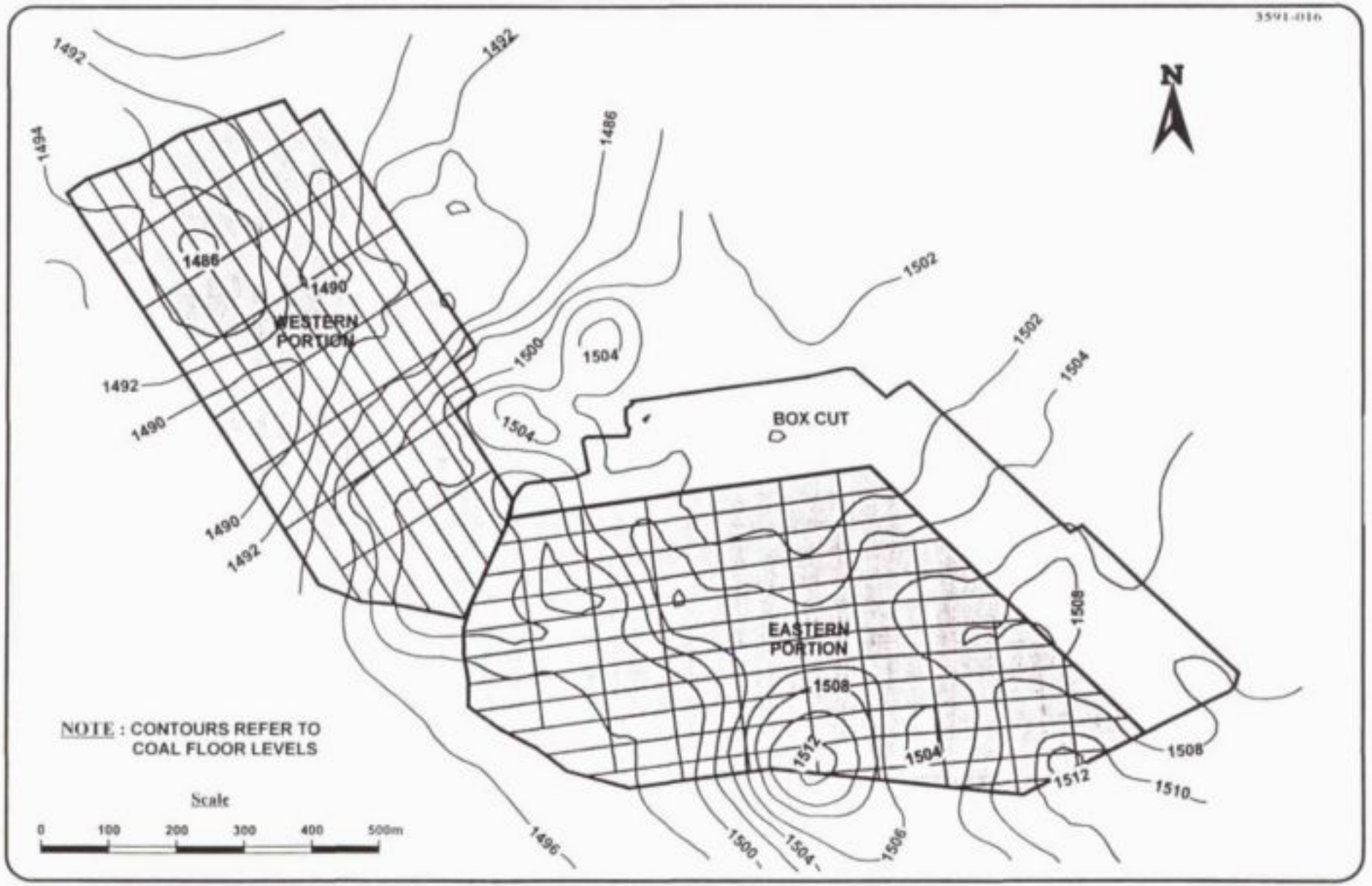

Figure 6.1 (a) : General layout of opencast coal pit

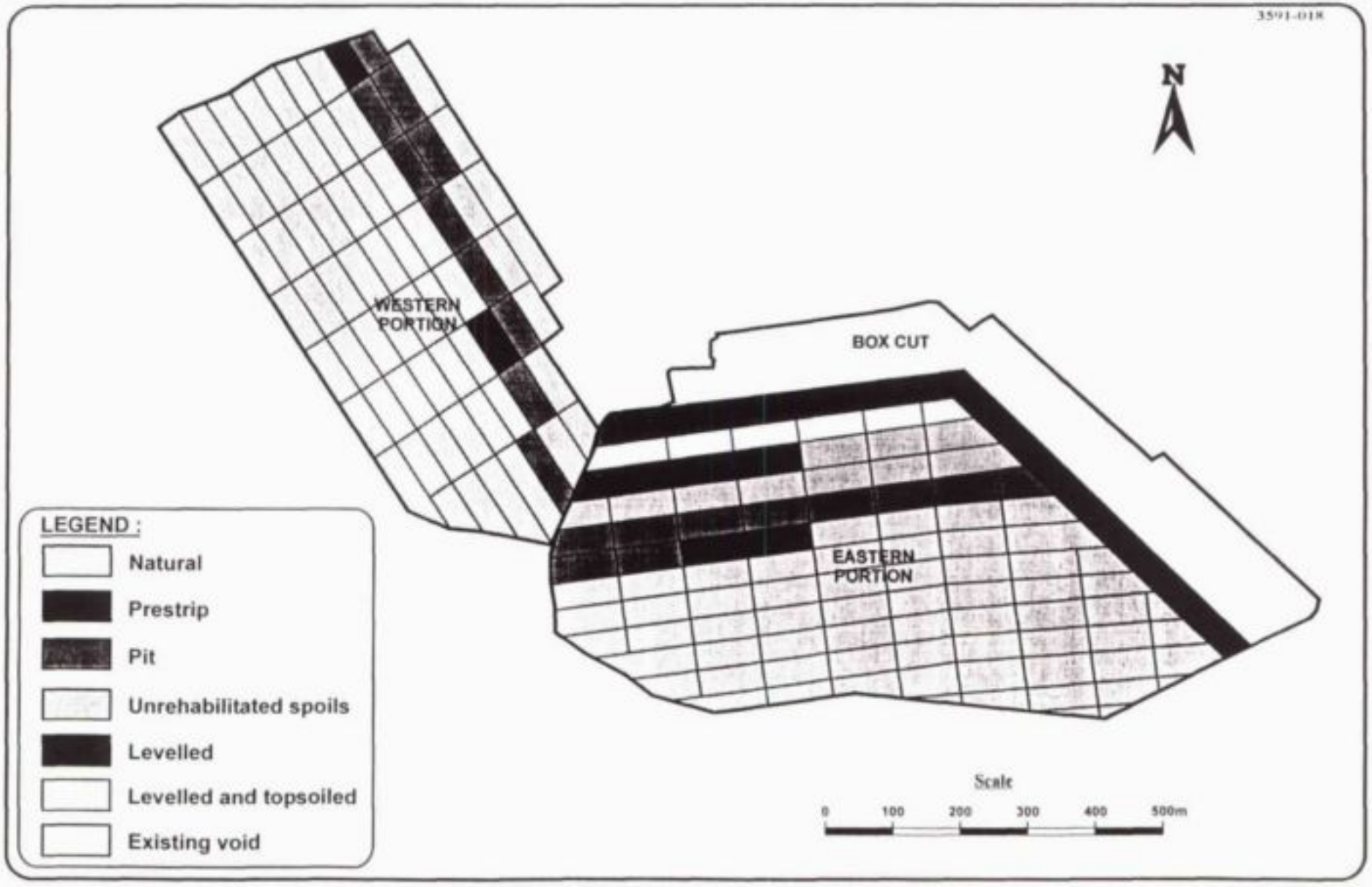

Figure 6.1 (b) : Status of opencast mining blocks, after first year of mining

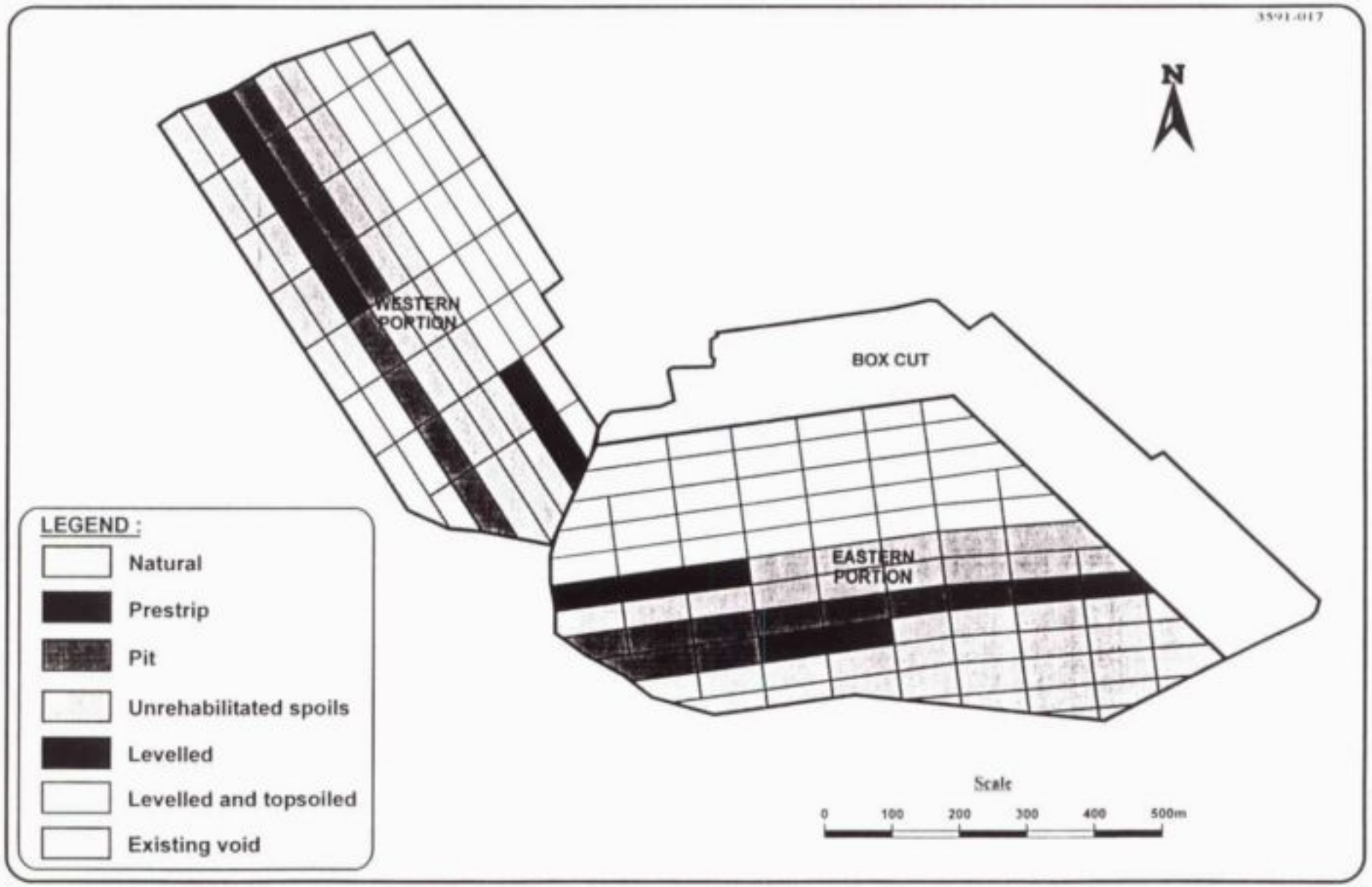

Figure 6.1 (c) : Status of opencast mining blocks, after third year of mining

- natural conditions
- prestripped
- pit floor
- unrehabilitated spoils
- levelled spoils
- levelled and topsoiled
- fully rehabilitated (vegetated) spoils

Besides the individual mining blocks, the generic mine water model allowed in-spoil water storage, local depressions on the rehabilitated surface, polluted water dams and a pit floor sump which can be incorporated to represent the water system. An in-spoils storage area and a pit floor sump were used together with the individual blocks to model the pit water balance. The surface recharge water was routed to the in-spoils water storage area and the surface runoff from the prestripped areas and the unrehabilitated spoils was routed to the pit floor. The runoff from the upslope natural areas was assumed to be diverted around the pit water system by berm walls. Similarly, the surface runoff from the rehabilitated areas was assumed to flow out of the system, due to the free draining post-mining topography created behind the mining front.

The default values for the generic mine water model were used in the simulation of this demonstration pit. The only pit-specific water quantity-related variable was the groundwater influx. The pit operation potentially intercepted a number of water bearing aquifers including:

- a shallow, perched aquifer
- fractured Karoo rock aquifer
- aquifer associated with the coal seam itself

The groundwater make to the pit was estimated to average 2 420 m^3/month, over the operational life of the pit. This value will obviously marginally change with time, as the size of the pit increases.

6.3 Modelling results

The pit water model described was employed to simulate the water system over the length of the active mining period.

The historical local rainfall gauge records were analysed to identify periods of dry, wet and average hydrological cycles. A 58 month, moving average of rainfall was used to identify these cycles and simulations were conducted for the following three rainfall scenario's:

- **Wet case scenario**

A wet hydrological cycle using the rainfall records for the period April 1986 to 31 January 1991 was simulated. The total depth of rain over the 58 month period was 3 959 mm.

- **Probable scenario**

An average hydrological cycle using the rainfall records for the period 1 April 1972 to 31 January 1997 was simulated. The total depth of rain over the 58 month period was 3 491 mm.

- **Dry case scenario**

A dry hydrological cycle using the rainfall records for the period 1 April 1991 to 31 January 1996 was simulated. The total depth of rain over the 58 month period was 2 623 mm.

The three hydrological scenarios were simulated to demonstrate the range of probable water volumes that may be generated during the mining operation. These are summarised in **Table 6.3(a)** in terms of average monthly water flows/volumes for the different components of the water balance. These averages are for the full 58 month period of simulation.

The groundwater entering the pit during the operational phase does not change, as it is not influenced to a large extent by rainfall. The only part of the groundwater that is directly influenced by rainfall is the volume of water in the perched aquifer, but this contributes a small amount to the overall groundwater inflow volume.

Table 6.3(a) : Anticipated average water generation (m^3/month) during active pit mining operations

Water Element	Wet Case Scenario (m^3/month)	Probable Scenario (m^3/month)	Dry Case Scenario (m^3/month)
1. Recharge flows			
Rehabilitated spoils (400 mm topsoil & vegetation)	1 740	1 641	1 074
Topsoiled spoils (400 mm)	1 669	1 568	1 003
Levelled Spoils	175	162	101
Unrehabilitated Spoils	2 286	1 979	1 314
Sub Total	**5 870**	**5 350**	**3 492**
2. Groundwater flows	**2 420**	**2 420**	**2 420**
3. Runoff flows			
Rehabilitated spoils (400 mm topsoil & vegetation)	3 124	1 410	1 588
Topsoiled spoils (400 mm)	585	750	740
Levelled Spoils	56	60	39
Unrehabilitated Spoils	623	707	184
Pre-stripped area	62	51	11
Pit floor	4 746	4 218	2 854
Upslope catchment	1 364	842	346
Sub Total	**10 560**	**8 038**	**5 773**
Total	**18 850**	**15 808**	**11 685**

In general, the analysis of the modelling results indicated that:

- a relatively large contribution of the pit water make originates from surface runoff. It is therefore important to divert runoff from rehabilitated areas and the upslope pre-stripped areas away from the pit. It is not practical to divert all such runoff away from the pit. For example, the constructed berms to divert the upslope runoff away from the pit, have to be relocated periodically, as mining advances. This results in a situation where there is always, albeit a small, upslope area draining towards the pit.

- the surface recharge through the different types of spoils material in various stages of rehabilitation, grows in significance with time. By the end of the pit operation, this component of the water balance is the most significant. Model simulations using different rates of surface rehabilitation, demonstrate the importance of rapid surface rehabilitation behind the mining front.

- the groundwater inflow along the pit perimeter is a small, but still significant component of the water balance. For the most probable hydrological scenario, the groundwater inflow corresponded to approximately 15% of the total pit water make. This value depends entirely on the local geology and geohydrology of the mined land. The simulated 15% contribution is typical for relatively small opencast pits on the Mpumalanga Highveld Coalfields.

- pit water generation is quite sensitive to the actual rainfall. A comparison of the simulated excess pit water generation for different rainfall/hydrological scenarios indicated that it can differ substantially from dry to wet years.

- the relative contribution from surface runoff, surface recharge and groundwater flows to the total pit water make changes with time. During the early life of the mine, the surface runoff dominates the water balance. Towards the end of the operational life of the pit, surface recharges, especially through unrehabilitated spoils areas, become progressively more important.

The pit water production is also seasonal. The simulated monthly excess pit water generation is shown graphically on **Figure 6.3(a)**. The pit water production peaks in late summer and decreases to low values in winter. It is also noticeable that the peak monthly excess water production increases with time. This can be attributed to the increasing size of land disturbed by mining and contributing to the pit water generation.

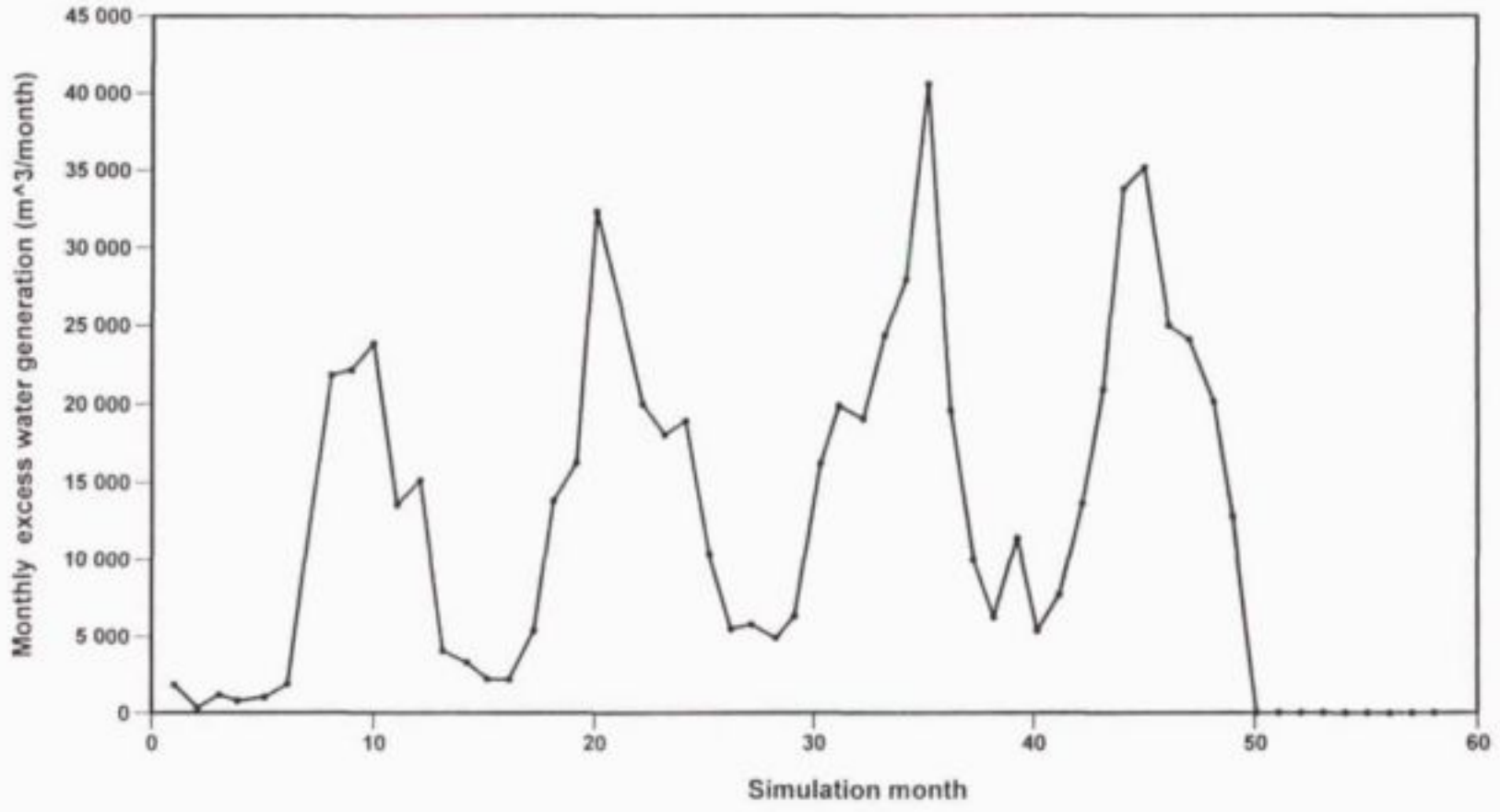

Figure 6.3 (d) : Seasonal variation in simulated pit water generation (Wet case scenario)

7. CONCLUSIONS

Development of a generic opencast mine water model has confirmed that the water system is indeed very complex. A large number of mining, hydrological, geochemical and other variables have to be taken into consideration. The project also confirmed that quasi-empirical models and prediction models based on some average rainfall and typical mine configuration can be very misleading in the prediction of mine water flow and quality.

As the environmental pressures on mining and related operations to cut back on the pollution load emanating from such operations increase, it will become increasingly important to develop accurate prediction tools to assess the generation of excess polluted water from opencast mining operations. Opencast mine water systems are further complicated by the fact that they are open to hydrological influences. This is unlike a closed circuit industrial process, where the water circuit and balance are typically dictated largely by production rates. Opencast mining operations will have to take due cognisance of the environmental risks associated with different hydrological events. The generic model allows such risk assessment by analysing the response of a mining operation to different hydrological sequences. This allows one to develop a quantitative understanding of the risk associated with extreme rainfall/runoff events.

The generic model can also be used to conduct a sensitivity analysis to develop an understanding of the response of the opencast mine water system to different variables. This allows the mine operator to develop, for example, an understanding of the sensitivity of excess mine water production to different mining sequences. The benefit associated with accelerated spoils levelling, topsoiling and vegetation can now be quantified in terms of a reduction in excess water make. Sensitivity analyses in general confirmed that it is essential to have realiable information and data on mine scheduling and mine layout, accurate prediction of runoff associated with a different type of disturbed surfaces, reliable information on the recharge through the rehabilitation cover into the spoils and the geochemical characteristics of the spoils, specifically in terms of reactive pyrite and available carbonate minerals.

The data inputs to the generic opencast mine water model are onerous, but these inputs are required as a minimum to develop a reliable understanding of the mine water system. The initial use of the model for a specific opencast pit, therefore, requires the commitment of adequate resources and time to prepare the input data. Once the model has been configured with the available input data, it then becomes very easy to use and it is possible to look at a number of different mining schedules, rehabilitation strategies, hydrological sequences, etc. without further substantial input requirements.

The practical application of the model to the mining industry will, however, require further training and exposure of mining engineers, environmental officers and water system managers to the model. It is therefore recommended that the Commission gives consideration to the sponsoring of workshops to expose people to the model, develop confidence in the application of the model and to form a nuclear user group which can, in future, assist in the enhancement and refinement of the model.

Consideration should also be given to further research in a number of aspects which we now understand to be critical in the simulation of an opencast mine water system. These aspects include the following:

- Runoff generation from surfaces disturbed or modified by opencast mining operations. A large body of knowledge exists on rainfall/runoff characteristics for small and large catchments in South Africa. The Commission has, in the past, sponsored the development and verification of these models on different types of catchments. We have applied the best available knowledge to the generic mine water model. It is,

however, appropriate to launch a research project to confirm the rainfall/runoff characteristics from surfaces, disturbed or modified by mining. These surfaces include access ramps and ramp slopes, pit floors, mining spoils in different states and different levels of rehabilitation.

- The recharge (infiltration) of rainfall through the rehabilitation cover into the spoils material is a dominant influence over the long term in any opencast mine water system. The Commission has already undertaken research on this topic and we believe that the research work should be continued.

- There is still a general lack of knowledge on the hydrodynamic characteristics of different South African spoils materials. The water retention and water flow characteristics need to be established for a broad spectrum of South African spoils, using techniques which have been applied with success internationally. The model had to rely on international experience and this needs to be extrapolated to South African conditions.

- There is also a general lack of information on the geochemical characteristics and the geochemical behaviour of South African spoils. It is only in recent times that static acid based accounting tests and kinetic leach column tests have been conducted. We need to expand our knowledge to include some full scale research work on the long term behaviour of spoils material under controlled conditions. In general it would appear that the pyrite mineral contained in coal spoils is slowly oxidised and that the pyrite oxidation products are slowly mobilised from the spoils. It will be of value to our understanding of the geochemical behaviour of spoils to undertake full scale investigations into the migration of oxygen within actual spoils bodies and the accumulation of oxidation products.

BIBLIOGRAPHY

ALEXANDER, M. 1977. **Introduction To Soil Microbiology**. John Wiley and Sons, New York. 2nd ed. p. 467.

ALPERS, C.N. and NORDSTROM, D.K. 1991. **Chemical Evolution of Extremely Acid Mine Waters at Iron Mountain, California : Are There Any Lower Limits to pH**. Second International Conference on the abatement of Acid Drainage. Montréal. Canada. 16-18 September 1991.

ANDERSON, W.C. and YOUNGSTROM, M.P. 1976. **Coal pile leachate - Quantity and quality characteristics**. Journal of the Environmental Engineering Division, Proc of ASCE. Vol 102 No EE6. Dec. 1976.

ARIS, R. 1959. **Diffusion and reaction in flow systems of Turner's structures.** Chemical Engineering Science. Vol 10. pp 80-87.

ARIS, R. 1978. **Mathematical Modelling Techniques.** Pitman, London.

BABCOCK, R.E., GREEN, D.W. and PERRY, R.H. 1966. **Longitudinal dispersion mechanisms in packed beds.** A.I.Ch.E.J. Vol 12(5). pp 915-927.

BARNES, H.L. and ROMBERGER, S.B. 1968. **Chemical Aspects of Acid Mine Drainage**. J. Water Poll. Control Fed. Vol 40, No 3. Part 1. March 1968.

BART, R.A. and CARUCCIO, F.T. 1986. **The effect of limestone treatments on the rate of acid generation from pyritic mine gangue.** Environmental Geochemistry and Health. 1986, Vol 8, No 3, pp 71(8).

BECKER, B., GRAFF, M. and NäVEKE, R. 1993. **Initiation of bacterial sulphate reduction in acidic overburden dumps from lignite surface mining**. WISA Proc. of the 3rd biennial conference. Durban, South Africa. pp 24-26. May 1993.

BENJAMIN, L., LOWENTHAL, R.E., and MARAIS, G.V.R. 1977. **Calcium carbonate precipitation kinetics, Part 2 : Effects of Magnesium**. Water SA Vol. 3 No. 3. July 1977.

BENNET, J.W. and RITCHIE, A.I.M. 1991. **Measurements of the Transport of Oxygen into two rehabilitated waste rock dumps**. Second International Conference on the abatement of Acid Drainage. Montréal. Canada. 16-18 September 1991.

BOOTY, W.G., LAM, D.C.L., WONG, I. and ????? 1991. **Water quality modelling system for acid mine drainage**. Second International Conference on the abatement of Acid Drainage. Montréal. Canada. 16-18 September 1991.

BRADHAM, W.S. and CARUCCIO, F.T. 1991. **A comparative study of tailings analysis using acid/base accounting, cells, columns and soxhlets**. Second International Conference on the abatement of Acid Drainage. Montréal. Canada. 16-18 September 1991.

BRITTON, R.R. and GOZON, J.S. 1991. **Acid mine drainage control by re-mining**. Second International Conference on the abatement of Acid Drainage. Montréal. Canada. 16-18 September 1991.

BRODIE, M.J., BROUGHTON, L.M. and ROBERTSON, A.M. 1991. **A conceptual rock classification system for waste management and a laboratory method for ARD prediction from rock piles**. Second International Conference on the abatement of Acid Drainage. Montréal. Canada. 16-18 September 1991.

BROUGTON, L.M., CHAMBERS, R.W. and ROBERTSON, A. M. 1992. **Mine Rock GuidHelines - Design and Control of Damage Water Quality**. Steffen Robertson & Kirsten (B.C.) Inc.

BROUGHTON, L.M. and ROBERTSON, A. M. **Modelling of leachate quality from acid generation waste rock dumps**. Second International Conference on the abatement of Acid Drainage. Montréal. Canada. 16-18 September 1991.

BROWN, A. **Proposal for the mitigation of acid leaching from tailings using a cover muskeg peat.** Second International Conference on the abatement of Acid Drainage. Montréal. Canada. 16-18 September 1991.

BURT, R.A. and CARUCCIO, F.T. 1986. **The effect of limestone treatments on the rate of acid generation from pyritic mine gangue.** Environ. Geochem. and Health 8(3). p. 71-78.

CARUCCIO, F.T. 1968. **An evaluation of factors affecting acid mine drainage production and the ground water interactions in selected areas of western Pennsylvania: Proceedings of the Second Symposium on Coal Mine Drainage Research.** Monroeville, Pennsylvania. pp 107-151.

CARUCCIO, F.T. 1976. **The Character of Drainage as a Function of the Occurrence of Framboidal Pyrite and Ground Water Quality in Eastern Kentucky.** Proceedings of the Symposium coal mine drainage. Research Natl. Coal Association. Bitium Coal Research. Vol 1.

CARUCCIO, F.T. and GEIDEL, G. 1986. **An evaluation of mine waste-overburden analytical techniques.** Proceedings of the 1984 National Symposium on Mining, Hydrology, Sedimentology and Reclamation. Lexington, Kentucky.

CARUCCIO, F.T., GEIDEL, G. and PELLETIER, A. 1978. **Geochemical factors affecting coal mine drainage quality.** In reclamation of drastically disturbed lands. Ed by F.W. Schaller and P. Sutton. American Society of Agronomy. Madison, Wisconsin. pp 129-148.

CATHLES, L.M. 1979. **Predictive Capabilities of a Finite Difference Model of Copper Leaching in low grade Industrial Sulfide Waste Dumps.** Math. Geol. Vol. 11. pp 175-191.

CATHLES, L.M. and APPS, J.A. 1975. **A Model of the Dump Leaching Process that incorporates oxygen balance, heat balance and air convection.** Metallurgical Transactions B. Vol 6B. pp 617-624.

CATHLES, L.M. and SCHLITT, W.J. 1980. **A Model of the Dump Leaching Process that incorporates oxygen balance, heat balance and two dimensional air convection.** Proceedings of the symposium or leaching and recovering copper from as-mined materials. Ed. by W.J. Schlitt, Las Vegas. 26 February 1980, pp 9-15.

CATHLES, L.M. 1983. **Removal of Pyrite from Coal by Heap Leaching**. US Bureau of Mines, Department of the Interior. Open File Report 138-83 (PB 83-238758).

CLAYTON, J.A. **Problems in Industrial Water Systems Proceedings**. The South African Industrial Water Association Symposium. 27 & 28 September 1990.

CLAYTON, J.A., DE VILLIERS, M.G., MAREE, J.P. and PIENAAR, G. 1990. **Calcium carbonate neutralization of acidic effluents in a fluidised bed**. Proceedings of the Southern African Industrial Water Association Symposium - Problems in industrial water systems. Witkoppen, Johannesburg, RSA. 27-28 September 1990.

COLLIN, M. 1987. **Mathematical modelling of water and oxygen transport in layered soil covers for deposits of pyritic mine tailings.** Licentiate Treatise. Royal Institute of Technology, Stockholm, Sweden.

CRAVOTTA, III, C.A., BRADY, K.B.C., SMITH, M.W. and BEAM, R.L. 1990. **Effectiveness of the Addition of Alkaline Materials at surface coal mines in preventing or abating acid mine drainage : Part 1. Geochemical Considerations.** Mining and Reclamation Conference and Exhibition, April 23-26. Charleston, West Virginia.

DAMA, L. and McDONALD, A.J. 1983. **Drainage Quality at Deep Coal Mines Sites**. Water Resources Bulletin (American Water Resources Association). Vol. 19, No. 2.

DAVIS, E.C. and BOEGLY, W.J. 1981. **A Review of water quality issues associated with coal storage**. Journal of Environmental Quality. Vol 10, No. 2. April - June 1981.

DAVIS, G.B. 1983. **Mathematical modelling of rate-limiting mechanisms of pyritic oxidation in overburden dumps**. Department of Mathematics. University of Wollongong, New South Wales.

DAVIS, G.B. and RITCHIE, A.I.M. 1986. **A Model of oxidation in pyritic mine waste I : Equations and Approximate Solutions.** Appl. Math. Modelling. Vol 10. pp 314-322.

DAVIS, G.B., DOHERTY, G. and RITCHIE, A.I.M. 1986. **A Model of oxidation in pyritic mine waste II : Comparison of Numerical and Approximate Solutions.** Appl. Math. Modelling. Vol 10. pp 323-329.

DOEPKER, D.D. 1991. **Column leach study IV : Factors affecting the dissolution of metals from sulfidic metal - mine tailings**. Second International Conference on the abatement of Acid Drainage. Montréal. Canada. 16-18 September 1991.

DOEPKER, D.D. and DRAKE, P.L. 1991. **Laboratory study of submerged metal-mine tailings 3 : Factors influencing the dissolution of metals.** Second International Conference on the abatement of Acid Drainage. Montréal. Canada. 16-18 September 1991.

DONALDSON, E.C., KENDALL, R.F. and BAKER, B.A. 1975. **Surface area measurement of geologic materials.** Soc. Petrol. Eng. J. Vol 15. pp 111-116.

DU PLESSIS, H.M. 1983. **Using lime treated acid mine water for irrigation.** Water Science and Technology. Vol 15, No 2, pp 145-154.

ELBOUSHI, I.M. 1975. **Amount of water needed to initiate flow in rubbly rock particles.** J. Hydrol. Vol 27. pp 275-284.

ERIKSSON N. and DESTOUNI G., 1994. **Modelling Field-Scale Transport of Weathering Products in Mining Waste Rock Dumps.** Third International Conference on the Abatement of Acidic Drainage. Pittsburgh, USA.

EVANGELOU, V.P., PHILLIPS, R.E. and SHEPARD, J.S. 1982. **Salt generation in pyritic coal spoils and its effect on saturated hydraulic conductivity.** Soil Science Society of America Journal. Madison, Wisconsin. Vol 46, No 3, pp 457-460.

FEASBY, D.G., BLANCHETTE, M. and TREMBLAY, G. 1991. **The mine environment neutral drainage (MEND) program**. Second International Conference on the abatement of Acid Drainage. Montréal. Canada. 16-18 September 1991.

FERGUSON, K.D. and MORIN, K.A. 1991. **The prediction of acid rock drainage - lessons from the database**. Second International Conference on the abatement of Acid Drainage. Montréal. Canada. 16-18 September 1991.

FILIPEK, L.H., GORMLEY, J.T., EWING, R. and ELLSWORTH, D. 1991. **Kinetic acid-prediction studies as aids to waste-rock and water management during advanced exploration of a massive sulfide deposit**. Second International Conference on the abatement of Acid Drainage. Montréal. Canada. 16-18 September 1991.

GEIDEL, G. 1979. **Alkaline and acid production potentials of overburden material : the rate of release.** Reclamation Review, 1979, Vol 2, No 3-4, pp 101-107.

GERALD C.F. 1968. **Applied Numerical Analysis"** Addison-Wesley Publishing Company.

GHADIRI, H. and ROSE, C.W. **Modelling Chemical Transport in Soils**. Centre for Catchment and in-stream research. Griffith University. Australia. Lewis Publishers.

GOLDHABER, M.B. 1982. **Experimental study of metastable sulfur oxy-anion formation during pyrite oxidation at pH 6 - 9 and 30°C.** Am. Jour. Sci. Vol 283. pp 193-217.

GOTTSCHLICH, D.E., GREENFIELD, P.F. and BELL, P.R.F. 1987. **Treatment requirements for acid drainage from coal storage heaps**. J. Environmental Engineering. Vol. 113, No. 2. April 1987.

GRISHIN, S.I. and TUOVINEN, O.H. 1988. **Fast kinetics of Fe^{2+} oxidation in packed bed reactors**. Applied and Environmental Microbiology. Vol. 54, No. 12. December 1988.

GROENEWOLD, G.H. and BAILEY, M.J. 1979. **Instability of Contoured Strip Mine Spoils - Western North Dakota.** Ecology and Coal Resource Development. Ed. by M.K. Wali. pp 685-692.

HALBERT, B.E., IBBOTSON, B.G. and SCHARER, J.M. 1980. **Development of Application of a Water Quality Model for use in an Environmental Assessment.** Water Pollution Research Journal of Canada. Vol 15. pp 59-72.

HALL, W.G. 1982. **The kinetics of leaching of organic carbon from in-situ spent shale**. Ph.D. thesis. Lawrence Berkely Laboratory. University of California. May 1982.

HARRIES, J.R. and RITCHIE, A.I.M. 1981. **The use of temperature profiles to estimate the pyritic oxidation rate in a waste rock dump from an open cut mine, Water, Air and Soil Pollution**. Vol 15. pp 405-423.

HART, W.M., BATARSEH, K.I., SWANEY, G.P. and STILLER, A.H. 1991. **A rigorous model to predict the AMD production rate of mine rock**. Second International Conference on the abatement of Acid Drainage. Montréal. Canada. 16-18 September 1991.

HAWKINS, J.W. and ALJOE, W.W. 1991. **Hydrologic characteristics of a surface mine spoil aquifer**. Second International Conference on the abatement of Acid Drainage. Montréal. Canada. 16-18 September 1991.

HELZ, G.R., DAI, J.H., KIPAK, R.J., FRENDINGER, N.J. and RADWAY, J.C. 1987. **Processes controlling the composition of acid sulphate solutions evolved from coal.** Applied Geochemistry. Vol 2. pp 427-436.

HILL, D.W. 1969. **Neutralisation of acid mine drainage**. Journal of the Water Pollutio Control Federation. Oct 1969, Vol 41, No 10, pp 1702-1715.

HODGSON, F. 1992. **The Preliminary Evaluation of the Impact of Coal Strip Mining on Groundwater Resources at Optimum Colliery**. Preliminary Geohydrological Report. June 1992.

HODGSON, F. March 1993. **An Investigation into Water Quality in the Olifants catchment**. Institute for Groundwater Studies. Bloemfontein.

HOFFMAN, M.R., FAUST, B.C., PONDS, F.A., KOO, H.H. and TSUCHIYA, H.M. 1981. **Kinetics of the Removal of Iron Pyrite from Coal by Microbial Catalysis.** Applied Environmental Microbiology. Vol 42. No 2. pp 259-271.

HOOD, W. and OERTER, O. 1984. **A leaching column method for predicting effluent quality from surface mines: Proceedings of the Symposium on Surface Mining Hydrology, Sedimentology, and Reclamation.** Lexington, Kentucky, College of Engineering, University of Kentucky. pp. 271-277.

JAYNES, D.B. 1983. **Atmosphere and temperature within a reclaimed coal stripmine and a numerical simulation of acid mine drainage from stripmined lands.** Ph.D. thesis. Department of Agronomy. Pennsylvania State University. March 1983.

JAYNES, D.B., ROGOWSKI, A.S. and PIONKE, H.B. 1984. **Acid mine drainage from reclaimed coal strip mines : Model description**. Water Resources Research. Vol. 20, No. 2. Febr 1984.

JAYNES, D.B. 1991. **Modelling acid mine drainage from reclaimed coal stripmines**. Second International Conference on the abatement of Acid Drainage. Montréal. Canada. 16-18 September 1991.

JONES, D.R., CHAPMAN, B.M. and JUNG, R.F. 1992. **Experimental and computer modelling studies of acid leaching of rundle oil shale**. Water Resources. Vol. 26, No. 2.

KARATHARASIS, A.D. 1988. **Aluminium and iron equilibrium in soil solutions and surface waters of acid mine watersheds.** Journal of Environmental Quality. Oct - Dec 1988. Vol 17, No 4, pp 534(9).

KARATHARASIS, A.D., THOMPSON, Y.L. and EVANGELOU, V.P. 1990. **Temporal solubility trends of aluminium and iron leached from coal spoils and contaminated soil materials.** Journal of Environmental Quality. Madison, Wisconsin. Vol 19, No 3, pp 389-395.

KARGI, F. and WIESSMAN, J.G. 1984. **A dynamic mathematical model for microbial removal of pyritic sulfur from coal.** Biotechnology and Bioengineering. Vol 26, No 6. pp 604-612.

KEMPE, J.O. 1983. **Review of water pollution problems and control strategies in the South African mining industry.** Water Science and Technology, Oxford. Vo. 15, No 2, pp 27-58.

KLEINMAN, R.L.P., CRERAR, D.A. and PACELLI, R.R. 1981. **Biogeochemistry of acid mine drainage and a method to control acid formation**. Mining Engineering. March 1981. p. 300-305.

KONDOS, P.D., MacDONALD, R.J.C. and ZINCK, J.M. 1991. **Studies on the removal of heavy metals from acidic mineral effluents**. Second International Conference on the Abatement of Acid Drainage. Montréal. Canada. 16-18 September 1991.

KUCERA, E. 1965. **Contribution to the theory of chromatography-linear non-equilibrium elution chromatography.** J. Chromat. Vol. 19. pp 237-248.

KWONG, Y.T.J. 1991. **Acid generation in waste rock as exemplified by the mount Washington minesite, British Columbia, Canada**. Second International Conference on the abatement of Acid Drainage. Montréal. Canada. 16-18 September 1991.

LAI, J.L. and LO, K.S.L. 1992. **Modelling of solute transfer to surface runoff**. Wat. Sci. Tech. Vol. 26, No. 7-8, pp. 1851-1856, 1992. Great Britain.

LAPAKKO, K and ANTONSON, D. 1991. **Mixing of limestone with acid producing rock**. Second International Conference on the abatement of Acid Drainage. Montréal. Canada. 16-18 September 1991.

LAPIDUS, L. 1957. **Flow distribution of diffusion in fixed-bed two phase reactors**. Industrial and engineering Chemistry. Vol. 49, No. 6. June 1957.

LUTHER G.W. 1987 Pyrite Oxidation and Reduction : Molecular Orbital Considerations. Geochem and Cosmochim Acta V53; 3193 - 3200.

MALOUF, E.E. and PRATER, J.D. 1961. **Role of Bacteria in the Alteration of Sulfide Minerals.** Journal of Metals. Vol. 13, No 5. pp. 353-356.

MAREE, J.P., DU PLESSIS, P., VAN DER WALT, C.J., SUZUKI, M., BALLEY, D. and DAHLBERG, A.G. 1992. **Treatment of acidic effluents with limestone instead of lime.** Water Science and Technology. Proceedings of the 16th Biennial Conference. Part 1, Washington DC. Vol 26, No 1 & 2, pp 345-355.

MAREE, J.P., GERBER, A. and HILL, E. 1987. **An integrated process for biological treatment of sulphate containing industrial effluents**. Journal of Water Pol. Contr. Fed. Vol. 59, No. 12, pp 1069-1074. Dec. 1987.

MAREE, J.P. and HILL, E. 1989. **Biological removal of sulphate from industrial effluents and concomitant production of sulphur**. Wat Sci Tech. Vol. 21, pp 265-276. 1989.

McNABB, A., McADAM, G.B. and BRADFORD, E. 1975. **A coupled diffusion model for the reduction of agglomerates of iron oxide granules.** Met. Trans B 6. pp 593-600.

MILLER, S.D., JEFFERY, J.J., WONG, J.W.C. 1991. **Use and misuse of the acid-base accounting for AMD prediction**. Second International Conference on the abatement of Acid Drainage. Montréal. Canada. 16-18 September 1991.

MORIN, R.A., CHERRY, J.A., DAVE, N.K. 1988. **Migration of acidic groundwater seepage from uranium tailings impoundments : Field study and conceptual hydrogeochemical model**. Journal of Contaminant Hydrology. Vol. 2, pp 271-342. 1988.

NEBGEN, J.W. 1981. **Inhibition of acid mine drainage formation : The role of insoluble iron compounds.** Journal of Environmental Sciences. May - June '981, Vol 24, No 3, pp 23(5).

NICHOLSON, R.V. 1984. **Pyrite oxidation in carbonate-buffered systems : Experimental kinetics and control by oxygen diffusion in a porous medium**. Ph.D. thesis. University of Waterloo. Ontario.

NORDSTROM, D.K., JENNE, E.A. and BALL, J.W. 1979. **Redox Equilibria of Iron in acid mine waters**. American Chemical Society. 1979.

NORTH, A.H., SMITH, E.E. and SHUMATE, K.S. 1972. **Pyritic systems : A mathematical model.** EPA-Technol. Series 14010 EAH, Rep. No. 665771.

PALMER, C.D. 1983. **Modelling Hyderogeochemical Processes with the Mass Transfer Model WATE6M-SE.** PhD thesis, University of Waterloo. pp. 374.

PIONKE, H.B., ROGOWSKI, A.S. and DE ANGELIS, R.J. 1980(a). **Controlling the rate of acid loss from strip mine spoil**. J. Environ. Qual. Vol. 9, No. 4. 1980.

PIONKE, H.B., ROGOWSKI, A.S. and MONTGOMERY, C.A. 1980(b). **Percolate quality of strip mine spoil**. Transactions of the ASAE. pp. 621-628.

RAO, P.S.C., JESSUP, R.E., ROLSTON, D.E., DAVIDSON, J.M. and KILCREASE, D.P. 1980a. **Experimental and mathematical description of non-absorbed solute transfer by diffusion in spherical aggregates.** Soil Sci. Soc. Am. J. Vol 44. pp 684-688.

RAO, P.S.C., JESSUP, R.E., ROLSTON, D.E. and DAVIDSON, J.M. 1980b. **Solute transport in aggregated porous media : Theoretical and experimental evaluation.** Soil Sci. Soc. Am. J. Vol 44. pp 1139 - 1146.

RAUCH, H.W., WHITE, W.B. 1977. **Dissolution kinetics of carbonate rocks 1. Effects of lithology on dissolution rate.** Water Resources Research. Vol. 13, No 2. pp 381-394.

REHN, B.W., GROENEWOLD, G.H. and MORIN, K.A. 1980. **Hydraulic Properties of Coal and Related Materials, Northern Great Plains.** Ground Water. Vol 18, No 6. pp 329-342.

RENTON, J.J. 1983. **Evaluation of acid mine water generation an acid mine drainage potential of coal and coal associated rocks**. Water Research Institute. West Virginia University. Morgantown, Aug. 1983.

RENTON, J.J., RYMER, T.E. and STILLER, A.H. 1988. **A laboratory procedure to evaluate the acid producing potential of coal associated rocks.** Mining Science and Technology. Vol 7. pp 227-235.

RITCEY, G.M. 1991. **Deep water disposal of pyritic tailings - A simulation for acid prediction**. Second International Conference on the abatement of Acid Drainage. Montréal. Canada. 16-18 September 1991.

RITCHIE, A.I.M. 1977. **Heap leaching. Gas diffusion rate-limited model.** AAEC/E429.

ROGOWSKI, A.S., PIONKE, H.B. and BROYAN, J.G. 1977. **Modelling the impact of strip mining and reclamation processes on quality and quantity of water in mined areas : A review**. Journal of Environmental Quality. Vol. 6, No. 3. July - September 1977.

ROGOWSKI, A.S., PIONKE, H.B. and BROYAN, J.G. 1980. **Percolate Quality of Strip Mine Spoil.** Transactions of the ASAE.

ROGOWSKI, A.S. and WEINRICH, B.E. 1981. **Modelling water flux on strip-mined land.** Trans. ASAE. Vol 24. pp 935-940.

RYMER, T.E., SKOUSEN, J.G., RENTON, J.J., ZONDLO, A.M. and ZIEMKIEWICZ, P.F. 1991(a) **Undetected sources of detectable acid mine drainage : Some statistical considerations in rock sampling**. Second International Conference on the abatement of Acid Drainage. Montréal. Canada. 16-18 September 1991.

RYMER, T., RENTON, J.J., ZIEMKIEWICZ, P.F. 1991(b) **Isolation of critical predictive acid producing parameters from variable field data using advanced computer technology**. Second International Conference on the abatement of Acid Drainage. Montréal. Canada. 16-18 September 1991.

RYMER, T., STILLER, A.and RENTON, J. 1989. **The Effect of pyrite grain clustering on total sulfur analysis.** Proceedings of the 9th Annual West Virginia surface mine drainage task force symposium, Morgantown, West Virginia.

SASOWSKY, I.D. and WHITE, W.B. 1993. **Geochemistry of the Obey River Basin, north-central Tennessee : A case of acid mine water in a karst drainage system.** Journal of Hydrology. Vol 146, No 1 & 4, pp 29-48.

SCHARER J.M. 1994 **Mathematical Simulation of a Waste Rock Heap**. Third International Conference on the Abatement of Acidic Drainage. Pittsburgh.

SCHARER, J.M., GARGA, V., SMITH, R.and HALBERT, B.E. 1991. **Use of state for assessing acid generation in pyritic mine tailings**. Second International Conference on the abatement of Acid Drainage. Montréal. Canada. 16-18 September 1991.

SCHULZ, H.D. 1988. **Laboratory determination of carbonate dissolution kinetics in groundwater by measuring saturation length.** Geochimica-Cosmochimica-Acta, Oxford. Vol 52, No 11, pp 2651-2657.

SINGER, P.C., STUMM, W. 1970. **Acidic mine drainage : The rate determining step**. Science. Vol 167. Feb. 1970.

SMITH, A. 1989. **Some implications of characterization, acid generation and leachability test data to waste rock and spent ore disposal.** Annual meeting of Soc. Mining Engineers, February 1989. Las Vegas, Nevada.

SMITH, A. and BARTON-BRIDGES, J. 1991. **Considerations in the prediction and control of acid drainage impact from mining wastes on water resource utilization**. EPPIC 1991. Environmental Conference : Water. Randburg, South Africa. 16-17 May 1991.

SMITH, J.R., LUTHY, R.G. and MIDDLETON, A.C. 1988. **Microbial ferrous iron oxidation in acidic solution**. Journal of Wat. Poll. Cont. Fed. Vol. 60, No. 4. April 1988.

SMITH, R.M. and SOBEK, A.A. 1978. **Physical and chemical properties of overburdens, spoils, wastes, and new soils.** Reclamation of Drastically Disturbed Lands. Ed. by F.W. Schaller and P. Sutton. (American Society of Agronomy, Madison, Wisconsin. pp. 149-172.

SOBEK, A.A., SCHULLER, W.A., FREEMAN, J.R. and SMITH, R.M. 1978. **Field and laboratory methods applicable to overburdens and mine soils.** United States Environmental Protection Agency. EPA 600/2-78-054. Cincinnati, Ohio.

STEFFEN, ROBERTS & KIRSTEN. 1989. **Draft acid rock drainage technical guide**. Volume 1, 2. Prepared for the British Columbia AMD Task Force.

STEFFEN, ROBERTS & KIRSTEN. 1992. **Mine Rock Guidelines. Design and control of drainage water quality**. Report No. 93301. Saskatchewan Environment and Public Safety. Mines Pollution Control Branch. April 1992.

STUMM, W. and MORGAN, J.J. 1981. **Aquatic chemistry - An introduction emphasizing chemical equilibria in natural waters**. John Wiley and Sons. New York. pp 780.

SUGIO, T. 1985. **Role of ferric iron-reducing system in sulphur oxidation of Thiobacillus ferroxidans**. J. Bacteriology. Vol 44. pp 1401-1416.

THOMPSON, J.G. 1980. **Acid mine water in South Africa and their amelioration**. Water SA. Vol. 6, No. 3. July 1980.

TROEH, F.R., JABRO, J.D. and KIRKHAM, D. 1982. **Gaseous diffusion equations for porous materials.** Geoderma Vol 27. pp 239-253.

TURNER, G.A. 1958. **The flow structure in packed beds.** Chem. Engng. Sci. Vol 7. pp 156-165.

TUTTLE, J.H. 1969. **Microbial dissimilatory sulfur cycle in acid mine water**. Journal of Bacteriology. Vol. 97**(2)**, pp 594-602.

VLEK, P.L.G., BLOM, Th. J.M., BEEK, J. and LINDSAY, W.L. 1974. **Determination of solubility product of various iron hydroxides and jarosite by the chelation method.** Soil Science Society America Journal. Vol. 38. pp 429-432.

WEEKS, E.P., EARP, D.E. and THOMPSON, G.M. 1982. **Use of atmospheric fluorocarbons F-11 and F-12 to determine the diffusion parameters of the unsaturated zone in the southern high plains of Texas.** Water Resources Research. Vol 18. pp 1365-1378.

WICKS and GROVES. 1993. **Acid Mine Drainage in Carbonate Terrains : Geochemical Processes and rates of calcite dissolution.** Journal of Hydrology. 1993, Vol 146, pp 13(15).

WIRRIES, D.L. and McDONELL, A.J. 1983. **Drainage quality at deep coal mine sites**. Water Resources Bulletin. American Water Resources Association. Vol. 19, No. 2. April 1983.

YANFUL, E.K. 1991 **Engineered soil covers for reactive tailings management : Theoretical concepts and laboratory development**. Second International Conference on the abatement of Acid Drainage. Montréal. Canada. 16-18 September 1991.

YOSHIDA, F. and KOYANAGI, T. 1958. **Liquid phase mass transfer rates and effective interfacial area in packed absorption columns**. Industrial and engineering chemistry. Vol. 50, No. 3. March 1958.

GENERIC SIMULATION MODEL FOR

OPENCAST MINE WATER SYSTEMS

APPENDIX A

Parameter tables for SCS based
hydrological modelling

Runoff Curve Numbers for selected agricultural, suburban and urban land uses

LAND USE	TREATMENT/PRACTICE/DESCRIPTION	HYDROLOGICAL CONDITION	Hydrological Soil Group						
			A	A/B	B	B/C	C	C/D	D
Fallow	Straight row		77	82	86	89	91	93	94
Row crops	Straight row	Poor	72	77	81	85	88	90	91
	Straight row	Good	67	73	78	82	85	87	89
	Planted on contour	Poor	70	75	79	82	84	86	88
	Planted on contour	Good	65	70	75	79	82	84	86
	Conservation structures	Poor	66	70	74	77	80	81	82
	Conservation structures	Good	62	67	71	75	78	80	81
Garden and truck crops	Straight row		45	56	66	72	77	80	83
	Straight row	Good	68	71	75	79	81	83	84
Small grain	Straight row	Poor	65	71	76	80	84	86	88
	Straight row	Good	63	69	75	79	83	85	87
	Planted on contour	Poor	63	69	74	79	82	84	85
	Planted on contour	Good	61	67	73	78	81	83	84
	Planted on contour - winter rainfall region	Good	63	66	70	75	78	80	81
	Conservation structures	Poor	61	67	72	76	79	81	82
	Conservation structures	Good	59	65	70	75	78	80	81
Close seeded legumes or Rotational meadow	Straight row	Poor	66	72	77	81	85	87	89
	Straight row	Good	58	65	72	75	81	84	85
	Planted on contour	Poor	64	70	75	80	83	84	85
	Planted on contour	Good	55	63	69	74	78	81	83
	Conservation structure	Poor	63	68	73	77	80	82	83
	Conservation structure	Good	51	60	67	72	76	78	80
Sugarcane	Straight row: trash burnt	-	43	55	65	72	77	80	82
	Straight row: trash mulch	-	45	56	66	72	77	80	83
	Straight row: limited cover	-	67	73	78	82	85	87	89
	Straight row: partial cover	-	49	60	69	73	79	82	84
	Straight row: complete cover	-	39	50	61	68	74	78	80
	Planted on contour: limited cover	-	65	70	75	79	82	84	86
	Planted on contour: partial cover	-	25	46	59	67	75	80	83
	Planted on contour: complete cover	-	6	14	35	59	70	75	79
Pasture or veld (range)	-	Poor	68	74	79	83	86	88	89
	-	Fair	49	61	69	75	79	82	84
	-	Good	39	51	61	68	74	78	80
	Planted on contour	Poor	47	57	67	75	81	85	88
	Planted on contour	Fair	25	46	59	67	75	80	83
	Planted on contour	Good	6	14	35	59	70	75	79
Irrigated pasture		Good	35	41	48	57	65	68	70
Meadow		Good	30	45	58	65	71	75	81
Woods		Poor	45	56	66	72	77	80	83
		Fair	36	49	60	68	73	77	79
		Good	25	47	55	64	70	74	77
Scrub	Brush - winter rainfall region	-	28	34	44	53	60	64	66
Orchards	Winter region, understory of crop cover	Good	39	44	53	61	66	69	71
Forests/ plantations	Humus depth 25 mm; Compactness:	compact	52	62	72	77	82	85	87
		moderate	48	58	68	73	78	82	85
		loose/friable	37	49	60	66	71	74	77
	Humus depth 50 mm; Compactness:	compact	48	58	68	73	78	82	85
		moderate	42	54	65	70	75	78	81
		loose/friable	32	45	57	62	67	71	74
	Humus depth 100mm; Compactness:	compact	41	53	64	69	74	77	80
		moderate	34	47	59	64	69	72	75
		loose/friable	25	37	50	56	61	64	67
	Humus depth 150mm; Compactness:	compact	37	49	60	66	71	74	77
		moderate	30	43	56	61	66	69	72
		loose/friable	18	33	47	52	57	61	65
Urban/suburban land uses	Open spaces, parks, cemeteries	Good (75% + grass cover)	39	51	61	68	74	78	80
		Fair (50-75% grass cover)	49	61	69	75	79	82	84
	Commerical/business areas	85% impervious	89	91	92	93	94	95	95
	Industrial districts	72% impervious	81	85	88	90	91	92	93
	Residential: lot size 500m²	65% impervious	77	81	85	88	90	91	92
	1000m²	38% impervious	61	69	75	80	83	85	87
	1350m²	30% impervious	57	65	72	77	81	84	86
	2000m²	25% impervious	54	63	70	76	80	83	85
	4000m²	20% impervious	51	61	68	75	78	82	84
	Paved parking lots, roofs, etc.		98	98	98	98	98	98	98
	Streets/roads: tarred, with storm sewers, curbs		98	98	98	98	98	98	98
	gravel		76	81	85	88	89	90	91
	dirt		72	77	82	85	87	88	89
	dirt-hard surface		74	79	84	88	90	91	92

Runoff Curve Numbers for conservation tillage (after Rawls and Richardson, 1983)

LAND USE	COVER TREATMENT OR PRACTICE	HYDROLOGICAL CONDITION	RUNOFF CURVE NUMBERS BY HYDROLOGICAL SOIL GROUP A	B	C	D
Fallow	Straight row		77	86	91	94
	Straight row + conservation tillage	Poor*	75	84	09	92
	Straight row + conservation tillage	Good*	74	83	87	90
Row crops	Straight row	Poor	72	81	00	91
	Straight row	Good	67	78	85	09
	Straight row + conservation tillage	Poor*	71	79	86	89
	Straight row + conservation tillage	Good*	64	75	82	85
	Planted on contour	Poor	70	79	84	88
	Planted on contour	Good	65	84	82	86
	Planted on contour + conservation tillage	Poor*	69	78	83	87
	Planted on contour + conservation tillage	Good*	64	74	80	04
	Conservation structures	Poor	66	74	80	82
	Conservation structures	Good	62	71	70	81
	Conservation structures + conservation tillage	Poor*	65	73	79	81
	Conservation structures + conservation tillage	Good*	61	70	76	79
Small grains	Straight row	Poor	65	76	84	88
	Straight row	Good	63	75	03	07
	Straight row + conservation tillage	Poor*	64	74	02	86
	Straight row + conservation tillage	Good*	60	72	80	84
	Planted on contour	Poor	63	74	82	85
	Planted on contour	Good	61	73	81	84
	Planted on contour + conservation tillage	Poor*	62	73	81	84
	Planted on contour + conservation tillage	Good*	60	72	79	82
	Conservation structures	Poor	61	72	79	82
	Conservation structures	Good	59	70	78	81
	Conservation structures + conservation tillage	Poor*	60	71	78	81
	Conservation structures + conservation tillage	Good*	58	69	76	79

* Less than 20 % of the surface is covered with residue (less than 800 kg/ha for row crops or 350 kg/ha for small grain).

* More than 20 % of the surface is covered with residue (more than 850 kg/ha for row crops or 350 kg/ha for small grain).

Hydrological classification of soil forms and series found in southern Africa (Source : Schulze, 1984)

Legend

A - low runoff potential
B - moderately low potential
C - moderately high potential
D - high runoff potential
c - crusting
l - leaching
t - texture
w - water table

Cl - clay
S - sand
lm - loam
0 - no/low interflow potential
X - some interflow potential
XX - high interflow potential

Soil Form	Code	Soil Series	SCS Group -ing	SCS Adjust-ment Factor	Typical Text-ural Class	Inter-flow Poten-tial
ARCADIA C/D	Ar 40	Arcadia	C/D		Cl	0
	Ar 11	Bloukrans	C/D		Cl	0
	Ar 21	Clerkness	C/D		Cl	0
	Ar 41	Eenzaam	C/D		Cl	0
	Ar 20	Gelykvlakte	C/D		Cl	0
	Ar 10	Mngazi	C/D		Cl	0
	Ar 32	Nagana	C/D		Cl	0
	Ar 12	Koukloof	C/D		Cl	0
	Ar 31	Rooidraai	C/D		Cl	0
	Ar 30	Rydalvale	C/D		Cl	0
	Ar 42	Wanstead	C/D		Cl	0
	Ar 22	Zwaarkrygen	C/D		Cl	0
AVALON B	Av 13	Ashton	A/B	+l	SLm	X
	Av 26	Avalon	B		SClLm	X
	Av 12	Banchory	A	+l/+t	S	X
	Av 27	Bergville	B/C	-t	SCl	X
	Av 37	Bezuidenhout	C	-t/-l	SCl	X
	Av 33	Bleeksand	B/C	-l	SLm	X
	Av 34	Heidelberg	B/C	-l	SLm	X
	Av 20	Hobeni	A/B	+t	LmS	X
	Av 14	Kanhym	A/B	+l	SLm	X
	Av 24	Leksand	B		SLm	X
	Av 10	Mastaba	A	+l/+t	LmS	X
	Av 32	Middelpos	B	+t/-l	S	X
	Av 31	Koolveld	B	+t/-l	LmS	X
	Av 25	Newcastle	A/B	+t	SLm	X
	Av 17	Normandien	B	+l/-t	SCl	X
	Av 22	Rossdale	A/B	+t	S	X
	Av 16	Ruston	B	+l	SClLm	X
	Av 36	Soetmelk	B/C	-l	SClLm	X
	Av 21	Uithoek	A/B	+t	LmS	X
	Av 30	Viljoenskroon	B	+t/-l	LmS	X
AVALON (contd)	Av 23	Villiers	B		SLm	X
	Av 11	Welverdiend	A	+l/+t	LmS	X
	Av 35	Windmeul	B	+t/-l	SLm	X
	Av 15	Wolweberg	A	+l/+t	SLm	X
BAINSVLEI A/B	Bv 23	Ashkelon	A/B		SLm	X
	Bv 36	Bainsvlei	B	-l	SClLm	X
	Bv 12	Camelot	A	+t	S	X
	Bv 20	Chelsea	A	+t	LmS	X
	Bv 30	Delwery	A/B	+t/-l	LmS	X
	Bv 13	Dunkeld	A/B		SLm	X
	Bv 16	Elysium	A/B		SClLm	X
	Bv 10	Hlatini	A	+t	LmS	X
	Bv 34	Kareekuil	B	-l	SLm	X
	Bv 31	Kingston	A/B	+t/-l	LmS	X
	Bv 26	Lonetree	A/B		SClLm	X
	Bv 25	Maanhaar	A	+t	SLm	X
	Bv 11	Makong	A	+t	LmS	X
	Bv 27	Metz	B	-t	SCl	X
	Bv 22	Oosterbeek	A	+t	S	X
	Bv 37	Ottosdal	B/C	-t/-l	SCl	X
	Bv 24	Redhill	A/B		SLm	X
	Bv 32	Trekboer	A/B	+t/-l	S	X
	Bv 15	Tygerkloof	A	+t	SLm	X
	Bv 33	Vermaas	B	-l	SLm	X
	Bv 21	Vungama	A	+t	LmS	X
	Bv 35	Wedgewood	A/B	+t/-l	SLm	X
	Bv 17	Wilgenhof	B	-t	SCl	X
	Bv 14	Wykeham	A/B		SLm	X
BONHEIM C	Bo 41	Bonheim	C/D	-t	LmS	0
	Bo 20	Bushman	C		SClLm	0
	Bo 30	Dumasi	C		SClLm	0
	Bo 31	Glengazi	C/D	-t	SCl	0
	Bo 10	Kiora	C		SClLm	0
	Bo 21	Rasheni	C/D	-t	SCl	0
	Bo 11	Stanger	C/D	-t	SCl	0
	Bo 40	Weenen	C		SClLm	0

Table (continued)

Soil Form	Code	Soil Series	SCS Group -ing	SCS Adjust-ment Factor	Typical Text-ural Class	Inter-flow Poten-tial
ESTCOURT (contd)	Es 12	Potela	D		S/Slm	II
	Es 16	Rosemead	D		SCILm/SCI	II
	Es 32	Soldaatskraal	D		S/SLm	II
	Es 34	Uitvlugt	D		SLm/SCILm	II
	Es 15	Vredenhoek	D		LmS/SCILm	II
	Es 17	Zintwala	D		SCI/CI	II
FERNWOOD A	Fw 40	Brinley	C	-w	SLm	II
	Fw 11	Fernwood	A		SLm	0
	Fw 21	Langebaan	A		SLm	0
	Fw 42	Mambone	C	-w	SLm	II
	Fw 10	Maputa	A		SLm	0
	Fw 20	Motopi	A		SLm	0
	Fw 22	Saldanha	A		SLm	0
	Fw 12	Sandveld	A		SLm	0
	Fw 30	Shasha	B	-w	SLm	II
	Fw 41	Soetvlei	C	-w	SLm	II
	Fw 32	Trafalgar	B	-w	SLm	II
	Fw 31	Warrington	B	-w	SLm	II
GLENCOE B	Gc 16	Appam	B		SCILm	I
	Gc 33	Beatrix	B/C	-i	SLm	I
	Gc 20	Boskuil	A/B	+t	LmS	I
	Gc 15	Delmas	A/B	+t	SLm	I
	Gc 10	Driepan	A/B	+t	LmS	I
	Gc 24	Dunbar	B		SLm	I
	Gc 26	Glencoe	B		SCILm	I
	Gc 37	Grespan	C	-t/-i	SCI	II
	Gc 11	Hartog	A/B	+t	LmS	II
	Gc 13	Klipstapel	B		SLm	II
	Gc 32	Kwezana	B	+t/-i	S	II
	Gc 34	Leeudoorn	B/C	-i	SLm	II
	Gc 36	Leslie	B/C	-i	SCILm	II
	Gc 27	Ontevrede	B/C	-t	SCI	II
	Gc 21	Penhoek	A/B	+t	LmS	II
	Gc 31	Ribblesdale	B	+t/-i	LmS	II
	Gc 17	Shotton	B/C	-t	SCI	II
	Gc 23	Strathree	B		SLm	II
	Gc 22	Talana	A/B	+t	S	II
	Gc 12	Tranendal	A/B	+t	S	II
	Gc 35	Uitskot	B	+t/-i	SLm	II
	Gc 30	Vlakpan	B	+t/-i	LmS	II
	Gc 14	Weltevrede	B		SLm	II
	Gc 25	Wesselsnek	A/B	+t	SLm	II
GLENROSA B/C	Gr 28	Achterdam	B/C		SCILm	I
	Gr 27	Dothole	B/C		SCILm	I
	Gr 24	Dunvegan	B/C		SLm	I
	Gr 15	Glenrosa	B	+t	SLm	I
	Gr 13	Kanonkop	B/C		SLm	I
	Gr 22	Knapdaar	B	+t	S	I
	Gr 26	Lekfontein	B/C		SCILm	I
	Gr 25	Lomondo	B	+t	SLm	I
	Gr 21	Majeng	B	+t	LmS	I
	Gr 20	Malgas	B	+t	LmS	I
	Gr 10	Martindale	B	+t	LmS	I
	Gr 11	Orsbi	B	+t	LmS	I
	Gr 12	Paardeberg	B	+t	S	I
	Gr 14	Platt	B/C		SLm	I
	Gr 29	Ponda	C	-t	SCI	I
	Gr 18	Robmore	B/C		SCILm	I
	Gr 19	Saintfaiths	C	-t	SCI	I
	Gr 23	Southfield	B/C		SLm	I
	Gr 17	Trevanian	B/C		SCILm	I
	Gr 16	Williamson	B/C		SCILm	I
GRIFFIN A	Gf 10	Burnside	A		SLm	0
	Gf 11	Cleveland	A		SCILm	0
	Gf 32	Cradock	B	-t/-i	SCI	0
	Gf 20	Erfdeel	A		SLm	0
	Gf 13	Farmhill	A/B	-t	CI	0
	Gf 12	Griffin	A/B	-t	SCI	0
	Gf 22	Ixopo	A/B	-t	SCI	0
	Gf 30	Runnymeade	A/B	-i	SLm	0
	Gf 33	Slagkraal	B	-t/-i	CI	0
	Gf 21	Umzinkulu	A		SCILm	0
	Gf 31	Welgemoed	A/B	-i	SCILm	0
	Gf 23	Zwagershoek	A/B	-t	CI	0
HOUWHOEK C	Hh 20	Albertinia	C		LmS	I
	Hh 10	Elgin	C		LmS	I
	Hh 21	Garcia	C		SLm	II
	Hh 31	Gouna	B/C	+t	SLm	II
	Hh 30	Houwhoek	B/C	+t	S	I
	Hh 11	Stormsrivier	C		SLm	II

Table (continued)

Soil Form	Code	Soil Series	SCS Group -ing	SCS Adjust-ment Factor	Typical Text-ural Class	Inter-flow Poten-tial
CARTREF C	Cf 10	Amabele	B/C	+t	LmS	0
	Cf 12	Arrochar	C		SCILm	0
	Cf 13	Byrne	C/D	-t	SCl	0
	Cf 21	Cartref	C		SLm	0
	Cf 22	Cranbrook	C		SCILm	0
	Cf 30	Grovedale	B/C	+t	S	0
	Cf 31	Kusasa	B/C	+t	SLm	0
	Cf 32	Noodhulp	C		SCILm	0
	Cf 11	Rutherglen	C		SLm	0
	Cf 20	Waterridge	B/C	+t	LmS	0
CHAMPAGNE D	Ch 11	Champagne	D		SLm	0
	Ch 21	Ivanhoe	D		SCILm	0
	Ch 10	Mposa	D		SLm	0
	Ch 20	Stratford	D		SCILm	0
CLOVELLY A/B	Cv 33	Annandale	B	-l	SLm	0
	Cv 18	Balgowan	B	-t	Cl	0
	Cv 40	Bleskop	A	+t	LmS	0
	Cv 36	Blinkklip	B	-l	SCILm	0
	Cv 17	Clovelly	B	-t	SCl	0
	Cv 28	Clydebank	B	-t	Cl	0
	Cv 35	Denhere	A/B	+t/-l	SLm	0
	Cv 46	Dudfield	A/B		SCILm	0
	Cv 11	Geelhout	A	+t	LmS	0
	Cv 25	Gutu	A	+t	SLm	0
	Cv 47	Klippan	B	-t	SCl	0
	Cv 38	Klipputs	B/C	-t/-l	Cl	0
	Cv 10	Lismore	A	+t	LmS	0
	Cv 12	Lundini	A	+t	S	0
	Cv 34	Makuya	B	-l	SLm	0
	Cv 14	Mossdale	A/B		SLm	0
	Cv 48	Nelspan	B	-t	Cl	0
	Cv 27	Newport	B	-t	SCl	0
	Cv 16	Oatsdale	A/B		SCILm	0
	Cv 23	Ofazi	A/B		SLm	0
	Cv 41	Oranje	A	-t	LmS	0
	Cv 32	Paleisheuwel	A/B	+t/-l	S	0
	Cv 31	Sandspruit	A/B	+t/-l	LmS	0
	Cv 22	Sebakwe	A	+t/-l	S	0
	Cv 45	Skipskop	A	+t	SLm	0
	Cv 21	Sonnenblom	A	+t	LmS	0
	Cv 26	Southwold	A/B		SCILm	0
CLOVELLY (contd)	Cv 15	Soweto	A	+t	SLm	0
	Cv 24	Springfield	A/B		SLm	0
	Cv 30	Sunbury	A/B	+t/-l	LmS	0
	Cv 37	Summerhill	B/C	-t/-l	SCl	0
	Cv 42	Thornhill	A	+t	S	0
	Cv 44	Torquay	A/B		SLm	0
	Cv 20	Tweefontein	A	+t	LmS	0
	Cv 43	Vaalbank	A/B		SLm	0
	Cv 13	Vidal	A/B		ClLm	0
CONSTAN -TIA B	Ct 25	Cintsa	B		Lm/SCILm	II
	Ct 12	Constantia	B		LmS	I
	Ct 23	Dwesa	B		SLm/SCILm	II
	Ct 22	Fencote	B		S/SCILm	II
	Ct 13	Harkerville	B		SLm	0
	Ct 24	Kromhoek	B		SCl/SCILm	II
	Ct 14	Noetzie	B		SLm	0
	Ct 20	Palmyra	B		LmS/SCILm	II
	Ct 10	Strombolis	B		LmS	I
	Ct 11	Tokai	B		S	I
	Ct 21	Vlakfontein	B		LmS/SCILm	II
	Ct 15	Wynberg	B		SLm	0
DUNDEE B/C	Du 10	Dundee	B/C		SLm	0
ESTCOURT D	Es 20	Assegaai	D		LmS/SCILm	II
	Es 11	Auckland	D		LmS/SLm	II
	Es 22	Avontuur	D		S/SCILm	II
	Es 35	Balfour	D		LmS/SCILm	II
	Es 40	Beerlaagte	D		LmS/SCILm	II
	Es 37	Buffelscrif	D		SCl/Cl	II
	Es 42	Darling	D		S/SCILm	II
	Es 13	Dohne	D		SLm/SCILm	II
	Es 31	Elim	D		LmS/SLm	II
	Es 33	Enkelboom	D		SLm/SCILm	II
	Es 36	Estcourt	D		SCILm/SCl	II
	Es 14	Grasslands	D		SLm/SCILm	II
	Es 41	Heights	D		LmS/SCILm	II
	Es 10	Houdenbeck	D		LmS/SLm	II
	Es 21	Langkloof	D		LmS/SCILm	II
	Es 30	Mozi	D		LmS/SLm	II

Table (continued)

Soil Form	Code	Soil Series	SCS Group-ing	SCS Adjust-ment Factor	Typical Text-ural Class	Inter-flow Poten-tial
HUTTON A	Hu 10	Alloway	A		LmS	0
	Hu 11	Arnot	A		LmS	0
	Hu 18	Balmoral	A/B	-t	Cl	0
	Hu 25	Bontberg	A		SLm	0
	Hu 22	Chester	A		S	0
	Hu 24	Clansthal	B		SLm	0
	Hu 27	Doveton	A/B	-t	SCl	0
	Hu 17	Farningham	A/B	-t	SCl	0
	Hu 31	Gaudam	A	-1/+t	LmS	0
	Hu 47	Hardap	A/B	-t	SCl	0
	Hu 16	Hutton	A		SClLm	0
	Hu 21	Joubertina	A		LmS	0
	Hu 15	Kyalami	A		SLm	0
	Hu 23	Lichtenburg	A		SLm	0
	Hu 40	Lowlands	A		LmS	0
	Hu 43	Maitengwe	A		SLm	0
	Hu 37	Makatini	B	-t/-1	SCl	0
	Hu 44	Malonga	A		SLm	0
	Hu 33	Mangano	A/B	-1	SLm	0
	Hu 38	Marikana	B	-t/-1	Cl	0
	Hu 14	Middelburg	A		SLm	0
	Hu 48	Minhoop	A/B	-t	Cl	0
	Hu 32	Moriah	A	-1/+t	S	0
	Hu 26	Msinga	A		SClLm	0
	Hu 41	Nyala	A		LmS	0
	Hu 35	Portsmouth	A	-1/+t	SLm	0
	Hu 42	Quaggafontein	A		S	0
	Hu 30	Roodepoort	A	-1/+t	LmS	0
	Hu 46	Shigalo	A		SClLm	0
	Hu 36	Shorrocks	A/B	-1	SClLm	0
	Hu 12	Stonelaw	A		S	0
	Hu 45	Vergenoeg	A		SLm	0
	Hu 28	Vimy	A/B	-t	Cl	0
	Hu 13	Wakefield	A		SLm	0
	Hu 20	Whithorn	A		LmS	0
	Hu 34	Zwartfontein	A/B	-1	ClLm	0
INANDA A	Ia 10	Fountainhill	A		SClLm	0
	Ia 11	Inanda	A		SCl	0
	Ia 12	Sprinz	A		Cl	0
INHOEK C	Ik 11	Coniston	C/D	-t	SCl	0
	Ik 10	Cronley	C		SClLm	0
	Ik 21	Drydale	C/D	-t	SCl	0
	Ik 20	Inhoek	C		SClLm	0
KATSPRUIT C/D	Ka 10	Katspruit	C/D		SCl	0
	Ka 20	Killarney	C/D		SCl	0
KRANSKOP A	Kp 10	Kipipiri	A		SClLm	0
	Kp 11	Kranskop	A		SCl	0
	Kp 12	Umbumbulu	A		Cl	0
KROONSTAD C/D	Kd 17	Avoca	C/D		SClLm/SCl	II
	Kd 16	Bluebank	C/D		SClLm/SCl	II
	Kd 22	Katarra	C/D		S/SClLm	II
	Kd 20	Koppies	C/D		LmS/SClLm	II
	Kd 13	Kroonstad	C/D		SLm/SClLm	II
	Kd 14	Mkanbati	C/D		SLm/SClLm	II
	Kd 10	Rocklands	C/D		LmS/SLm	II
	Kd 15	Slangkop	C/D		LmS/SClLm	II
	Kd 12	Swellengift	C	+t	S/SLm	II
	Kd 18	Uitspan	C/D		SClLm/SCl	II
	Kd 21	Umtentweni	C/D		LmS/SClLm	II
	Kd 11	Velddrif	C/D		LmS/SLm	II
	Kd 19	Volksrust	D	-t	SCl/Cl	II
LAMOTTE A/B	Lt 10	Alsace	A/B		LmS	I
	Lt 21	Burgundy	B	+c	LmS	II
	Lt 14	Chamond	A/B		SLm	I
	Lt 22	Franschhoek	B	+c	LmS	II
	Lt 25	Hooghalen	B	+c	SLm	II
	Lt 12	Lamotte	A/B		LmS	I
	Lt 11	Leperis	A/B		LmS	I
	Lt 15	Lillesand	A/B		SLm	I
	Lt 20	Lorraine	B	+c	LmS	II
	Lt 24	Ringwood	B	+c	SLm	II
	Lt 23	Tillberga	B	+c	SLm	II
	Lt 13	Vevey	A/B		SLm	I
LONGLANDS C	Lo 22	Albany	C/D	-t	SClLm	II
	Lo 32	Chitsa	C/D	-t	SClLm	II

Table (continued)

Soil Form	Code	Soil Series	SCS Group -ing	SCS Adjust-ment Factor	Typical Text-ural Class	Inter-flow Poten-tial
LONGLANDS (contd)	Lo 21	Longlands	C		SLn	XX
	Lo 10	Orkney	C		LnS	XX
	Lo 30	Tayside	C		S	XX
	Lo 31	Vaalsand	C		SLm	XX
	Lo 20	Vasi	C		LmS	XX
	Lo 11	Waalsand	C		SLm	XX
	Lo 12	Waldene	C/D	-t	SCILm	XX
	Lo 13	Winterton	C	-t	SCI	XX
MAGWA A/B	Ma 12	Frazer	A/B		CI	0
	Ma 11	Magwa	A/B		SCI	0
	Ma 10	Milford	A	+t	SCILm	0
MAYO C	My 10	Mayo	C		SCILm	0/X
	My 11	Msinsini	C/D	-t	SCI	0/X
	My 21	Pafuri	C/D	-t	SCI	0/X
	My 20	Tshipise	C		SCI	0/X
MILKWOOD C	Mw 10	Dansland	C		SCILm	0/X
	Mw 21	Graythorne	C/D	-t	SCI	0/X
	Mw 11	Milkwood	C/D	-t	SCI	0/X
	Mw 20	Sunday	C		SCILm	0/X
MISPAH C	Ms 21	Hillside	C		SCILm	XX
	Ms 22	Kalkbank	C		SCILm	XX
	Ms 11	Klipfontein	C		SCILm	XX
	Ms 12	Loskop	C		SCILm	XX
	Ms 23	Misgund	C		SCILm	XX
	Ms 10	Mispah	C		SCILm	XX
	Ms 20	Muden	C		SCILm	XX
	Ms 13	Plettenberg	C		SCILm	XX
	Ms 14	Winchester	C		SCILm	XX
	Ms 24	Vredendal	C		SCILm	XX
NOMANCI B	No 11	Lusiki	B		SCI	0
	No 10	Nomanci	B		SCILm	0
OAKLEAF B	Oa 43	Allanridge	B		SLn	0
	Oa 45	Calueque	A/B	+t	SLn	0
	Oa 21	Doornkraagte	A/B	+t	LmS	0
OAKLEAF (contd)	Oa 25	Hazelwood	A/B	+t	SLn	0
	Oa 17	Highflats	B/C	-t	SCI	0
	Oa 22	Holpan	A/B	+t	S	0
	Oa 36	Jozini	B		SCILn	0
	Oa 23	Kirkton	B		SLn	0
	Oa 13	Klipplaat	B		SLm	0
	Oa 37	Koedoesvlei	B/C	-t	SCI	0
	Oa 16	Leeufontein	B		SCILm	0
	Oa 26	Letaba	B		SCILm	0
	Oa 34	Levubu	B		SLm	0
	Oa 46	Limpopo	B		LCILn	0
	Oa 41	Lovedale	A/B	+t	LmS	0
	Oa 11	Madwaleni	A/B	+t	LmS	0
	Oa 24	Magersfontein	B		SLm	0
	Oa 27	Makulek	B/C	-t	SCI	0
	Oa 12	Mbanyana	A/B	+t	S	0
	Oa 47	Mutale	B/C	-t	SCI	0
	Oa 42	Nzulila	A/B	+t	S	0
	Oa 30	Oakleaf	A/B	+t	LmS	0
	Oa 44	Okavango	B		SLm	0
	Oa 31	Oshikango	A/B	+t	LmS	0
	Oa 15	Pollock	A/B	+t	SLm	0
	Oa 14	Rockford	B		SLm	0
	Oa 32	Sezela	A/B	+t	S	0
	Oa 10	Snaldeel	A/B	+t	LmS	0
	Oa 33	Vaalriver	B		SLm	0
	Oa 35	Venda	A/B	+t	SLm	0
	Oa 40	Voorspoed	A/B	+t	LmS	0
	Oa 20	Warrenton	A/B	+t	LmS	0
PINEDENE B	Pn 27	Airlie	B/C	-t	SCI	I
	Pn 12	Bethlehem	A	+t/+I	S	I
	Pn 25	Chatsworth	A/B	+t	SLn	I
	Pn 15	Eykendal	A	+t/+I	SLm	I
	Pn 10	Fortuin	A	+t/+I	LmS	I
	Pn 13	Greymead	A/B	+I	SLn	I
	Pn 22	Hermanus	A/B	+t	S	I
	Pn 17	Kilburn	B	-t/+I	SCI	I
	Pn 32	Kleinrivier	B	+t/+I	S	I
	Pn 36	Klerksdorp	B/C	-I	SCILn	I
	Pn 31	Nootwagt	B/C	-I	SLn	I
	Pn 33	Oewer	B/C	-I	SLm	I
	Pn 16	Oswerf	A/B	+I	SCILn	I
	Pn 30	Papiesvlei	B	+t/-I	LmS	I
	Pn 14	Pinedene	A/B	+I	SLn	I

Table (continued)

Soil Form	Code	Soil Series	SCS Group -ing	SCS Adjust-ment Factor	Typical Text-ural Class	Inter-flow Poten-tial
PINEDENE (contd)	Pn 11	Radyn	A	+t/+1	LmS	X
	Pn 20	Rotterdam	A/B	+t	LmS	X
	Pn 31	Stormsvlei	B	+t/-1	LmS	X
	Pn 26	Suurbraak	B		SClLm	X
	Pn 24	Tulbagh	B		SLm	X
	Pn 23	Vyeboom	B		SLm	X
	Pn 21	Wemmershoek	A/B	+t	LmS	X
	Pn 37	Witpoort	C	-t/-1	SCl	X
	Pn 35	Yzerspruit	B	+t/-1	SLm	X
RENSBERG D	Rg 10	Phoenix	D		Cl	X
	Rg 20	Rensberg	D		Cl	X
SHEPSTONE A	Sp 12	Addington	A		LmS	0
	Sp 11	Bitou	A		LnS	0
	Sp 13	Gouritz	A		SLm	0
	Sp 15	Inhaminga	A		SLm	0
	Sp 22	Kunjane	A		LmS/SClLm	0
	Sp 23	Pencarrow	A		SLm/SClLm	0
	Sp 24	Portobello	A		SLm/SClLm	0
	Sp 25	Pumula	A		SLm/SClLm	0
	Sp 14	Robberg	A		SLm	0
	Sp 21	Shepstone	A		LmS/SClLm	0
	Sp 2[illegible]	Southbroom	A		LmS/SClLm	0
	Sp 10	Tergniet	A		LmS	0
SHORT-LANDS B	Sd 11	Argent	B		SCl	0
	Sd 10	Bokuil	A/B	+t	SClLm	0
	Sd 30	Ferry	B		SClLm	0
	Sd 21	Glendale	B/C	-1	SCl	0
	Sd 20	Kinross	B	-1/+t	SClLm	0
	Sd 12	Richmond	B/C	-t	Cl	0
	Sd 22	Shortlands	C	-1/-t	Cl	0
	Sd 31	Sunvalley	B/C	-1	SCl	0
	Sd 32	Tugela	C	-1/-t	Cl	0
STERK-SPRUIT D	Ss 27	Antioch	D		SCl	X
	Ss 13	Bakklysdrift	D		SLm	X
	Ss 15	Dehoek	D		LmS	X
	Ss 10	Diepkloof	D		LmS	X
STERK-SPRUIT	Ss 17	Driebaden	D		SCl	X
	Ss 21	Graafwater	D		LnS	X
	Ss 25	Grootfontein	D		LnS	X
	Ss 20	Halseton	D		LmS	X
	Ss 24	Hartbees	D		SLm	X
	Ss 12	Ruacana	D		S	X
	Ss 22	Silwana	D		S	X
	Ss 23	Stanford	D		SLm	X
	Ss 26	Sterkspruit	D		SClLm	X
	Ss 16	Swaerskloof	D		SClLm	X
	Ss 11	Tina	D		LnS	X
	Ss 14	Toleni	D		SLm	X
SWARTLAND C/D	Sw 12	Breidbach	D	-t	Cl	X
	Sw 21	Broekspruit	C/D		SCl	X
	Sw 32	Hogsback	D	-t	Cl	X
	Sw 40	Malekata	C/D		SCl	X
	Sw 41	Nyoka	C/D		SCl	X
	Sw 42	Ondraai	D	-t	Cl	X
	Sw 22	Prospect	D	-t	Cl	X
	Sw 10	Reveillie	C/D		SClLm	X
	Sw 30	Rosehill	C/D		SClLm	X
	Sw 11	Skilderkrans	C/D		SCl	X
	Sw 31	Swartland	C/D		SCl	X
	Sw 20	Uitsicht	C/D		SClLm	X
TAMBAN-KULU C	Tk 10	Fenfield	C		SClLm	X
	Tk 20	Loshoek	C		SClLm	X
	Tk 21	Masala	C/D	-t	SCl	X
	Tk 11	Tabenkulu	C/D	-t	SCl	X
VALS-RIVIER C/D	Va 31	Arniston	C/D		SCl	X
	Va 32	Chalumna	C	-t	Cl	X
	Va 21	Craven	C/D		SCl	0
	Va 10	Herschel	C/D		SClLm	X
	Va 12	Lilydale	D	-t	Cl	0
	Va 41	Lindley	C/D		SCl	X
	Va 22	Marienthal	C	-t	Cl	0
	Va 42	Sheppardveie	D	-t	Cl	X
	Va 10	Sunnyside	C/D		SClLm	0

Table (continued)

Soil Form	Code	Soil Series	SCS Group-ing	SCS Adjust-ment Factor	Typical Textural Class	Inter-flow Potential
VALS-RIVIER (contd)	Va 40	Valsrivier	C/D		SCILm	X
	Va 11	Waterval	C/D		SCl	0
	Va 20	Zuiderzee	C/D		SCILm	0
VILA-FONTES A/B	Vf 45	Blombosch	A/B		SLm/SCILm	XX
	Vf 23	Blythdale	A/B		SLm/SCILm	XX
	Vf 31	Brenton	A/B		LmS	XX
	Vf 24	Chantilly	A/B		CLm/SCILm	XX
	Vf 44	Dassenhoek	A/B		SLm/SCILm	XX
	Vf 21	Fairbreeze	A/B		LmS/SCLm	XX
	Vf 43	Geelbek	A/B		SLm/SCILm	XX
	Vf 11	Hudley	A/B		LmS	XX
	Vf 22	Klaarwater	A/B		LmS/SCILm	XX
	Vf 34	Knysna	A/B		SLm	XX
	Vf 40	Kransduinen	A/B		LmS/SCILm	XX
	Vf 20	Matigulu	A/B		LmS/SCILm	XX
	Vf 41	Mazeppa	A/B		LmS/SCILm	XX
	Vf 35	Meulvlei	A/B		SLm	XX
	Vf 10	Moreland	A/B		LmS	XX
	Vf 14	Moyeni	A/B		SLm	XX
	Vf 25	Nhamecala	A/B		SLm/SCILm	XX
	Vf 33	Rheebok	A/B		SLm	XX
	Vf 30	Sedgefield	A/B		LmS	XX
	Vf 32	Swinton	A/B		LmS	XX
	Vf 13	Tinley	A/B		SLm	XX
	Vf 42	Vallance	A/B		LmS/SCILm	XX
	Vf 15	Vilafontes	A/B		SLm	XX
	Vf 12	Zeekoe	A/B		LmS	XX
WASBANK C	Wa 12	Burford	C		SCILm	XX
	Wa 13	Endicott	C/D	-t	SCl	XX
	Wa 30	Hamman	B/C	+t	S	XX
	Wa 10	Hoopstad	B/C	+t	LmS	XX
	Wa 11	Kromvlei	C		SLm	XX
	Wa 20	Rondevlei	B/C	+t	LmS	XX
	Wa 31	Sandvlei	B/C	+t	SCILm	XX
	Wa 22	Warrick	C		SCILm	XX
	Wa 21	Wasbank	C		SLm	XX
	Wa 32	Winterveld	C		SCILm	XX
WESTLEIGH C	We 10	Chinde	B/C	+t	LmS	X
	We 32	Davel	C		SCILm	X
	We 22	Devon	C		SCILm	X
	We 20	Kosi	B/C	+t	LmS	X
	We 30	Langkuil	B/C	+t	S	X
	We 31	Paddock	B/C	+t	SLm	X
	We 12	Rietvlei	C		SCILm	X
	We 13	Sibesa	D	-t	SCl	X
	We 11	Westleigh	C		SLm	X
	We 21	Witsand	C		SLm	X
WILLOW-BROOK D	Wo 21	Chinyika	D		SCl	0
	Wo 10	Emfuleni	D		SCILm	0
	Wo 20	Saresdale	D		SCILm	0
	Wo 11	Willowbrook	D		SCl	0